



Sustainable Civil Engineering Structures and Construction Materials, SCESCM 2016

Shear behavior of high-volume fly ash concrete as replacement of Portland cement in RC beam

Ade Lisantono^{a,*}, Haryanto Yoso Wigroho^a, Roy Arnol Purba^a

^a*Department of Civil Engineering, Universitas Atma Jaya Yogyakarta, Jl. Babarsari 44, Yogyakarta 55281, Indonesia*

Abstract

An experimental program was conducted to study the shear behavior of high-volume fly ash concrete as replacement Portland cement of Reinforced Concrete (RC) beams. Eight beam specimens were tested in this study. Two beams used normal concrete as control beams, while six others beams used High-Volume Fly Ash Concrete (HVFAC) as a replacement of Portland cement by mass (two beams with 50 % of fly ash; two beams with 60 % fly ash; and two beams with 70 % of fly ash). The beams had longitudinal bars, and with stirrups were kept constant in the bending-test region. There were no shear reinforcements in the shear-test regions. The results showed that increasing substitutions of fly ash as replacement of Portland cement tend towards a reduction of shear strength and led the HVFAC beams became brittle. Comparing all the series of HVFAC beams that better results could be achieved by the beams with 50 % of fly ash due to the higher shear strength than the beam with 60 % and 70 % of fly ash. The HVFAC beams failed in shear due to low shear strength of the beams

© 2017 The Authors. Published by Elsevier Ltd.

Peer-review under responsibility of the organizing committee of SCESCM 2016.

Keywords: high-volume fly ash; OPC replacement; shear strength;

1. Introduction

Indonesia's construction industry has been emerged since several decades ago. As emerging of construction industry in Indonesia, a need of building material for construction also increase. Concrete has been emerged as a famous material for building due to easily in making and forming the concrete, and of course concrete structures is more resistant from corrosion than steel structures. The basic materials for making concrete are Portland cement, fine

* Corresponding author. Tel.: +62-274-487711; fax: +62-274-487748.

E-mail address: adelisantono@mail.uajy.ac.id

aggregates and coarse aggregates. The Portland cement is the most essential ingredient in production of concrete. However, Portland cement also contributes to the global warming due to carbon dioxide (CO₂) emissions as a side effect of Portland cement production. Roy [1] stated that Portland cement contribution to global warming because of production of one ton ordinary Portland cement will produce one ton CO₂ which is released to the air.

One of the solutions for this global warming issue is reducing the utility of Portland cement in production of concrete. To reduce the Portland cement in production of concrete is the use of supplementary cementitious materials. Bilodeau and Malhotra [2] stated that the most available supplementary cementitious material is fly ash which is produced by coal-burning thermal power stations. Fly ash has been used as supplementary cementitious material in concrete since 1937 [3]. According to American Concrete Institute [4], fly ash is categorized into three classes: class N, F, and C based on the chemical compositions. Study of utilization of fly ash as supplementary in concrete has been extensively conducted since several decades ago [2, 5-9]. The utilization of fly ash as supplementary in concrete has benefit such as reducing heat generation, low permeability, and high durability [10]. Therefore, development of utilization of fly ash as supplementary in concrete is still promising for the future.

In the early, fly ash was used as replacement of cement limited into the range of 15-25 % [11]. While for high strength concrete the portion of replacement at 35 % to control peak hydration temperature [12]. In the next development, a high volume fly ash concrete (HVFAC) where the replacement of cement with fly ash at least at 50 % was developed [13-14]. These studies had shown that HVFAC has lower shrinkage, creep, and water permeability, and has higher modulus of elasticity compared to the conventional concrete. Koyama et al. [15] investigated the mechanical properties of concrete beam made of a large amount of fly ash where the cement content was kept constant, the results showed that the shear strength and deformability of the beam increased as the mixed quantity of fly ash increased. Rao et al. [16] investigated shear resistance of high volume fly ash reinforced concrete beams without web reinforcement where the replacement of cement with the portion of 0 % and 50 % and with the various longitudinal tensile steel reinforcement, the result showed that shear strength of the beam increased with increasing of longitudinal tensile steel ratio. Soman and Sobha [17] also investigated the shear and behavior of high volume fly ash concrete with the replacement of fly ash 50 %, the result showed that the HVFAC beams improved the deflection and the load carrying capacity of the beams. Thangaraj, R., and Thenmozhi, R. [18] investigated the performance of high volume fly ash concrete structures with the replacement of cement of 50 %, 55 %, and 60 %, it was observed that the compressive strength of HVFAC was improved by about 50 % cement replacement. Arezoumandi et al. [10] conducted an experimental program on shear behavior of high-volume fly ash concrete versus conventional concrete with the replacement of cement of 50 %, and 70 %, the results showed that the HVFAC beams gave the superior shear strength compared to the conventional concrete beams.

There were several investigations on shear strength of the HVFAC beams. However it is still questionable in what portion of fly ash replacement which makes the maximum shear strength of the HVFAC beams. Therefore, this research will conduct the experimental program to investigate the shear behavior of high-volume fly ash concrete beams as a replacement of cement. The various portion of fly ash replacement in this research were 50 %, 60 %, and 70 %.

2. Experimental program

2.1. Materials

The Portland Pozzolan Cement (PPC) was used in this study. The water used in this study was taken from the Laboratory of Structures and Materials. The fine and coarse aggregates were taken from local materials. The fine aggregates were passed through sieve 4.75 mm. The specific gravity and fineness modulus of fine aggregates were 2.77 and 2.92, respectively. While the coarse aggregates used in this research were passed through 20 mm and retained on 10 mm sieve. The specific gravity and fineness modulus of coarse aggregates were 2.68 and 7.16, respectively. The fly ash class F was used in this study. To enhance the workability of concrete a super plasticizer was used to make the concrete. The mix design of concrete was designed following the ACI 211.1-91 [19]. The mix proportion per m³ of concrete with 0 % replacement of cement was as follows: Portland Pozzolan Cement=336.07 kg; water=207.39 kg; coarse aggregates=892.09 kg; fine aggregates=958.67 kg, and with super plasticizer=2.073 kg. For HVFAC with the

replacement 50 %, 60 %, and 70 % of cement, just replaced the cement in the proportion with 50 %, 60 %, and 70 % of fly ash, respectively.

2.2. Materials testing

To see the chemical composition of fly ash, the fly ash was tested in the Laboratory of Chemical Engineering, Universitas Gadjah Mada. The tested result of fly ash was shown in Table 1. It can be seen that the fly ash can be classified as fly ash type F.

Table 1. The chemical composition of fly ash.

No	Chemical element	Content (%)	Note
1	SiO ₂	43.250	
2	Al ₂ O ₃	27.492	
3	Fe ₂ O ₃	11.292	
4	SiO ₂ + Al ₂ O ₃ + Fe ₂ O ₃	82.034	> 70 %
5	Loss on Ignition	-	
6	CaO	7.246	< 10 %
7	MgO	7.125	
8	SO ₃	1.499	
9	K ₂ O	0.864	
10	Na ₂ O	-	
11	H ₂ O	-	

Reinforcement bar with diameter of 12 mm was used for longitudinal bar, and reinforcement bar with diameter of 6 mm was used for stirrup. The yield stress of reinforcement bars was obtained according to the guidelines in ASTM E8/E8M-09 [20], Standard Test Methods for Tension Testing of Metallic Materials. Universal Testing Machine (UTM) with capacity of 30,000 kgf was used to conduct the tension test of reinforcement bars. The average yield stresses of 240 MPa were obtained for both reinforcing bars of 12 mm and 6 mm.

2.3. Specimens preparation

Cylinder specimens with the size of 150 mm x 300 mm were cast for testing of compressive strength and modulus elasticity of concrete. Thirty six cylinder specimens were tested in this study (see Table 2).

Table 2. The number of cylinder specimens.

Cylinder Designation	Fly ash content (%)	For 7 days testing	For 14 days testing	For 28 days testing
0FA	0	3	3	3
50FA	50	3	3	3
60FA	60	3	3	3
70FA	70	3	3	3

Eight beam specimens were tested in this study. Two beams used normal concrete as control beams, while six others beams used High-Volume Fly Ash Concrete (HVFAC) as a replacement of portland cement by mass (two beams with 50 % of fly ash; two beams with 60 % fly ash; and two beams with 70 % of fly ash). The beams had a rectangular section of 150 mm x 260 mm and overall length of 2600 mm. The beams had longitudinal bars with diameter of 12 mm. Three bars were for bottom reinforcement and two bars for top reinforcement. The shear reinforcements used diameter of 6 mm with stirrups spacing of 100 mm were kept constant in the bending-test region, and there were no shear reinforcements in the shear-test regions. The beam designation and the number of the beam in every variant can be seen in Table 3.

Table 3. The beam designation and the number of beam specimens.

Beam Designation	Fly ash content (%)	The number of beam specimen
B1-Normal	0	2
B2-Normal	0	
B1-50FA-SS	50	2
B2-50FA-SS	50	
B1-60FA-SS	60	2
B2-60FA-SS	60	
B1-70FA-SS	70	2
B2-70FA-SS	70	

2.4. Setup of beam specimens

The beam specimens were tested on the loading frame of the Laboratory of Structures and Materials. The actuator with load capacity of 250 kN was used to test all beam specimens. The specimen was tested under load control. A transfer beam was used to transfer the load from the actuator to the beam specimen. The beams were simply supported and loaded symmetrically under two-point-loading. A Linear Variable Differential Transformers (LVDT) was used to measure deflection of the specimen. The LVDT was placed at the middle of the specimen. Measured data of load and deflection were read through a computer driven data acquisition system using data logger. The setup of the beam specimen was shown in Fig.1.

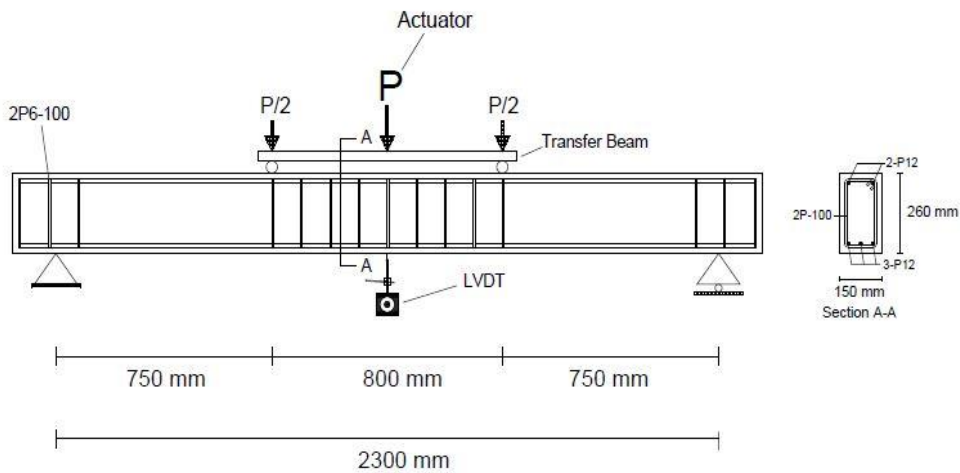


Fig.1. Setup of beam specimen

3. Results and discussion

3.1. Properties of concrete

The average density, compressive strength, and modulus of elasticity of concrete tested at 28 days were shown in Table 4. It can be seen from Table 4 that the average density of HVFAC increased when the content of fly ash increased. While the average compressive strength and modulus of elasticity of HVFAC decreased when the content of fly ash increased. Compare to the normal concrete, it can be seen also from Table 4 that the average compressive strength and average modulus of elasticity of HVFAC were lower than normal concrete.

Table 4. The mechanical properties of concrete.

Code	Fly ash content (%)	Average density (Kg/m ³)	Average Compressive Strength (MPa)	Average Modulus of Elasticity (MPa)
0FA	0	2256.222	20.441	22527.32
50FA	50	2252.100	15.342	15200.28
60FA	60	2305.669	13.753	14541.86
70FA	70	2402.134	11.672	11482.64

3.2. Shear Behavior of HVFAC Beam

The first crack was observed visually during the testing specimen. The first crack load was noted as the load at first crack occurred. The first crack load of every beam specimen was presented in Table 5. It can be seen from Table 5 that the average first crack load of HVFAC beams was lower than the control beam. It can be seen also that the first crack load of HVFAC beams decreased when the replacement of the cement by fly ash was increased.

Table 5. The first cracking load of every beam specimen.

Beam Designation	Fly ash content (%)	The load at first crack (kN)	Average load at first crack (kN)
B1-Normal	0	26.12	31.31
B2-Normal	0	36.50	
B1-50FA-SS	50	25.50	22.30
B2-50FA-SS	50	19.10	
B1-60FA-SS	60	22.00	18.73
B2-60FA-SS	60	15.46	
B1-70FA-SS	70	21.85	18.55
B2-70FA-SS	70	15.25	

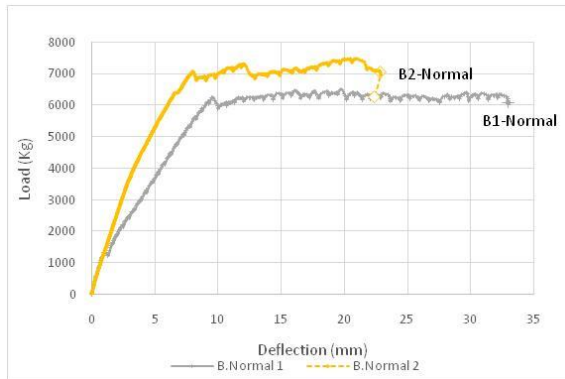
The ultimate load of every beam specimen was shown in Table 6. Compared to the control beam, it can be seen that the average ultimate load of HVFAC beams were lower than the control beam. It can be seen also that the ultimate load of HVFAC beam was decreased when the replacement of cement by fly ash was increased. Among the HVFAC beams, it can be seen that the HVFAC beam with 50 % fly ash was the optimum replacement of fly ash, because it had the largest ultimate load compared to others HVFAC beams. If the HVFAC beam with 50 % fly ash had the largest ultimate load, it means that the HVFAC beam with 50 % fly ash had the largest shear strength compared to others HVFAC beams.

Table 6. The ultimate load of beam specimens.

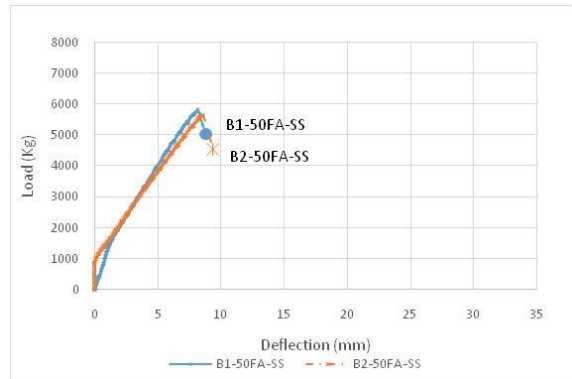
Beam Designation	Fly ash content (%)	Ultimate load (kN)	Average ultimate load (kN)
B1-Normal	0	65.094	70.003
B2-Normal	0	74.912	
B1-50FA-SS	50	58.091	57.263
B2-50FA-SS	50	56.434	
B1-60FA-SS	60	55.256	48.869
B2-60FA-SS	60	42.482	
B1-70FA-SS	70	38.182	41.893
B2-70FA-SS	70	45.604	

The load-deflection relationship of every beam specimen was shown in Fig. 2(a); (b); (c); and (d). It can be seen from Fig. 2(a), the load-deflection behavior of B1-Normal and B2-Normal (control beams) were virtually identical. Before first cracking the curve increased linearly which was presenting elastic behavior. After cracking, the curve increased nonlinearly up to an ultimate load. After reaching the ultimate load, the curve decreased non-linearly and

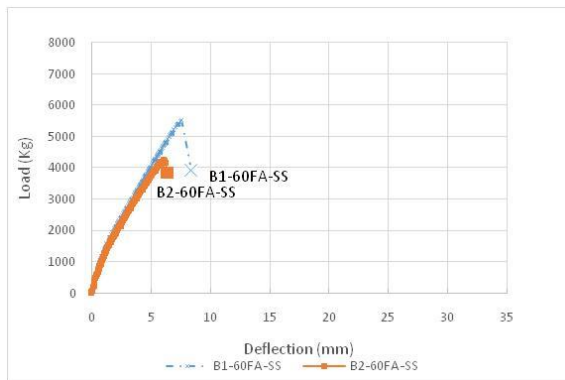
proceeded with a section of an approximately horizontal curve, indicating a state of yielding and large deformation of the beam before collapse.



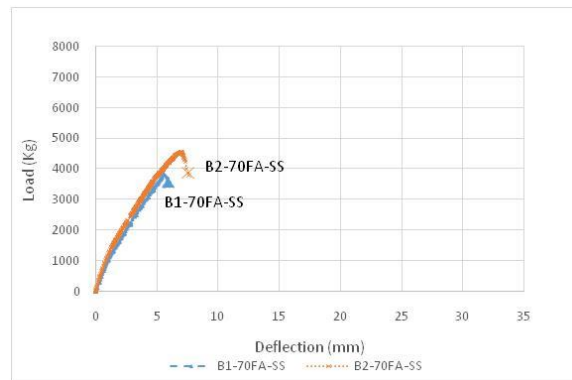
(a) Load-deflection of B1-Normal and B2-Normal



(b) Load-deflection of B1-50FA-SS and B2-50FA-SS



(c) Load-deflection of B1-60FA-SS and B2-60FA-SS



(d) Load-deflection of B1-70FA-SS and B2-70FA-SS

Fig.2. The load-deflection relationship of beam specimens

While the load-deflection of the HVFAC beams (B1-50FA-SS; B2-50FA-SS; B1-60FA-SS; B2-60FA-SS; B1-70FA-SS; and B2-70FA-SS) were virtually also identical (see Fig. 2(b), (c), and (d)). Before cracking, the curve displayed linearly elastic behavior. After cracking, the curve increased nonlinearly until reaching the ultimate load. After reaching the ultimate load, the load drop rapidly prior to collapse. The collapse of the HVFAC beams was indicated with a sudden failure and large shear crack in shear-test-region (region without stirrups).

The comparison among the beam specimens can be seen in Fig. 3. It can be seen that the control beams were more ductile compared to the HVFAC beams. It indicated that replacement of cement by fly ash made the HVFAC beams brittle due to the lower compressive strength of HVFAC beams compared to the control beams.

The crack pattern of beam specimens was shown in Fig. 4. The control beams (B1-Normal and B2-Normal) failed in flexure. The first crack appeared in the maximum moment region, and then followed by additional flexural crack which developed vertically. As the load increased, a small inclined flexure-shear crack appeared then the beam gave large deformation prior to collapse. While all HVFAC beams failed in shear. The first crack appeared in the maximum moment region, and then followed by additional flexural crack. As the load increased, a large inclined flexure-shear crack appeared between the load and support then the beam was collapse suddenly. It indicated that the shear strength of the HVFAC was low and it was easily to be crack in the shear-test-region.

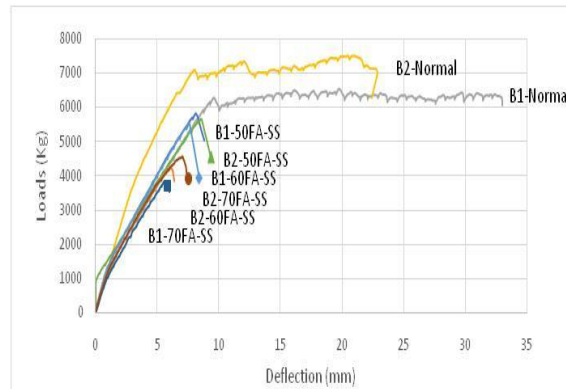


Fig. 3. Comparison load-deflection relationship among the beam specimens

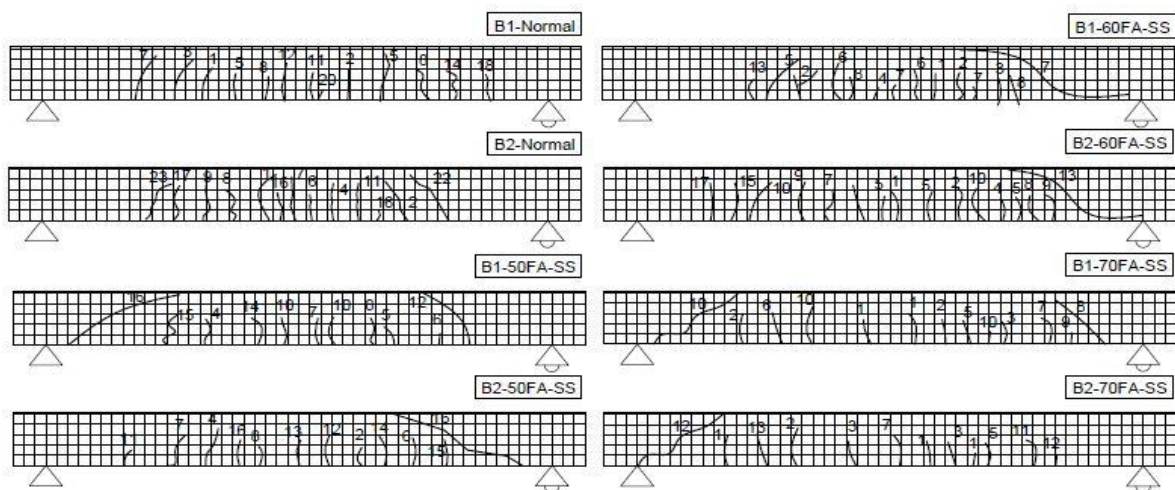


Fig. 4. The crack pattern of beam specimens.

4. Conclusions

Based on the obtained experimental results, the following conclusion can be drawn:

- Increasing the substitutions of fly ash as replacement of portland cement tend towards a reduction of shear strength and led the HVFAC beams became brittle.
- Comparing all the series of HVFAC beams that better results could be achieved by the beams with 50 % of fly ash due to the higher shear strength than the beam with 60 % and 70 % of fly ash.
- The HVFAC beams failed in shear due to the low shear strength of the beams.

Acknowledgements

The experimental program reported herein was made possible due to fund of Internal Research Grant of Civil Engineering Department, Faculty of Engineering, Universitas Atma Jaya Yogyakarta. The authors gratefully acknowledge of this financial support. The authors would like to thanks to the Head and Staff of Laboratory of Structures and Materials, Department of Civil Engineering, Faculty of Engineering, Universitas Atma Jaya Yogyakarta for the use of their research facilities. In this chance, the authors would like also to thanks to Daniel Krisna Mukti for the help during the testing of the specimens in the Laboratory of Structures and Materials.

References

- [1] Roy, D.M., Alkali-activated cements, opportunities and challenges. Cement and Concrete Research, 1999, pp. 249-254.
- [2] Bilodeau, A., and Malhotra, V.M., High-volume fly ash system: Concrete solution for sustainable development, ACI Materials Journal, 97(1), 2000, pp. 41-48.
- [3] Davis, R.E., Carlson, R.W., Kelly, J.W., and Davis, H.E., Properties of cements and concretes containing fly ash. Journal American Concrete Institute, 33(5), 1937, pp. 577-612.
- [4] ACI Committee 232, Use of fly ash in concrete. ACI 232.2R-03, 2003, Farmington Hills, MI.
- [5] Malhotra, V.M., Zhang, M.H., Read, P.H., and Ryell, J., Long-term mechanical properties and durability characteristics of high-strength/high-performance concrete incorporating supplementary cementing materials under outdoor exposure conditions. ACI Materials Journal, 97(5), 2000, pp. 518-525.
- [6] Bilodeau, A., Sivasundaram, V., Painter, K.E., and Malhotra, V.M., Durability of concrete incorporating high volume of fly ash from sources in the USA, ACI Materials Journal, 91(1), 1994, pp. 3-12.
- [7] Langley, W.S., Carette, G.G., and Malhotra, V.M., Strength development and temperature rise in large concrete blocks containing high volumes of low-calcium (ASTM Class F) fly ash. ACI Materials Journal, 89(2), 1992, pp. 362-368.
- [8] Sivasundaram, V., Carette, G.G., and Malhotra, V.M., Mechanical properties, creep, and resistance to diffusion of chloride ions of concretes incorporating high volume of ASTM class F fly ash from seven different sources. ACI Materials Journal, 88(4), 1991, pp. 384-389.
- [9] Langley, W.S., Carette, G.G., and Malhotra, V.M., Structural concrete incorporating high volumes of ASTM class F fly ash. ACI Materials Journal, 86(5), 1989, pp. 507-514.
- [10] Arezoumandi, M., Volz, J.S., Ortega, C.A., and Myers, J.J., Shear behaviour of high-volume fly ash concrete versus conventional concrete: Experimental study. ASCE Journal of Structural Engineering, 141 (3), 2015.
- [11] Berry, E.E., Hemmings, R.T., Zhang, M.H., Cornelious, B.J., and Golden, D.M., Hydration in high-volume fly ash binders, ACI Materials Journal, 91(4), 1994, pp. 382-389.
- [12] Myers, J.J., and Carrasquillo, R.L., Mix proportioning for high-strength HPC bridge beams, ACI Special Publication 189, Detroit, MI, pp. 37-56.
- [13] Malhotra, V.M., Superplasticized fly ash concrete for structural application. Concrete International, 8(12), pp. 28-31.
- [14] Gopalan, M.K., Nucleation and pozzolanic factors in strength development of class F fly ash. ACI Materials Journal, 90(2), 1993, pp. 117-121.
- [15] Koyama, T., Sun, Y.P., Fujinaga, T., Koyamada, H., and Ogata, F., Mechanical properties of concrete beam made of a large amount of fine fly ash. Proceeding of the 14th World Conference on Earthquake Engineering, October 12-17, 2008, Beijing, China.
- [16] Rao, R.M., Mohan, S., and Sekar, S.K., Shear resistance of high volume fly ash reinforced concrete beams without web reinforcement. International Journal of Civil and Structural Engineering, 1 (4), 2011, pp. 986-993.
- [17] Soman, M., and Sobha, K., Strength and behaviour of high volume fly ash concrete. International Journal of Innovative Research in Science, Engineering and Technology, 3(5), 2014, pp. 12416-12424.
- [18] Thangaraj, R., and Thenmozhi, R., Performance of high volume fly ash in concrete structures. IOSR Journal of Mechanical and Civil Engineering, 3(1), 2012, pp. 28-33.
- [19] ACI Committee 211, Standard practice for selecting proportions for normal, heavyweight, and mass concrete (ACI 211.1-91), ACI Manual of Concrete Practice, Part I, 1995, pp. 211.1-1 to 211.1-38.
- [20] ASTM, American society for testing and materials annual book of ASTM standards. Vol. 04.09, 2008, West Conshohocken, PA.



Sustainable Civil Engineering Structures and Construction Materials, SCESCM 2016

Composite engineering – direct bonding of plastic PET films by plasma irradiation

Tamio Endo^{a,b,*}, Lakshmi Reddy^c, Hiroaki Nishikawa^d, Satoru Kaneko^e,
Yoshinobu Nakamura^f, Kazuhiro Endo^g

^aFaculty of Engineering, Mie University, Japan

^bFaculty of Engineering, Gifu University, Gifu 5011193, Japan

^cS.V.D. College, Cuddapah, India

^dFaculty of Biology-Oriented Science and Technology, Kinki University, Japan

^eKanagawa Industrial Technology Center, Japan

^fGraduate School of Engineering, University of Tokyo, Japan

^gKanazawa Institute of Technology, Japan

Abstract

This article reviews “plasma bonding” of plastic films. Polyethylene terephthalate (PET) films can be bonded directly by oxygen plasma irradiation and heat-press at low temperatures of 100–160°C. Functional groups of COOH and OH were detected on the irradiated surface. The irradiated films were kept in the atmosphere for six years, yet they can be bonded tightly. The irradiated surface is extremely active just after the irradiation, and it is still considerably active after five years. Dry- and wet-peel tests on the bonded films suggest that there are two elements, hydrogen bonding and chemical bonding. The films are bonded weakly by these two elements at lower press temperatures due to low densities of bonds, while they are bonded strongly by high density of the pure chemical bonds at higher temperatures. The hydrogen bonding is broken by water penetration into the interface, causing smaller peel strength under the wet-peel test. FTIR results on the non-irradiated, irradiated and bonded samples indicate that COOH and OH groups are created at the surface, they are responsible for the both bondings. The OH is consumed during the heat-press bonding, then dehydrated condensation reaction can be proposed for the chemical bonding. Cross-linking layer may be the origin for the long lifetime of the irradiated active surface.

© 2017 The Authors. Published by Elsevier Ltd.

Peer-review under responsibility of the organizing committee of SCESCM 2016.

* Corresponding author. Tel.: +81-90-4084-0075.

E-mail address: endotamio@yahoo.co.jp

Keywords: plasma bonding; PET; chemical bonding; irradiation effect.

1. Introduction

1.1. Utility of PET films

Biaxially oriented polyester polymer (PolyEthylene Terephthalate :PET) films have strong merits such as high mechanical strength, high electrical insulation, high transparency, high heat resistance and low-temperature durability. Then they are used for various applications, for example, magnetic tape bases, liquid crystal display touch panels, food packages[1], and back-sheets in solar cell panels [2,3].

In most of important utilities, low cost PET is mainly used in laminates with various plastic films. A biaxially oriented PET film possesses high performance, it has oriented molecular chains and crystallized structure. A graphic formulae of PET molecule is shown in Fig. 1, composed of C, H, O, and benzene ring. Then the biaxial oriented PET (we call this simply as PET henceforth) cannot be bonded with each other at temperatures lower than melting point (258°C). That is, it has no heat-sealing nature. For this reason PET films are coated with layers having the heat-sealing nature using glues and organic solvents when they are used for the food packages [1].

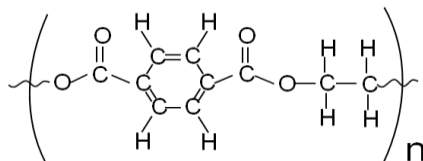


Figure 1. Graphic formulae of PET. It is feasible that the left end is terminated by H and the right by OH.

1.2. Solar cell back-sheets and issues of glue

A clean energy is urgently necessary in the world. One of essential technologies is the solar cell electric generation. It is important to further improve power generation efficiency, weight and durability for wider applications. A cost performance is also an important factor. Usually laminated PET film is used for the back-sheet of solar cell panel, as shown in Fig. 2. Alternatively a PVF/PET/PVF trilayer structure using fluoropolymer PVF (polyvinyl fluoride) was proposed by DeBergalis [4]. It is expected by this lamination that electrical isolation is increased, moisture permeation is decreased and cost is minimized. The other types of trilayer back-sheets also consist of PET films, and these are laminated using glues and organic solvents as well. But the organic solvents cause environmental and health issues, then we should withdraw the organic solvents during the coating process. Further the glues cause performance deterioration of devices in a long term use.

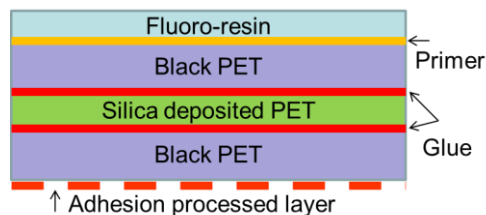


Figure 2. An example of back-sheet of solar cell panel.

1.3. Short lifetime of irradiated surface

To solve such problems, we developed a technique of plasma irradiation-induced direct bonding of plastic films without using any glues [5]. Normally the plasma irradiation effects on the plastic surfaces have very short lifetime,

say several days [6]. A reason for it was reported by Occhiello et al [7], that plasma-generated functional groups turn-back inside at the surface. We, however, report here that the PET films, kept for six years in the atmosphere after the plasma irradiation, can still be bonded very tightly in our work. It is quite strange that the activated surface by the plasma can be kept so long, because generally the surface must be easily inactivated due to reaction with the atmosphere (O₂, N₂, H₂O, Na, Cl, S etc.) even if the generated functional groups do not turn-back inside. New concepts should be proposed for such ultralong lifetime of the plasma irradiation effect.

1.4. Inorganic films on PET

The plasma-induced activation of plastic film surface is also an important technique when we deposit inorganic thin films such as ZnO and TiO₂ on plastic films in flexible devices. Banerjee and Endo et al. [8] have reported that crystalline ZnO thin film is successfully deposited on PET film at 90°C utilizing DC-sputtering plasma. Hao et al. [9] reported that electrophoresis chip needs gold deposition on the plastic films, and Audronis et al. [10] reported that Cu deposition is selectively enhanced on plasma-irradiated surface of PET.

1.5. Some reports on plasma effects

It is valuable to mention in this review on some recent reports by several authors regarding the plasma irradiations to the plastic surfaces. Effects of plasma irradiations and their chemical analyses on the plastic surfaces were reported by Cioffi et al. [11] and others [9-14]. Cioffi mentioned that tensile strength of PET fiber-reinforced composites can be improved by the plasma irradiation. Setsuhara et al. [12,14] mentioned on etching effects of the plasma, and Yang et al. [13] mentioned on increase in surface energy of the irradiated surfaces. Effects on biological responses of adhesion variations on the plasma-irradiated surfaces were reported. Katsikogianni et al. [15] mentioned that bacteria adhesion is reduced by the plasma irradiation due to increase in surface energy, while Vesel et al. [16] mentioned that the adhesion of polysaccharide fucoidan on the plasma-irradiated PET surface can be increased. Pandiyaraj et al. [17,18] reported that scotch tape adhesive strength can be increased on plasma-irradiated PET surface which is related to surface roughness, and surface energy of the irradiated PET is increased due to creation of polar groups. They mentioned a very important phenomenon that crystallinity of PET is improved by the plasma irradiation.

The plasma induced bonding effects were reported by Dai et al. [19] for between PET and PSMA (poly styrene-co-maleic anhydride), and by Hao et al. [9] for between PET and PET. Dai et al. mentioned that the plasma-irradiated PET and PSMA can be bonded at low press temperatures of 120-160°C, and this is induced by chemical reactions. However, when they tried to peel off, the laminated sample showed adherent failure implying not so strong adhesion. The plasma-induced chemical reaction for the chemical bonding at such low temperatures were reported also by Scott et al. [20] and Marechal et al. [21]

The most closely related research to our work was done by Hao et al. [9] reporting that amorphous PET can be bonded at very low press temperatures of 65-75°C just after the plasma irradiation. The amorphous PET has softening temperatures of 60-70°C, then this softening is one of the causes for such the very low bonding temperatures. They also mentioned a quite important point that some condensation reactions are possible to occur between the irradiated interface. Friedlich [22] published a book recently summarizing the plasma effects on plastic surfaces. He suggested that plasma-induced functional groups are –OH, –COOH, –C=O and O-bridge at the irradiated surface. The present authors [23-27] have reported the related papers concerning PET-PET and PET-PVF direct bondings by the plasma irradiations.

1.6. Scheme of this work

We tried to directly bond PET films without using such coatings and adhesive glues, and found that exposures of oxygen plasma was effective. After the exposure, PET films can be directly bonded with each other very tightly, i.e., showing the heat-sealing nature. They can be bonded with, for instance, glass plate also at low temperatures as 100°C.

In this review paper we introduce our experimental results on various chemical analyses on the exposed surface of PET films, and we discuss mechanisms for the direct tight bonding. Chemical bonding due to condensation reactions

and hydrogen bonding concerning the plasma irradiation-induced functional groups such as –OH and –COOH, are the most possible origins.

2. Experimental Procedure

2.1. Samples and plasma irradiations

It has been known so far that unique chemical reactions occur on the surface of polymer resins when they are irradiated by plasma. Complicated collisions due to high energy particles involved in the plasma induce such reactions. This is a reason why the reactions are unique and they cannot take place in usual soft chemical processes. Thus we can obtain higher hydrophilic and adhesive properties of the irradiated surface, called as surface modifications by the plasma [28,29]. However, the effects are usually kept only in short periods, say one week at most [30]. We tried to obtain the plasma equipment system which assures persistent effects of the plasma modifications.

In this experiment we used PET film samples (Lumirror, Toray) which were produced by two-axes stretch method (biaxially oriented PET). The sample size is 100 mm width and 200 mm length. The film thickness is 100 μm usually with surface roughness of around 0.5 nm, and 3.5 μm for Fourier Transform Infrared (FTIR) measurement. The film with 1 μm thickness was specially used when we prepared the bonded sample for the FTIR-Transmission measurement. The film samples were attached on a grounded drum electrode (150 mm diameter, 150 mm width) in a bell-jar-type vacuum chamber as shown in Fig. 3 [5]. The chamber was evacuated down to a range of 5-10 Pa, then O_2 gas was introduced with 20 cc/min to the chamber oxygen pressures of 15-40 Pa. Oxygen plasma was generated between the drum electrode and counter electrode with application of ac voltage at powers of 15 W (500 V, 30 mA)-75 W, and the drum electrode was rotated at 0.5 m/min. The moving sample was irradiated by the plasma for around 10 sec at energy of $E=200\text{-}1000 \text{ W}\cdot\text{min}/\text{m}^2$. The irradiated sample was taken out from the chamber to the normal atmosphere.

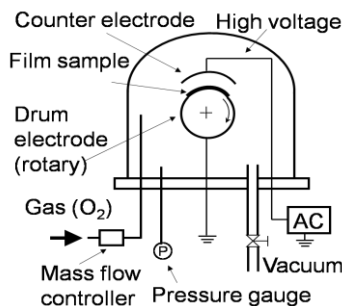


Figure 3. Plasma irradiation apparatus in a vacuum chamber. Sample film is attached on the rotating drum electrode. Plasma is generated between the drum and counter electrodes.

2.2. Bonding processes and strength evaluations

One part of the irradiated films were immediately pressed with their irradiated surfaces faced at various press temperatures T_p . Some of them were bonded tightly but others were loosely bonded or not bonded depending on T_p . We employed two methods of the heat-press as shown in Figs. 4(a) and 4(b). One is (a) heated roll-press at a pressure of 3 kg/cm^2 with a rolling rate of 0.45 m/min at T_p from 70 to 160 $^\circ\text{C}$, and the other is (b) heated plate-press (Kitagawa Seiki, VH-1[5] at a pressure of 10 kg/cm^2 at a fixed $T_p=140^\circ\text{C}$ for 10 min. The other part of the irradiated films were kept in the normal atmosphere for six years, after that they were heat-pressed by the same way mentioned above.

Bonding strength of the heat-pressed films was measured as peel strength S_p using T-type 180 $^\circ$ -peel test (Touyouseiki Seisaku, E-L) at a pulling rate of 50 mm/min as shown in Fig. 5 under JIS-C-2151 standard. It gives 180 $^\circ$ -peel strength S_p . Two processes were employed, one is called dry-peel test without water drops, the other is called wet-peel test with water drops at the bonded interface as shown in Fig. 5.

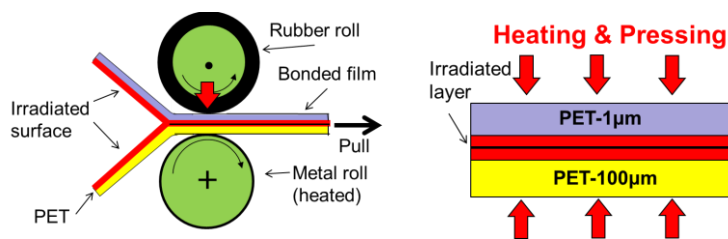


Figure 4. Heat press, (a) heated roll-press, (b) heated plate-press. Larger size of the sample film is necessary for FTIR measurement, then (b) is used.

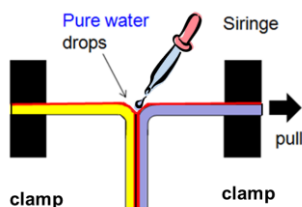


Figure 5. 180°(T)-peel test. Dry-peel without water drops, wet-peel with water drops.

2.3. Sample characterizations

The surface morphologies were observed on the irradiated films and non-irradiated films using Atomic Force Microscopy (AFM) (VecoDigital Instrument, Nano Scope III). Surface roughness R_a (mean value) was evaluated by AFM images.

The sample surface was chemically analyzed by X-ray Photoelectron Spectroscopy (XPS) (VG Scientific, ESCALB220iXL). Chemical bonding states and compositions were characterized on the sample surfaces. The samples were measured by Gas Chemical Modification Method (GCM) to get information on functional groups [31]. Trifluoroacetic anhydride (TFAA) was used to detect hydroxyl group (-OH). Poly vinyl alcohol was used as standard sample for the TFAA reaction. Trifluoroethanol with Di-ter-butylcarbodiimide and pyridine were used to detect carboxyl group (-COOH). Polyacrylic acid was used as standard sample for 2,2,2-trifluoroethanol reaction. To obtain mean molecular weight, Gel-Permeation-Chromatography (GPC) measurement was performed on the samples using a Type-515 water.

The irradiated and press-bonded samples with the roll-press (a) were characterized by the peel test, and a pure water contact angle θ was measured on the corresponding irradiated film surfaces. The samples with the plate-press (b) were characterized by FTIR. One special sample (irradiated and press-bonded) was prepared using 100 μm and 1 μm thicknesses for FTIR-Transmission measurement. The other part of the irradiated samples were kept in the atmosphere for five years, then the angle θ was measured on these sample surfaces.

The angle θ was measured on the non-irradiated samples in the atmosphere at 25°C under 55% humidity, and on the irradiated surface of samples just after the irradiation. The irradiated samples were kept in the atmosphere for five years, and the angle θ was measured. These samples kept in the atmosphere were heated at various elevating temperatures T_h for 10 min in the atmosphere, then the angle θ was measured at room temperature on these heated samples.

Chemical bonding states of the samples were characterized by FTIR with two methods as shown in Figs. 6(a) and 6(b). One was Attenuation Total Reflection (ATR) method on the non-irradiated and irradiated samples, the Infrared (IR) incident beam was introduced from the irradiated surface for the irradiated sample as shown in (a). The other was transmission method on the non-irradiated (100 μm thickness), irradiated (100 μm) and bonded samples (total 101 μm). The IR incident beam was introduced from the irradiated surface for the irradiated sample, and from the 1- μm side for the bonded sample with 1- μm /100- μm layer structure as shown in (b).

In order to investigate chemical nature (cross-linking) of the plasma-irradiated surface layer, we conducted solubility test of the irradiated sample. The non-irradiated and irradiated sample films with 40 mm x 40 mm were cut

into small pieces. They were put in o-chlorophenol (OCP) solution heated at 90°C in water bath for 30 min. Then remnant in the solution was observed by eyes.

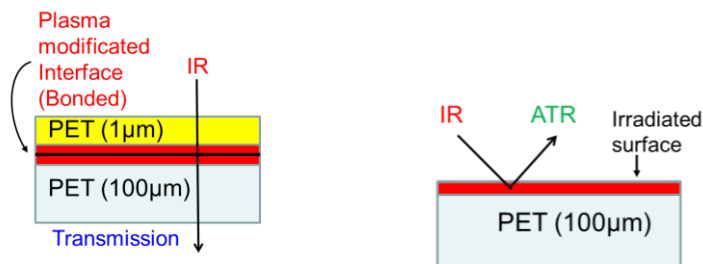


Figure 6. Schematic drawing for FTIR measurements. (a) ATR type and (b) Transmission type. In case of the irradiated sample, IR beam is introduced from the irradiated surface in (b).

3. Experimental Results

3.1. Press bonding temperature by peel test

The result of peel strength S_p vs heat-press temperature T_p by dry-peel test is shown in Fig. 7 for the laminated film which was roll-pressed immediately after the plasma irradiation. The films are not bonded below $T_p=90^\circ\text{C}$, but the films are strongly bonded above 120°C . When the sample was pulled with peel strength beyond 7 N/cm, it showed cohesion failure. This cohesion failure indicates that the two films are bonded more tightly than the material chemical bonding strength of original PET film. The non-irradiated films are not bonded even at the highest T_p of 160°C . It indicates that the films cannot be bonded by heating only. This is a well-known fact, i.e., PET has no heat-sealing nature below its melting point (258°C). These two results imply that the plasma-irradiated surface is enormously activated to make bonding reaction under the low pressure at low temperatures below the melting point [13,15,17,18].

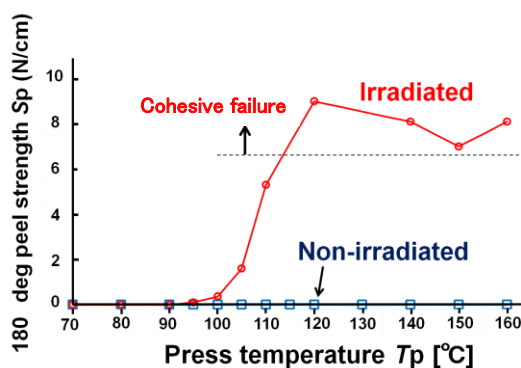


Figure 7. 180°(T)-peel strength (bonding strength) S_p vs press temperature T_p for the samples pressed just after the plasma irradiation. The sample shows cohesive failure beyond the pulling strength of 7 N/cm.

3.2. Surface morphology by AFM

AFM surface morphologies are shown in Fig. 8 for (a) the non-irradiated film and (b) the irradiated film. The mean surface roughness R_a is 0.46 nm and 0.53 nm for the non-irradiated and irradiated films, respectively. This increase by the plasma irradiation is negligibly small, and we have additional results which show that the roughness is rather reduced after the irradiation. Thus we can rule out an anchor effect for the origins of tight bonding by the plasma irradiation. Looking the surface morphologies carefully, we can recognize that micro-spike-like ragged fluctuation observed on the non-irradiated film is disappeared after the irradiation. It implies that weak-boundary-layer (WBL)

adhered on the non-irradiated film surface is removed by the irradiation.[32]. This may indicate further that the irradiated surface is chemically activated because active dangling bonds are created due to the WBL removal.

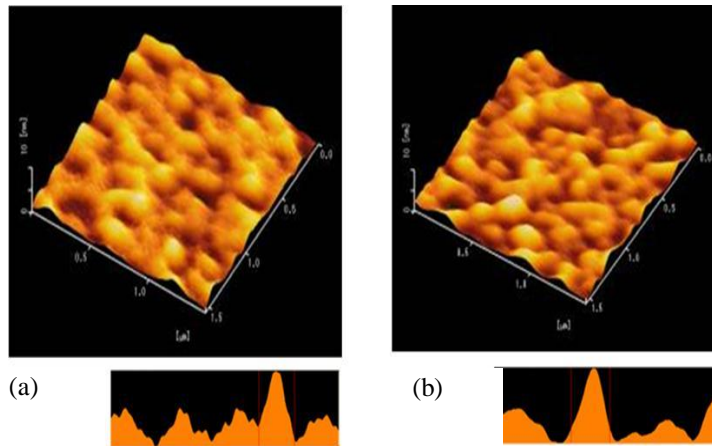


Figure 8. AFM surface images and sectional profiles for (a) non-irradiated ($R_a=0.46$ nm) and (b) irradiated ($R_a=0.53$ nm) PET films ($1.5 \times 1.5 \mu\text{m}$ area).

3.3. Surface chemical states by XPS

The results of XPS on C1s-related peaks normalized by C-C bond intensity are shown in Fig. 9(a), and N1s-related peak in Fig. 9(b), for the non-irradiated and irradiated film surfaces as a function of binding energy. It is known that the intensity corresponding to C=O (carbonyl group) bond indicated in Fig. 9(a) by an arrow around 287 eV is increased noticeably, and an apparent increase is recognized for C-O and C-N bonds. It should be noted that we cannot actually observe the peak corresponding to C=O because it is located between the neighbouring large peaks. We compare the intensities of C1s-related peaks for typical functional groups, their numerical values are shown in Table 1. Obviously the C=O bond intensity is appeared, then we can conclude at least that C=O is created by the irradiation. Although actually C-O is increased, the numerical value for C-O and C-N in Table 1 is not changed due to subtraction of the C=O peak tail from the C-O and C-N peak (Fig. 9(a)).

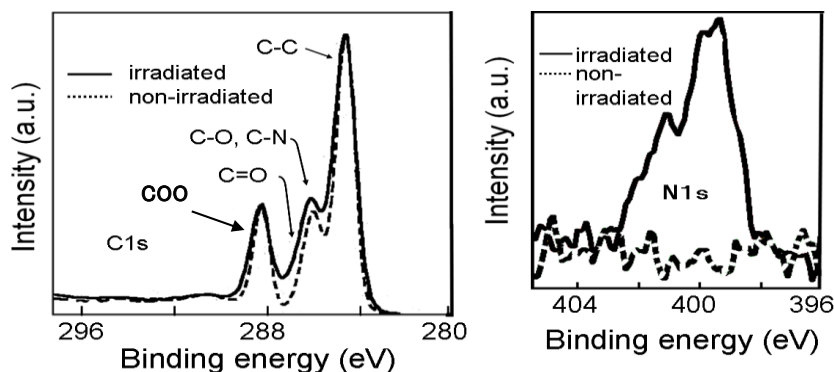


Figure 9. XPS spectra for the non-irradiated and irradiated PET film surfaces. (a) C1s-related peaks, (b) N1s-related peak.

Table 1. XPS peak intensity ratios of C1s-related peaks for various chemical states.

	π - π^*	COO	C=O	C-O C-N	CH _x , C-C C=C
non-irradiated (%)	5	18	-	22	55
irradiated (%)	4	17	3	22	54

Table 2. Surface compositions (atom%) and atomic ratios normalized by C in parentheses obtained by XPS.

	C	O	N
non-irradiated (%)	72.0 (1.0)	28.0 (0.390)	0 (0)
irradiated (%)	68.7 (1.0)	30.6 (0.445)	0.4 (0.005)

We calculated compositions for the surfaces of the films using XPS results, the numerical values are shown in Table 2. An atomic ratio of Oxygen is 0.390 for the non-irradiated film, quite close to the molecular nominal value of 0.4. This indicates the result is precise and reliable. After the irradiation the Oxygen composition is much increased to 0.445 from the nominal value. Then we can expect that the Oxygen-related functional groups other than C=O must be created at the surface by the irradiation. Those must be COOH and OH. The increase in C-O may be caused by creation of C-OH. In Table 1, the numerical value for COO is relatively decreased, because it is affected by the relative increase in C=O. Actually COO (properly COOH) should be increased. This is known from a broadening of the 289 eV-peak. This peak comes from the COO bond connecting to the benzene ring in the original molecular structure (see Fig. 1) in the non-irradiated PET. After the irradiation, the higher energy broadening comes from additionally created COOH groups at the surface, the peak energy of them is little higher than that of the original COO existing inside the molecule.

Fig. 9(b) clearly shows an appearance of N for the irradiated film. It is curious that Nitrogen is appeared after the irradiation. This is probably because the irradiated surface is chemically active then it is nitrogenized with air at room temperature after the irradiated sample was taken out from the chamber to the atmosphere.

3.4. Functional groups by GCMM and molecular weight by GPC

We show the results of GCMM in Table 3 for amounts of -OH (hydroxyl group) and -COOH (carboxyl group). These functional groups (especially COOH) are strikingly increased after the irradiation. Then the above discussions that COOH and OH are increased (created), can be supported. Table 4 shows the results of GPC, indicating that a mean molecular weight is decreased after the irradiation. This means that original long molecular chains are broken into shorter chains. The shorter chains must be terminated by the functional groups such as C=O, -COOH and -OH.

Table 3. Amounts of -OH and -COOH normalized by C obtained by GCMM. The COOH is increased much compared with the OH after the irradiation. The OH and COOH exist in the non-irradiated film as the terminators of polymer molecule.

	-OH/C	-COOH/C
non-irradiated (%)	0.003	0.001
irradiated (%)	0.008	0.016

Table 4. Mean molecular weights obtained by GPC.

	Mean molecular weight
non-irradiated (%)	32100
irradiated (%)	29700

3.5. Bonding after six years, dry-peel and wet-peel tests

The irradiated PET films were kept in the normal atmosphere for six years, then roll-pressed. The result of Sp vs Tp by the dry-peel test is shown in Fig. 10 for the laminated film which was heat-pressed six years after the plasma irradiation. The result is almost the same with that shown in Fig. 7 for the sample bonded immediately after the plasma irradiation. The sample showed the cohesive failure beyond the peel strength of 6 N/cm above Tp=110°C. It implies that the activated surface by the plasma can be kept in the atmosphere so long as six years, it is incredible.

The wet-peel test was done on the samples also bonded six years after the irradiation. The result is shown in Fig. 10. The peel strength is considerably weaker for the wet-peel test than for the dry-peel test in Tp range of 100-130°C,

however it is the same for the both for $T_p > 140^\circ\text{C}$. These two results indicate that there are two types of bonding elements, one element is not stable for (broken by) the water but the other element is very stable for (not broken by) the water.

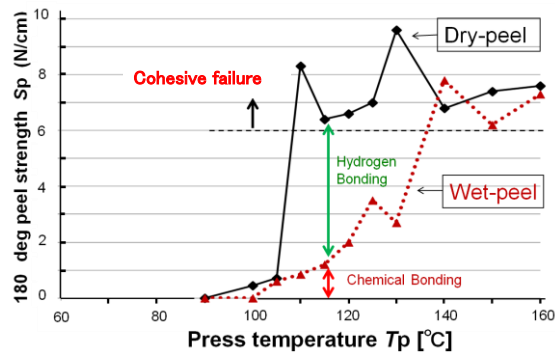


Figure 10. $180^\circ(\text{T})$ -peel strength (bonding strength) S_p vs press temperature T_p for the samples pressed six years after the plasma irradiation. The results from normal dry-peel and particular wet-peel tests are shown. The samples show cohesive failure beyond the pulling strength of 6 N/cm.

3.6. Bonding strength and contact angle (surface activity)

To investigate a reason why the activated surface can be kept so long, we measured the water contact angle θ for the irradiated samples kept in the atmosphere. The result is shown in Fig. 11. The angle θ before the irradiation shows 60 deg, and just after the irradiation it shows 18 deg at 25°C . This clearly indicates that the non-irradiated surface (larger θ) is inactive (low surface energy) but the irradiated surface (smaller θ) is excessively active (high surface energy). This irradiated sample was kept in the atmosphere for five years then the angle θ was measured, showing 38 deg. This indicates that the activated surface was gradually inactivated in five years, but it was not restored to the original state, that is “half-activated”. This sample was heated in the atmosphere at various elevating T_h from 50 to 240°C for 10 min then the angle θ was measured at room temperature. The angle θ increases with increasing T_h up to 48 deg at 240°C . It clearly indicates that the half-activated surface becomes more inactive probably due to thermal annihilation of the plasma-created functional groups. However, it is important that its surface is slightly more active compared with that of the non-irradiated sample ($\theta = 60$ deg).

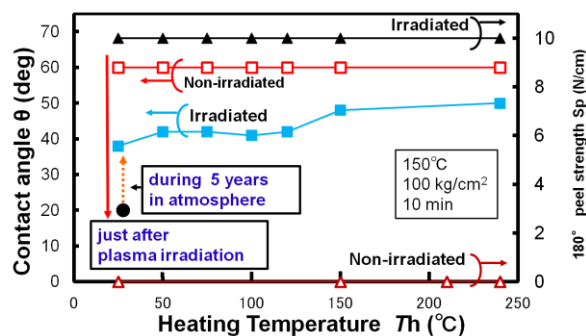


Figure 11. Pure water contact angle θ vs heating temperature T_h , and $180^\circ(\text{T})$ -peel strength S_p vs T_h for the non-irradiated and irradiated samples. The contact angle was measured at room temperature after heating.

We tried the heat-press and peel test on these samples heated at various T_h . The result of S_p vs T_h is shown in Fig. 11. It must be surprise that all the films can be bonded tightly even if the sample is heated at the highest T_h of 240°C . This means the surface activation with $\theta = 48$ deg is enough for the bonding. But a possibility cannot be denied that state of activation of the heated sample is different from that of the non-heated sample. However the most useful result is that the films kept in the atmosphere for five years after the irradiation can be bonded tightly even the surface

activation of this sample ($\theta=38$ deg) is restored considerably from that of the sample just after the irradiation ($\theta=18$ deg). This result confirms the result of Figs. 10, that is, the surface activation is considerably restored during the long atmosphere exposure but is still sufficient for the tight bonding.

3.7. COOH by FTIR (ATR)

In order to clarify origins for the bonding, the water-induced weakening of bonding, and the ultralong lifetime of plasma irradiation effect at the surface, we investigated chemical bonding states of the PET films by the FTIR. The FTIR-transmission spectrum for the non-irradiated PET film with 3.5 μm thickness is shown in Fig. 12. Here we assign only two peaks as C=O stretching mode at 1716 cm^{-1} and OH stretching mode at 3430 cm^{-1} , those are analyzed in this work. The C=O bond is involved in the original PET molecule as shown in Fig. 1, but the OH bond is not involved in the molecule originally. Then the OH bond absorption must be resulted from the termination-members of polymer, H can be added at the left and OH can be added at the right hand side of the molecule in Fig. 1. This is a reason why the OH absorption is very small compared with high absorption peaks coming from the main polymer molecular bond members.

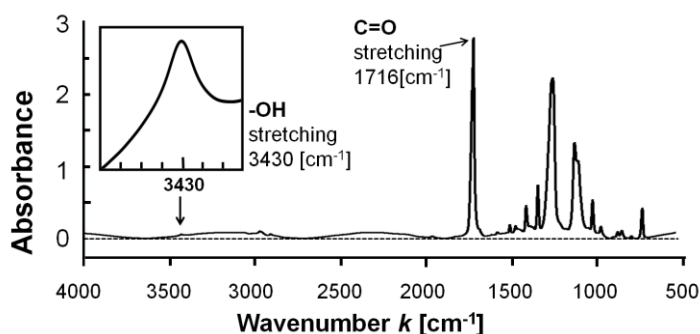


Figure 12. FTIR transmission spectrum for the non-irradiated PET film with 3.5 μm thickness. Many peaks are observed but we pick up only related two peaks for C=O and OH bonds.

The FTIR-ATR is very sensitive to the surface (1-3 μm) of sample due to reflection mode, then we employed it to investigate the plasma-irradiated surface. The FTIR-ATR spectra around 1716 cm^{-1} for the non-irradiated and irradiated samples (100 μm) are shown in Fig. 13. The peak heights are normalized using a constant peak of benzene ring. After the irradiation, the absorption band is shifted to the lower wavenumber k then the absorption is increased in the lower k region. Its difference is very small then we took the differential spectrum (irradiated – non-irradiated) around 1716 cm^{-1} .

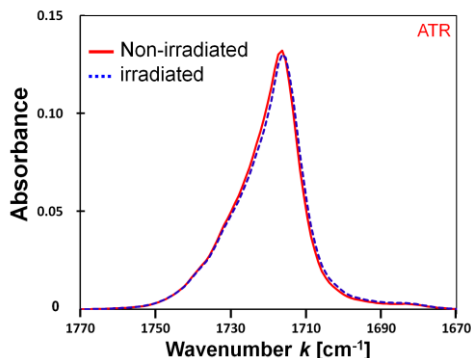


Figure 13. FTIR-ATR spectra near 1716 cm^{-1} for the non-irradiated and irradiated samples. The two peaks are normalized by stable strong peak arising from benzene ring (not shown). The lower k -shift is observed for the peak of the irradiated sample.

The result is shown in Fig. 14. It shows the minimum at 1719 cm^{-1} and the maximum at 1711 cm^{-1} . The minimum corresponds to the C=O bond inside the original PET molecule, indicating this bond is broken by the irradiation then its absorption is decreased. The maximum must correspond to the C=O bond in carboxyl COOH group (O=C=O-H) formed at the PET surface by the irradiation. The lower shift of k , corresponding to lower frequency shift of vibration, may be induced by surface COOH dimer coupling and hydrogen bonding.

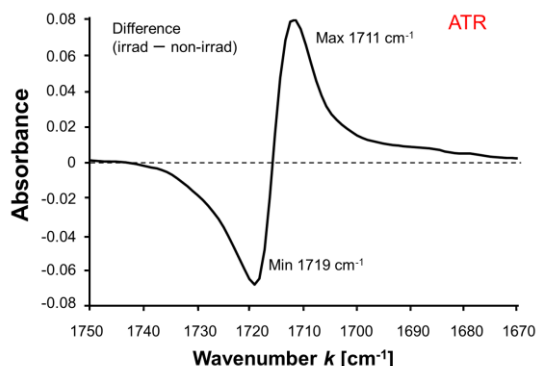


Figure 14. FTIR-ATR differential spectrum (irradiated – non-irradiated) corresponding to Figure 13.

3.8. OH by FTIR

The expanded FTIR transmission spectra around 3430 cm^{-1} related to OH bond are shown in Fig. 15 for the three samples of non-irradiated (100 μm thickness), irradiated (100 μm) and bonded PET (1- $\mu\text{m}/100\text{-}\mu\text{m}$). Further expansion around the peaks is inserted, from which we can recognize that the peak for the irradiated sample is increased from that for the non-irradiated sample, and the peak for the bonded sample is slightly decreased from that for the irradiated sample but still much larger than that for the non-irradiated sample. This result indicates as follows. The non-irradiated PET has OH bond due to termination of PET polymer as schematically drawn in the insert. By the irradiation, hydroxyl OH group is created at the surface, then the absorption is increased. After the heat-press bonding, a part of the created OH remain causing the increased absorption, but the other part of the created OH are consumed probably due to some chemical reactions under the heat-press because the absorption for the bonded sample (having two irradiated surfaces) is not two-times larger than that for the irradiated sample (having one irradiated surface).

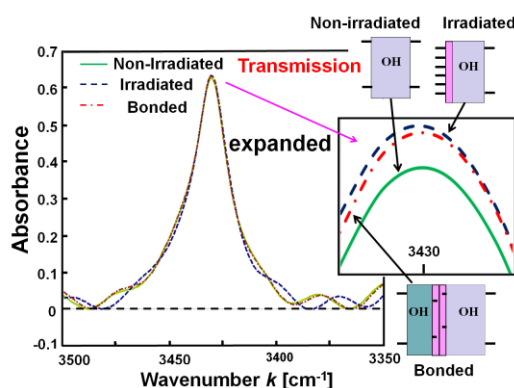


Figure 15. FTIR transmission spectra near 3430 cm^{-1} for the non-irradiated, irradiated and bonded samples. The sample pictures are shown in the figure, where bars indicate the OH bond. Before the irradiation, the OH bonds already exist in the non-irradiated film as the terminators. After the irradiation, the OH bonds increase on the irradiated surface. After the bonding, the OH bonds decrease at the interface due to chemical reactions. Inset shows expansion of the peaks attached with sample pictures.

3.9. Cross-linking layer by OCP

Here we mention on results of OCP solution test. The non-irradiated PET film was dissolved completely in OCP solution. Though, a remnant was observed for the irradiated film. It indicates the plasma-irradiated surface is modified from the pure PET polymer, which is not dissolved. The modified layer must be a cross-linking layer.

4. Discussions

We discuss the origins of plasma induced low temperature bonding of PET films, the water- induced weakening of bonding and the ultralong lifetime of plasma-irradiated active surface.

4.1. Dehydrated Condensation Reaction (DCR)

It is known from the results of XPS and FTIR that the COOH group and OH group are created at the PET surface by the oxygen plasma irradiation. This is quantitatively confirmed by the GCMM, the rate of creation is much larger for the COOH (16 times) than OH (2.7). It can be understood that the OH is more involved than the COOH in the non-irradiated original PET as the polymer terminator. Figure 16 shows schematic pictures of two irradiated PET surfaces before heat-press (top) and after heat-press (bottom). Figure 16(a) shows the PET surfaces with high dose of irradiation where high densities of the COOH and OH are formed, while (b) shows the surfaces with low dose where low densities of the COOH and OH are formed. Under the moderate heat-press these active functional groups might induce a Dehydrated Condensation Reaction (DCR) at the interface as schematically shown in Fig. 16(a) and 16(b). It does not need excessively high pressure and temperature to get DCR because (1) the COOH and OH are quite active and (2) the densities of them are quite high. Probably the high densities of surface COOH and OH are more important for the strong bonding.

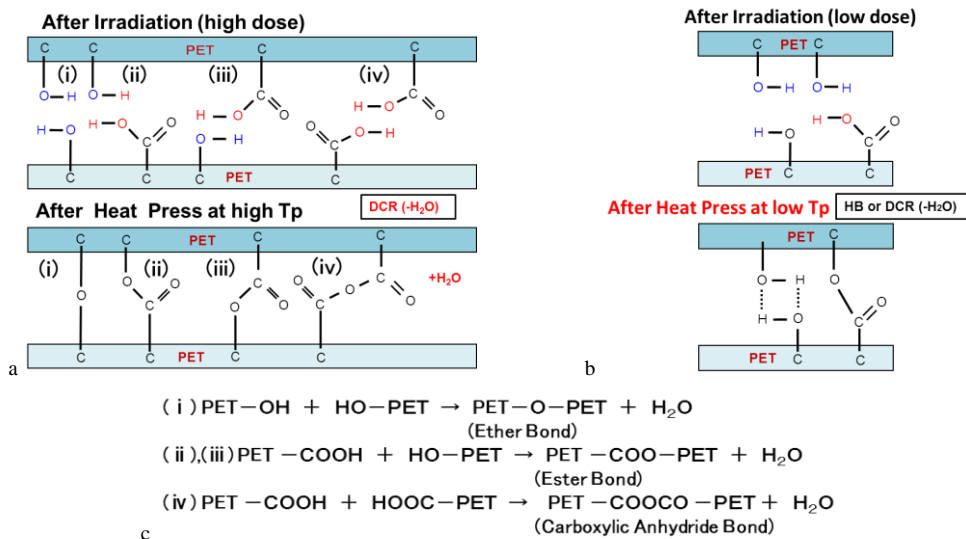


Figure 16. Models for the bonding mechanism. (a) High dose irradiation and high temperature press. The high densities of COOH and OH groups are created on the surface (top), leading to the high densities of bonds (bottom). The solid lines indicate the chemical bonds. (b) Low dose irradiation and low temperature press. It should be noted that, in this experiment, actually the sample was irradiated with high dose, but the low temperature presses were conducted. The dotted lines indicate the hydrogen bonds. (c) Presumed dehydrated condensation reactions between the two irradiated PET films under the heat press, corresponding to (a). These reactions produce water H₂O.

Dai et al. [19] and Hao et al. [9] also suggested that the chemical reactions can take place at such low temperatures under the press [20,21], Hao et al. [9] especially indicated a possibility of the condensation reaction. As a result, after the heat-press they form strong chemical bonds such as PET-O-PET (ether bond), PET-COO-PET (ester bond) and

PET-COOCO-PET (carboxylic anhydride bond) as shown in the bottom of (a). Their DCR formula are shown in Fig. 16(c). This must be the origin for the strongest bonding between the two irradiated PET for $T_p > 120^\circ\text{C}$ in Fig. 7 and for $T_p > 140^\circ\text{C}$ in the dry-peel test in Fig. 10 because substantial thermal energy can be supplied in these high temperature ranges.

While the weaker bondings (smaller peel strength S_p) observed in $90 < T_p < 120^\circ\text{C}$ in Fig. 7, and in $90 < T_p < 110^\circ\text{C}$ for the dry-peel test in Fig. 10, are caused by insufficient DCR due to shortage of thermal energy for the reaction. Then the films are bonded by small number (low density) of DCR bondings as simply shown in Fig. 16(b). In such the insufficient conditions, the hydrogen bonding is more possible as indicated in the bottom picture. This hydrogen bonding is discussed in more detail later. This figure also shows a possible situation for the low dose. When the irradiation dose is not high enough, the COOH and OH are created but their densities are low as shown in the top picture. Then the densities of DCR bondings are low as shown in the bottom picture, resulting in the weaker film bonding.

The amorphous PET can be bonded at around $65\text{--}75^\circ\text{C}$ as observed by Hao et al. [9] Our result of bonding temperature of 100°C is higher, because our biaxially oriented PET sample is crystalline. More exact reason must be clarified hereafter.

4.2. Hydrogen bonding

On the other hand, the weaker bonding in $100 < T_p < 130^\circ\text{C}$ for the wet-peel test in Fig. 10 suggests that there are two bonding elements, one must be the chemical bonding (DCR bonding) and the other must be hydrogen bonding between the created COOH and OH groups, as mentioned above. Not all of the created COOH and OH can take DCR even under the high heat-press because of insubstantial thermal energy and time, resulting in the hydrogen bonding (mixed with the chemical bonding). During the wet-peel test, the water can penetrate into the interface easily as shown in the top of Fig. 17 because the interface is well open to the water (see Fig. 5). Then, the water breaks this direct hydrogen bonding connecting the PET films directly. As the result, the water molecules (H_2O) form weaker secondary hydrogen bonding mediated by H_2O molecules as schematically shown in Fig. 17. Then during the wet-peel test the two PET films are loosely bonded only by the chemical bonding formed by the part of created COOH and OH groups. Thus we can divide the bonding elements into the chemical bonding and hydrogen bonding for the insufficient temperatures of $100 < T_p < 130^\circ\text{C}$, these are indicated by two vertical arrows in Fig. 10. In the low T_p region, the hydrogen bonding is major, but with increasing T_p , the DCR chemical bonding becomes major gradually, then finally the films are bonded only by the high density of chemical bondings at the highest region of $T_p > 140^\circ\text{C}$.

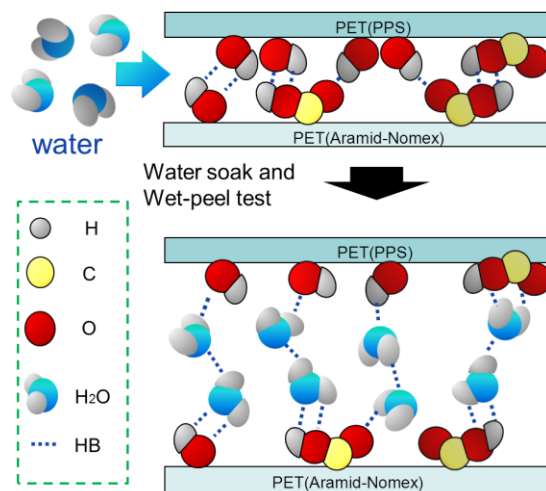


Figure 17. Model for the weaker peel strength under the wet-peel test. Water molecules can penetrate into the opened bonding interface (top) and break the “direct hydrogen bonds (HB)” connecting PET-PET directly. This results in the H_2O -mediated secondary hydrogen bonds (bottom). In this experiment, two PET films were used. (We tried to use PPS and Aramid, and obtained the same results).

4.3. Long lifetime of irradiation-induced active surface

The question why the plasma irradiated surface has so long lifetime for the bonding, is very difficult to answer. One of the answers might be the cross-linking reaction at the irradiated surface. As Occhiello et al. [7] suggested, the plasma-created COOH and OH turn-back inside from the surface. However in our case, the plasma-created COOH and OH cannot turn-back inside from the surface due to protection by the cross-linking layer [33], then they remain at the surface so long. Hudis et al. [34] reported that the cross-linking occurs by activated species created by inert gas plasma, called as CASING. The other origin might be water coverage of the irradiated surface. The plasma-created COOH and OH are covered with adsorbed H₂O in the atmosphere, they are forming the hydrogen bonding with H₂O. Then the COOH and OH are preserved in the atmosphere. In this case we should consider why the COOH and OH are activated again when the PET films are heat-pressed six years after the irradiation. Probably such hydrogen bond with H₂O is broken easily by the heat-press due to evaporation, resulting in restoring of active COOH and OH.

We do not have yet rigid answers to the mechanism for ultralong lifetime of irradiate active surface in the atmosphere which is effective to the bonding of PET for six years after the irradiation. We have to study more on the surface of PET irradiated by “our plasma” henceforth.

5. Summary

The direct laminations of engineering plastic films without using glues are very useful for their practical applications, because each elemental film can cover weak properties of other elements. We worked on fundamental research to clarify the mechanism of plasma irradiation-induced tight bonding of the plastic PET films.

The functional groups of COOH and OH are detected on the plasma irradiated PET surface by XPS, FTIR and GCMM. The COOH numbers are larger than OH.

The oxygen plasma-irradiated PET films can be bonded tightly by the heat-press at temperatures higher than 100°C just after the irradiation. The films kept in the atmosphere for six years after the irradiation, can be strongly bonded. The results of water contact angle show that the film surface is extremely active just after the irradiation, and it becomes less active in the atmosphere with time going, but is still active considerably even after five years. This is the reason why the films can be bonded after six years.

The difference of peel strength between the dry- and wet-peel tests suggests that there are two forms of bonding, the hydrogen bonding and chemical bonding. Both are effective in the lower temperatures of 100-130°C for the weaker bonding due to the low densities of bonds. While the high density of pure chemical bonding is effective at the highest temperatures of 140-160°C for the strong bonding.

The FTIR results indicate that the plasma-created COOH and OH groups at the surface are responsible for the both bondings. After the heat-press bonding, the OH numbers in the bonded sample are decreased compared with those on the irradiated surface before the bonding. This indicates that OH is consumed during the heat-press bonding. Thus the dehydrated condensation reaction is suggested for the chemical bonding. We can propose by the wet-peel test that the water can penetrate into the bonded interface, and break the hydrogen bonding, resulting in the weaker peel strength.

The irradiation effects at the surface on the bonding can be preserved in the normal atmosphere for six years. It is proposed that the cross-linking layer and water adsorption with hydrogen bonding at the irradiated surface are the origins for ultralong lifetime of the plasma-induced active surface.

This review paper describes the fundamental research of our works on the plasma-bonding of various plastic films. Then we mentioned only the PET film here. We have developed some application researches as well on various plastic films such as aramid paper (Aramid), polyimide (PI) and poly phenylene sulfide (PPS), and obtained good achievements. For example, the <PVF/PET/PVF> trilayer can be used for the solar cell back-sheet, the <Aramid/PI/Aramid> is actually used for insulator sheets in motors of the high speed train (Shinkansen), and <Aramid/PPS/Aramid> is actually used for insulator sheets in EV motors of Mitsubishi i-MiEV and Outlander. We would like to review these application oriented researches in other occasions.

References

- [1] S. Adachi: Convertech 354 (2002) 40.

- [2] E. Sugimoto: *Electronic Parts and Materials* 47 (2008) 103.
- [3] K. Ino and E. Sugimoto: *Convertech* 355 (2002) 40.
- [4] M. DeBergalis: *J. Fluorine Chem.* 125 (2004) 1255.
- [5] M. Yokura, T. Hayashi, T. Yoshii, Y. Maeda, and T. Endo: *Trans. Mat. Res. Soc. Japan* 35[1] (2010) 191.
- [6] N. Inagaki, K. Narushima, S. Ijima, Y. Ikeda, S. K. Lim, Y. W. Park, and K. Miyazaki:
- [7] *J. Adhesion Sci. Technol.* 17 (2003) 1457.
- [8] E. Occhiello, G. Morra, F. Garbassi, and P. Humphrey: *J. Appl. Polym. Sci.* 42 (1991) 551.
- [9] A N. Banerjee, C. K. Ghosh, K. K. Chattopadhyay, H. Minoura, A. K. Sarkar, A. Akiba, A. Kamiya, and T. Endo: *Thin Solid Films* 496 (2005) 112.
- [10] Z. Hao, H. Chen, X. Zhu, J. Li, and C. Liu: *J. Chromatography A* 1209 (2008) 246.
- [11] M. Audronis, S.J. Hinder, P. Mack, V. Bellido-Gonzalez, D. Bussey, A. Matthews, and M.A. Baker: *Thin Solid films* 520 (2011) 1564.
- [12] M. O. H. Cioffi, H. J. C. Voorwald, and R. P. Mota: *M. Characterization* 50 (2003) 209.
- [13] Y. Setsuhara, K. Cho, K. Takenaka, A. Ebe, M. Shiratani, M. Sekine, M. Hori, E. Ikenaga, H. Kondo, O. Nakatsuka, and S. Zaima: *Thin Solid films* 518 (2009) 1006.
- [14] L. Yang, J. Chen, Y. Guo, and Z. Zhang: *Appl. Surface Sci.* 255 (2009) 4446.
- [15] Y. Setsuhara, K. Cho, K. Takenaka, M. Shiratani, M. Sekine, and M. Hori: *Surface & Coatings Tech.* 205 (2011) S484.
- [16] M. Katsikogianni, E. Amanatides, D. Mataras, and Y.F. Missirlis: *Colloids and Surfaces B: Biointerfaces* 65 (2008) 257.
- [17] A. Vesel, M. Mozetic, and S. Strnad: *Vacuum* 85 (2011) 1083.
- [18] K. N. Pandiyaraj, V. Selvarajan, R.R. Deshmukh, and M. Bousmina: *Surface & Coatings Tech.* 202 (2008) 4218.
- [19] K. N. Pandiyaraj, V. Selvarajan, R.R. Deshmukh, and C. Gao: *Vacuum* 83 (2009) 332.
- [20] C-A. Dai, Y-H. Lee, A-C. Chiu, T-A. Tsui, K-J. Lin, K-L. Chen, and M-W. Liu: *Polymer* 47 (2006) 8583.
- [21] C. Scott and C. Macosko: *J. Polym. Sci. Part B, Polym. Phys* 32 (1994) 205.
- [22] P. Marechal, G. Coppens, R. Legra, and J-M. Dekoninck: *J. Polym. Sci. Part A, Polym. Chem* 33 (1995) 757.
- [23] J. Friedrich: *The Plasma Chemistry of Polymer Surface: Advanced Techniques for Surface Design* (Wiley-VCH, Weinheim, 2012).
- [24] T. Hayashi, M. Kato, M. Yokura, K. Uehara, X. Guo, Y. Nakamura, and T. Endo: *World J. Engineering* 7 [Suppl.2] (2010) 520.
- [25] M. Yokura, T. Hayashi, H. Katsumata, G. Xiang, T. Yoshii, M. Matsui, and T. Endo: *World J. Engineering* 7 [Suppl.2] (2010) 519.
- [26] M. Yokura, K. Uehara, G. Xiang, A. Okamoto, Y. Nakamura, L. Reddy, and T. Endo: *World J. Engineering* 8[Suppl.3] (2011) 1275.
- [27] M. Yokura, K. Hanada, K. Uehara, M. Nagashima, H. Nishikawa, Y. Nakamura, H. Kezuka, K. Endo, and T. Endo: *Proc. Int. Conf. Composites/Nano Engineering (Beijing)* (2012) CDROM.
- [28] M. Yokura, K. Uehara, G. Xiang, K. Hanada, Y. Nakamura, L.S. Leddy, K. Endo, and T. Endo: *Mater. Res. Soc. Symp. Proc.* 1454 (2012) 201.
- [29] S. Teii: *The Journal of Institute of Electrical Engineers of Japan* 107 (1987) 1096.
- [30] H. Kobayashi and S. Hirose: *Electronic Parts and Materials* 20 (1981) 151.
- [31] H. Iriyama: *Convertech* 356 (2002) 46.
- [32] Y. Nakayama, T. Takahagi, F. Soeda, K. Hatada, S. Nagaoka, J. Suzuki and A. Ishitani: *J. Polym. Sci. Polym. Chem.* 26 (1988) 559.
- [33] M. Mito: *The Mechanism of Organic / Inorganic Interface*, Ed. by K. Fukushima (Science & Technology, Tokyo, 2006) pp. 3-9.
- [34] Y. Iriyama and J. Yasuda: *Appl. Polym. Sci., Appl. Polym. Symp.* 42 (1998) 97.
- [35] M. Hudis: *Techniques and Applications of Polymer Chemistry*, Eds J. R. Hollahan and A. T. Bell (John Wiley and Sons, New York, 1974) p.113.



Sustainable Civil Engineering Structures and Construction Materials, SCESCM 2016

Europe goes green

Adrian J.M. Leijten^{a,*}^a*Department of the build environment, Eindhoven University of Technology, PO Box 513, Eindhoven 5600 MB, The Netherlands*

Abstract

At the UN-Paris conference in 2015 countries accepted the challenge to fight Green House Gas emissions (GHG) during the next decades in an attempt to stop global warming. In Europe the aim is that all future new buildings aim at nearly zero-energy consumption and be highly material efficient whilst the existing building stock will be refurbished at a rate of 2% annually. Numerous international scientific studies have found that timber-framed buildings result in lower GHG emissions than their steel and concrete counterparts. For green building construction (relative) new timber products and connection methods conquer the market such as Cross Laminated Timber products. CLT products allow fast and cost effective execution of the building while structural limitations and disadvantages of the traditional timber frame construction are overcome. Examples of multi-storey timber structures are presented. These steps forward were ministered by the development of innovative timber fastener connections like self-tapping screws and reinforced dwv tube connections.

© 2017 The Authors. Published by Elsevier Ltd.

Peer-review under responsibility of the organizing committee of SCESCM 2016.

Keywords: timber structures; GHG; sustainability; CO₂;CLT;Connections; dwv;

1. Introduction

Step by step the issue of global warming is being recognized as a potential threat for human living conditions on Earth. A key parameter in this struggle to get control over the greenhouse gas emission known as the CO₂, increasing share of renewables and improving energy efficiency. "Sustainable development is the need of the day so that we can conserve and keep our resources for our future generations. All the ill effects that we see today – effects like global warming etc. are the effects of our ruthless exploits of our natural resources which we have consumed at such alarming

* Corresponding author. Tel.: +31-40-247-3928

E-mail address: a.j.m.leijten@tue.nl

rate that some of it is depleted or is on the verge of becoming extinct. Sustainable development means development or creating assets by consuming the least resources", [1].

2. European Position

In March 2011, the European Commission published a Communication entitled “A Roadmap for moving to a competitive low carbon economy in 2050”, [2]. This Roadmap builds on the Europe 2020 flagship initiative for a resource-efficient Europe as part of a series of long-term policy plans in areas such as transport, energy and climate change. The Communication sets out key elements that should shape the EU's climate action helping the EU become a competitive low carbon economy by 2050. The Europe 2020 Strategy for smart, sustainable and inclusive growth includes five headline targets that set out where the EU should be in 2020. One of them relates to climate and energy; Member States have committed themselves to reducing greenhouse gas emissions (GHG) by 20%, increasing the share of renewables in the EU's energy mix to 20%, and achieving the 20% energy efficiency target by 2020. The EU is currently on track to meet two of those targets, but will not meet its energy efficiency target unless further efforts are made. The document describes the cost-effective pathway to reach the EU's objective of cutting greenhouse emissions by 80-95% of 1990 levels by 2050 in order to keep climate change below 2°C. The EC Roadmap 2050 also points to the role of the built environment in achieving the 80% reduction target.

The built environment provides low-cost and short-term opportunities to reduce emissions, first and foremost through improvement of the energy performance of buildings. The Commission's analysis shows that emissions in this area could be reduced by around 90% by 2050, a larger than average contribution over the long-term. This underlines the importance of achieving the objective of the recast Directive on energy performance of buildings that new buildings built from 2021 onwards will have to be nearly zero-energy buildings. This change the situation considerably, Fig. 1.

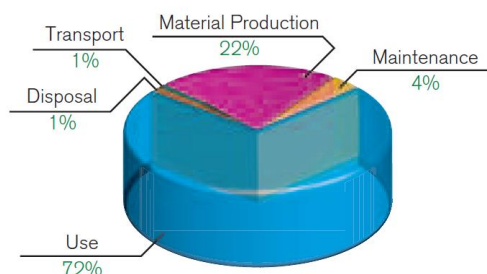


Fig. 1. Energy use across the life-cycle of a house, [6].

Today, new buildings should be designed as intelligent low- or zero-energy buildings. The extra cost of this can be recovered through fuel savings. A greater challenge, however, is the refurbishment of the existing building stock, and in particular how to finance the necessary investments. Wood and wood-based products have a specific role to play in this context. There is a strong development potential for wood-based constructions in structural and non-structural applications, both for new buildings as for renovation purposes.

In the explanatory memorandum to this EU-commission proposal as mentioned in [3], the EC states that "In addition to the opportunities directly linked to forestry and agriculture, there are potential mitigation benefits in the related industries (e.g. pulp and paper, wood processing) and renewable energy sectors if agricultural land and forests are managed for production of timber and energy. Whilst carbon is stored in trees and in other plants and soils, it can also be stored for several decades in products (e.g. construction wood). Industry and consumer oriented policies can make an important contribution to increasing the long term use and recycling of wood and/or the production of pulp, paper and wood products, thereby replacing more emission-intensive equivalents (e.g. concrete, steel, plastics made from fossil fuels). (...) Studies show that for each ton of carbon in wood products substituted for non-wood products an average greenhouse gas emission reduction of approximately two tons of carbon can be expected". As mentioned in [3], the woodworking industry welcomes this legislative proposal as it puts the EU in the driver's seat in the implementation of a realistic policy of emission reductions and towards closing the accounting CO₂ savings and emissions from forest related industry welcomes the move from the EC to start implementing the accounting for

harvested wood products, thereby recognizing the contribution these wood products deliver to climate change mitigation, and calls for a rapid adoption of this principle.

It is widely accepted that, globally, permanent deforestation and land use change contributes for an estimated 20% to GHG emissions. However, this type of deforestation does not take place in Europe and European forests can by no means be considered as net carbon emission sources. European forests grow yearly by around 834.000 hectares (581.000 hectares for the EU 27). Recent Fig.s also confirm that not more than 60 % of the net annual increment is being harvested in European forests available for wood supply and the growing stock is estimated 24 billion m³ emissions of the EU. Wood derived from sustainably managed forests continues to store this carbon and can substitute non-renewable and less environmentally friendly materials and products", Fig. 2.

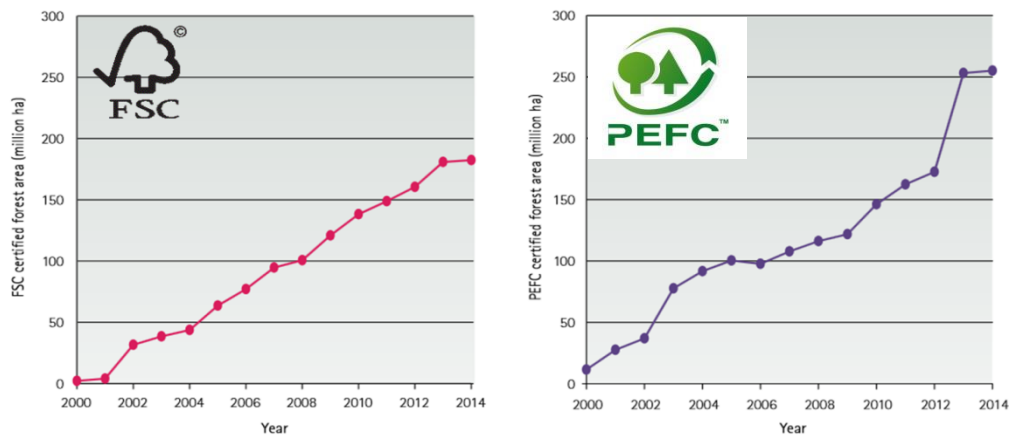


Fig. 2. Area of International forest management certification (2000-2014), source FAO.

The position of the European wood working industry is that unfortunately, the positive role of wood in housing is not always fully recognized in the green building rating schemes which are currently in operation. Some of these schemes have in fact worked against the use of wood. The European Economic Social Community (EESC) therefore calls for generally-accepted LCA methodologies to be used that recognize all the advantages and disadvantages of the building material, including carbon storage. Encouraging the use of wood products is the greenest choice: by using the full potential of wood (sink and substitution effects) in buildings, Europe could reduce emissions of CO₂ by 300 million tons (between 15 and 20%). The EESC recognizes that by using green building materials it is possible to achieve effective energy savings in buildings, Fig. 3. The relative influence of the building design as such on the environmental impact of the whole life cycle is huge, especially in the use phase. The environmental performance depends to a large extent on environmental and climate conditions of the building site and a full range of (urban) planning parameters. Due to progressive technical developments, buildings might require less and less operating energy in the future. The importance of life cycle calculations for the production phase will increase consequently.

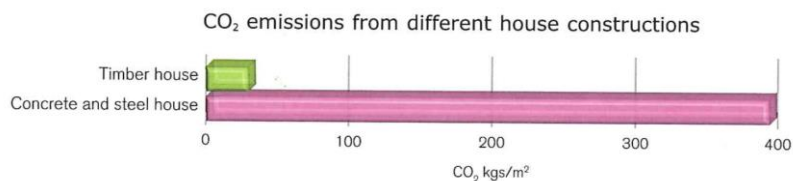


Fig. 3. The difference in CO₂ emissions from the materials and construction content of two houses is 370 kg/m² (Tratek/SCA, Materials Production and Construction)

This is why efforts for reducing a building's carbon footprint and increasing its energy efficiency will become even more important during the production and construction phases of a building project. It makes little sense to attribute 'green' labels to construction products and buildings when these important parameters, as well as the recyclability and end of life uses of the materials are not rightly considered and/or when excessive weight is attributed to less relevant

indicators. Besides that, benchmarks at European level are not helpful, as conditions in – for instance – Scandinavian and Mediterranean countries are quite different". A Swedish study, [3] undertaken in 2001 compared the embodied energy and CO₂ emissions from the construction of two similar houses, one made from timber, the other from steel and concrete. The difference of 2 300 MJ/m² energy used in the materials and construction of the houses is enough to heat one of the houses for 6 years, while the 370 kg/m² difference in CO₂ emissions is equivalent to the emissions from 27 years' heating – or driving 130 000 km in a Volvo S80.

2.1. European Standard Organization CEN/TC315

The European standardization organization CEN has, since some years, been working with sustainable constructions within CEN/TC 350. It is responsible for the development of voluntary horizontal standardized methods for the assessment of the sustainability aspects of new and existing construction works and for standards for the environmental product declaration of construction products. The standards will be generally applicable (horizontal) and relevant for the assessment of integrated performance of buildings over its life cycle. The standards show how to calculate and present sustainability, but not what is good or bad. Sustainability includes environmental, economic and social aspects. An Environmental Product Declaration (EPD) is made by the producer and will be the input for the evaluation of the whole building. Product category rules have been developed in order to compare different products. The new European harmonized standard EN 15804 sets core rules for the creation of Environmental Product Declarations (EPD) for building products and materials. This standard gives the basis for a uniform calculation and declaration of product-related environmental information all over Europe.

3. Developments in durability

Durability is always an aspect that needs to be considered dependent of the exterior application of structural timber. Humidity, light and temperature are key parameters that drive the durability performance. Surface treatments are not really the long term solution as regular inspection is required to check the quality of the protection. The environmental demands have diverted the focus from adding toxic substances or oil derivate substances to change the molecular structure of the wood fibers to modification methods using non-toxic substances. Basically one can improve the durability by impregnation or by modification based on chemical or biological treatments. The latter can be a heat treatment with the aim to change the chemical composition that is responsible for the decay process. Products of this kind usually have excellent durability but as the treatment changes the chemical composition of the hemo-cellulose the material becomes brittle. For structural use these products are not always suited.

3.1. Acetylation

A promising chemical modification process that has been developed the last decades is based on acetylation. Acetylation is a revolutionary wood modification process, which has been known and studied for over 80 years. It involves the reaction of wood (or wood particles) with acetic anhydride, through which the free -oh (hydroxyl) groups – causing the shrink and swell of wood and the susceptibility to decay - within the cell wall are replaced by more stable and hydrophobic non-toxic acetyl groups, naturally occurring in wood. As a result, the stability and durability of the wood significantly increases, Fig. 4.

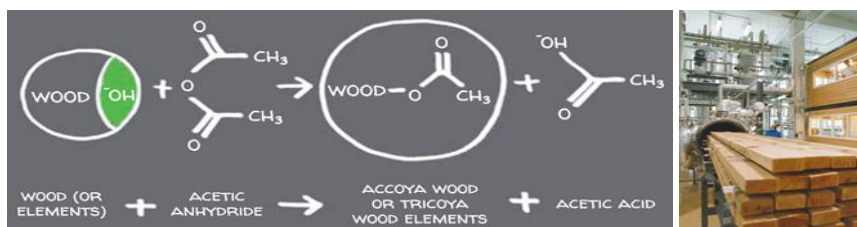


Fig. 4. Chemical modification with acetic anhydride (source www.accoya.com)



Fig. 5. Termite resistance of Acetylated wood (top) compared to non-treated wood of the same wood species (below).



Fig. 6. Bridge at Sneek (NL) highest load category (left); Bridge support during erection stage (right).

The co-product of this process is acetic acid, otherwise known as vinegar in its dilute form, which is reused in a wide range of industries. For example, the largest of the two timber road bridges in Sneek (2008), the Netherlands comprises 1200 cubic meters of acetylated wood (accoya) as a result, 1080 tons of CO₂ ($0.9 \text{ ton CO}_2/\text{m}^3 \times 1200 \text{ m}^3$) are locked in the bridge for nearly a century (anticipated lifespan is 80 years), Fig. 6. This is equivalent to eliminating the annual CO₂ emissions of 432 typical western European households for their energy need accoya wood is fully reusable and recyclable - non-toxic and

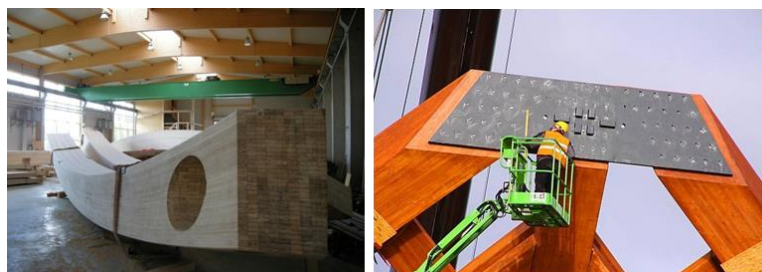


Fig. 7. Curved and twisted glued laminated member (left); 80mm thick steel plate to connect the members at the top (right).

100% biodegradable - waste wood gets high quality second life. The wood species is radiate pine from New Zealand. The bridge spans 35 m and is 12m wide and 16m high and has a steel designed bridge deck and weighs 420 tons. It is designed to carry up to 60 ton vehicles. Except for the two the lower chord beams that carry the bridge desk all other are curved and twisted, Fig. 7 (left). The cross-sectional dimensions of the bottom chord exceed 1m² and are assembled by gluing together multiple but separately produced glued laminated beams. The load transfer from the truss members

at the top is accomplished by a steel-timber connection using glued-in rods and an 80mm thick twisted steel plate, Fig. 7 (right).

4. Innovative products and connections

The structural use of Laminated Veneer Lumber (LVL), consisting of glued 3 to 6mm thick veneer layers in parallel or cross-wise layered, has proven to be an excellent method to enhance the mechanical properties of wood. Its market is well established in Europe and North-America. The concept of cross-wise layered material like the veneers in plywood and LVL have been adopted for the production of CLT (or X-Lam) but now with layers of sawn timber wood, up to 45mm thickness, Fig. 8 (left). The result is that the low perpendicular to grain (in-plane) properties have vanished.



Fig. 8. Five layered Cross-Laminated-Wood (left); Application of CLT in a self-supporting roof (right).

The CLT product can therefore be used for walls, floors and roofs. For roofs it can be designed as a self-supporting structure, as shown in Fig. 8 (right), where the folded roof part kept together with self-tapping screws to form the load bearing structure. This way the attic is not obstructed by internal structural supporting members or frames.

From many years, a great effort in research has been made to estimate the dissipative capacity and thus the seismic vulnerability of timber structures that can be built with several connection techniques: light-frame panels, cross-laminated panels and moment transmitting frames, to mention a few. Within this last category, one of the most used fasteners are the dowel-type fasteners like dowels and bolts. They are applied to connect the timber members. Studies by Leijten and Brandon [11-12] have shown that local reinforcement of the connection area with Densified Veneer Wood (DVW) results in mechanical properties superior to all other existing timber connections. The DVW layer, which is constituted by plywood compressed at high temperature, is glued to the timber members to avoid premature splitting and improve the stress distribution, Fig. 9 (a). The concentrated stresses introduced by the fasteners are taken by the DVW and distributed over a large glued surface into the timber, and the critical cross-section is hence reinforced with DVW, Fig. 9 (b).

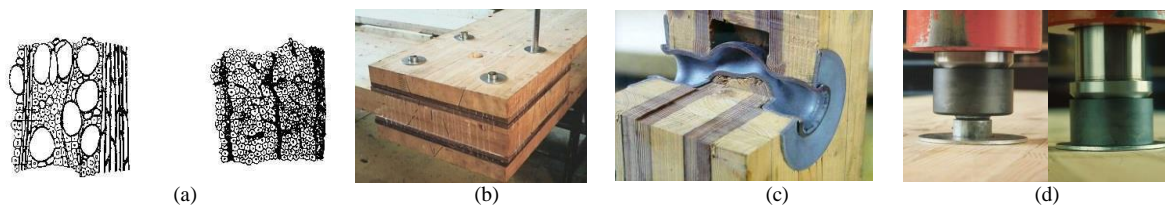


Fig. 9. Before and after densification to dvw (a); Assembly of tubes in moment connection (b); Expansion of tube diameter (c); Cut-open test specimen after loading (d).

The DVW is layered cross-wise in order to obtain isotropic material behaviour. The lay-up of the layers and the high density make the material more homogeneous, resulting in less variation in strength. The strength of DVW is related to the density of the material. In the DVW connection large diameter fasteners are being used, steel hollow

tubes. Compared to a (solid) bolt or dowel, the tube has significantly higher deformation capacity, Fig. 9 (c). During assembly the tubes are expanded in the oversized pre-drilled holes with a hydraulic actuator, to remove the hole clearance, Fig. 9 (d). The strength and stiffness per fastener compared to a dowel in non-reinforced timber is enhanced by a factor of four and eight, respectively. This assembly procedure increases the initial stiffness and assures immediate load carrying capacity, similarly to what happens in steel structures with pre-stressed bolts. The favourable ductility and small scatter in experimental test results makes this connection an excellent candidate for seismic design. On-going studies into the seismic load reduction factor q indicate appropriate values of $q=5$. The strength and stiffness capacity are such that in moment transmission column-beam connections applying only two tubes the full moment capacity of the timber members can be attained, Fig. 10.



Fig. 10. Examples of timber frame buildings with two expanded tubes per moment transmitting connection having the same moment capacity as the glued laminated timber beams.

4.1. Multi-storey timber building

Comparative research shows that using wood constructions in buildings instead of a concrete or a brick one is beneficial to tackle climate changes [5]. In this reference publication the following cases are elaborated. "The Austrian case studies analyses primary energy input and CO₂ emissions over the life cycle of high energy efficient residential buildings (Passive houses and Nearly Zero Energy Buildings - NZEB). Three existing buildings that represent typical residential buildings according to the Austrian building typology (developed within the EU project TABULA) have been chosen for this analysis. However, the wood construction systems they incorporate are quite innovative and not yet common in Austria.

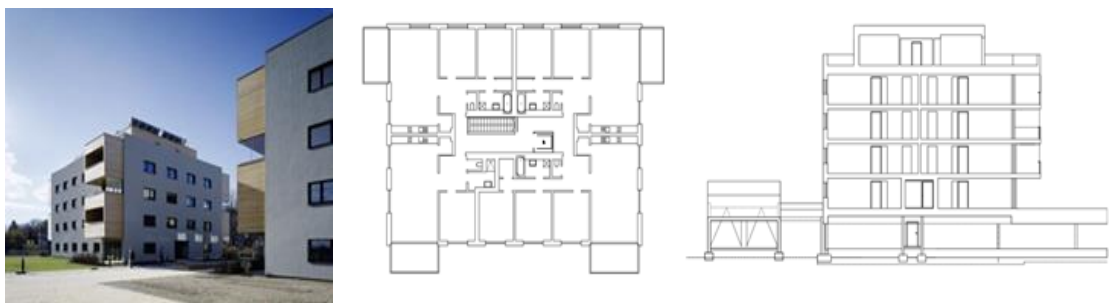


Fig. 11. Passive Mühlweg apartments Vienna

Just one example is the multi-storey building in Mühlweg (Vienna) is a passive energy, multi-storey residential building, Fig. 11. The apartment complex consists of four blocks comprising 70 flats for approximately 200 inhabitants in total. It was built within the financial means of the social housing fund. The residual heat is provided by a combined

solar/gas heating system. All apartments are supplied with fresh air by a central ventilation system. The basement, the staircase and the load-carrying system of the first floor are made of concrete; the three upper floors and the attic floor show a solid wood construction. The characteristic structure of the building is a cross laminated timber (CLT) construction. External walls are made of a prefabricated cross-laminated wood construction with mineral wool between wooden lathes as insulation material. The exterior side of the wall is covered with wood or plastered wood panels.

What's said to be the world's tallest wood tower, at 24 storeys, is scheduled to start construction this coming fall in Vienna, Austria. The 84-metre tall, 19,500-square-metre HoHo is expected to cost roughly €65 million (about \$90 million Canadian), and when completed, will contain apartments, offices, restaurants and a spa.

5. Conclusions

The European Commission aims at moving to a competitive low carbon economy in 2050. The construction sector holds a significant potential for lowering greenhouse gas emissions. With new buildings becoming more energy efficient, the energy demand and carbon footprint of construction materials becomes increasingly important. Wood-based building materials have several direct and indirect climate related advantages. However, strong political actions will be needed in order to utilise this potential for the mitigation of climate change.

The new European harmonized standard EN 15804 sets core rules for the creation of Environmental Product Declarations (EPD) for building products and materials. This standard gives the basis for a uniform calculation and declaration of product-related environmental information all over Europe.

New developments in wood engineered products like Cross-Laminated-Timber and innovative connections allow structural timber to be applied for more types of building than ever before. Future practicing engineers should be more aware of the typical advantages of building with wood to reduce the CO₂ footprint and contribute to the climate change issue.

Acknowledgement

The author gratefully acknowledges the assistance and contribution by the European Confederation of Woodworking Industries.

References

- [1] Panandike N, Panandiker S. Effective Use of Building Materials for Sustainable Development, In Proceedings of IABSE Symposium, Bangkok, Thailand, Sept 9-11, 2009.
- [2] Communication from the commission to the European parliament, the council, the European economic and social committee and the committee of the regions, Brussels, COM (2011) 112 final, 8-3-2011
- [3] Preparation of a CEI-Bois Position paper on the “Commission Communication on Sustainable Buildings” Draft version 1,- 08.01.2014 For discussion in WG Sustainability and WG Construction, www.CEI-Bois.org
- [4] Factsheet on CEN TC 350 activities, Sustainability by CEI-Bois, www.CEI-BOIS.org
- [5] CEI-Bois (2011): Tackle climate change, use wood, 2nd edition, CEI-Bois (Ed.), Brussels.
- [6] Pohlmann, C. M. (2002) Ökologische Betrachtung für den Hausabau – Ganzheitliche Energie – und Kohlendioxidbilanzen für zwei verschiedene Holzhauskonstruktionen, PhD thesis, Universität Hamburg Fachbereich Biologie.
- [7] Tratek/SCA, September 2003, ‘Materials Production and Construction’.
- [8] RTS Building Information Foundation, 2001, ‘Environmental Reporting for Building Materials’ – 1998 – 2001 and Ministry for Environment, Denmark, 2001, ‘The Environmental Impact of Packaging Materials’.
- [9] Castañeda F. , Criteria and indicators for sustainable forest management: international processes, current status and the way ahead, FAO, Unasylva 203, Vol. 51, 2000.
- [10] Gasparri E, Prefabricated external wall system for tall cross-laminated timber buildings, PhD-thesis, Dep of arch, built environment and construction engineering, Politecnico Milano, CICLO XXVIII, 2016.
- [11] Leijten, A.J.M. & Brandon, D. (2013). Advances in moment transferring dwv reinforced timber connections: analysis and experimental verification, Part 1. *Construction and Building Materials*, 43, 614-622. doi: 10.1016/j.conbuildmat.2013.03.020
- [12] Brandon, D. & Leijten, A.J.M. (2014). Advances in moment transferring dwv reinforced timber connections: numerical analyses and verification, Part 2. *Construction and Building Materials*, 56, 32-43. doi: 10.1016/j.conbuildmat.2014.01.026



Sustainable Civil Engineering Structures and Construction Materials, SCESCM 2016

Wood frame floor model of LVL *Paraserianthes falcataria*

Ali Awaludin^{a,*}, Anita Firmanti^b, Muslikh^a, Hendra Theodarmo^a, and Dani Astuti^a

^aDepartment of Civil and Environmental Engineering, Gadjah Mada University, Yogyakarta, 55281, Indonesia

^bMinistry of Public Works and Housing, Republic of Indonesia, Indonesia

Abstract

This paper develops wood frame floor made from laminated veneer lumber (LVL) *Paraserianthes falcataria* as an effort to further utilize this new emerging and sustainable building material in building applications such as multi-story dwelling houses. This LVL *Paraserianthes falcataria* is a typical of fast growing timber species planted in artificial forests to help mitigation of greenhouse gases. The work consisted of two consecutive activities: searching best shape of floor joist, and conducting full-scale test of prototype of the wood frame floor. Two models of joist section were developed, I-shape and Box-shape having equal height of 300 mm. Flexural test upon these two models of joist indicated that the Box-shape joist had better flexural stiffness and resistance than the I-shape joist. The prototype of floor system having size of 1200 mm by 2400 mm and were loaded in several loading configurations before finally loaded until failure. The test results found that the prototype of floor system had a uniform load capacity of 18.75 kN/m² corresponds to allowable floor deflection and 52.5 kN/m² at the ultimate condition.

© 2017 The Authors. Published by Elsevier Ltd.

Peer-review under responsibility of the organizing committee of SCESCM 2016.

Keywords: LVL *Paraserianthes falcataria*, I-shape joist, Box-shape joist, bending test, wood frame floor

1. Introduction

Recently laminated veneer lumber (LVL) is available in Indonesian markets. LVL is one type of structural composite lumber (SCL) products that is produced by gluing veneers of wood together into sizes common for solid-sawn [1]. *Paraserianthes falcataria* (or commercially known as *Sengon*) is the wood species used to produce LVL in Indonesia. This is because *P. falcataria* is a fast-growing timber species and is widely planted by Indonesian forest communities [2]. LVL *Paraserianthes falcataria* uses veneers 2.2 mm thick, which are hot-pressed with melamine

* Corresponding author. Tel.: +62-274-545675; fax: +62-274-545676.

E-mail address: ali.awaludin@ugm.ac.id

urea-formaldehyde under 0.6-0.7 MPa pressure and 105-110°C temperature. First author's previous study found that this LVL had an average oven-dry specific gravity of 0.26 and moisture content of 12.8% [2]. Owing to know that the source of *Paraserianthes falcataria* timber used by this LVL is community forests, which are managed in a sustainable way and help offset the greenhouse gasses, authors classify this LVL *Paraserianthes falcataria* as a sustainable and green building material. First author of this paper since 2012 has started an intensive research to utilize LVL *Paraserianthes falcataria* for structural purposes. Racking performance of wooden shear walls made from this LVL was presented in 2013 [3], while research on connection system as well as knee-joint of gable frame made from this LVL is still under review process for possible publications. This presented paper summarized the authors' work in developing the wood frame floor made from LVL *Paraserianthes falcataria* as well as finding best configuration of built-up joist of the floor.

2. Built-up Joists

Wood frame floors can be found in multi-storey dwelling houses or offices of timber constructions. It is designated to support direct loads from occupants and transfer them to beams and columns of a frame system. Wood frame floors consist of repetitive joists at a prescribe spacing sheathed with either boards or wood structural panels attached to the top surface [4, 5]. Figure 1 shows various built-up joists commonly developed using wooden-base materials and they are categorized in general as I-shape and Box-shape [6].

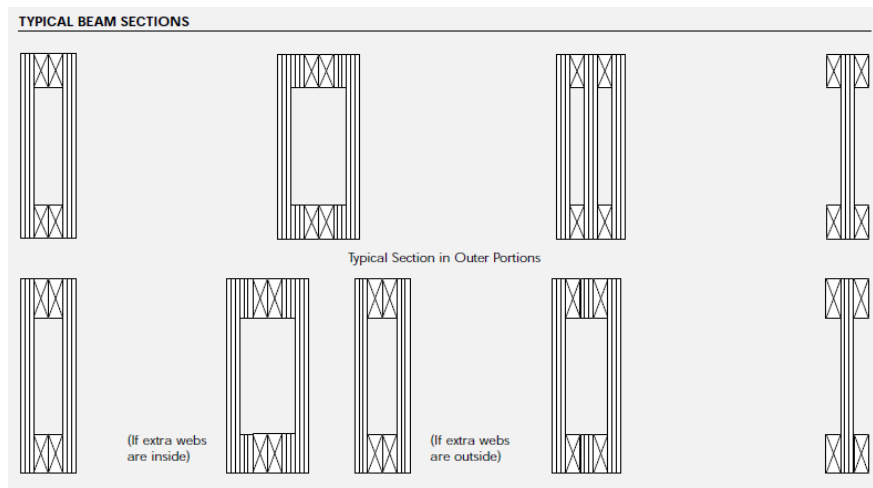


Fig 1. Typical built-up joists in wood frame floor [6]

In this study two types of built-up joist were fabricated as can be seen in Fig 2 where they had an equal height of 300 mm. They are I-section joist and Box-section joist. These two built-up joists were composed of LVL *Paraserianthes falcataria* having cross-section of 40 mm by 60 mm and 9 mm thick plywood of *Paraserianthes falcataria* connected with common nails CN55 (diameter 2.8 mm) and CN75 (diameter 3.2 mm) as shown in Fig. 2. Two replicates were prepared for each type of built-up joist and all specimens were tested according to a four-point bending configuration test as shown in Fig. 3 where the span length of the built-up joist was 2400 mm. These joists were loaded monotonically until failure and their deflection were continuously measured through four displacement transducers (LVDTs).

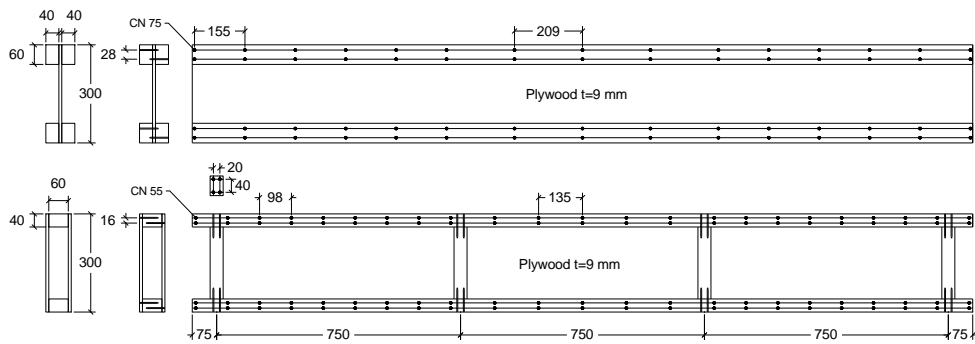


Fig 2. I-section and Box-section built-up joists (unit in millimeter)

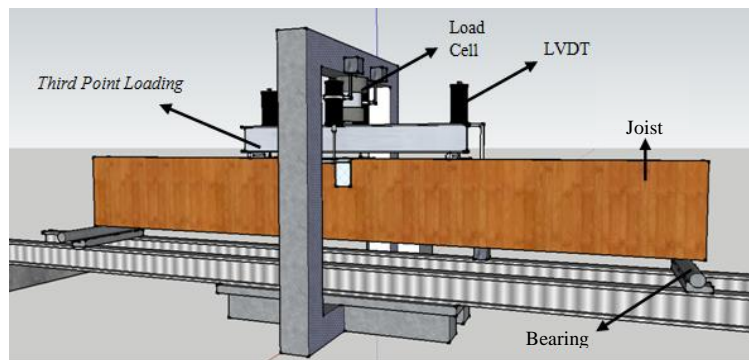


Fig 3. Four-point bending test of Box-section built-up joist

Figure 4 shows the load-deflection curves of the I-section and Box-section built-up joists obtained from the experiment; indicating that bending capacity and stiffness of the box-section built-up joists are much higher than that of the I-section built-up joists. Bending capacity of the I-section and Box-section was 14.37 kN and 23.99 kN, respectively. Bending stiffness (EI) of the joists was evaluated using Eq. 1 where P is the applied load, L is the clear span length, and Δ_b is bending deformation which is expressed in Eq. 2 [7].

$$EI = \frac{23PL^3}{1296\Delta_b} \quad (1)$$

$$\Delta_b = \Delta - \Delta_s = \Delta - \frac{PL}{4kAG} \quad (2)$$

In the above Equation, Δ_s is shear deformation, A is cross-sectional area of the joist, G is shear modulus, and k is shape factor. Applying those formulation, bending stiffness of the I-section and Box-section built-up joist was found, respectively, equal to $315 \times 106 \text{ Nmm}^2$ and $582 \times 106 \text{ Nmm}^2$.

Failure of Box-section built-up joist is bending at mid-span where crack initiated at the bottom (tension side) and propagated to the upper part of the cross-section. This indicates that shear capacity of the Box-section joist is sufficient to resist the applied shear force as it has two layers of plywood. In the case of I-section built-up joist, the failure was due to shear failure of the web (one layer of plywood) that finally left two flanges of the I-section supported the rest of loading (see Fig. 5). Results of this experiment suggested that the Box-section built-up joist is recommended for further use in the wood frame floor study.

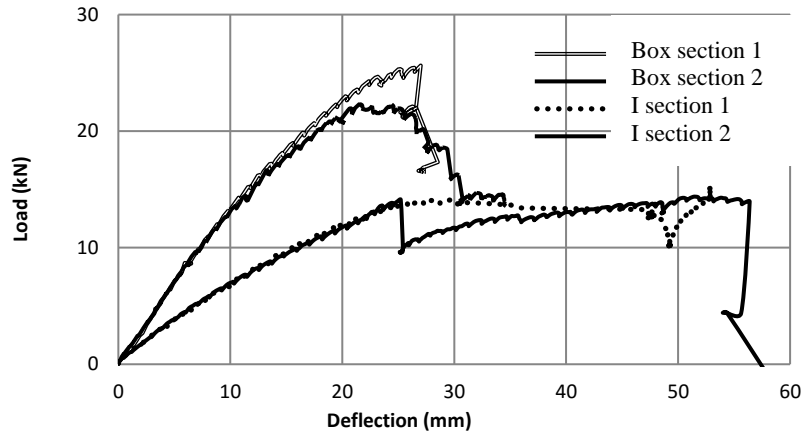


Fig 4. Load vs. deflection of I-section and box-section built-up joists



Fig 5. Failure mode of Box-section (left) and I-section (right) built-up joists under bending test

3. Wood Frame Floor

The production of wood frame floor is shown in Fig 5 which is composed of 4 Box-section built-up joists having an identical spacing of 300 mm and one structural panel at the top which is plywood of 20 mm thick. The plywood is connected to the joists in total using 52 common nails (CN 50, 13 nails per each joist). This wood frame floor was loaded on top of the structural plywood by gravity loads: a uniform load of concrete cylinders and group of people as illustrated in Fig. 6a and 6b. In addition to this uniform load, the wood frame floor was also loaded only at mid-span, reflecting as single line load (see Fig. 6c and 6d). During load test, deflection of the wood frame floor was measured by two dial gauges and the applied load was increased step by step.

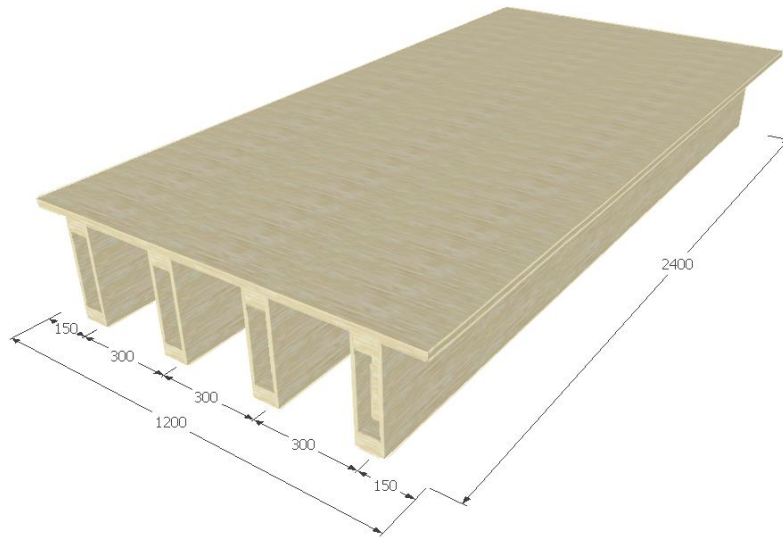


Fig 6. Production of wood frame floor (unit in millimeter)

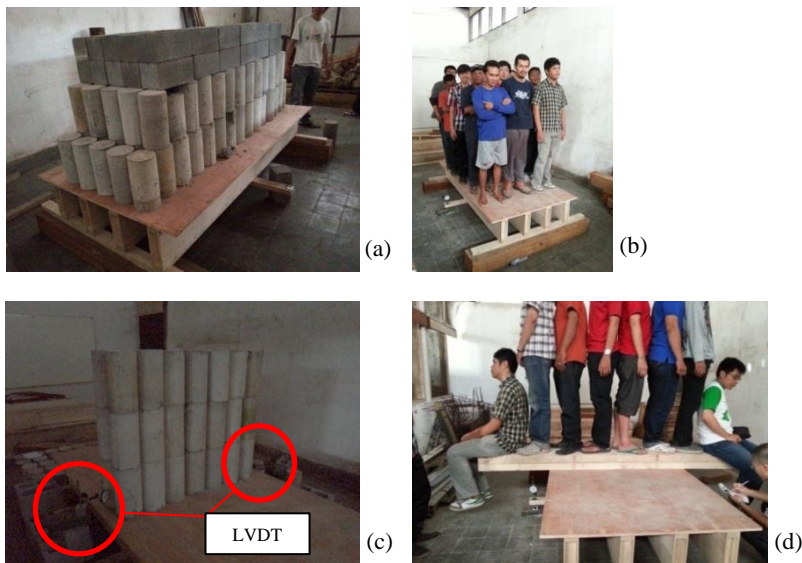


Fig 7. Test of wood frame floor under gravity loads

Figure 8 shows load-deflection curve of the wood frame floor under four different loading configurations where magnitude of deflection was the average of two displacement measurements. It is well observed that the linear relationship between load and deflection is still applied up to maximum load considered in the experiment. In the case of uniform concrete load configuration, the maximum load is 21.5 kN (corresponds to 3 mm displacement) and this is equivalent to a uniform load of 7.46 kN/m² as the floor area is 2.88 m² (1.2 m by 2.4 m). The slopes of the curves which indicate bending stiffness of the floor are in general similar especially when it is loaded under single line load either concrete load or people load.

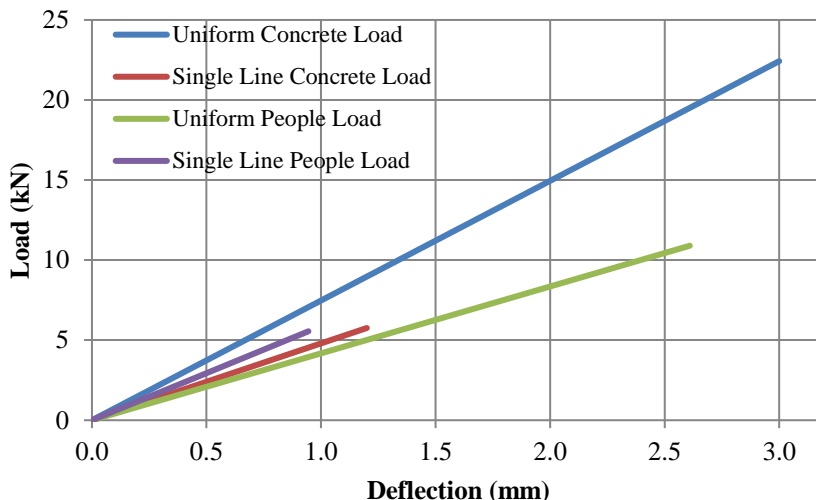


Fig 8. Load-deflection curve the wood frame floor under 4 types of gravity load

After completing this test, the wood frame floor was divided into two symmetrical parts to undergo further load test until failure according to test set-up shown in Fig. 9. One specimen was loaded by two loading points at one-third span, and the other specimen was loaded uniformly through wooden blocks. During the test five LVDTs were used to measure deflection of wood frame floor at both mid-span and one-third span. Load-displacement curves of these two wood frame floor specimens obtained from the experiment are presented in Fig 10 where the maximum load of the wood frame floor under uniform loading, which is 63 kN (or equivalent to 52.5 kN/m²), is higher than that of the wood frame floor under two-point load at one-third span (57 kN). Unfortunately the LVDT#1 (see Fig. 10a) was stop during the test of wood frame floor under two-point loading due to improper installation of LVDT holder. Assuming that allowable deflection of this wood frame floor equaled to $L/300$, which is 8 mm (2400 mm/300), it is found that the total of uniform load corresponds to this allowable deflection is 22.4 kN (or equivalent to a uniform load 18.75 kN/m²). This load is still within the elastic portion of the curve shown in Fig. 10b. This magnitude of uniform load that corresponds to allowable deflection is extremely greater than that generally specified in many standards of residential constructions (2.5 kN/m²).

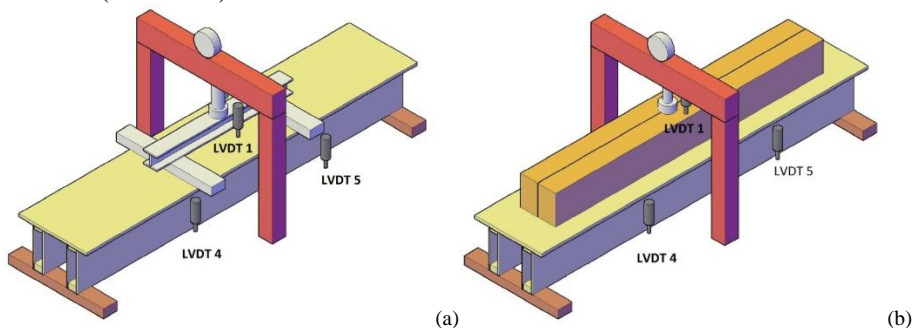


Fig 9. Load test of wood frame floor up to failure: a) using two-point loading; b) using uniform loading

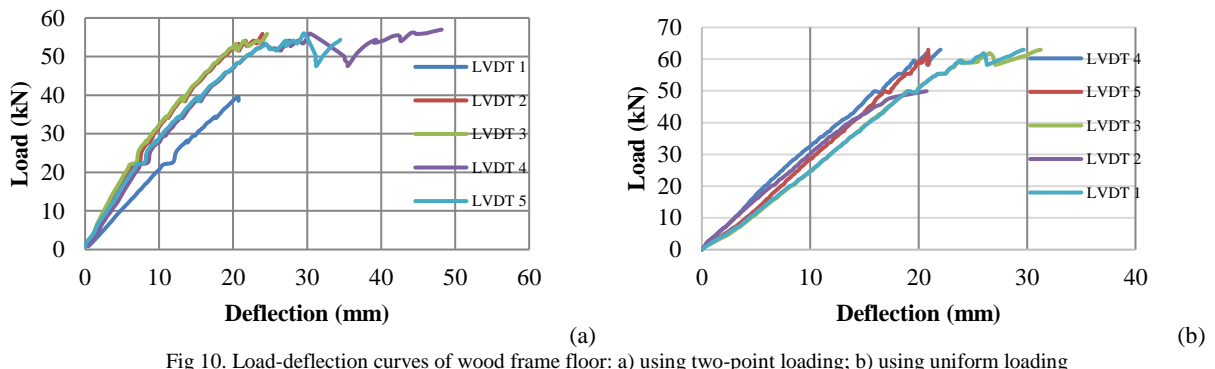


Fig 10. Load-deflection curves of wood frame floor: a) using two-point loading; b) using uniform loading



Fig 11. Photos of failure of the wood frame

The rest of this paper is used to evaluate the load bearing capacity of the wood frame floor considering two different failure modes: bending failure and shear failure of the built-up joist along with plywood sheet at the top. Assuming that all elements formed wood frame floor cross-section are fully composite, the calculation showed that bending capacity of the wood frame floor is 70.58 kNm, which is equivalent to the total of uniform load of 177 kN. While shear capacity of the floor is 29.89 kN which corresponds to an equivalent to the total of uniform load of 59.78 kN. Detailed calculation belongs to the authors due to limitation of number of page. This analytical bearing load is almost the same as the maximum load obtained from the experiment, which is 63 kN for the floor under uniform loading. The failure of the wood frame floor of the experiment is shown in Fig 11 which most failure concentrated at both ends of the floor specimens due to large shear force. This shear force compressed the joist creating opening or separation among the elements of the joist.

4. Final Remarks

This paper summarizes a series of experimental works to develop wood frame floor made from LVL *Paraserianthes falcataria*, a new sustainable and green construction materials recently available in Indonesian markets. The works consisted of an evaluation of two kinds of built-up joist: I-section and Box-section, and followed by an examination of 1.2 m by 2.4 m wood frame floor under various loading configuration. Results of the tests showed that box-section built-up joists had greater bending stiffness and capacity than the I-section built-up joists. Test of the wood frame floor which is composed by four Box-section built-up joists and one layer of plywood connected through nail fasteners indicated that the bearing load corresponds to allowable deflection of $L/300$ is 18.75 kN/m². This finding concludes that the proposed wood frame floor model made from LVL *Paraserianthes falcataria* is accepted for practical applications in residential constructions.

Acknowledgements

The authors wish to thank PT. Sumber Graha Sejahtera for providing LVL *Paraserianthes falcataria* used in this study. Sincerely thanks also goes to Ms. Khamida Nur Faizah for help adjusting layout and template of this paper.

References

- [1] Moody, R.C., Hernandez, R., Liu, J.Y., Glued Structural Members, Wood Handbook – Wood as an engineering material, U.S. Department of Agriculture, Forest Service, Forest Products Laboratory, 1999.
- [2] Awaludin, A., Development of Structural Walls made from LVL Sengon (*Paraserianthes falcataria*): Basic Mechanical Properties, Proc. 1st International Conference on Sustainable Civil Engineering Structures and Construction Materials (SCESCM), Yogyakarta, 2012, pp. 299-302.
- [3] Awaludin, A., Pribadi, A., Satyarno, I., Racking resistance of *Paraserianthes falcataria* wooden panel under monotonic load, Proc. of Civil Engineering Conference in Asia-Pacific Region (CECAR), Jakarta, paper # 79, 2013.
- [4] Boise Cascade, Simple Framing System : A Technical Guide Floor & Roof Framing Costruction BS5268 PART 2:2002 Version, 2013
- [5] APA, Design and Fabrication of Glued Plywood-Lumber Beams in Plywood Design Specification. APA, USA, 1998.
- [6] APA, Performance Rated I-Joists, Form No. 2725E. APA, USA, 2012.
- [7] Gere & Timoshenko, S., Mechanics of Materials. Wadsworth, Inc. UK, 1985.



Sustainable Civil Engineering Structures and Construction Materials, SCESCM 2016

On the confined high-strength concrete and need of future research

Antonius^{a,*}, Iswandi Imran^b and Prabowo Setiawan^a

^a*Department of Civil Engineering, Universitas Islam Sultan Agung, Semarang-Indonesia*

^b*Structural Engineering Research Group, Department of Civil Engineering, Institut Teknologi Bandung, Bandung- Indonesia*

Abstract

Investigation about requirements of confining reinforcement on the structure of high-strength concrete has been progressed significantly since the last three decades. Research carried out intensively on high-strength concrete, produces a material which has a relatively brittle nature. Various parameters of the confining reinforcement design have been varied to obtain the optimal results regarding the behavior of high-strength concrete, especially for columns comprehensively. This paper discussed about the development roadmap of confined high-strength concrete research, includes constitutive equations of confined high-strength concrete developed by researchers. In this paper modified of analytical model for confined normal to high-strength concrete is also proposed. Results of this further discussion were associated with the need of the development research of confining reinforcement on high-strength concrete material adapted to the material properties and zones in Indonesia.

© 2017 The Authors. Published by Elsevier Ltd.

Peer-review under responsibility of the organizing committee of SCESCM 2016.

Keywords: High-strength concrete; strength; constitutive equations; confinement model

1. Introduction

Infrastructure development requires excellent material quality and durable so many innovations to produce a material that has a high quality have been intensively conducted. High strength-concrete ($f'_c \geq 50$ MPa) has superior mechanical properties and durability compared with normal-strength concrete because of the hardness of the breakdown of a high and a lower porosity. However, high-strength concrete material is brittle, less ductile and more sensitive to aspects of the planning and execution of construction compared with materials made of normal strength

* Corresponding author. Tel.: +62-81228659970; fax: +62-24-6582455.

E-mail address: antonius@unissula.ac.id

concrete. High-strength concrete material's brittleness is characterized by the occurrence of crack propagation occurring faster than the crack propagation on normal strength concrete. This in turn leads to a more rapid loss of effectiveness of the concrete cover on the column, or the occurrence of which is premature shear failure on reinforced concrete beams. Brittle effect of high-strength concrete is generally solved by installing a confining reinforcement so that high-strength concrete is more ductile. Some researchers have been investigating the behavior of high-strength concrete columns by reviewing the compressive strength of concrete, confining reinforcement (i.e. ratio, spacing, yield stress) or configurations reinforcement and proposing design equations especially to ensure the safety and ductility of the columns that accept earthquake loads [1, 2].

This paper discusses the behavior of high-strength concrete, especially in the column structure that aims to evaluate some design equations that have been developed and adopted in the planning regulations. Confined concrete constitutive equations that affect the need of confining reinforcement are also discussed and compared to identify the accuracy of each model against experimental results that have been done by the author. At the end of the paper the development model of confinement of a general nature, which can be applied to normal and high-strength concrete.

2. The axial capacity of the concrete column

The axial capacity of the concrete column (P_o) to the concentric axial load is determined by the equation below.

$$P_o = \alpha f_c' (A_g - A_c) + A_s f_y \quad (1)$$

Equation (1) does not take into account the effect of confinement. SNI 2847-2013 [3] to stipulate the value of α is equal to 0.85 for various concrete compressive strength. NZS 3101-2006 [4] also sets the value of α of 0.85 in the equation above but applies for concrete compressive strength up to 55 MPa. If the concrete compressive strength is higher then:

$$\alpha = 0.85 - 0.004 (f_c' - 55) \quad (2)$$

The α value is limited to no less than 0.75. Equation (2) shows that NZS has been accommodating the decrease of the column axial capacity when using high-strength concrete.

Next the above equation accuracy with experimental results of high-strength concrete column against concentric load which has been done by several researchers have evaluated [5]. Figure 1 shows the relationship between $\rho_s f_s / f_c'$ and the ratio between the axial load test results ($P_{exp.}$) to the axial capacity of columns by SNI (Equation 1). From these relationships show that the confining reinforcement ratio (ρ_s) significant role in increasing the capacity of the axial column. The higher the ratio of the installed confining reinforcement, the more increase the axial capacity will be. Generally from the image it is also be seen that the value of α is quite safe in the value of 0.85 when the value $\rho_s f_s / f_c'$ is higher than 30. Conversely, when the ratio $\rho_s f_s / f_c'$ lower, even below 20, then it is quite risky when using the 0.85 factor in the calculation of the column axial capacity. The results show that α values espoused in the SNI need to be modified to accommodate high-strength concrete.

Besides affecting the amount of axial capacity, one of the failure mechanism of high-strength concrete column is results cover spalling prematurely. Figure 2 shows data of test results by Cusson & Paultre [6] and Antonius [7] that the strain ratio at the time of the cover concrete spalling of the unconfined concrete peak strain under 1 on columns made of high-strength concrete. Cover spalling behavior of high-strength concrete column that affects the equation stress blocks of concrete which is often used for design against bending. Modification of the equation block stress for high-strength concrete has also been proposed by several investigators, including by Bae & Bayrak [8] and Mertol [9].

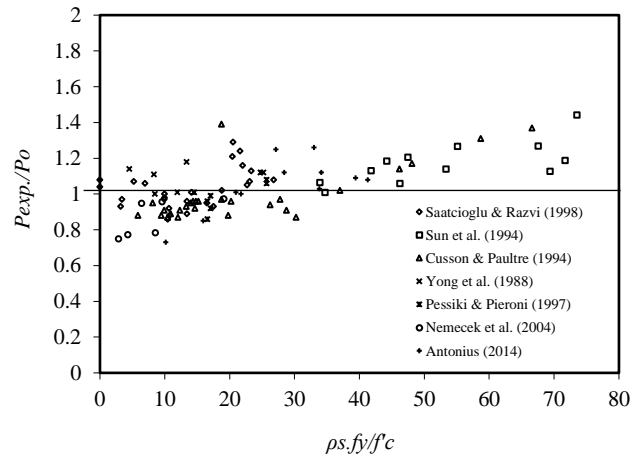


Figure 1. Axial Capacities of columns [5]

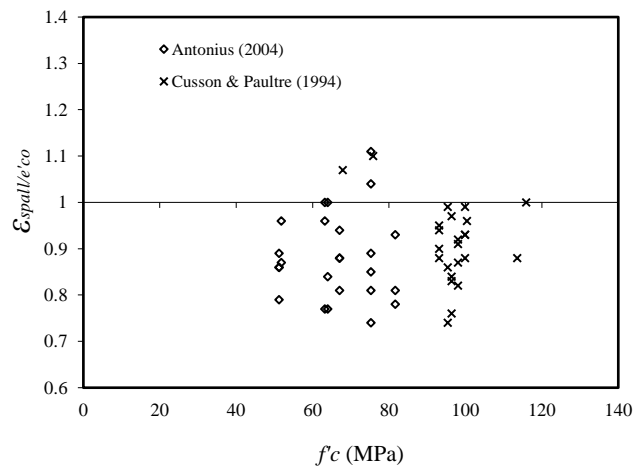


Figure 2. Relation between concrete strength and vs $\varepsilon_{spall}/\varepsilon'_{co}$

3. Constitutive equations of confined high-strength concrete

It is known that the design philosophy of confining reinforcement is that when it receives a seismic load the column axial force after the cover spalling remains well preserved. Volumetric ratio of confining reinforcement required in the column is determined by the magnitude of the increase in the strength of confined concrete or K value. Equation K value up to now has been widely proposed and generally adapted to the conditions in each researchers' country.

3.1. Strength enhancement of confined concrete (K)

3.1.1. Model by Muguruma et al.

Muguruma et al. [10] proposed a K value equation based on experimental results on the concrete with the compressive strength of 20-160 MPa. Therefore, the model can be applied to normal and high-strength concrete. It is reported that the model can be used to analyze the concrete with confinement that have a normal and high yield strength strength.

K value equation is mathematically written:

$$K = \frac{\bar{\sigma}_m}{f'_c} = (1 + 49.C_c) \tag{3}$$

$$C_c = 0.313 \rho \frac{\sqrt{f_{yh}}}{f'_c} \left(1 - 0.5 \frac{s}{w}\right) \tag{4}$$

C_c coefficient depends on the ratio of confining reinforcement (ρ), yield stress of confining reinforcement (f_{yh}), compressive strength of concrete (f'_c), spaced confining reinforcement (s) and the core cross-sectional area of reinforcement (w). The above equation does not take into account the effect of the configuration of the reinforcement. Confining reinforcement assumed has been yielded at the time of peak response.

3.1.2. Model by Diniz & Frangopol

Diniz & Frangopol [11] developed a constitutive model that can be applied to concrete compressive strength of 120 MPa. K value is determined by the following equation:

$$K = \frac{f'_{cc}}{f'_c} = 1 + \left(1.15 + \frac{3048}{f'_c}\right) \frac{f_{le}}{f'_c} \tag{5}$$

Equation (5) in units of psi. Confinement index is calculated by the formula:

$$f_{lat.} = \frac{A_{sh} \cdot f_{yt}}{d_e \cdot s_p} \tag{6}$$

in which $A_{sh} = \lambda \cdot A_{st}$.

Equation (6) shows that Diniz considers the confining reinforcement has been yielded at the time of maximum response. λ form factor is the reinforcement configuration. C_f factor is used to correct the value of the stress supplied by confining reinforcement by the following equation:

$$C_f = 1 - \frac{s}{d_c} \tag{7}$$

So that the effective lateral stress is:

$$f_{le} = C_f \cdot f_{lat.} \tag{8}$$

3.1.3. Model by Legeron & Paultre

Legeron & Paultre [12] proposed a model of confinement that can be applied to normal and high-strength concrete. K value is calculated by:

$$K = \frac{f'_{cc}}{f'_c} = 1 + 2.4(I'_e)^{0.7} \tag{9}$$

Confinement index I'_e formulated:

$$I'_e = \frac{f'_{le}}{f'_c} \tag{10}$$

Where f'_{le} is the effective lateral stress. The stress on the confining reinforcement is obtained by calculating the first strain of confinement at the time of the concrete reinforcement stress reaches a maximum, and then calculate the stress that corresponds to the stress on the stress-strain diagram. Legeron model has been used as the main reference to lower the design equation reinforcement of confinement with regard axial load level as well as in the design of confining reinforcement against seismic loads [13].

3.1.4. Model by Antonius et al.

Antonius et al. [1] proposed a high-strength concrete confinement model based on experimental results of concrete concentric round cross-section of the load. Strength enhancement of the confined concrete is below:

$$K = \frac{f'_{cc}}{f'_{co}} = 1 + 3.7 \left(\frac{f_2}{f'_{co}} \right)^{0.9} \quad (11)$$

f_2 is a effective lateral stress where the coefficient of confinement effectiveness for square section who adopt the equation proposed by Mander [14]. Results of investigations conducted by Antonius, stress of confining reinforcement at the time of peak response is not always yield, hence the stress to a square cross-section column is calculated by the equation below.

$$f_s = E_s \left\{ 0.0004 \cdot \ln \left[\frac{(s/d_c)}{\rho_s \sqrt{f'_c}} \right] + 0.002 \right\} \quad (12)$$

3.2. Validation of K equations to the experimental results

The K equations above will then be validated with data from experiments conducted by Antonius & Imran [15] on the testing of confined normal and high-concrete with square cross-section (Table 1).

Table 1. Experimental data of square section under concentric loadings [15]

Specimen	f'_c (MPa)	Confining steel			$P_{max.}$ (kN)	f'_{cc} (MPa)	K
		Conf.	\emptyset -spacing	ρ_s (%)			
AL5	34		5.5 – 50	2.01	301.84	33.80	1.16
AM5	45		5.5 – 50	2.01	381.77	42.75	1.12
AH5	67		5.5 – 50	2.01	533.23	59.71	1.10
BL5	34		5.5 – 50	3.43	300.86	33.69	1.37
BM5	45		5.5 – 50	3.43	453.39	50.77	1.33
BH5	67		5.5 – 50	3.43	631.64	70.73	1.29
CL5	34		5.5 – 50	3.02	329.26	36.87	1.27
CM5	45		5.5 – 50	3.02	375.25	42.02	1.24
CH5	67		5.5 – 50	3.02	606.63	67.93	1.10
DL5	34		5.5 – 50	3.63	390.88	43.77	1.50
DM5	45		5.5 – 50	3.63	444.01	49.72	1.30
DH5	67		5.5 – 50	3.63	558.41	62.53	1.16

Figure 3 is a validation result value K based on models that have been developed with a K value of experimental results in Table 1 above. Prediction value K based on Legeron proposed is generally over-estimating the value of K the experimental results. While it is generally the value of K based on the proposal Muguruma, Diniz and Antonius underestimate the experimental results. These results indicate that each proposed K value depends on the nature of the material used by each researcher. The reviewed parameters are also vary, depending on the estimated highly influential and appropriate conditions of each country.

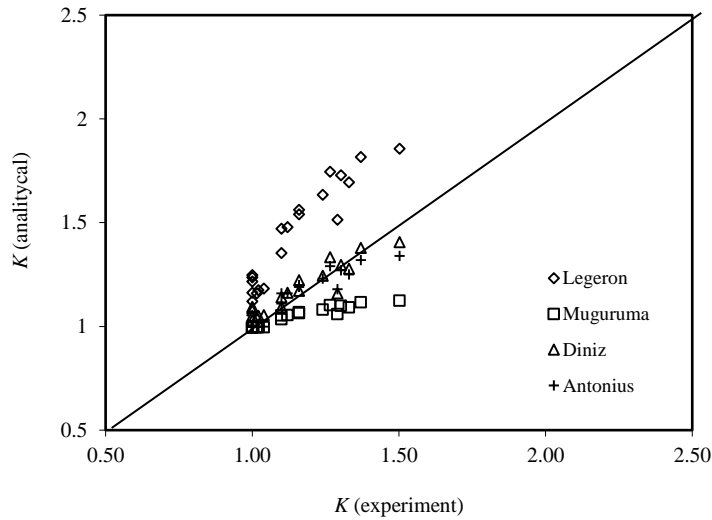


Figure 3. *K* values of models versus experimental values

4. Modification of confinement model

K values discussed above basically determines the stress-strain behavior of confined concrete too. The results of investigations of confinement models for high-strength concrete are very different from each other especially in modeling the behavior of post-peak [16]. In this paper, a confinement model that will be validated with experimental results based on the data in Table 1 above is going to be developed, wherein the compressive strength of concrete cover normal and high-strength concrete with various configurations of confining reinforcement. The base-model proposed by Antonius et al. [1], derived based on a large volume of test data from concentrically tested columns which is modified to develop a general confinement models with a wide range of compressive strength. Stress-strain parameters were unchanged from the model proposed in 2001 are outlined below. Ascending and descending branch are:

$$f_c = \frac{f'_{cc} \left(\frac{\epsilon_c}{\epsilon'_{cc}} \right)^r}{r - 1 + \left(\frac{\epsilon_c}{\epsilon'_{cc}} \right)^r} \tag{13}$$

$$f_c = f'_{cc} - (\epsilon_c - \epsilon'_{cc}) \frac{0.15 \cdot f'_{cc}}{(\epsilon_{85c} - \epsilon'_{cc})} \tag{14}$$

Furthermore, the parameters strain are:

$$\epsilon_{co}' = 0,0004 \cdot (f'_{co})^{0.45} \tag{15}$$

$$\epsilon'_{cc} = \epsilon'_{co} [1.94(K - 1) + 1] \tag{16}$$

Stress of confining reinforcement is determined by equation (12). Furthermore, the model modification made is the value equation of *K*, ductility parameters (ϵ_{85c}), effective lateral stress and residual stress (f_r).

4.1. Strength enhancement of confined concrete (K) and residual stress (f_r)

The K equation based on triaxial tests of high-strength concrete has been developed by Imran et al. [17] using Ottosen criteria which is adopted to estimate the strength increase in normal and high-strength concrete columns due to confinement. The K equation is:

$$K = \frac{f'_{cc}}{f'_{co}} = \left(\frac{f_l}{f'_{co}} - 0.327 \right) + \sqrt{1.7606 + 16.1714 \frac{f_l}{f'_{co}}} \quad (17)$$

And for the residual strength envelope:

$$\frac{f_r}{f'_{co}} = \left(\frac{f_l}{f'_{co}} - 0.327 \right) + \sqrt{0.1069 + 19.479 \frac{f_l}{f'_{co}}} \quad (18)$$

Failure strength envelope shown in figure 4 states that the value equation K proposed in this model has a non-linear shape and tend to be equal to the value equation K of Mander et al. [14], Xie et al. [18] and Ansari & Li [19]. The K value equation is also derived from the triaxial testing in which each uses yield criteria. Another phenomenon that is visible in the picture is the value equation K by Richart [5], and is the basis for determining the volumetric ratio of confining reinforcement by SNI, is under estimation of lateral low stress (up to $f_2/f'_{co} \sim 0.5$), compared with other equations.

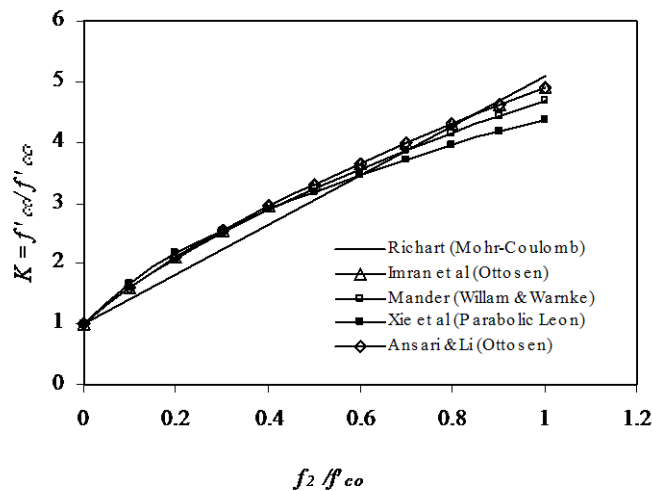


Figure 4. Failure strength envelope of K models

4.2. Ductility parameter

In the value of K in the above equation affects the behavior of confined concrete ductility. The data of test results round cross-section column by Antonius [1] and a square cross-section column test data by Antonius & Imran to be subsequently combined to determine the parameters of the new ductility. Results of regression yields the equation (see Figure 5):

$$\varepsilon_{sc} = \varepsilon'_{cc} + 3.10^{-5} \cdot e^{3.1K} \quad (19)$$

4.3. Effective lateral stress

It has been observed that for confined concrete with square sections that for spacings of ties greater than least dimension of the column the confining effects are negligible [15], therefore the lateral stress for square section with a correction factor proposed by Diniz & Frangopol [11] is adopted:

$$f_2 = k_e \left(1 - \frac{s}{d_c} \right) \left(\frac{\rho_s}{2} \cdot f_s \right) \tag{20}$$

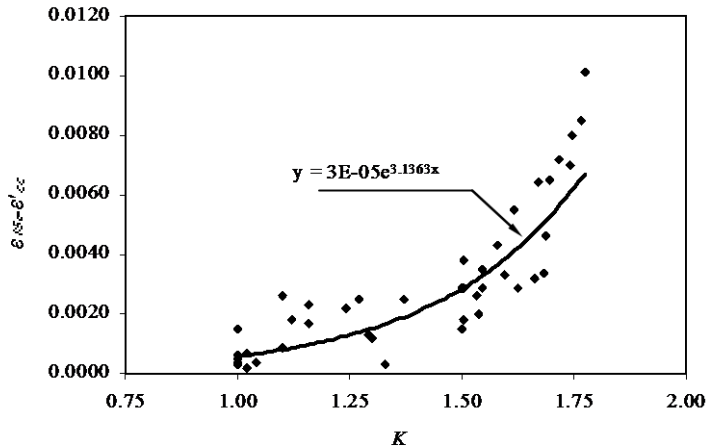


Figure 5. Regression of ϵ_{85c} equation

5. Corroboration with the experimental results

The modified stress-strain relationship for confined concrete is then used to simulate experimental results of reinforced concrete columns in Table 1 above. The comparisons of the modified model with specimens for square sections showed in Figure 6 through 9. It can be seen from those figures that the modified model simulate the stress-strain of confined normal and high-strength concrete on the pre and post peak response satisfactorily.

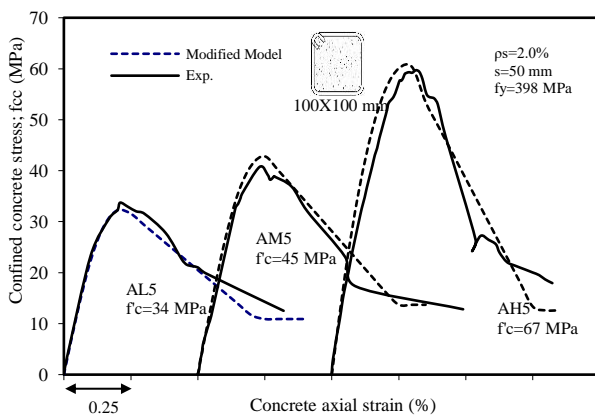


Figure 6. Modified model vs experimental results for A configuration

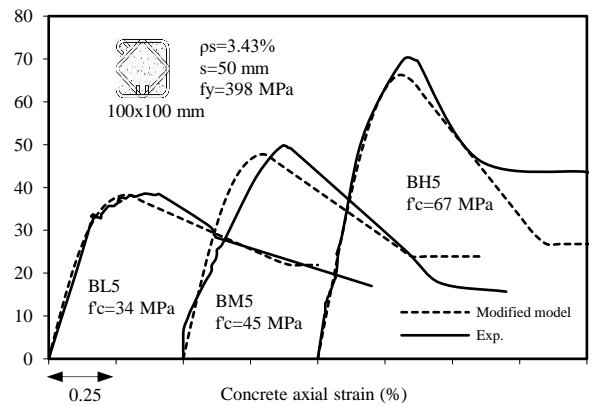


Figure 7. Modified model vs experimental results for B configuration

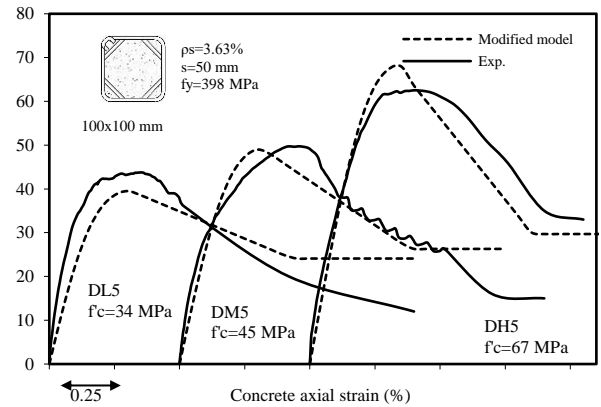
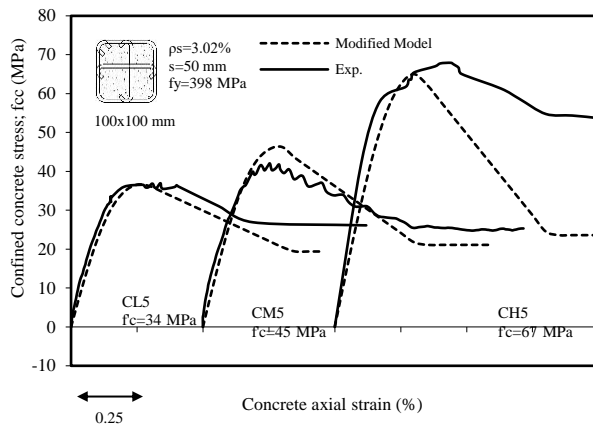


Figure 8. Modified model vs experimental results for C configuration Figure 9. Modified model vs experimental results for D configuration

6. Conclusion

Further studies on calculation of axial capacity on high strength concrete columns are needed, where the coefficient α in equation (1) needs to be reviewed and modified. Premature cover spalling occurs in high strength concrete, even data from previous study cover spalling occurs in concrete compressive strength from 50 MPa. Equation of the increases of the strength of confined concrete developed by researchers has different characteristics from one another, and in general the results of performed tests are verified by yield criteria. In general, the K value especially for high-strength concrete uses non-linear equations. Modification of confinement models applied for concrete with a wide range of compressive strength was presented.

In the derivation, the concrete strength increase ($= K$), due to the symmetrical confinement was adopted with triaxial stress of data through the Ottosen criteria. Within the verification, the performance of the modified simulation models in the stress-strain behavior of the confined normal and high-strength concrete columns to the column tests under concentric loadings was found satisfactory. In line with previous author recommendation [20], research progress has been achieved regarding with the confined high-strength concrete, it still needs to be developed further mainly experimental program to cyclic loading is expected very useful in order to complete the concrete regulations in Indonesia (SNI).

References

- [1] Antonius, Behaviour of High-Strength Concrete Columns Subjected to Concentric and Eccentric Axial Loads, Dissertation, Institut Teknologi Bandung, 2001 (in Indonesian).
- [2] O. Bayrak, Seismic Performance of Rectilinearly Confined High-Strength Concrete Columns, Ph.D. Dissertation, Univ. of Toronto, 1999.
- [3] Indonesian National Standard, Requirements of Structural Concrete for Building, SNI-2847-2013 (in Indonesian).
- [4] New Zealand Standard, Concrete and Structures Standard, Part 1-The Design of Concrete Structures, NZS 3101: Part 1: 2006.
- [5] Antonius, Performance of High-Strength Concrete Columns Confined by Medium Strength of Spirals and Hoops, Asian Journal of Civil Engineering, 15(2), 2014, pp.245-258.
- [6] D. Cusson, P. Paultre, Experimental Study of High-Strength Concrete Columns Confined by Rectangular Ties, Proc. of High-Strength Concrete Conf., Norway, June 20-23, 1993 pp.136-145.
- [7] Antonius, The Influence of Lateral Reinforcement to the Cover Spalling Mechanisms for High-Strength Concrete Column Structures, Proceeding of National Conference Earthquake Engineering II, UGM Yogyakarta, January, 2004, pp.168-176 (in Indonesian).
- [8] S. Bae, O. Bayrak, Stress Block Parameters fo High-Strength Concrete Members, ACI Structural Journal, 100(5), 2003, pp. 626-636.
- [9] H.C. Mertol, S. Rizkalla, P. Zia, A. Mirmiran, Characteristics of Compressive Stress Distribution in High-Strength Concrete, ACI Structural Journal, 105(5), 2008, pp.626-633.
- [10] H. Muguruma, M. Nishiyama, F. Watanabe, Stress-strain Curve Model for Concrete with a Wide-Range of Compressive Strength, Proc. of High-Strength Concrete Conf., Norway, 1993, pp. 314-321.
- [11] S.M.C. Diniz, D. M. Frangopol, Strength and Ductility Simulation of High Strength Concrete Columns, Journal of Structural Eng. ASCE, 123(10), 1997, pp.1365-1374.

- [12] F. Legeron, P. Paultre, Uniaxial Confinement Model for Normal and High-Strength Concrete Columns, *Journal of Struct. Eng. ASCE*, 129(2), 2003, pp. 241-252.
- [13] P. Paultre, F. Legeron, Confinement Reinforcement Design for Reinforced Concrete Columns, *Journal of Structural Eng. ASCE*, 134(5), 2008, 738-749.
- [14] J.B. Mander, M.J.N. Priestley, R. Park, Theoretical Stress-Strain Model for Confined Concrete, *Journal of Structural Eng. ASCE*, 114(8), 1988, pp.1804-1824.
- [15] Antonius, I. Imran, Experimental Study of Confined Low, Medium and High-Strength Concrete Subjected to Concentric Compression, *ITB Journal of Engineering Science*, 44(3), 2012, pp. 252-69.
- [16] U.K. Sharma, P. Bhargava, S.K. Kaushik, Behavior of Confined High Strength Concrete Columns under Axial Compression, *Journal of Advanced Concrete Technology*, 3(2), 2005, pp.267-81.
- [17] I. Imran, Suharwanto, M. Moestopo, D. Brahmantyo, Stress-Strain Response of Confined High-Strength Concrete, *Journal of Civil Eng. ITB*, 8(3), 2001, pp.135-144 (in Indonesian).
- [18] J. Xie, E. Elwi, J.G. MacGregor, Numerical Investigation of Eccentrically Loaded High-Strength Concrete Tied Columns, *ACI Structural Journal*, 93(4), 1996, pp.449-461.
- [19] F. Ansari, Q. Li, High-Strength Concrete Subjected to Triaxial Compression, *ACI Materials Journal*, 95(6), 1998, pp. 747-755.
- [20] Antonius, Studies on The Provisions of Confining Reinforcement for High-Strength Concrete Column, *Procedia Engineering*, Vol.95, 2nd SCESCM, 23-25 Sept., 2014, pp.100-111.



Sustainable Civil Engineering Structures and Construction Materials, SCESCM 2016

Role of organizational factors affecting worker safety behavior: A Bayesian Belief Network Approach

Bonaventura H.W. Hadikusumo^a, Bhanupong Jitwasinkul^a, Abdul Qayoom Memon^{a,*}

^aSchool of Engineering and Technology, Asian Institute of Technology, P.O. Box 4, Klong Luang, Pathumthani 12120, Thailand

Abstract

Several investigations on major occupational accidents are demonstrating interest in role of organizational factors. Investigations and evidences manifest that “the root causes involved more than technical or human failures” [1]. Thus, focusing on organizational factors is an important issue in safety as a means of mitigating accident in the workplace. First step for assessing the influence of organizational factors is to identify the relevant organization factors. Out of 22 factors identified from literature review, seven important factors were finalized for Thailand construction industry: communication, culture, management commitment, leadership, organization learning, empowerment, and reward system. At final phase, Bayesian Belief Network was used for handling the complex causality and providing the strategies to enhance the safety work behaviors. According to first alternative, 73.3% of safety work behavior was reached by manipulating management commitment, participation, learning and leadership nodes simultaneously. The second alternative accomplished about 74.6% of safety work behavior when the leadership, management commitment, participation and intention node were assigned to favorable state. For the third alternative, 77.7% of safe work behavior could be obtained by controlling leadership, management commitment, participation and perceived behavioral control node.

© 2017 The Authors. Published by Elsevier Ltd.

Peer-review under responsibility of the organizing committee of SCESCM 2016.

Keywords: Organizational factors, Worker behavior, Bayesian belief network

1. Introduction

Occupational accidents not only generate losses in property damage but also provoke a decrease in employee’s morale, productivity, quality of products and services, public image, customer relations, and organization’s reputation.

* Abdul Qayoom Memon. Tel.: +66944046058; fax: +0-000-000-0000 .

E-mail address: abdul.qayoom@ait.asia

In light of these economic and social costs, it is important that safety professionals and researchers require better understanding on the events preceding occupational injuries, as well as the relevant contributory factors that may influence in any individual's safety work behaviors. In Thailand, governmental and non-governmental agencies are active in development and promoting occupational safety in construction industry. Therefore, every project in Thailand has to be intergraded with safety program in day-to-day operations in order to increase safety performance. Besides that, there is still a need to reach the targeted outcomes, even though accidents in downward trend [2]. This indicates that these efforts are not adequate to handle at-risk work behaviors on the construction sites. It is important here to note that not only people are considered as contributing factors but also organizational factors shape the context that contributes to at-risk work behavior [3]. Thus, organizational factors have been recognized as the means of mitigating accidents in the workplace and improve the worker safety behavior.

2. Problem statement

Findings from several studies revealed and underpinned the idea that the majority of occupational accidents are caused by people rather than unsafe working environments [4,5]. Accordingly, findings indicate that approximately 80 percent of occupational injuries caused by at-risk behaviors while 15 percent caused by risk working conditions and the last five percent is inevitable [6,7,8]. This particularly brings attention to safety professional to recognize the importance of employee's behaviors as major root cause. The prominence of organizational factors in human error has been particularly acknowledged. Evidences from previous researches have supported the contribution of organizational factors on organizational safety performance. However, the effect of organizational factors in the field of work behavior in construction industry has hardly been examined. It is not easy to determine the implication on the improvement of the safety work behaviors in conjunction with the influence of organizational factors because of their complexities from the multiple causal relations between organizational factors, psychological precursors and safety work behaviors, especially in the complex construction safety scenarios. Thus, appropriate analytical approach should be capable of handling the complex causality from their interactions among organizational factors, psychological precursors and individual safety work behaviors within a built environment. Hence, inconsistency in the influences of causal relationships could be determined by various quantitative methods such as traditional inferential statistic or probabilistic model (Bayesian belief network). The achieved results and explanations should further enable the safety experts provide policy and procedures to increase safe work behaviors by considering the certain inferences of causative factors.

3. Methodology

Fig. 1. illustrates the research paradigm. Both qualitative and quantitative approaches have been used. After thorough literature review, a set of organizational factors have been identified. Through triangulation, key important organizational factors were finalized by expert opinion. After that causality analysis has been carried out using Bayesian belief network to develop strategies to improve the worker safety behavior.

4. Identification of organizational factors

The success or failure of the organization is reliant on the collaboration of all departments, identification of organizational factors, therefore, is based on perspective regarding on how an organization and its people cooperate within their environment. Therefore, the first step of systematic approach for evaluating the influence of organizational factors must sufficiently identify the key organization factors. Thus, a system theory has been adopted as a blueprint for a framework to identify and investigate the organizational factors. This theory provided the concept that attempt to integrate classical and human relation approaches. This phase utilizes the realism paradigm and the case study approach to decide how an organization and its people interrelate within their environment and to provide an illustrative framework because realism research is capable of "searching towards an understanding of the common reality of any system in which many people operate inter-dependently"[9]. Therefore, this study proposes 22 organizational factors including organizational culture, ownership, safety culture, leadership, personnel selection, reward system, resource allocation, communication, and management commitment, coordination of work,

formalization, organizational knowledge, empowerment, centralization, goal prioritization, organizational learning, technical knowledge, time urgency, problem identification, role/responsibilities, performance evaluation, and training.

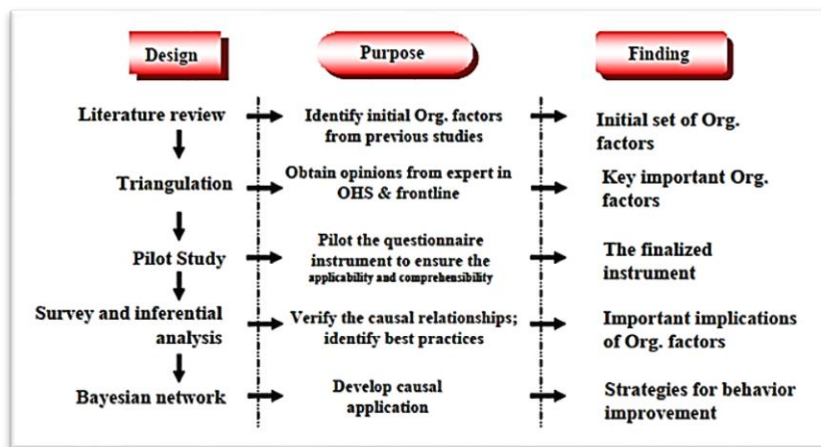


Fig. 1. Research Paradigm

5. Key organizational factors

Authors aimed to classify suitable organizational factors. It can be in terms of process or analysis approach [10,11]. According to the analysis approach offered by Osborn et al. [10], categories contain two main dimensions, i.e. organizational contingencies and intermediate outcomes. Organizational contingencies include four groups of organizational factors: governance, context, environment, and design. The latter category, known as intermediate outcomes, has four organizational factors: innovation, quality, efficiency, and compliance. This approach is founded on the organizational structure. Besides the organizational analysis approach, Jacobs and Haber [11] introduced a perspective to determine valid relationships between organizational factors and safe work procedure. It tries to determine how an organization works, versus how it is structured. For this reason, this study used the perspective of Jacobs and Haber [11] to determine how an organization and its people intermingle within their environment, since the success or failure of the organization is reliant on the relations of all departments. After focus group interviews with HSE experts and front line workers, following seven key important organizational factors were finalized.

5.1. Safety culture

Commonly, culture refers to the set of key values, beliefs, understandings, and norms that people of an organization share. Moreover, culture strengthens commitment for attainment of the organizational goal and establishes direction through explanation and also supports the standards of behaviors [12]. Sorensen [13] suggested that it is reasonable to consider organizational culture as application of the larger concept of culture, and safety culture could be represented as subset of organizational culture. Maximum HSE managers approved that safety culture development is important for reliably handling work behaviors and supporting safety awareness. Health & safety manager in Thailand said:

“When our people take risks for production targets or for any reason, frontline management investigates and considers how and why they do not follow procedure. This management action explicitly states that risk is unacceptable. These practices could govern work behaviors. On the other hand, if frontline management turns praise blind eye or gives praise when people accomplish tasks by violating safety rules, it means that frontline management has nonverbally stated that it is OK. This risk work behavior will continue.”[14]

Results from inferential analysis indicate that safety policy consistently applied into specific actions and motivating subordinate to work safely has strong negative associations with at-risk work behaviors. Strong correlation values range from -0.61 to -0.72. These strong inverse associations of safety culture development substantially implied that

motivating subordinate to work safely from management level could help reduce the occurrences of a-risk work behaviors in construction projects.

5.2. *Communication*

Numerous HSE managers intensely insisted that a two-way communication process establishes trust from consultative safety activities between different stakeholders in projects, because it can generate a shared understanding of risk and assistance to resolve conflicts that may arise about risk management decisions [15,16]. According to HSE manager in Thailand:

“Keeping open and honest communication greatly supports the risk management in a cross-disciplinary team as well as consultative. By breaking down the conventional hierarchical style, we can gain the benefit of our people’s ideas and knowledge sharing. Such open communication builds commitment to our safety goal as well as also establishing trust. These help support compliance with risk control and any safety initiatives.”[14]

5.3. *Empowerment*

Empowerment refers to the process that allows one to obtain the official authority and power. In general, this notion simply refers to process that provide subordinates with opportunities. Gibson [17] provided definition of empowerment as "individual's recognition, promotion and improvement of his abilities to achieve his own requirements, solve their own problems and mobilize resources to control their own lives by helping them to build a critical awareness of the situation and ease the proposition of a plan of action". Instead of trying to govern workers, empowerment is an approach that empowers the individual to regulate his environment and achieves self-determination [18]. For this reason, empowerment aims to establish work conception of increasing the involvement and motivation of frontline workers with moderate utilization of supervision as a control system and flat structure where decision-making authority tends to be downward. It is mentioned in the extensive literatures that the greater empowered workers are beneficial in mitigating the accident rate. However, in this study only 1st operatives testified the application of empowerment scheme. As per HSE manager in Thailand:

“Accordingly, workers are freely allowed to raise safety concerns, suggestions and has right to stop work whenever they found suspicious incidences. Peer-to-peer observations help us maintain safety awareness of workers. We also use the intrinsic rewards of meaningful work and the opportunity to learn and growth. Diversity of workforce on site will pool their area of expertise to achieve at procedures that are better than one could come up alone. Thus self-control of employee’s work behaviors at workplace and continuous learning will be arrived.”[14]

The most at-risk work behaviors have negative association with the actual implication of empowerment. The results of statistic inferences showed moderate correlation strengths between implications of empowerment and safe work behaviors.

5.4. *Management commitment*

Management commitment has been extensively acknowledged as a key ingredient of organizational success in competitive arenas regarding the attainment of certain aspects such as quality, production, job satisfaction and safety. Generally, exhibiting management commitment through its substantive actions helps improve employee commitment [19]. In particular, considerable findings found that management commitment has been exhibited to positively affect the work behaviors of organizational members, with remarkable examples originating from the occupational safety profession. Likewise, frontline respondents stated that they weigh the significance of safety concern from substantive action of top management [14].

The results of statistic inferences showed five of six key implications of management commitments, excluding the practices of resource allocations, have moderate correlation coefficients (r) with at-risk work behaviors. Their correlation coefficient values range from 0.5 to 0.6. In the light of these findings, it could be addressed that the construction projects where managements exhibit and implement the higher standard of commitment to occupational safety are most likely to lower occurrences of at-risk behaviors and improved safety work behaviors.

5.5. Leadership

The concept of leadership continues to evolve as the need of organizations change. As dynamic and reciprocal natures occurring among people, leadership plays an important role in influencing organizational members toward the attainment of certain goals. Reed [20] has defined leadership as the art of accomplishing change through people. The visible commitment and guiding example of leadership as modeling of the behaviors are critical for bringing about organizational safety. In particular, several researchers have put their attempts for investigating the relationship between leadership and occupational health and safety. Maximum HSE manager exposed that active role of leadership strongly inspires the safe work behavior of their subordinates. Safety performance will progress where the role of the leader is accepted and the leader makes employees admit the significance of safety [14].

The results of statistic inferences show that there is a strong negative correlation between encouraging frontline workforce discussion about safety by management and at-risk behaviors. Result from perception-based survey indicates correlation values in which their strength are greater than 0.57. The results of statistic investigations showed that three of eight key implications of leadership have strong correlation coefficients (r) with compliance behaviors to safety regulations and procedures. Thus, these strong associations between actual implications of leadership at workplace and safe work behaviors implied that implementing more participative and supportive style of leadership in construction projects could lead to better safety work behaviors at construction projects.

5.6. Organization Learning

Another vital feature to constantly sustain the employees' awareness and competency is organizational learning. Several problems have no ready-made solutions and require that members throughout the organization think in new ways and learn new values and attitude. Previous mistakes and failures are principally considered as elemental ingredients of learning and incident management. Case studies exhibited those HSE managers from organization that pays high attention to continuous learning vintages better performance. A number of HSE managers strongly agreed that learning empowers the creation of an organizational environment that encourages human development to meet the probability of organizational adaptability, and to avoid stability traps and self-satisfaction

According to results of statistical analysis negative association exists between regular rehearsal of training and at-risk work behaviors. Such correlation coefficient values range from -0.564 to -0.74. The slightly less correlation also found between reviews of proactive and preventive and at-risk work behaviors. In the light of these findings, it can be mentioned that the construction projects where implications of learning on board are most likely to lower occurrences of at-risk behaviors and promote safety work behaviors [14].

5.7. Reward system

In business arena, organizations extensively apply certain reward systems to motivate individuals and improve morale. Reward systems are conducted in different ways. Organizations commonly implement extrinsic and intrinsic reward to encourage and retain their people within the organization. Organization always endeavor motivation in their members to contribute to perform their activities in a safe manner. Such safety reward schemes are generally designed to handle risk behaviors and reinforce safe behaviors. HSE managers also claimed that "the most important issue is how strongly the worker is intrinsically motivated rather than motivated by tangible benefit." They propose a so-called "intrinsic safety motivation." One of HSE managers of construction organizations in Thailand said:

"Using merely 'carrot and stick' seems like seducing workers into complying with safety regulations as well as participating in certain safety initiatives. This will hardly cultivate internal motivation or consistently maintain safe work behavior. Instead, using intrinsic motivation coupled with extrinsic motivation yields better results. This makes workers recognize how important their well-being is to themselves and their families [14].

Besides selected significant factors, not all factors were acknowledged as important factors for assisting risk work behavior reduction, endorsing safety compliance or reassure safe work behaviors. Time urgency, centralization, goal prioritization and formalization were identified as less important in influencing risk work behaviors. Therefore

these were not recognized as contributing factors. Their consequences for safety might be considered as part of administration and received low priority with respect to safe work behavior.

Result of statistic inferences analysis indicated that there are strong positive associations between implications of reward system and safety work behaviors. Positive correlations exist between implementing reward schemes and safe work behaviors. In particular, a correlation of 0.664 exists between incentive for participation and compliance with safety regulation behaviors.

6. Network development

Bayesian Belief network (BBN) offers important capabilities to establish such complex causal relationships. This graphical network could determine and quantify complicated relations in accordance with specific evidence within built environment. For this reason, this study adopted this technique within aim to provide insight into influence of organizational factors and psychological precursors on safety work behaviors in construction projects as well as identifying practical combinations of key organizational factors to manipulate such factors that have the strongest influences on safety work behavior in complex construction scenarios. The main concerns with Bayesian network development is about lack of a clearly defined process. This study adapted the systematic steps of network construction from Sigurdsson et al.[21] shown in fig. 2.

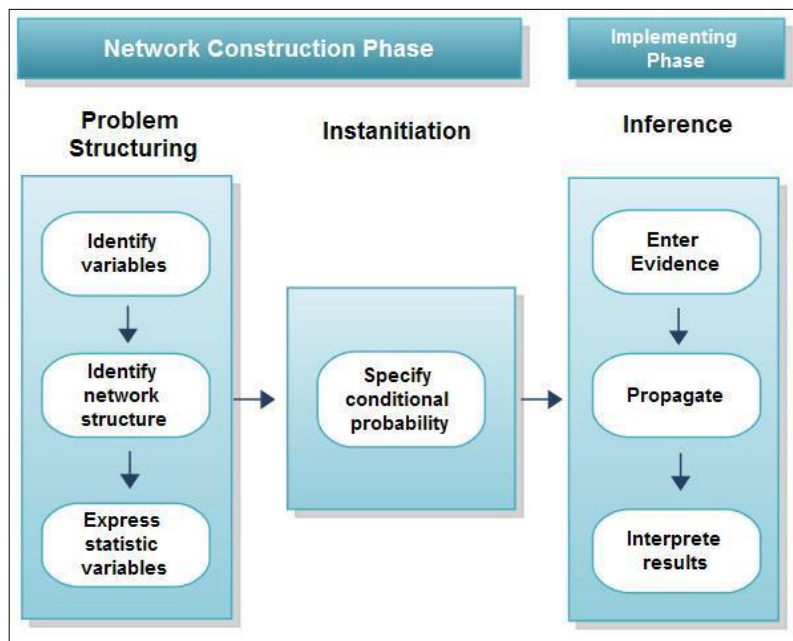


Fig. 2. Bayesian belief network process

To develop the Bayesian network in predicting safety work behaviors, and in order to obtain individual attitudes, beliefs and actual implications of organizational factors regarding occupational health and safety, a perception-based survey of frontline workers in Thai construction project was conducted. Building projects in Bangkok and surrounding provinces were participated as population samples for this analysis. According to system theory framework and how an organization works, seven out of twenty-two important organizational factors: communication, culture, management commitment, leadership, organization learning, empowerment, and reward system were finalized.

According to critical review of the behavioral literature, Theory of Planned Behavior could be one appropriate among work-related behavior models because it has particular characteristics: (1) consisting of precursor intent constructs covering the wide range of motivation, intention and behavior inaction, and (2) the proof of validity examining from a number of empirical studies in behavioral science e.g. Christian and Armitage [22], Johnson,

Musial et al. [23] ;Armitage and Arden [24] ;Armitage and Conner [25]. For this reason, this study adopted TPB as the reasonable basis for the development of BBN explaining safety work behaviors.

In Bayesian probability analysis, every entity requires assigning the prior conditional probabilities to the hypotheses. These prior conditional probabilities are typically acquired from knowledge of the prevailing circumstance. Due to limitation, the states at each node are kept at level 3 (Good, Average, Poor) to limit the number of surveys to possible limits. The developed BBN is shown in Fig. 3

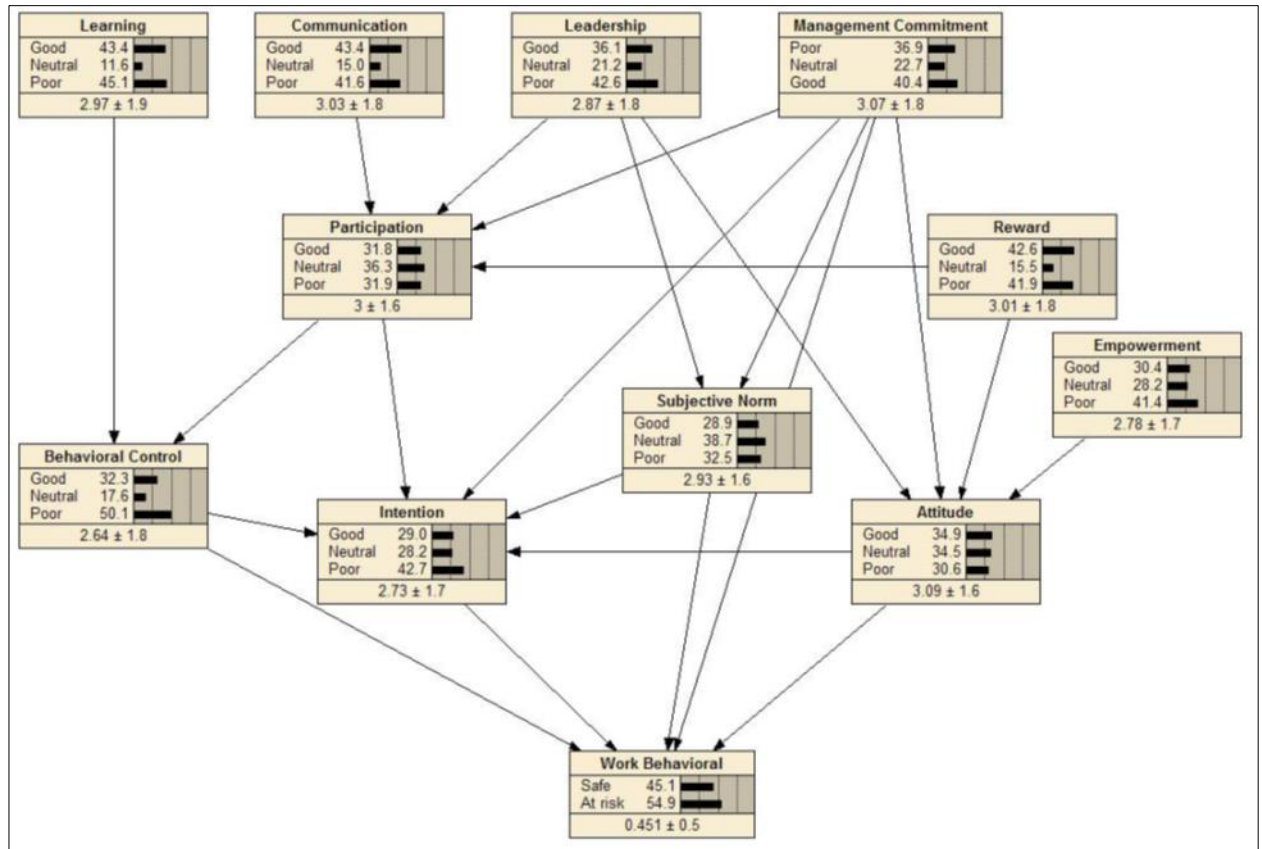


Fig. 3. Bayesian belief network

7. Results

7.1. Simple strategy

If implication states of management commitment change from poor to good, the probability of safety work behaviors ranged from 36.09% to 53.12%, which represents a sensitivity of 47.19%. This demonstrates that the favorable implications of management commitments seem essential to help improve safety work behaviors. Thus, in devising a simple strategy from manipulating organizational factor to improve safety work behavior, network recommend to particularly control the favorable implications of management commitments, which seem very essential to help improve safety work behaviors. Besides organizational factors, the psychological precursors of TPB archetype also play important roles in safety work behavioral enaction. As mediators, sensitivity of non-root nodes was higher than root nodes like organizational factors. In other words, safety profession should put their attempt to promote implications of such organizational factors that would lead to favorable state of psychological precursors.

7.2. Joint strategy

Considerable investigations are allowed to identify the appropriate combination of favorable states according to controlling variables. The obtained schemes enable safety professional achieve the attainment of high level probability of safety work behaviors. Realizing that there is an optimistic perspective in alternative scenarios, favorable state are assigned into potential variables, which might play an important role in establishing the safety environment and encouraging safe work behaviors. The presented alternatives highlight the useful implications that might lead to high probability of (wb=good) which are greater than 70%. According to first alternative, 73.3% of safety work behavior (wb=good) was reached by manipulating management commitment, leadership, learning and participation node simultaneously. The second alternative accomplished about 74.6% of safety work behavior (wb=good) when the leadership, management commitment, participation and intention node are assigned to favorable state (ls=good; mc=good; pa=good and in=good). For the highest alternative, 77.7% of safety work behavior (wb=good) could be obtained by controlling leadership, management commitment, participation and perceived behavioral control node (ls=good; mc=good; pa=good and pb=good).

8. Conclusion & recommendations

A number of optimistic scenarios are examined to determine the condition predictive ability of an early demonstrative guess in combination of implications regarding organizational factors. Due to limitation of time and budget, the sample size was limited but development of Bayesian belief application should incorporate more sample size in order to enhance the level of model reliability and robustness. Further research could be broadened to investigate other construction project categories. Apart from building projects, infrastructure and industrial projects have different scale and degree of technological complexity and to overcome drawback of perception-based survey, safety professionals should adopt direct observation method as means for collecting safety work behaviors.

Journal publications related with this article

1. Jitwasinkul, B., & Hadikusumo, B. H. (2011). Identification of important organisational factors influencing safety work behaviours in construction projects. *Journal of Civil Engineering and Management*, 17(4), 520-528.
2. Jitwasinkul, B., Hadikusumo, B. H., & Memon, A. Q. (2016). A Bayesian Belief Network model of organizational factors for improving safe work behaviors in Thai construction industry. *Safety science*, 82, 264-273.

References

- [1] Seo, D.-C. (2005). "An explicative model of unsafe work behavior." *Safety Science* 43(3): 187-211.
- [2] Siriruttanapruk, S. and P. Anantagunlathi (2004). "Occupational health and safety situation and research priority in Thailand." *Industrial health* 42(2): 135-140.
- [3] Papazoglou, I. A. and O. Aneziris (1999). "On the quantification of the effects of organizational and management factors in chemical installations." *Reliability Engineering & System Safety* 63(1): 33-45
- [4] Stranks, J. W. (1994). *The handbook of health and safety practice*, Financial Times Management.
- [5] Garavan, T. N. and F. O'Brien (2001). "An investigation into the relationship between safety climate and safety behaviours in Irish organisations." *Irish Journal of Management* 22(1): 141.
- [6] Petersen, D. (1984). "Human-error reduction and safety management."
- [7] Sawacha, E., S. Naoum, et al. (1999). "Factors affecting safety performance on construction sites." *International Journal of Project Management* 17(5): 309-315.
- [8] Vredenburg, A. G. (2002). "Organizational safety: which management practices are most effective in reducing employee injury rates?" *Journal of Safety Research* 33(2): 259-276.
- [9] Sobh, R. and C. Perry (2006). "Research design and data analysis in realism research." *European Journal of marketing* 40(11/12): 1194-1209.
- [10] Osborn, R., J. Olson, et al. (1983). *Organizational analysis and safety for utilities with nuclear power plants: perspectives for organizational assessment. Volume 2.*[PWR; BWR], Pacific Northwest Lab., Richland, WA (USA)
- [11] Jacobs, R. and S. Haber (1994). "Organizational processes and nuclear power plant safety." *Reliability Engineering & System Safety* 45(1): 75-83
- [12] Cox, S. and R. Flin (1998). "Safety culture: philosopher's stone or man of straw?" *Work & Stress* 12(3): 189-201.
- [13] Sorensen, J. (2002). "Safety culture: a survey of the state-of-the-art." *Reliability Engineering & System Safety* 76(2): 189-204.

- [14] Jitwasinkul, B. and B. H. Hadikusumo (2011). "Identification of Important Organisational Factors Influencing Safety Work Behaviours in Construction Projects." *Journal of civil engineering and management* 17(4): 520-528.
- [15] Parker, S. K., C. M. Axtell, et al. (2001). "Designing a safer workplace: importance of job autonomy, communication quality, and supportive supervisors." *Journal of Occupational Health Psychology* 6(3): 211
- [16] Choudhry, R. M. and D. Fang (2008). "Why operatives engage in unsafe work behavior: Investigating factors on construction sites." *Safety Science* 46(4): 566-584
- [17] Gibson, C. H. (1991). "A concept analysis of empowerment." *Journal of advanced nursing* 16(3): 354-361.
- [18] Wilkinson, A. (1998). "Empowerment: theory and practice." *Personnel Review* 27(1): 40-56
- [19] Niehoff, B. P., C. A. Enz, et al. (1990). "The impact of top-management actions on employee attitudes and perceptions." *Group & Organization Management* 15(3): 337-352.
- [20] Reed, T. K. (1996). "A new understanding of " followers" as leaders: emerging theory of civic leadership." *Journal of Leadership & Organizational Studies* 3(1): 95-104
- [21] Sigurdsson, J., L. Walls, et al. (2001). "Bayesian belief nets for managing expert judgement and modelling reliability." *Quality and Reliability Engineering International* 17(3): 181-190
- [22] Christian, J. and C. J. Armitage (2002). "Attitudes and intentions of homeless people towards service provision in South Wales." *British Journal of Social Psychology* 41(2): 219-231.
- [23] Johnson, J. A., D. L. Musial, et al. (2005). "INTRODUCTION TO THE FOUNDATIONS OF AMERICAN EDUCATION, 13/e."
- [24] Armitage, C. J. and M. A. Arden (2002). "Exploring discontinuity patterns in the transtheoretical model: An application of the theory of planned behaviour." *British journal of health psychology* 7(1): 89-103.
- [25] Armitage, C. J. and M. Conner (2001). "Efficacy of the theory of planned behaviour: A meta-analytic review." *British Journal of Social Psychology* 40(4): 471-499.



Sustainable Civil Engineering Structures and Construction Materials, SCESCM 2016

Numerical study on lateral-torsional buckling of honeycomb beam

DannyGunawan^a, Bambang Suryoatmono^{b,*}

^a*Departement of Civil Engineering, Tarumanagara University, Jakarta, Indonesia*

^b*Department of Civil Engineering, Parahyangan Catholic University, Bandung, Indonesia*

Abstract

A honeycomb beam is a non-prismatic wide flange beam with constant spaced hexagonal holes throughout its length. Most design codes, including Specification for Structural Steel Buildings (ANSI/AISC 360-10) do not provide provisions for lateral-torsional buckling of non-prismatic beam. In this paper, lateral-torsional buckling of honeycomb beam is studied numerically using finite element analysis (FEA). Nonlinear time history analysis is performed to simulate the behavior of the beam loaded perpendicular to its major axis gradually from zero until lateral-torsional buckling occurs. Two loading conditions are considered, namely concentrated and uniformly distributed loads. Nonlinear behavior of steel material and the presence of residual stress in the beam are considered in the analysis. The beam is assumed to be simply supported and laterally supported at both ends so that the unbraced length of the beam is the same as the beam length. Honeycomb beams with various dimensions and various unbraced length are analyzed. The lateral-torsional buckling moments obtained from finite element analyses are compared with those computed using equations in ANSI/AISC 360-10 assuming the beams were prismatic without any holes. Based on this comparison, simplified equations to predict lateral-torsional buckling moments or LTB strength of honeycomb beams under major axis bending are proposed in this paper.

© 2017 The Authors. Published by Elsevier Ltd.

Peer-review under responsibility of the organizing committee of SCESCM 2016.

Keywords: honeycomb beam; non-prismatic; lateral-torsional buckling; residual stress; nonlinear time history analysis

1. Introduction

The use of honeycomb or castellated beam in steel structure increases recently, The presence of holes in such beam makes it lighter compared to an I beam of the same dimension. However, the analysis of such section,

* Corresponding author. Tel.: +62-222-033-691; fax: +62-222-031-110.

E-mail address: suryoatm@unpar.ac.id

especially to obtain lateral-torsional buckling (LTB) strength is difficult due to its non-prismatic nature. Gandomi and others [1] have developed a prediction model for the load capacity of honeycomb steel beams based on a reliable database. The model relates the load capacity to the geometrical and mechanical properties of the honeycomb beams. In the present study, a different approach has been developed. Nonlinear time history finite element analyses were conducted to obtain the lateral-torsional buckling strength of honeycomb beams. Assuming the beams were prismatic without any holes, other analyses were conducted in accordance to standard procedure, namely ANSI/AISC 360-10 [2]. The honeycomb reduction factors are then proposed based on those two analyses.

2. Lateral-torsional Buckling of Prismatic Member

If a beam is bent about its major axis, lateral-torsional buckling (LTB) may occur. During LTB, the beam not only deflects in transverse direction, but also deforms in lateral direction accompanied by torsion of the cross section. As seen in Fig. 1, to increase the bending moment that cause LTB, M_n , one possible measure is by reducing the distance between the beam lateral supports L_b . According to AISC 360-10 [2], nominal LTB strength M_n of a compact wide flange beam are determined as follows:

$$M_n = M_p \text{ when } L_b \leq L_r \tag{1}$$

$$M_n = \min \left(C_b \left[M_p - (M_p - 0.7S_x F_y) \frac{L_b - L_p}{L_r - L_p} \right] \text{ and } M_p \right) \text{ when } L_p < L_b \leq L_r \tag{2}$$

$$M_n = \min(F_{cr} S_x \text{ and } M_p) \text{ when } L_b > L_r \tag{3}$$

where

$$F_{cr} = C_b \frac{\pi^2 E}{\left(\frac{L_b}{r_{ts}}\right)^2} \sqrt{1 + 0.078 \frac{J}{S_x h_0} \left(\frac{L_b}{r_{ts}}\right)^2} \tag{4}$$

$$r_{ts}^2 = \frac{I_y h_0}{2S_x} = \frac{\sqrt{I_y C_w}}{S_x} \tag{5}$$

The limiting lengths L_p and L_r (see Fig. 1) are computed using

$$L_p = 1.76 r_y \sqrt{\frac{E}{F_y}} \tag{6}$$

$$L_r = 1.95 r_{ts} \frac{E}{0.7 F_y} \sqrt{\frac{J}{S_x h_0} + \sqrt{\left(\frac{J}{S_x h_0}\right)^2 + 6.76 \left(\frac{0.7 F_y}{E}\right)^2}} \tag{7}$$

Material properties used in ANSI/AISC 360-10 procedure are modulus of elasticity E and specified minimum yield stress F_y . Section properties employed in Eqs. (2) to (7) are torsional constant J , warping constant C_w , radius of gyration about y -axis r_y , elastic section modulus about the x -axis S_x , effective radius of gyration r_{ts} , and distance between the flange centroids h_0 ,

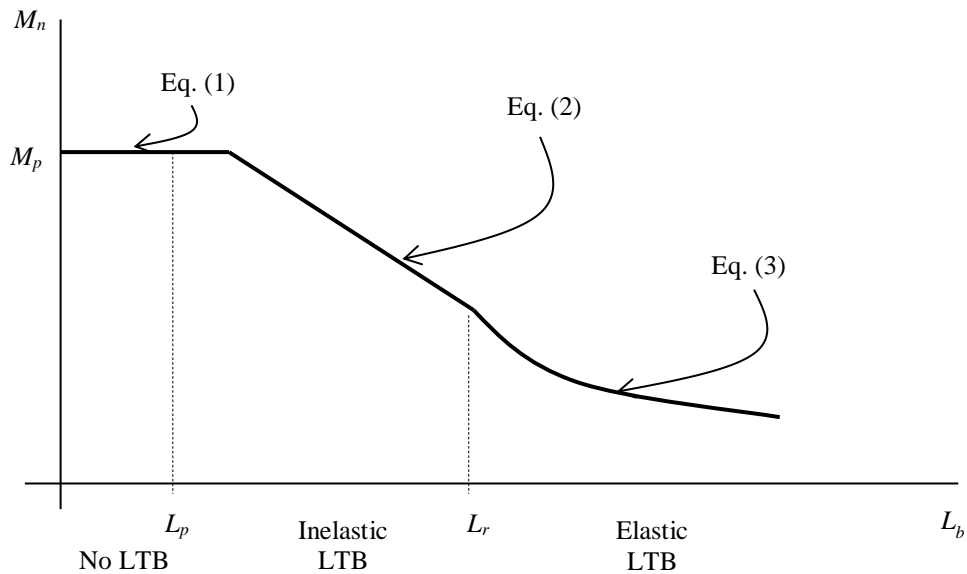


Fig. 1. Lateral-torsional buckling strength M_n of a beam subjected to bending about its major axis.

In this paper, a beam with lateral supports at its ends are studied. Two different loading conditions are considered, namely concentrated load at midspan and uniformly distributed load. For these two loading conditions, the lateral-torsional buckling modification factor for nonuniform moment diagrams C_b are 1.32 and 1.14, respectively [3].

3. Finite element model

To perform finite element analysis (FEA), the SAP2000 version 15 was employed. The analyses were both material and geometry nonlinear. The four-node quadrilateral shell elements and three nodes triangular shell elements were used in FEA. Shell element was chosen because this type of element can model both membrane and bending behaviors [5]. Fig. 2 shows the typical finite element mesh in the analyses along with LTB deformation. The boundary conditions were set in accord with the derivation of Eq. (3), namely both ends were transversely supported at neutral axes, both ends could rotate about lateral axis, and both ends were restrained against torsion [6].

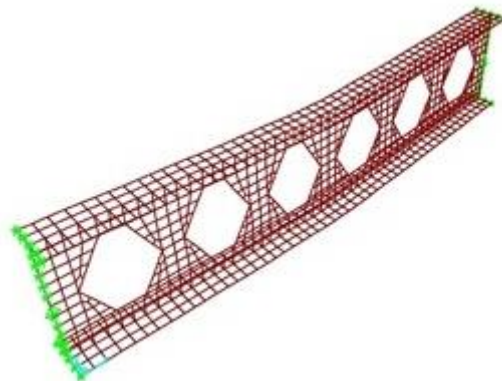


Fig. 2. Typical finite element mesh in FEA along with LTB deformation.

Two separate loading conditions were performed. One was concentrated load P applied on top flange as line load along the flange width, and the other one was uniformly distributed load w applied at top flange in the web plane. These loads were applied quasi-statically to simulate loadings in a testing laboratory. Before applying transverse loads, very small uniformly distributed lateral static loads were applied at top flange to activate lateral degree of freedom of the beam. Plot of transverse load versus lateral displacement of centerline at midspan was obtained for each FEA. The typical plot is shown in Fig. 3. The loads causing LTB were taken as the maximum loads from the plots. From simple statics, bending moment that cause LTB were computed using $M_n = \frac{1}{4}PL$ for concentrated load and $M_n = \frac{1}{8}wL^2$, where L is the beam span.

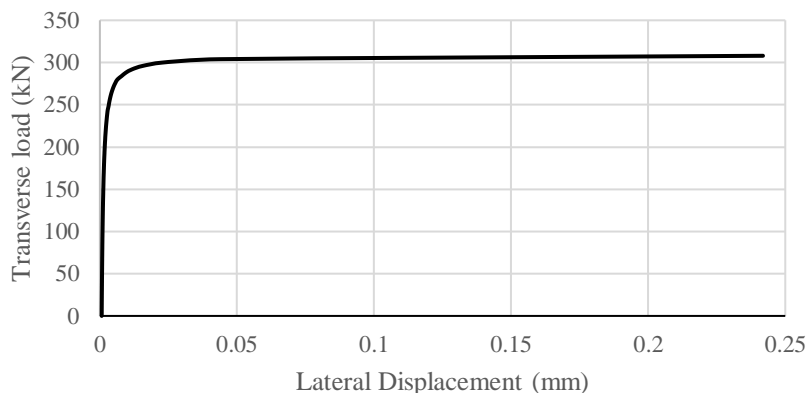


Fig. 3. Typical plot of transverse load versus lateral displacement of centerline at midspan as a result of nonlinear FEA

In hot-rolled sections, residual stress always exists due to rolling process. Therefore, in analysis of hot-rolled sections, including honeycomb, the presence of residual stress needs to be considered. In the FEA in this paper, the distribution of residual stress in honeycomb beam section was as seen in Figure 4. The maximum compressive residual stress f_{rc} at each flange tip was assumed to be $0.3F_y$. In Fig. 4(a) the tensile residual stress was such that the resultant of tension and compression stresses were zero. In a cross section with a hole as seen in Fig. 4(b), no residual stress was present in the web so the maximum tensile residual stress was the same as the maximum compressive residual stress.

Material behavior in FEA was assumed to be elastic perfectly plastic with yield stress $F_y = 240$ MPa. The presence of residual stress in the cross section was accounted for by modifying the yield stress of the material [4]. In the flange tip where the compressive residual stress was 72 MPa, for example, the modified compressive yield stress was 168 MPa and the modified tensile yield stress was 312 MPa.

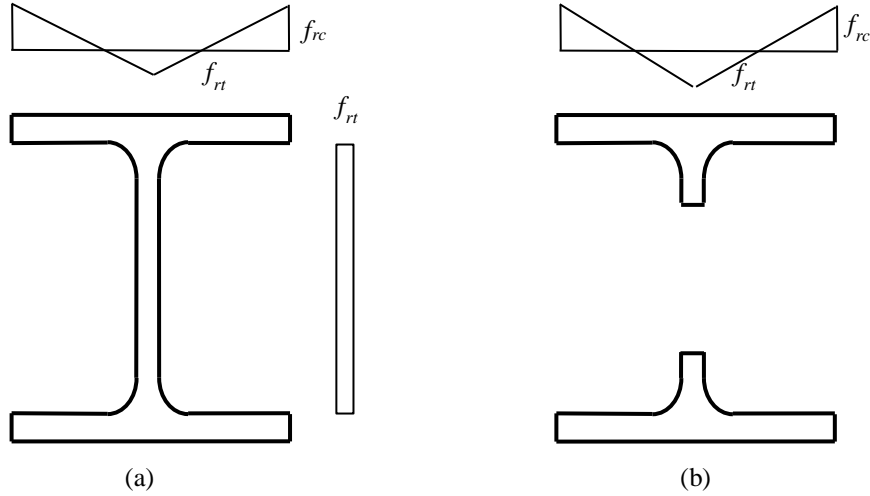


Fig. 4. Residual stress distribution in honeycomb, (a) in a cross section without hole, (b) in a cross section with hole.

4. Analysis results and discussion

Five honeycomb sections, namely HC 300, HC 450, HC 600, HC 750, and HC 900, with various laterally unbraced length L_b , were analyzed using nonlinear time history FEA described above to obtain LTB strength denoted as $(M_{nFEA})_{HC}$. Assuming there were no holes in the honeycomb beams, the LTB strengths for various L_b were computed using ANSI/AISC 360-10 procedure. These are denoted as $(M_{nAISC})_{prismatic}$. The results are shown in Fig. 5(a) for concentrated load case and Fig. 5(b) for uniformly distributed load case. It is obvious that the presence of holes reduces the LTB strength. If the honeycomb reduction factor is denoted by C_{HC} , then

$$C_{HC} = \frac{(M_{nFEA})_{HC}}{(M_{nAISC})_{prismatic}} \quad (8)$$

As seen in Fig. 5, the honeycomb reduction factor C_{HC} depends on both laterally unbraced length L_p and loading conditions. It is, therefore, two different regression functions are proposed in this study, one is for concentrated load case, and the other one is for uniformly distributed load case. To be on the safe side, the lowest values of C_{HC} in Fig. 5 were used in order to obtain the regression functions. The data along with the regression functions are shown in Fig. 6. For simply supported honeycomb beam laterally supported at both ends and loaded at midspan, the honeycomb reduction factor can be computed as a function of laterally unbraced length L_b using

$$C_{HC} = -0.0221 \left(\frac{L_b}{(L_p)_{prismatic}} \right)^3 + 0.2036 \left(\frac{L_b}{(L_p)_{prismatic}} \right)^2 - 0.338 \frac{L_b}{(L_p)_{prismatic}} + 0.2968 \quad (9)$$

where $(L_p)_{prismatic}$ is the limiting unbraced length for the limit state of yielding of the honeycomb beam neglecting the presence of holes. The similar function for uniformly distributed load is

$$C_{HC} = -0.0342 \left(\frac{L_b}{(L_p)_{prismatic}} \right)^3 + 0.3757 \left(\frac{L_b}{(L_p)_{prismatic}} \right)^2 - 1.015 \frac{L_b}{(L_p)_{prismatic}} + 0.8867 \quad (10)$$

The coefficient of determination r^2 for Eq. (9) and Eq. (10) are 0.9883 and 0.9969, respectively. This means that both equations are very close to the data used in the regression process.

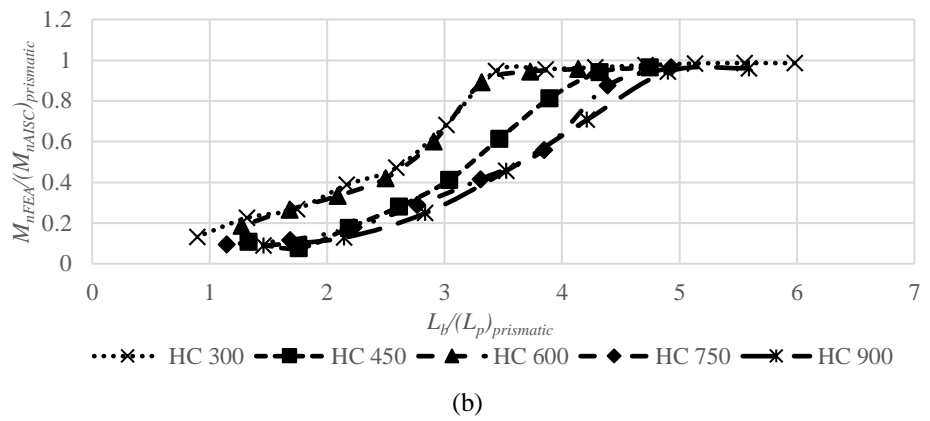
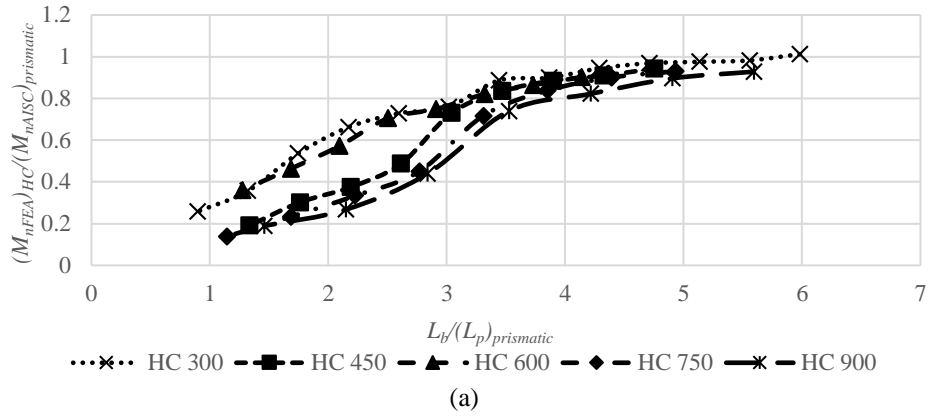
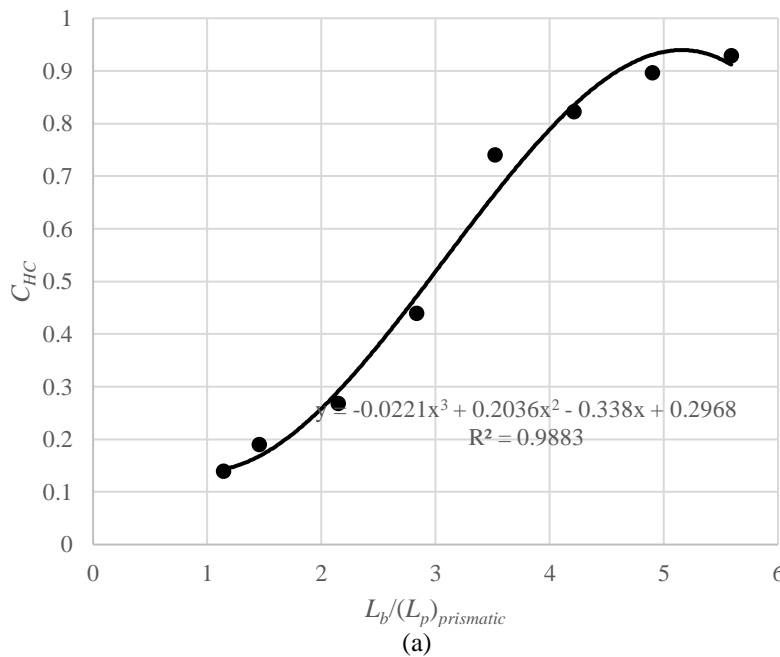


Fig. 5. Plot of $L_b/(L_p)_{prismatic}$ versus $M_{nFEA}/(M_{nAISC})_{prismatic}$ for (a) concentrated load case, and (b) uniformly distributed load case.



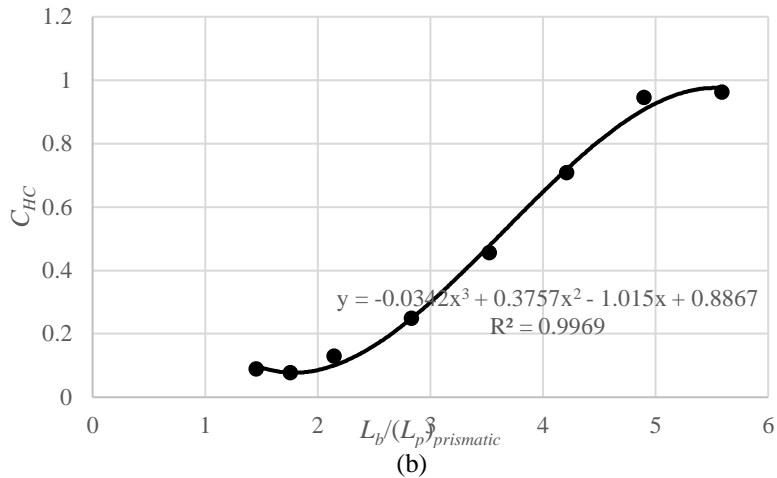


Fig. 6. Regression functions and data used to obtain the functions for (a) concentrated load case, and (b) uniformly distributed load case.

5. Conclusion

It can be concluded that nonlinear time history FEA can be used to model LTB of a honeycomb beam bent about its major axis considering both residual stress and material nonlinearity. To obtain LTB strength, the procedure in ANSI/AISC 360-10 can be used by assuming that the beam were prismatic without any hole and then applying honeycomb reduction factor because the beam actually has holes. This factor is smaller for shorter laterally unbraced length and depends on loading conditions. When laterally unbraced length L_b is six times the limiting unbraced length for the limit state of yielding $(L_p)_{prismatic}$ or more, the honeycomb reduction factor is very close to 1.0. This means that in that case the procedure in ANSI/AISC 360-10 can be used to obtain LTB strength of honeycomb beam neglecting the presence of holes. It should be noted, however, that the honeycomb reduction factor can be as low as 0.10 for very short laterally unbraced length L_b .

Acknowledgements

The authors wish to thank the Department of Civil Engineering, Parahyangan Catholic University for facilitating the finite element software that was employed in this numerical study.

References

- [1] A. H. Gandomi, et al., A new prediction model for the load capacity of castellated steel beams, J. of Constructional Steel Research 67(7), 1096-1105.
- [2] AISC, Specification for Structural Steel Buildings, ANSI/AISC 360-10, American Institute of Steel Construction, Chicago, Illinois, 2010.
- [3] W.T. Segui, Steel Design, Fifth ed., Cengage Learning, Stanford, 2012.
- [4] T.V Galambos and A.E. Surovek, Structural Stability of Steel, John Wiley & Sons, New Jersey, 2008.
- [5] CSI, Analysis reference manual for SAP2000, ETABS, SAFE and CSiBridge, Computers and Structures, Berkeley, California, 2013.
- [6] J.C. McCormac, S.F. Csernak, Structural Steel Design, fifth ed., Prentice-Hall, New Jersey, 2012.



Sustainable Civil Engineering Structures and Construction Materials, SCESCM 2016

Post-buckling behaviour of axially FGM planar beams and frames

Buntara Sthenly Gan^{a,*}, Trinh Thanh Huong^a, Nguyen Dinh Kien^b

^aDepartment of Architecture, College of Engineering, Nihon University, 1 Nakagawara, Koriyama, Fukushima 963-8642, Japan

^bDepartment of Solid Mechanics, Institute of Mechanics, Vietnam Academy of Science and Technology, 18 Hoang Quoc Viet, Hanoi, Vietnam

Abstract

Post-buckling analysis of planar beams and frames made of axially Functionally Graded Material (FGM) by using the finite element method is presented. The material property of the beams is assumed to vary linearly along the axis of beam direction. A non-linear beam element based on Timoshenko beam theory is formulated in the context of the co-rotational formulation. The non-linear equilibrium equations are solved by using the incremental/iterative procedure in combination with the arc-length control method. The obtained results are compared with the published references to verify the accuracy of the proposed formulation and the numerical procedure. The effect of the material distribution on the post-buckling response of the axially FGM structures is highlighted.

© 2017 The Authors. Published by Elsevier Ltd.

Peer-review under responsibility of the organizing committee of SCESCM 2016.

Keywords: Axially FGM; Large displacement analysis; Planar beam and frame structures; Finite element method

1. Introduction

The post-buckling behaviour of planar beams and frames is very important information for design engineers. Establishing equilibrium paths is the most common way of understanding the structures' behaviour in the post-buckling state. However, a major difficulty is the geometric nonlinearity when the structures undergo large displacement. Due to this challenge, it is difficult to analyse the post-buckling problem using analytical methods, and a numerical method, especially the finite element method, is often employed instead. In order to analyse the large displacements of the structures by the finite element method, a nonlinear finite element which makes it possible to model the nonlinear behaviour of the structures accurately is required. Many nonlinear finite elements in general and

* Corresponding author. Tel.: +81-(0)24-956-8735

E-mail address: buntara@arch.ce.nihon-u.ac.jp

beam elements in particular are available in the literature, some of which have been documented in well-known textbooks [1,2]. The nonlinear beam elements can be classified into three types, namely the total Lagrange formulation, the updated Lagrange formulation, and the co-rotational formulation [3]. In the co-rotational formulation which will be adopted in this article, the kinematics is described in an element-attached local coordinate system. The finite element formulation is firstly formulated in this local system and then transferred to a global system with the aid of transformation matrices. Among others, the elements proposed by Hsiao and Huo [4], Meek and Xue [5], Pacoste and Eriksson [6], and Nguyen [7] are some of the co-rotational beam elements for analysis of planar beams and frames which can be cited herewith.

Functionally graded material (FGM) has received great interest from many researchers and engineers for a long time because of its wide range of applications in structural mechanics. FGMs, which were introduced by Japanese scientists in 1984, can be formed by varying the percentage of constituents in any desired direction in order to create new materials with specific physical and mechanical properties [8]. The newly created materials have then been employed in many fields such as space projects, energy sectors, communication projects, defense industries, biomedicine, and miscellaneous others. Many investigations of FGM structures are available in the literature, and only contributions that are most relevant to the present work are discussed below. Trinh and Gan [9] developed a consistent shape function for a linearly solid tapered Timoshenko beam. Shahba et al. [10,11] employed the exact shape functions from a uniform homogenous Timoshenko beam segment to formulate a finite element formulation for computing natural frequencies and buckling loads of tapered axially FGM beams. Nguyen [12], Nguyen and Gan [13], and Nguyen et al. [14] derived the finite element formulation for studying the large displacement behaviour of FGM beams and frames. From the literature review, there exist many investigations of FGM beams and frames in the thickness direction; however, researches on the post-buckling analysis (with large displacement taken into account) of axially FGM structures are still limited. This paper aims to contribute research on the geometric nonlinearity in analysing the post-buckling behavior of axially FGM structures to the existing literature.

The present article investigates the post-buckling response of planar beams and frames made of axially FGM by using the finite element method. The material properties of the structures are assumed to vary linearly in the axial direction. A shear deformable nonlinear beam element, taking into account the effect of the material non-homogeneity, is formulated in the context of the co-rotational formulation. A consistent formulation of shape functions for a Timoshenko beam section made of axially FGM is derived based on the Hamilton principle. An incremental/iterative procedure in combination with the arc-length control method is employed to compute equilibrium paths. Numerical examples are given to demonstrate the accuracy and efficiency of the formulated element and to examine the effect of the material non-homogeneity on the instability behaviour of the structures.

2. Consistent shape functions for axially FGM beam element

2.1. Problem definition

In the Bernoulli-Euler beam, the cross-section of the beam is assumed to remain straight against the axis after it has deformed; hence no shear deformation is taken into account. Hence, the resulting shape functions contain only the length information of the beam inside the polynomial forms. For a short beam where the shearing deformation is a dominant factor for getting an accurate result, the Bernoulli-Euler beam is not recommended. Therefore, the Timoshenko beam has to be considered.

Reference [15] derived the shape functions for the Timoshenko beam (Fig. 1) by using Hamilton's principle to satisfy the homogeneous form of the static equations of equilibrium as

$$\frac{\partial}{\partial x} \left(EA \frac{\partial u}{\partial x} \right) = 0, \quad \frac{\partial}{\partial x} \left(\kappa AG \left(\frac{\partial w}{\partial x} - \theta \right) \right) = 0, \quad \frac{\partial}{\partial x} \left(EI \frac{\partial \theta}{\partial x} \right) + \kappa AG \left(\frac{\partial w}{\partial x} - \theta \right) = 0. \quad (1)$$

where A and I are the beam cross-section of the area and the area moment of inertia, respectively, E and G are the Young's and shear moduli of the beam material, respectively, and κ is the shear coefficient of the cross-section

geometry. The resulting common and widely used shape functions for a Timoshenko beam considering shear deformation can be obtained as

$$\left. \begin{aligned} N_{u1} &= \frac{l-x}{l}, \\ N_{u2} &= \frac{x}{l}, \\ \phi &= \frac{12}{l^2} \frac{E_0 I}{\kappa G_0 A} \end{aligned} \right\} \left\{ \begin{aligned} N_{w1} &= \frac{1}{1+\phi} \left[2\left(\frac{x}{l}\right)^3 - 3\left(\frac{x}{l}\right)^2 - \phi\left(\frac{x}{l}\right) + (1+\phi) \right] \\ N_{w2} &= \frac{l}{1+\phi} \left[\left(\frac{x}{l}\right)^3 - \left(2+\frac{\phi}{2}\right)\left(\frac{x}{l}\right)^2 + \left(1+\frac{\phi}{2}\right)\left(\frac{x}{l}\right) \right] \\ N_{w3} &= -\frac{1}{1+\phi} \left[2\left(\frac{x}{l}\right)^3 - 3\left(\frac{x}{l}\right)^2 - \phi\left(\frac{x}{l}\right) \right] \\ N_{w4} &= \frac{l}{1+\phi} \left[\left(\frac{x}{l}\right)^3 - \left(1-\frac{\phi}{2}\right)\left(\frac{x}{l}\right)^2 - \frac{\phi}{2}\left(\frac{x}{l}\right) \right] \end{aligned} \right\}, \left\{ \begin{aligned} N_{\theta1} &= \frac{6}{(1+\phi)l} \left[\left(\frac{x}{l}\right)^2 - \left(\frac{x}{l}\right) \right] \\ N_{\theta2} &= \frac{1}{1+\phi} \left[3\left(\frac{x}{l}\right)^2 + (4+\phi)\left(\frac{x}{l}\right) + (1+\phi) \right] \\ N_{\theta3} &= -\frac{6}{(1+\phi)l} \left[\left(\frac{x}{l}\right)^2 - \left(\frac{x}{l}\right) \right] \\ N_{\theta4} &= \frac{1}{1+\phi} \left[3\left(\frac{x}{l}\right)^2 - (2-\phi)\left(\frac{x}{l}\right) \right] \end{aligned} \right\} \quad (2)$$

where l is the element length, ϕ is the ratio of beam bending stiffness to shear stiffness, A and I are the cross-section area and moment of inertia of the uniform beam, E_0 and G_0 are the Young's and shear moduli of the material at the left end of the FGM beam, while $[N_{u1} \ N_{u2}]$, $[N_{w1} \ N_{w2} \ N_{w3} \ N_{w4}]$, and $[N_{\theta1} \ N_{\theta2} \ N_{\theta3} \ N_{\theta4}]$ are the nodal axial, transverse displacement, and rotational shape functions of the beam.

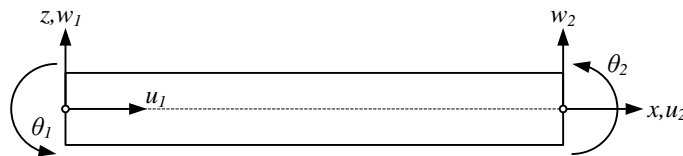


Fig. 1. Two-node six-degrees-of-freedom beam element

It can be observed that Eq. (2) is the predefined shape functions for homogeneous material (constant E) and uniform cross-section (constant A) of a Timoshenko beam. However, up to now, the shape functions have been widely used to derive the stiffness and mass matrices for Timoshenko beams with inherent inhomogeneity and nonuniformity. Hence, it is obvious that the behaviour of beams is inaccurately predicted in the analyses, and to solve this problem, quite a large number of beam divisions are required. Thus, unnecessary and unreasonable efforts are often made without understanding the nature of the problem. This problem can only be solved by using consistent and correct shape functions for the inhomogeneous Timoshenko beam element.

2.2. Consistent shape functions

A beam with length l and a rectangular cross-section and made of two different materials functionally graded along the beam axis is considered. The effective property P (representing the Young's modulus or shear modulus) of the beam materials is assumed to vary linearly in the beam axis as

$$P(x) = P_0 \left(1 + \frac{n-1}{l} x \right) \quad (3)$$

where P_0 represents the effective properties at $x=0$ of the beam and n is the ratio between the effective properties at both ends.

Nonhomogeneous axially FGM beams with Young's modulus of the beams vary as follows:

$$E(x) = E_0 \left(1 + \frac{x}{\ell} \right) \tag{4}$$

where $E(x)$ is the first order ($n = 2$) with respect to x . In this paper, Eq. (4) will be used for numerical verifications and examples.

Integrating the first term of Eq. (1) and solving for $u(x)$ results in

$$u(x) = \frac{1}{A} \int \frac{k_1}{E(x)} dx + k_2 = k_2 + \frac{k_1 \ell \ln[\ell + (-1+n)x]}{AE_0(-1+n)} \tag{5}$$

where k_l is an integration constant.

By applying the boundary conditions at both end nodes of the beam, where $u(x = 0) = u_1$ and $u(x = \ell) = u_2$, solving for k_1 and k_2 , and then substituting the result back into Eq. (5), the shape functions for the axial displacement of the beam can be obtained as

$$u(x) = \mathbf{N}_u = [N_{u1} \quad N_{u2}] \begin{Bmatrix} u_1 \\ u_2 \end{Bmatrix} \tag{6}$$

where $N_{u1} = \frac{(\ell - x)(\ell + n\ell + x - nx)}{\ell^2(1+n)}$; $N_{u2} = \frac{x(2n\ell + x - nx)}{\ell^2(1+n)}$.

It can be observed that the integration of the second term in Eq. (1) is encapsulated in the third term of Eq. (1). Hence, the transverse displacement $w(x)$ should be one order higher than the rotation $\theta(x)$ of the beam. Here, the transverse displacement and rotation fields can be expressed in polynomial equations as follows:

$$\begin{aligned} \theta(x) &= b_0 + b_1x + b_2x^2 \\ w(x) &= a_0 + a_1x + a_2x^2 + a_3x^3. \end{aligned} \tag{7}$$

After substituting Eq. (7) into the second and third terms of Eq. (1), the polynomial coefficients $b_0, b_1, b_2, a_0, a_1, a_2$ and a_3 in Eq. (7) are then represented by the integration constants c_1, c_2, c_3, c_4 , resulting in the rotational and transverse displacement equations as follows:

$$\theta(x) = -\frac{c_1}{I} \int \frac{xdx}{E(x)} + \frac{c_2}{I} \int \frac{dx}{E(x)} + c_3, \quad w(x) = \int \theta(x)dx + \frac{c_1}{\kappa A} \int \frac{1}{G(x)} dx + c_4 \tag{8}$$

The boundary conditions $w(x = 0) = w_1; \theta(x = 0) = \theta_1; w(x = \ell) = w_2; \theta(x = \ell) = \theta_2$ are applied to Eq. (8), solving for c_1, c_2, c_3, c_4 and then substituting the result back into Eq. (8). Here, this resulted in some natural logarithmic terms in Eq. (8), which leads to infinity when a homogeneous condition is imposed. To eliminate this problem, a cubic order Taylor series expansion scheme is used for representing the natural logarithmic terms in Eq. (8), which results in

$$w(x) = \mathbf{N}_w = [N_{w1} \quad N_{w2} \quad N_{w3} \quad N_{w4}] \begin{Bmatrix} w_1 \\ \theta_1 \\ w_2 \\ \theta_2 \end{Bmatrix}; \quad \theta(x) = \mathbf{N}_\theta = [N_{\theta1} \quad N_{\theta2} \quad N_{\theta3} \quad N_{\theta4}] \begin{Bmatrix} w_1 \\ \theta_1 \\ w_2 \\ \theta_2 \end{Bmatrix} \tag{9}$$

where

$$\begin{cases}
 N_{w1} = \frac{(\ell - x)(3(1+n)^2(\ell - x)(\ell + 2x) + (4\ell^2(1+n+n^2) + \ell(1+(4-5n)n)x + 4(n-1)^2x^2)\phi)}{(\ell^3(3(1+n)^2 + (4(1+n+n^2))\phi))} \\
 N_{w2} = \frac{(\ell - x)x(3(1+n)^3(\ell - x) + (\ell(2+n(7+n(2+n))) - (4(n-1))x)\phi)}{(\ell^2(3(1+n)^3 + (4(1+n))(1+n+n^2)\phi))} \\
 N_{w3} = \frac{x(3(1+n)^2(3\ell - 2x)x + (\ell^2(3+9n^2) - 3\ell(n-1)(-1+3n)x + 4(n-1)^2x^2)\phi)}{(\ell^3(3(1+n)^2 + (4(1+n+n^2))\phi))} \\
 N_{w4} = \frac{-\ell(\ell - x)x(3(1+n)^3x + \ell(1+2n)(1+3n^2)\phi - (4(n-1))n^2x\phi)}{(\ell^2(3(1+n)^3 + (4(1+n))(1+n+n^2)\phi))} \\
 N_{\theta1} = \frac{-18(1+n)^2(\ell - x)x}{(\ell^3(3(1+n)^2 + (4(1+n+n^2))\phi))} \\
 N_{\theta2} = \frac{(\ell - x)(3(1+n)^3(\ell - 3x) + (4(1+n+n^2))(\ell + n\ell + x - nx)\phi)}{\ell^2(3(1+n)^3 + (4(1+n))(1+n+n^2)\phi)} \\
 N_{\theta3} = \frac{18(1+n)^2(\ell - x)x}{\ell^3(3(1+n)^2 + (4(1+n+n^2))\phi)} \\
 N_{\theta4} = \frac{3(1+n)^3x(-2\ell + 3x) + (4(1+n+n^2))x(2n\ell + x - nx)\phi}{\ell^2(3(1+n)^3 + (4(1+n))(1+n+n^2)\phi)}
 \end{cases}$$

in which $\phi = \frac{12}{l^2} \frac{E_0 I}{\kappa G_0 A}$ with E_0 and G_0 being the Young's and shear moduli of the material at $x = 0$ of the FGM beam axis. It can be shown that for homogeneous material ($n = 1$), both the transverse and rotational shape functions in Eq. (9) become Eq. (2). It should be noted that in these consistent shape functions given by Eq. (9), the influence of the effective properties ratio, n , is reflected.

3. Finite element formulation

3.1. Global formulation

The co-rotational approach is a convenient way to formulate geometrically nonlinear finite elements in the global coordinate system. The central idea of the approach is to introduce a local coordinate system that continuously moves and rotates with the element during its deformation process. By using such a local system, the element deformation can be decomposed into a rigid body and pure deformation parts, and the geometric nonlinearity induced by the large body motion is incorporated in the transformation matrices. The element formulation is firstly formulated in the local system and then transferred into the global system with the aid of the transformation matrices. The main points of the co-rotational approach summarized below are closely related to the formulation described by Crisfield [3], and the formulation has been further developed by Pacoste and Eriksson [6] and Nguyen [7].

Figure 2 shows a two-node planar beam element and its kinematics in a global coordinate system (X,Z) . A local system (x,z) attached to the element is chosen; its origin is always at node 1 and its x -axis is directed to node 2. By choosing such a local system, the axial displacement at node 1 and the transverse displacement at both of the two nodes in the local system are always zero.

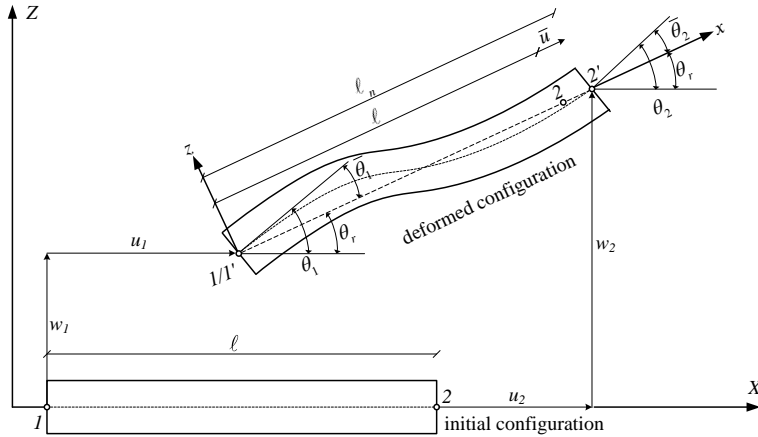


Fig. 2. A planar co-rotational beam element and its kinematics.

The local and global nodal displacement vectors are respectively given by

$$\bar{\mathbf{d}} = \{\bar{u} \quad \bar{\theta}_1 \quad \bar{\theta}_2\}^T, \quad \mathbf{d} = \{u_1 \quad w_1 \quad \theta_1 \quad u_2 \quad w_2 \quad \theta_2\}^T. \quad (10)$$

In Eq. (10) and hereafter, the superscript T denotes the transpose of a vector or a matrix and the bar is used to indicate that the variable is defined in the local system.

The vectors of nodal forces and moments associated with the nodal displacements of Eq. (10) are as follows:

$$\bar{\mathbf{f}}_{in} = \{\bar{N} \quad \bar{M}_1 \quad \bar{M}_2\}^T, \quad \mathbf{f}_{in} = \{N_1 \quad Q_1 \quad M_1 \quad N_2 \quad Q_2 \quad M_2\}^T. \quad (11)$$

The components of the local vector in Eq. (10) can be obtained from $\bar{u} = \ell_n - \ell$; $\bar{\theta}_1 = \theta_1 - \theta_r$; $\bar{\theta}_2 = \theta_2 - \theta_r$.

In Eq. (11), ℓ , ℓ_n and θ_r are the initial length, current length, and rigid rotation of the element, respectively, and can be computed from the coordinates of the nodes. Assuming that the strain energy U of the element has been derived, the element nodal force vector \mathbf{f}_{in} and the tangent stiffness matrix \mathbf{k}_t in the global system can be obtained by successive differentiation of the strain energy with respect to the nodal displacements:

$$\mathbf{f}_{in} = \frac{\partial U}{\partial \mathbf{d}} = \frac{\partial U}{\partial \bar{\mathbf{d}}} \frac{\partial \bar{\mathbf{d}}}{\partial \mathbf{d}} = \mathbf{T}_1^T \bar{\mathbf{f}}_{in}, \quad \mathbf{k}_t = \frac{\partial^2 U}{\partial \mathbf{d}^2} = \frac{\partial}{\partial \mathbf{d}} \left(\frac{\partial U}{\partial \bar{\mathbf{d}}} \frac{\partial \bar{\mathbf{d}}}{\partial \mathbf{d}} \right) = \mathbf{T}_1^T \bar{\mathbf{k}}_t \mathbf{T}_1 + \bar{N} \mathbf{T}_2 + (\bar{M}_2 + \bar{M}_3) \mathbf{T}_3. \quad (12)$$

In Eq. (12), $\bar{\mathbf{f}}_{in}$ and $\bar{\mathbf{k}}_t$ are the local nodal force vector and tangent stiffness matrix, respectively; \mathbf{T}_1 , \mathbf{T}_2 and \mathbf{T}_3 are the transpose matrices [6], which can be computed from Eq. (13) as:

$$\mathbf{T}_1 = \frac{\partial \bar{\mathbf{d}}}{\partial \mathbf{d}}, \quad \mathbf{T}_2 = \frac{\partial^2 \bar{u}}{\partial \mathbf{d}^2}, \quad \mathbf{T}_3 = -\frac{\partial^2 \theta_r}{\partial \mathbf{d}^2} \quad (13)$$

Equations (12) and (13) completely define the element formulation provided that the local nodal force vector and tangent stiffness matrix are known.

3.2. Local formulation

Consider a two-node beam element in a local system (x, z) , where the x -axis coincides with the neutral axis. Adopting Timoshenko beam theory, the axial and transversal displacements of any arbitrary point are given by

$$u(x, z) = u_0 - z\theta(x), \quad w(x, z) = w(x) \quad (14)$$

where u_0 is the axial displacement of a point at the neutral axis; z is the distance from the considered point to the x -axis, and $\theta(x)$ is the rotation of the cross-section. The axial and shear strains are deduced from Eq. (14) as:

$$\varepsilon = u_{0,x} + \frac{1}{2}w_{,x}^2 - z\theta_{,x} = \varepsilon_m + z\chi, \quad \gamma = w_{,x} - \theta \quad (15)$$

where a comma denotes the derivative with respect to the x variable; $\varepsilon_m, \chi, \gamma$ are the membrane strain, curvature strain, and shear strain, respectively. Assuming elastic behaviour, the axial and shear stresses associated with the strains of Eq. (15) are given by

$$\sigma = E(x)\varepsilon, \quad \tau = \kappa G(x)\gamma \quad (16)$$

where $E(x)$ and $G(x)$ are the effective Young's modulus and shear modulus, respectively; κ denotes the shear correction factor, which is equal to 5/6 for a rectangular section. In order to express the displacement at an arbitrary point in terms of the nodal displacements, it is necessary to introduce shape functions for u_0, w, θ . Noting that, $\bar{u}_1 = \bar{w}_1 = \bar{w}_2 = 0$, one can write

$$u_0 = \mathbf{N}_u \bar{\mathbf{u}}, \quad w = \mathbf{N}_w \bar{\boldsymbol{\theta}}, \quad \theta = \mathbf{N}_\theta \bar{\boldsymbol{\theta}} \quad (17)$$

where $\bar{\boldsymbol{\theta}} = \{\bar{\theta}_1 \quad \bar{\theta}_2\}^T$; $\mathbf{N}_u, \mathbf{N}_w, \mathbf{N}_\theta$ are the matrices of interpolating functions for w and θ , respectively. In the present work, the consistent shape functions of Eqs. (6) and (9) are employed to interpolate for u, w, θ , respectively.

The element formulated from the above unbalanced interpolating functions does, however, suffer from membrane locking [3]. In order to avoid this problem, the membrane strain in Eq. (15) is replaced by the effective strain, and by substituting Eqs. (14), (15), and (17) into Eq. (18), one gets

$$\varepsilon_{eff} = \frac{1}{\ell} \int_0^\ell \left(u_0 + \frac{1}{2} w_{,x}^2 \right) dx = \mathbf{b}_u \bar{\mathbf{u}} + \frac{1}{2\ell} \bar{\boldsymbol{\theta}}^T \left(\int_0^\ell \mathbf{b}_w^T \mathbf{b}_w dx \right) \bar{\boldsymbol{\theta}}. \quad (18)$$

where $\mathbf{b}_u = \frac{\partial \mathbf{N}_u}{\partial x}$ and $\mathbf{b}_w = \frac{\partial \mathbf{N}_w}{\partial x}$.

Using the concept of effective strain, one can express the virtual work in the form

$$\delta U = \int_V (\sigma \delta \varepsilon_{eff} + \tau \delta \gamma) dV = \int_0^\ell (N \delta \varepsilon_{eff} + M \delta \chi + Q \delta \gamma) dx = \int_0^\ell \left\{ N b_u \delta \bar{\mathbf{u}} + [N \mathbf{e}_\theta^T + M \mathbf{b}_\theta^T + Q (\mathbf{b}_w^T - \mathbf{N}_\theta^T)] \delta \bar{\boldsymbol{\theta}} \right\} dx \quad (19)$$

where $N = E(x)A\varepsilon_{eff}$; $M = E(x)I\chi$; $Q = \psi G(x)A\gamma$; $b_u = \frac{1}{\ell}$; $\mathbf{e}_\theta = \frac{\partial \varepsilon_{eff}}{\partial \boldsymbol{\theta}}$; $\mathbf{b}_\theta = -\frac{\partial \mathbf{N}_\theta}{\partial x}$.

Equation (19) gives the components of the local internal force vector as

$$\bar{f}_u = \int_0^\ell N b_u dx; \quad \bar{f}_\theta = \int_0^\ell [N e_\theta + M b_\theta + Q(\mathbf{b}_w - \mathbf{N}_\theta)] dx \tag{20}$$

The tangent stiffness matrix in the local system can be expressed by sub-matrices as follows:

$$\bar{\mathbf{k}}_t = \begin{bmatrix} \bar{\mathbf{k}}_{uu} & \bar{\mathbf{k}}_{u\theta} \\ \bar{\mathbf{k}}_{u\theta}^T & \bar{\mathbf{k}}_{\theta\theta} \end{bmatrix} \tag{21}$$

where

$$\begin{cases} \bar{\mathbf{k}}_{uu} = \bar{f}_{u,u} = \frac{1}{\ell^2} \int_0^\ell E(x) A dx, & \bar{\mathbf{k}}_{u\theta} = \bar{f}_{u,\theta} = \frac{1}{\ell} \int_0^\ell E(x) A e_\theta^T dx, \\ \bar{\mathbf{k}}_{\theta\theta} = \bar{f}_{\theta,\theta} = \int_0^\ell \left[E(x) A e_\theta e_\theta^T + N \mathbf{B} + E(x) I \mathbf{b}_\theta \mathbf{b}_\theta^T + G(x) A \psi (\mathbf{b}_w - \mathbf{N}_\theta) (\mathbf{b}_w^T - \mathbf{N}_\theta^T) \right] dx, \end{cases} \quad \text{and} \quad \mathbf{B} = \frac{\partial \mathbf{e}_\theta}{\partial \theta}.$$

Together, the local internal force vector (Eq. (20)), the stiffness matrices (Eq. (21)), and the transformation matrices (Eqs. (12) and (13)) completely describe the element formulation in the global coordinate system.

4. Numerical procedure

The formulated element internal force vector and tangent stiffness matrix are assembled to construct the structural equilibrium equations [3], which can be written in the form

$$\mathbf{g}(\mathbf{d}, \varphi) = \mathbf{q}_{in}(\mathbf{d}) - \varphi \mathbf{f}_{ext} \tag{22}$$

where the out-of-balance force vector \mathbf{g} is a function of the current structural nodal displacements \mathbf{d} and the loading parameter φ ; \mathbf{q}_{in} is the structural nodal force vector, assembled from the element force vector \mathbf{f}_{in} ; \mathbf{f}_{ext} is the constant external loading vector.

The nonlinear equations (23) can be solved by using an incremental/iterative procedure, and in order to trace a complete equilibrium path, the arc-length control method described by Crisfield [3] is employed.

5. Numerical examples

5.1. Formulation verification

To verify the accuracy of the present formulation and the numerical procedure of the uniform homogenous Timoshenko beam and uniform axially FGM Bernoulli-Euler beam under various boundary conditions (clamped–clamped, clamped–free, and hinged–hinged) subjected to axial load $P = 1$ N, a beam with a shear correction factor $\psi = 5/6$, Poisson’s ratio $\nu = 0.3$, $E_0 = 70$ GPa is considered. In analysing the Bernoulli-Euler beam problems, the shape functions derived in this paper can be used by using a large value of κ . The Young’s modulus of the axially FGM beam follows a linear variation along the x -axis as given in Eq. (4).

To facilitate the presentation of results, the dimensionless critical buckling parameter is introduced as

$$\bar{P} = \frac{P_{cr} L^2}{E_0 I}. \tag{23}$$

Tables 1 and 2 show, very good agreements between the critical loads obtained in the present work and those of references.

Table 1. Dimensionless critical load of a uniform homogenous Timoshenko beam.

Boundary Conditions	Clamped– Clamped	Hinged–Hinged	Clamped–Free
Present	17.6901	7.5464	2.2910
Reference [10]	17.7056	7.5472	2.2911
Theoretical	17.6896	7.5460	2.2910

Table 2. Dimensionless critical load of a uniform axially FGM Bernoulli-Euler beam.

Boundary Conditions	Clamped– Clamped	Hinged–Hinged	Clamped–Free
Present	57.3942	14.5113	3.1177
Reference [10]	57.3948	14.5113	3.1177
Reference [11]	57.3940	14.5112	3.1177

The critical loads of the simply supported beam made from steel and alumina with different numbers of elements are listed in Table 3. The first column includes the number of elements, the second column shows the critical loads of the beam using the uniform shape functions of Eq. (2) for interpolation, and the last column displays the critical loads of the beam using the newly derived shape functions of Eqs. (6) and (9).

As can be seen from the Table 4, the beam element based on the newly derived shape functions converges faster than the one based on the homogeneous shape functions. To achieve the convergence of buckling coefficient, the solution by using Eq. (2) which is the homogeneous shape functions requiring more than 12 element division, while by using Eqs. (6) and (9) only requiring one or two element divisions can achieve the convergence.

Table 3. Dimensionless critical load of a uniform steel–alumina beam element.

Element division	Eq. (2)	Eqs. (6) and (9)
1	16.5059	13.8780
2	14.0246	13.8763
3	13.9041	13.8752
4	13.8838	13.8745
5	13.8782	13.8745
6	13.8762	13.8745
7	13.8754	13.8745
8	13.8749	13.8745
9	13.8747	13.8745
10	13.8746	13.8745
11	13.8745	13.8745

Table 4. Buckling coefficient for cantilever beam made of steel–alumina (buckling coefficient $f_B = P_C L^2 / EI$ beam with width $b = 0.1$ m, height $h = 0.08$ m, and total length $L = 3$ m).

Element division	Eq. (2)	Eqs. (6) and (9)
1	14.7899	13.1711
2	14.6541	13.1709
4	14.3189	13.1708
6	14.0271	13.1708
8	13.7018	13.1708
12	13.1810	13.1708

5.2. Cantilever beam subjected to eccentric axial load

Consider the cantilever beam subjected to an eccentric axial load shown in Fig. 3a. This problem was previously analysed by Wood and Zienkiewicz [16] and by Nguyen [7]. The beam data are: $L = 100$ m, $b = 1$ m, $h = 1$ m, $E = 12$, and $G = E/2$. The load-displacement curves obtained by using only three beam elements are shown in Fig. 3b.

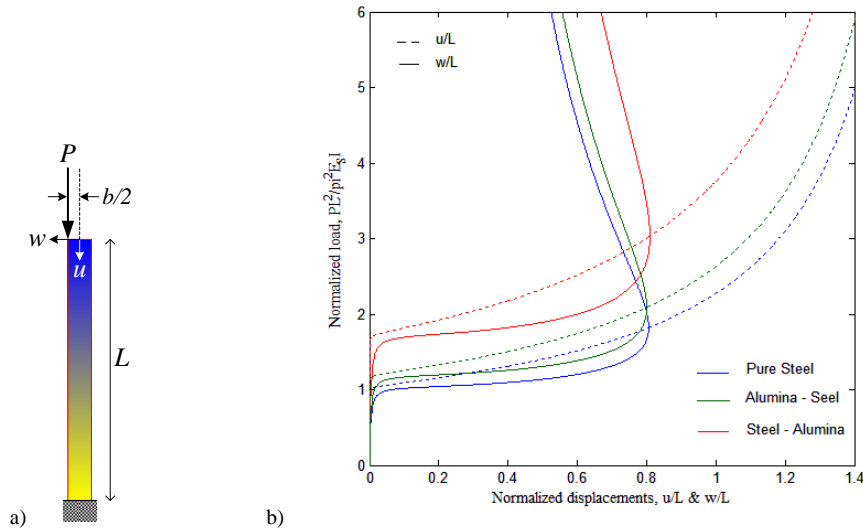


Fig. 3. Load–displacement relation for cantilever beam under eccentric axial load.

It can be observed from the figure that the pure steel material has the lowest buckling load compared with the linearly graded steel–alumina material. It is very interesting that even when the same linearly graded steel–alumina material is used, the buckling loads are significantly different depending on the side of the material being loaded or fixed. The buckling load can be increased by arranging only steel on the loading side and alumina on the fixed side, because the alumina has greater stiffness.

5.3. Williams' toggle FGM frame

The Williams' toggle frame (Fig. 4a), which has been employed by many authors to test their nonlinear beam elements, is considered here. The data for computation are as follows: $L = 12.943$ in (0.329 m), $H = 0.386$ in (0.01 m), $b = 0.753$ in (0.019 m), $h = 0.243$ in (0.006 m), and $E_o = 10.3 \times 106$ lb (7.1×104 MPa). In Fig. 4b, the load-displacement curves for the frame are obtained by using only two beam elements. The green curve corresponding to the homogenous material, which is in good agreement with the results obtained by Nguyen [7], is shown in round blue circles. The effect of the material distribution on the limit load of the FGM frame is clearly seen from the figure. The pure steel material has the lowest limit load compared with the graded steel–alumina material. Putting the graded distribution of alumina at the fixed ends and the steel at the peak of the frame will give the highest limit load of the frame subjected to a vertical loading P .

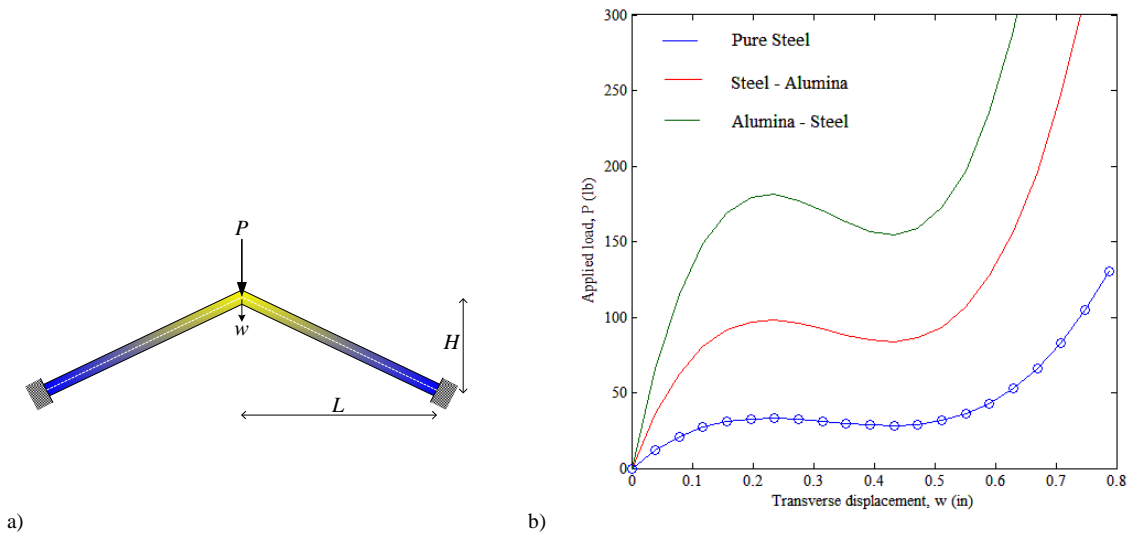


Fig. 4. Load–displacement curves for Williams' toggle frame.

5.4. Lee's FGM frame

An asymmetric frame under a concentrated vertical load P , as shown in Fig. 5a, which is also known in the literature as the Lee frame, is investigated. The problem has been previously analysed by Hsiao and Huo [4], Pacoste and Eriksson [6], and Nguyen [7]. The frame shows high nonlinearity with snap-through and snap-back behaviour, and thus this problem is a good example to test the behaviour of the beam element and the proposed numerical algorithm. The frame is assumed to be composed of steel and alumina graded material with geometric data of $L = 120$ cm, $b = 3$ cm, and $h = 2$ cm.

Figure 5b displays the load–displacement curves for the frame in two cases: the blue curves are for the pure steel frame and the red ones are for the steel–alumina frame. The blue curves for the homogenous steel frame are also compared with the results obtained by Nguyen [7], which coincided with the present results. Similarly to the previous example, placing the graded distribution with alumina at both hinged ends and steel at the joint of the frame will give the highest limit load of the frame subjected to a vertical loading P .

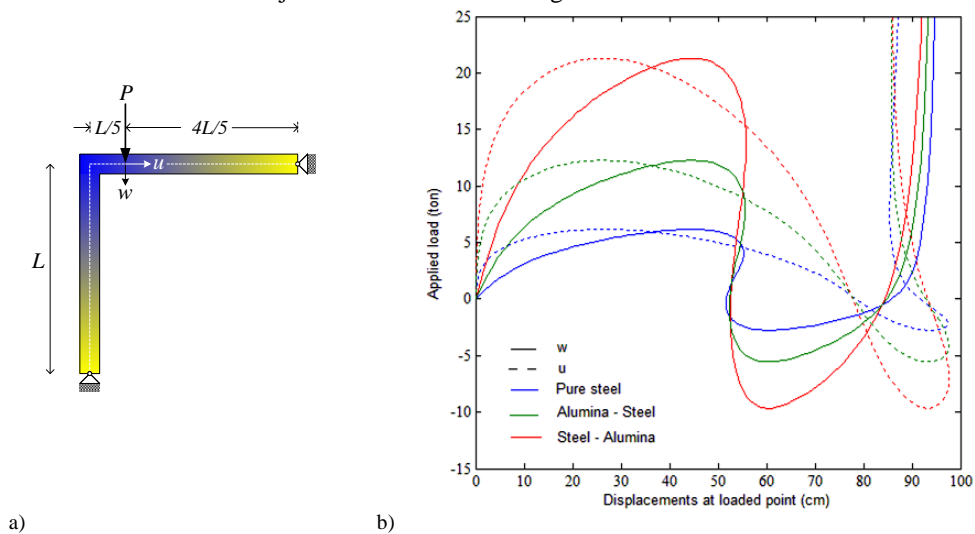


Fig. 5. Load–displacement curves for asymmetric frame.

6. Conclusions

A Timoshenko beam element for large displacement analysis of planar beam and frame structures has been formulated in the context of the co-rotational approach. Homogenously consistent shape functions, which are derived by solving the differential equations of a uniform Timoshenko beam element made of axial FGM, is employed for the formulation of the beam element. Using the formulated element, the equilibrium paths of the structures have been analysed with the aid of the incremental/iterative procedure combined with the arc-length control method. A number of numerical examples have been given to show the accuracy and efficiency of the formulated element.

From the present work, the following conclusions can be drawn:

1. Using the accurate shape functions which can incorporate material inhomogeneity will result in high efficient calculation in the finite element context, since the number of element divisions required can be suppressed significantly.
2. FGM beams subjected to axial loading show improvements in the limit of loadings and nonlinear behaviours in the post-buckling region.
3. Gradation between two or more materials, that is, FGM, is expected to give opportunities for material optimization in structural designs.

References

- [1] O.C. Zienkiewicz, R.L. Taylor, The finite element method. Vol. 2: Solid and fluid mechanics, dynamics and non-linear problems, fourth ed., McGraw-Hill, London, 1991.
- [2] T. Belytschko, W.K. Liu, B. Moran, Nonlinear finite elements for continua and structures, first ed., John Wiley & Sons, Chichester, 2000.
- [3] M.A. Crisfield, Non-linear finite element analysis of solids and structures, Vol. 1: Essentials, John Wiley & Sons, Chichester, 2010.
- [4] K.M. Hsiao, F.Y. Huo, Nonlinear finite element analysis of elastic frames, *Comput. Struct.* 26 (1987) 693–7014.
- [5] J.L. Meek, Q. Xue, A study on the instability problems for 2D–frames, *Comput. Method. Appl. Mech. Eng.* 136 (1996) 347–361.
- [6] C. Pacoste, A. Eriksson, Beam elements in instability problems, *Comput. Method. Appl. Mech. Eng.* 144 (1997) 163–197.
- [7] D.K. Nguyen, A Timoshenko beam element for large displacement analysis of planar beams and frames, *Int. J. Struct. Stab. Dyn.* 12:6 (2012) 1–9.
- [8] M. Koizumi, FGM activities in Japan, *Composites: Part B.* 28 (1997) 1–4.
- [9] T.H. Trinh, B.S. Gan, Development of consistent shape functions for linearly solid tapered Timoshenko beam, *J. Struct. Constr. Eng.*, 80:713 (2015) 1103–1111.
- [10] A. Shahba, R. Attarnejad, M. Tavanaie Marvi, S. Hajilar, Free vibration and stability analysis of axially functionally graded tapered Timoshenko beams with classical and non-classical boundary conditions, *Composites: Part B.* 42 (2011) 801–808.
- [11] A. Shahba, S. Rajasekaran, Free vibration and stability of tapered Euler–Bernoulli beams made of axially functionally graded materials, *Appl. Math. Model.* 36 (2012) 3094–3111.
- [12] D.K. Nguyen, Large displacement response of tapered cantilever beams made of axially functionally graded material, *Composites: Part B.* 55 (2013) 298–305.
- [13] D.K. Nguyen, B.S. Gan, Large deflections of tapered functionally graded beams subjected to end loads, *Appl. Math. Model.* 38 (2014) 3054–3066.
- [14] D.K. Nguyen, B.S. Gan, T.H. Trinh, Geometrically nonlinear analysis of planar beam and frame structures made of functionally graded material, *Struct. Eng. Mech.* 49:6 (2014) 727–743.
- [15] J.B. Kosmatka, An improved two-node finite element for stability and natural frequencies of axial–loaded Timoshenko beams, *Comput. Struct.* 57:1 (1995) 141–149.
- [16] R.D. Wood, O.C. Zienkiewicz, Geometrically nonlinear finite element analysis of beams, frames, arches and axisymmetric shells, *Comput. Struct.* 7 (1977) 725–735.



Sustainable Civil Engineering Structures and Construction Materials, SCESCM 2016

Local wisdom to a sustainable non-engineered brick building

Lumantarna, B.^{a,*}, Pudjistryadi, P.^a, Soetanto, R.M.^a, Hindrajaya, G.G.^a

^aCivil Engineering Department, Petra Christian University, Siwalankerto 121-131, Surabaya 60236, Indonesia

Abstract

With the increase of wealth, people tend to modernize their houses by replacing the traditional wooden houses to brick buildings. Unfortunately most of these “modern non-engineered buildings” collapsed during earthquake, while the traditional wooden houses remain undamaged. In previous studies, the authors have shown that the strength of the traditional building was in the construction of the columns which were not fixed to the ground but rested on top of flat stones, hence simulating friction base dampers.

In this study a typical non-engineered brick building is used as a prototype, it is also assumed that this building is built properly. Two types of building are considered, the first one has its tie beams anchored to the foundation. While in the second one, the tie beams are not anchored to the foundation, allowing the building to slide thus simulating friction damper. Both non-engineered brick buildings are subjected to spectrum consistent earthquake excitations with several return periods. The prototype building with anchors is treated as pinned on the anchor locations, while the one without anchor is treated as friction base isolation. A third building assuming no infilling brick wall is also analyzed as a comparison. The result shows that the two buildings can stand to earthquake with a return period of 500 and 2500 year, however the one with pinned base suffers some small damages. However the bare frame already showed extensive damages due to 500 year earthquake. It is worth to note that the building with friction base attracts only 66% of the total base shear of the one with pinned base.

© 2017 The Authors. Published by Elsevier Ltd.

Peer-review under responsibility of the organizing committee of SCESCM 2016.

Keywords: Friction base isolation; non-engineered brick building; seismic performance

1. Introduction

Although the first Indonesian earthquake code was introduced in 1971 [1], after more than forty years, despite all effort to disseminate the principle of good earthquake engineering design and construction, in recent earthquake events, such as Padang, October 2009, Bengkulu, September 2007, Yogyakarta, Mei 2006, Nias, March 2005, a lot of

* Corresponding author. Tel.: +62-31-2983394

E-mail address: bluman@petra.ac.id

modern buildings collapsed (Figure 1a), while traditional building such as Northern Nias, *Omo Hada* (Figure 1b) survived without any damage [2].



Fig. 1. (a) Nias 2005: Modern Building; (b) *Omo Hada* (Lase, 2005).



Fig. 2. (a) A three story shop house (Bengkulu September 17th 2007, private documentation); (b) Wooden house (Bengkulu September 17th 2007, private documentation).



Fig. 3. (a) *Uma Lengge*; (b) Base of *Uma Lengge*.

On the other hand with the increase of wealth people tend to renovate their wooden houses to modern brick houses, apparently brick house is a pride to the owner. Unfortunately the quality of work of the building is very inferior, hence during earthquake these “modern buildings” collapse (Figure 2a) while the wooden building (Figure 2b) next to the modern building in Figure 2a survived. In the previous paper, Lumantarna and Pudjisuryadi [3] reported that besides due to the light mass of the wooden house which attracts less inertia force, the traditional building survived due to the details of the columns connections to the foundation. In traditional buildings the columns are not fixed to the ground, thus simulating a friction base isolation system (Figures 3a and 3b).

2. Building Considered and Method

In this study, a typical non-engineered building suggested by Boen [4] is used as a prototype (Figure 4a). To enable slip between the upper structure and the lower structure, the anchors between the tie beams and the foundation are omitted (Figure 4b). This building (without anchor), the original building (with anchor), and a bare frame (without infilling wall) are subjected to earthquake with various return periods. SAP2000 v11 is used to perform the nonlinear time history analysis. The ground acceleration used for the excitation is a spectrum consistent ground acceleration which is modified from El Centro 18 May 1940 NS to the acceleration design spectrum [5] specific to the area where the buildings are. The modification of the earthquake record is performed using RESMAT, a software developed at Petra Christian University, Surabaya, Indonesia [6]. The original El Centro, the modified El Centro, and their response spectra compared to the design spectrum are shown in Figures 5a, 5b, and 5c respectively.

The building considered is modeled as a three dimensional frame (Figure 6). Three-strut model [7] is used to model the infilling brick wall with the width of strut is one-quarter of the diagonal length. The plastic hinge properties and the shear capacity of the beams are obtained using Cumbia [8]. A typical input to SAP2000 Nonlinear is shown in Figure 7 and 8. The building is arbitrarily assumed to be built on soft ground, in Palu, Sulawesi, Indonesia.

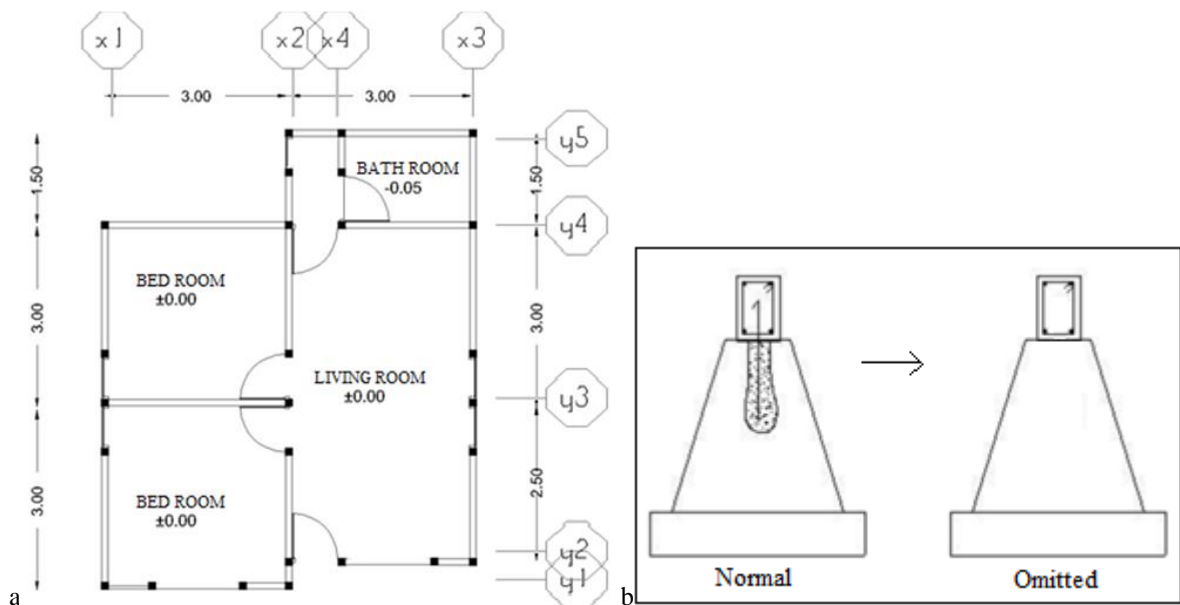


Fig. 4. Typical non-engineered brick building: (a) Plan of the building; (b) Anchors between tie beams to foundation (spaced every meter).

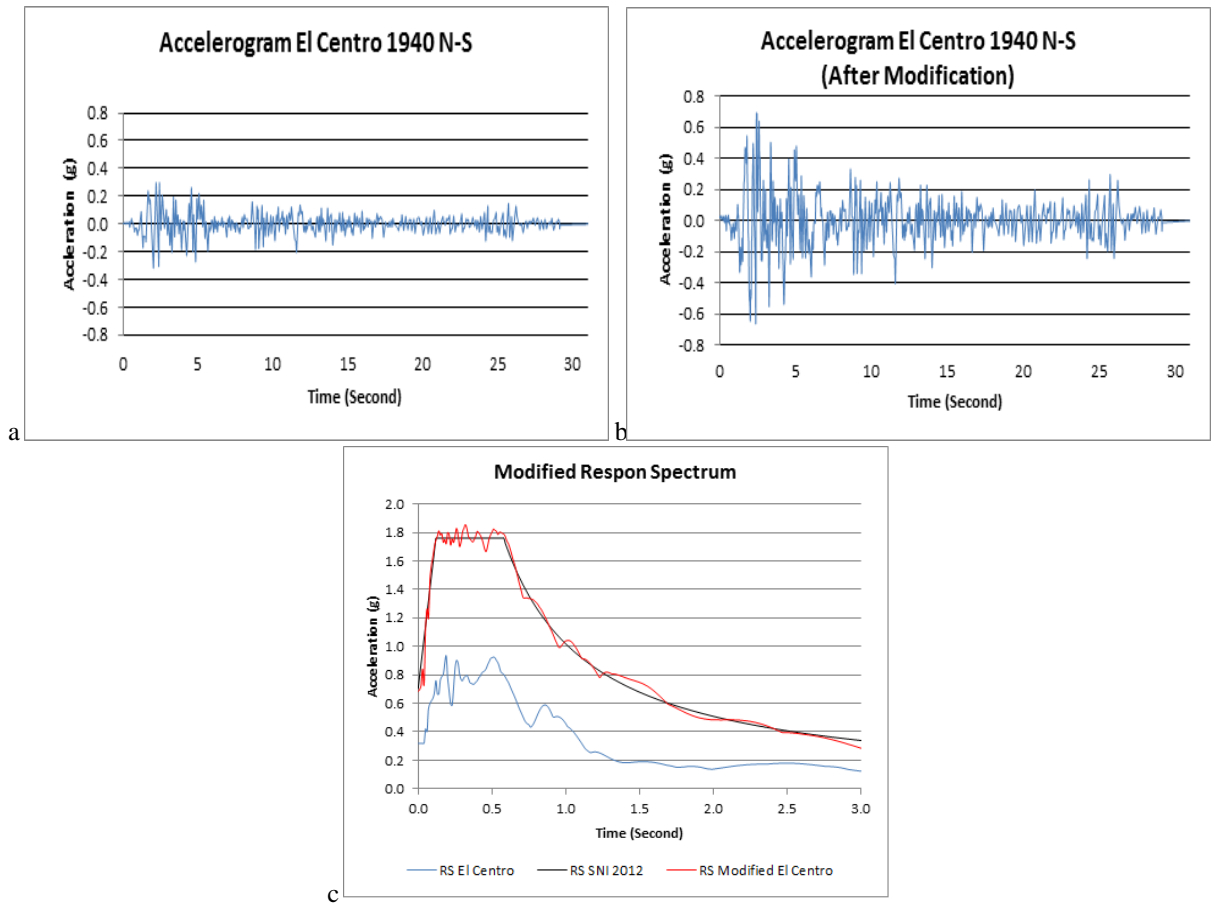


Fig. 5. El Centro 1940 N-S Component: (a) Original acceleration; (b) Modified acceleration (2500 years return period, Palu, Sulawesi, Indonesia); (c) Response Spectra

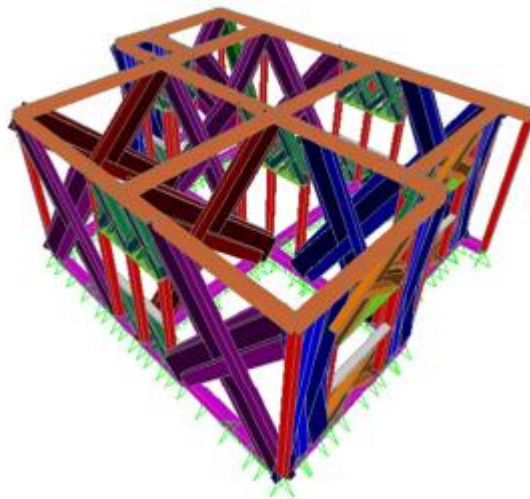


Fig. 6. Three dimensional structural model of the building (extrude view).

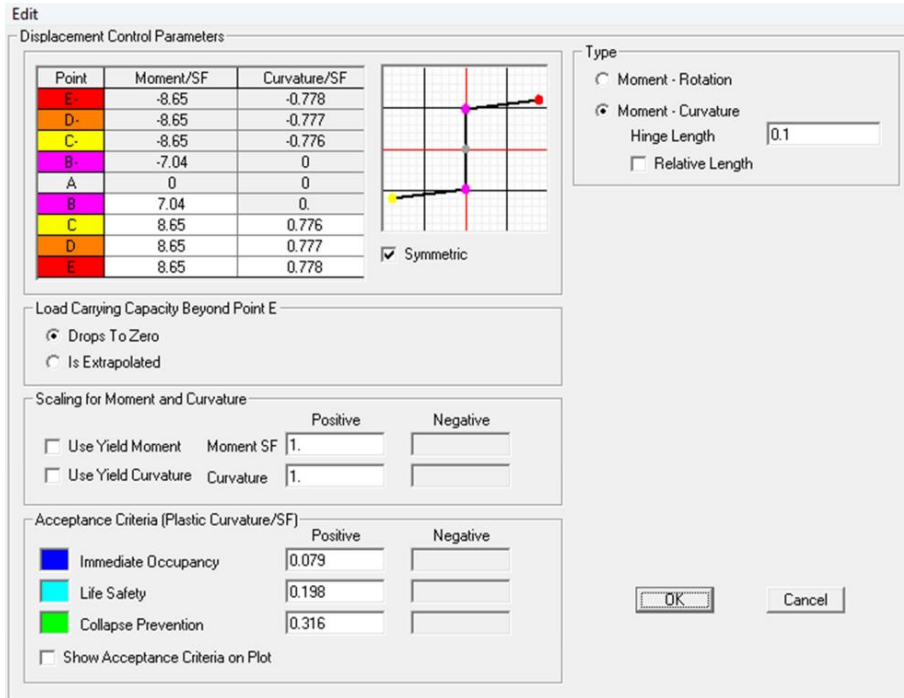


Fig. 7. Typical plastic hinge properties (bending capacity).

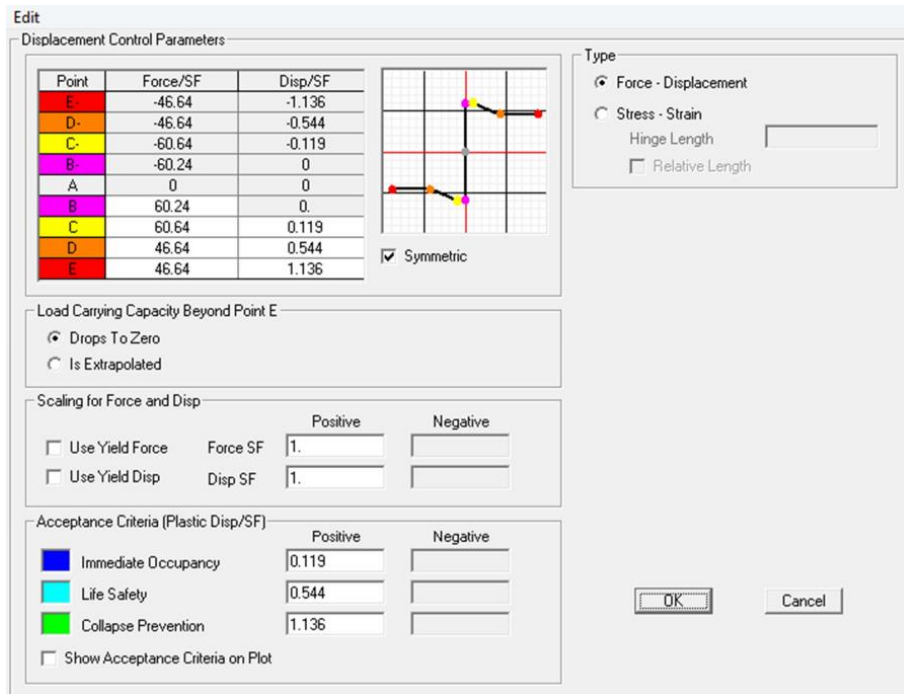


Fig. 8. Typical plastic hinge properties (shear capacity).

Friction base isolation relies on friction between the upper structure (in this case the tie beam) with the foundation. Friction is defined as (Figure 9):

$$f_s = \mu_s N \tag{1}$$

$$f_k = \mu_k N \tag{2}$$

In which, f_s , f_k , μ_s , μ_k , and N are the static friction force, kinetic friction force, static friction coefficient, kinetic friction coefficient, and normal force, respectively. To model the friction base damper, Friction Pendulum Isolators with radius is equal to zero (flat base) in SAP2000 v11 [9] are used, while for building with anchors, the anchors are assumed as hinges (pinned). The coefficients of static friction and kinetic friction for this research are set as much as 0.4.

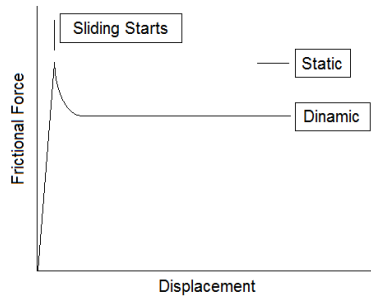


Fig. 9. Frictional force.

3. Analysis Results

3.1. Base Shear

Figures 10 and 11 show the total base shear of the two buildings due to earthquakes with 500, and 2500 years return period in X direction. While Table 1 shows comparison of maximum total base-shear in the two buildings due to earthquakes with 500 and 2500 years return period in the X direction.

It can be seen from Table 1, Figures 10, and 11 that the total base shear in the building with friction base is always smaller than the one with anchor. Comparison between the 500 and 2500 years shows that while the maximum base shear of the anchored base increases by 1.5, the friction base only increases 1.19 time. This indicates that the base of the friction base building already slips.

Table 1. Comparison of maximum Base-Shear in X direction for 500 and 2500 years.

Base Shear (N)	Earthquake in X direction					
	500 years			2500 years		
	Friction	Anchored	Anchored/ Friction	Friction	Anchored	Anchored/ Friction
Min (-)	-78,559	-84,210	1.07	-92,020	-129,833	1.41
Max (+)	99,727	132,455	1.32	118,254	199,801	1.67

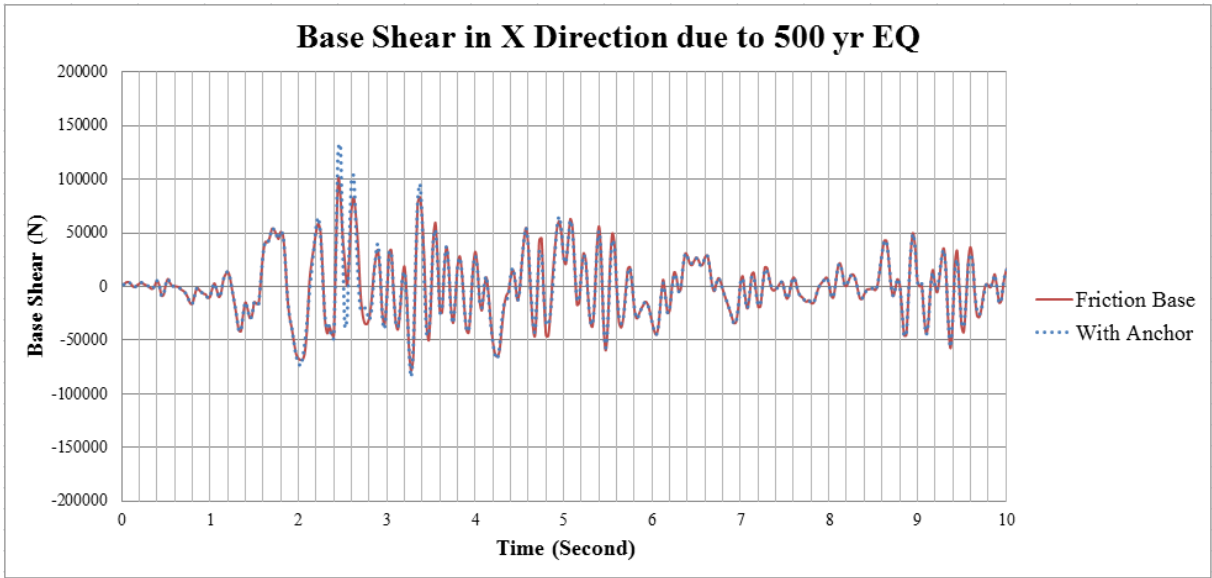


Fig. 10. Total Base Shear in X direction due to 500 years earthquake.

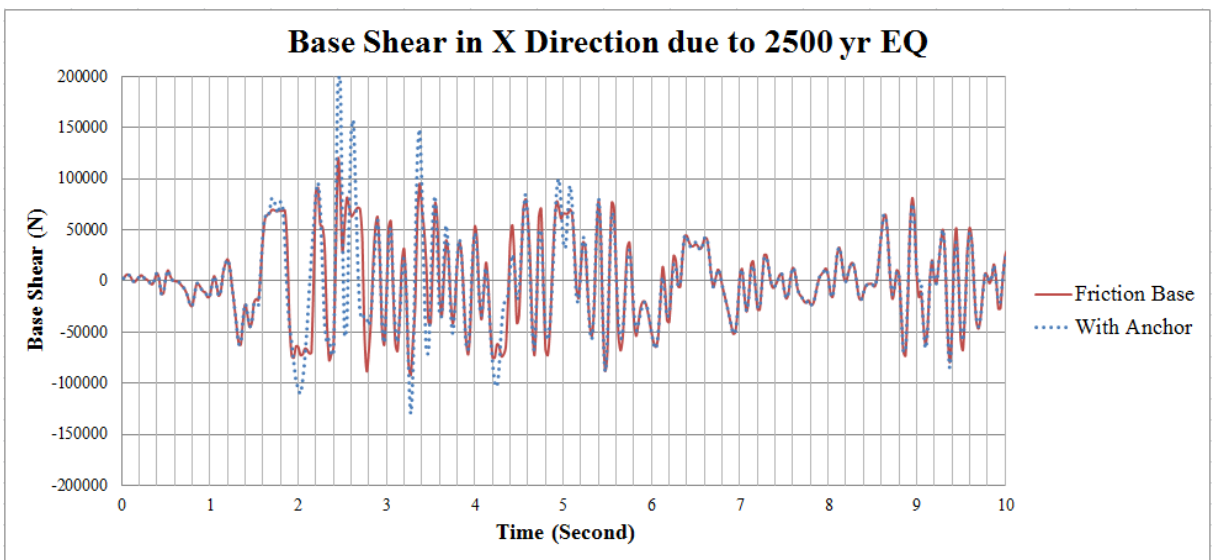


Fig. 11. Total Base Shear of building with friction base in X direction due to 2500 years earthquake.

3.2. Drift

Table 2 compares drift due to 500 and 2500 year earthquakes in the X direction between building with base isolation and with anchor. It can be seen that applying base isolation reduces the drift significantly.

Table 2. Comparison of drift due to earthquake in X direction.

Column IDs	Drift (%) due to Earthquake in the X direction					
	500 year			2500 year		
	Friction	Hinge	Friction/ Hinge	Friction	Hinge	Friction/ Hinge
K1	0.151	0.168	0.899	0.19	0.257	0.739
K2	0.151	0.167	0.904	0.189	0.257	0.735
K3	0.148	0.162	0.914	0.181	0.249	0.727
K4	0.148	0.162	0.914	0.181	0.249	0.727
K5	0.103	0.134	0.769	0.124	0.205	0.605
K6	0.104	0.134	0.776	0.125	0.205	0.610
K7	0.105	0.134	0.784	0.126	0.205	0.615
K8	0.081	0.103	0.786	0.104	0.158	0.658
K9	0.081	0.103	0.786	0.104	0.158	0.658
K10	0.082	0.103	0.796	0.105	0.158	0.665
K11	0.083	0.096	0.865	0.102	0.147	0.694
K12	0.082	0.095	0.863	0.102	0.147	0.694
K13	0.081	0.103	0.786	0.104	0.158	0.658
K14	0.082	0.096	0.854	0.102	0.147	0.694

3.3. Damages

The Analysis only showed slight damages in the anchored building due to 2500 year earthquake as shown in Figure 12. However the bare frame already showed extensive damages due to 500 year earthquake (Figure 13).

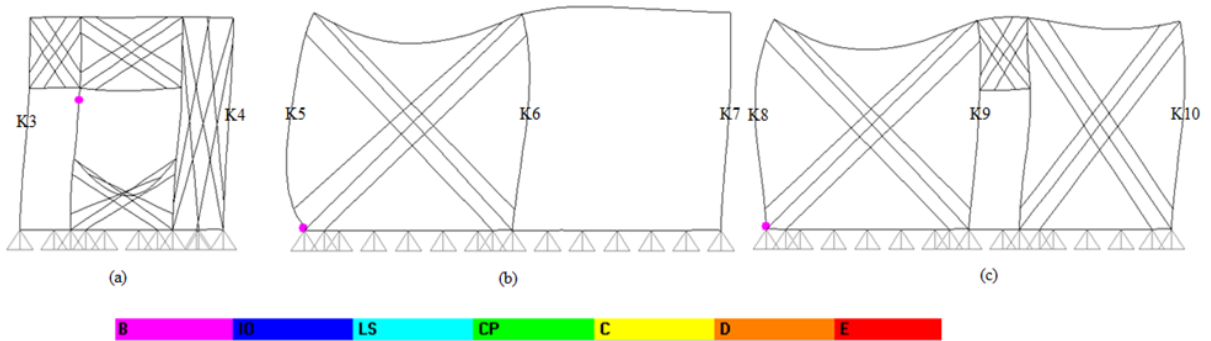


Fig. 12. Damages in (a) Frame Y2 (b) Frame Y3 (c) Frame Y4 due to 2500 year earthquake in the X direction Base Shear of building with anchor in X direction.

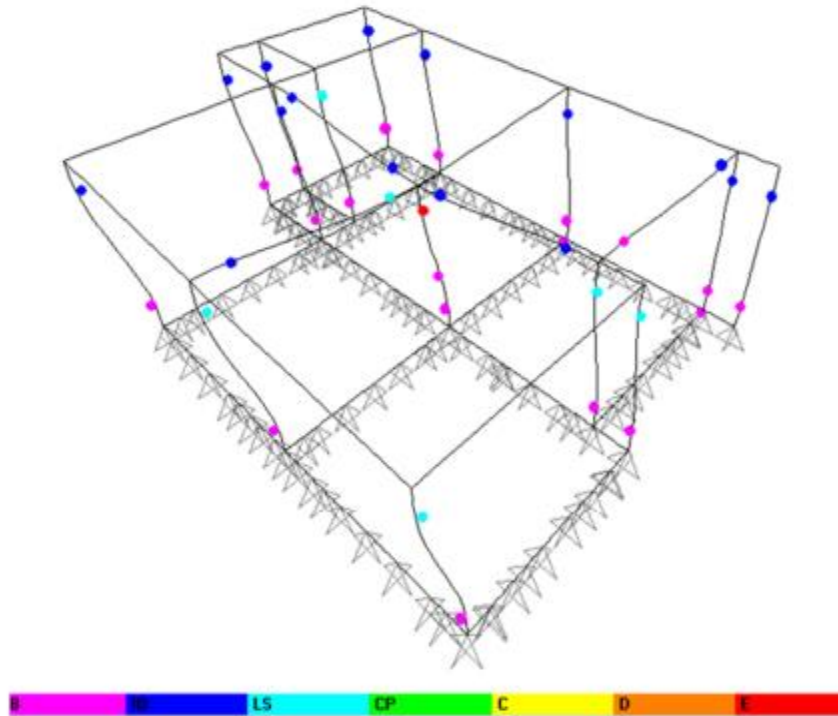


Fig. 13. Damages in bare frame due to 500 year earthquake in the X direction (at $t=6.6$ sec).

4. Conclusions

This study did not consider earthquake going in two directions, thus eliminating the possibility of walls already damaged due to load perpendicular to the wall (face load). If the infilling wall was damaged due to the face load, there is a possibility that the structure behave as bare frame and will possibly collapse.

It can be concluded that the non-engineered building suggested by Boen [4] will survive with very minimal damage to 2500 year earthquake if the structure is constructed soundly. However the friction base building behaves better by attracting only 66% of the total base shear and 68% of the average drift due to 2500 year earthquake of the traditional fixed base (anchored) building.

References

- [1] B. Lumantarna, Perkembangan peraturan pembebanan dan perencanaan bangunan tahan gempa, A paper presented in earthquake engineering seminar, Makasar, November 15th, 2007.
- [2] Y. Lase, Kontrol seismik pada rumah adat Nias, Proc. HAKI conference, Jakarta, Indonesia, 2005, pp. 1-10.
- [3] B. Lumantarna, and P. Pudjisuryadi, Key note lecture presented in the Thirteenth East Asia-Pacific Conference on Structural Engineering and Construction, Sapporo, Japan, September 11th-13th, 2013.
- [4] Boen, T., Membangun Rumah Tembokan Tahan Gempa. Jakarta, Indonesia, 2005.
- [5] Badan Standarisasi Nasional, Tata Cara Perencanaan Ketahanan Gempa untuk Struktur Bangunan Gedung dan Non Gedung, SNI 03-1726-2012, Indonesia, 2012.
- [6] B. Lumantarna, and M. Lukito, RESMAT Sebuah Program Interaktif untuk Menghasilkan Riwayat Waktu Gempa dengan Spektrum Tertentu, Proceedings of HAKI Conference, Jakarta, Indonesia, 1997.
- [7] H. B. Kaushik, D. C. Rai, and S. K. Jain, A Rational Approach to Analytical Modeling of Masonry Infills in Reinforced Concrete Frame Buildings, The 14th World Conference on Earthquake Engineering, Beijing, China, 2008.
- [8] L.M. Montejo, and M. J. Kowalsky, CUMBIA Set of Codes for the Analysis of Reinforced Concrete Members, California, United States, 2007.
- [9] Computer and Structures Inc., CSI Analysis Reference Manual, California, USA, 2007.



Sustainable Civil Engineering Structures and Construction Materials, SCESCM 2016

Toward bio-based geo- & civil engineering for a sustainable society

Henk M. Jonkers^{a,*}

^aDelft University of Technology, Stevinweg 1, 2628 CN Delft, The Netherlands

Abstract

The since 2010 running research program 'Bio-Based Geo & Civil Engineering for a Sustainable Society (BioGeoCivil)', funded by the Dutch technology foundation STW, aims to develop novel bio-based construction materials that can be used in Civil- and Geo-engineering constructions to enhance the sustainability performance of the sector. Rationale is that the sector produces still today excess amounts of waste in all life cycle phases of a construction, from building to use phase as well as end-of-life phase. Aim of the program is to mimic nature as 'building' processes in nature do not produce any waste as all elements, also residual material, is considered a high grade resource. In order to substantially improve the sustainability profile of the sector, upgrading of secondary- or byproducts must be achieved to allow functional performance similar to primary materials and resources. The challenge of the six currently running projects within the BioGeoCivil program is therefore not only to mimic nature but also to include bio-based materials or processes in civil- or geo-engineering applications which result, in comparison to traditional building products, in drastically improved performance both on sustainability and durability level. The six projects comprise: 1. Fungal biofilms (coating) for wood protection, 2. Bacteria-based repair and performance improvements of aged concrete structures, 3. Bacteria-based ground stabilization to mitigate liquefaction and piping of granular sediments, 4. Engineering of bacterial biofilms on buildings and infrastructure as a basis for natural protection, 5. Lift up Lowlands: upgrading of natural materials (bio-remediation of sludge) for sustainable lift up of low lying polder areas, and 6. Towards the development of carbon dioxide neutral renewable cement.

© 2017 The Authors. Published by Elsevier Ltd.

Peer-review under responsibility of the organizing committee of SCESCM 2016.

Keywords: Bio-based processes; civil- and geo-engineering; soil; concrete; cement

* Corresponding author. Tel.: +31 15 278 2313; fax: +31 12 278 6383.

E-mail address: h.m.jonkers@tudelft.nl

1. Introduction

Traditionally the disciplines of Civil- and Geo engineering sciences focus on building structures that are durable, i.e. last long. In recent decades sustainability practices are becoming more and more important and minimizing production of waste, emission of harmful components, saving of energy and recycling of elements and materials have become standard practices. However, in order to further and substantially improve both durability and sustainability performances of construction materials, technological innovations are required. Eminent requirement for these novel materials is that for their production and subsequent lifetime phases use of energy and dependence on use of finite resources, and emission of harmful substances for humans and environment are minimal. Use and implementation of bio-based materials and processes could make an important contribution to this aim as these are renewable by nature. The projects currently running in the BioGeoCivil program build further on concepts that have been are still being developed. One example is the development of self-healing materials in which limestone production by specific bacteria result in self-healing of cracks in concrete [1]. The ability to self-heal is widespread in nature and the used building concept here is based on damage management rather than damage prevention as in current man-made constructions [2]. The damage management concept used in nature generally requires much less resources in comparison to damage prevention as constructions built according to latter concept are usually over-dimensioned with respect to their required functional performance.

Main objectives of the BioGeoCivil program are therefore the development of biology-based materials as well as processes which can help to solve engineering challenges addressing sustainability performance while at the same time safeguarding required durability aspects such as sufficient strength are functional service lifetime performance. Figure 1 shows a schematic drawing of the main aim of the program, i.e. mimicking in trying to establish a fully circular resource and material approach in which no waste or other emissions are produced as all residual materials provide useful resources for other products or life cycle stages of the construction.

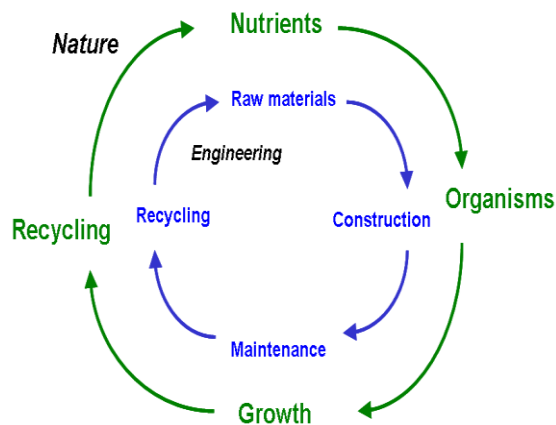


Figure 1: Resources and materials cycle in nature taken as inspiration for establishing fully circular material use in the civil- and geo-engineering building cycle.

In order to increase the chance of success, requirement for all six projects currently running in the BioGeoCivil program was that scientists from the different scientific disciplines biology and civil- and geo-engineering work closely together within each individual project.

The following main objectives were defined in the program [3] to achieve this goal:

1. Increase our fundamental knowledge of mechanisms nature uses to solve construction and functionality challenges we face in the field of geo and civil engineering
2. Develop robust biology-based technology, methods and processes that enable improved functionality and reduced environmental burden in geo and civil engineering applications

3. Define and demonstrate the requirements for upscaling: application of these findings in materials and processes in geo and civil engineering
4. Create a Dutch knowledge-platform of bio-based geo and civil engineering, combining representatives from research and industry, that enables the development of a strong research and economic infrastructure focused on sustainable geo and civil engineering

Six projects, in all of which as mentioned under objective 4 also industrial partners and governmental institutes defined as end-users participate, have been funded within the program scheme and these are titled:

1. Fungal biofilms (coating) for wood protection
2. Bacteria-based repair and performance improvements of aged concrete structures
3. Bacteria-based ground stabilization to mitigate liquefaction and piping of granular sediments
4. Engineering of bacterial biofilms on buildings and infrastructure as a basis for natural protection
5. Lift up Lowlands: upgrading of natural materials (bio-remediation of sludge) for sustainable lift up of low lying polder areas
6. Towards the development of carbon dioxide neutral renewable cement

2. BioGeoCivil Engineering program projects

2.1. Biofilms for Wood Protection (BioWoPro)

This research project builds further on findings by Sailer et al [4]. In latter research project it was found that specific species of fungi such as *Aureobasidium pullulans* can form biofilms on wood products which provide a protective natural and living coating. Growing such protective coatings on exposed outdoors wood constructions can provide a much more sustainable solution to wood protection in comparison to synthetic products which are usually based on environmentally unfriendly volatile organic solvents containing other environmental harmful active chemicals. Challenges in this project are particularly on characterization of microbial communities which develop on exposed outdoors wood products and furthermore to analyze how specific timber-protective fungal species can start to dominate these communities on the longer term. Also, the mechanistic functionality of fungal protection of timber products must be clarified.

In a subsequent study it was found that living biofilm coatings do provide functional protection of oil-treated wood surface against UV light and bio-degradation. Different types of wood such as from Yellow pine, beech, and Oregon pine treated with olive oil or linseed oil developed biofilm featuring different microbial communities. It was concluded in that study that the wood-oil-biofilm combination allows full recyclability while featuring at the same time a high eco-friendly profile, and is considered safe for humans both in application and during use [5].

2.2. Bio-based Repair and Performance Improvements of Aged Concrete Structures (BioRetrofit)

In the BioRetrofit project novel repair systems for existing aged and damaged concrete constructions are being developed. In contrast to currently available repair systems which are usually based on environmentally unfriendly materials such as acrylic resins, epoxy- or urethane or silicone-based polymers, these novel ones are based on bacteria that can precipitate specifically under alkaline conditions copious amounts of limestone. The produced limestone seals pores and cracks in concrete, resulting in waterproofing, protection of the embedded steel reinforcement against corrosion, and increased resistance against frost damage.

The process of bacterial limestone formation is based on metabolic conversion of specific feed sources such as calcium lactate under alkaline conditions according to the following bio-chemical reactions:



and subsequently:



The metabolic conversion of one molecule of calcium lactate thus results in the production of 6 molecules of calcium carbonate (limestone) provided that calcium hydroxide (portlandite) minerals are still present on the concrete crack or pore surface as these react with metabolically produced carbon dioxide to additional calcium carbonate.

Based on this principle two different concrete repair systems were developed, one liquid based two-component system and one cement-based repair mortar. Application of the liquid repair system resulted in substantial reduction of water permeability of cracked concrete specimens both before and after freeze and thaw cycles (Fig 2).

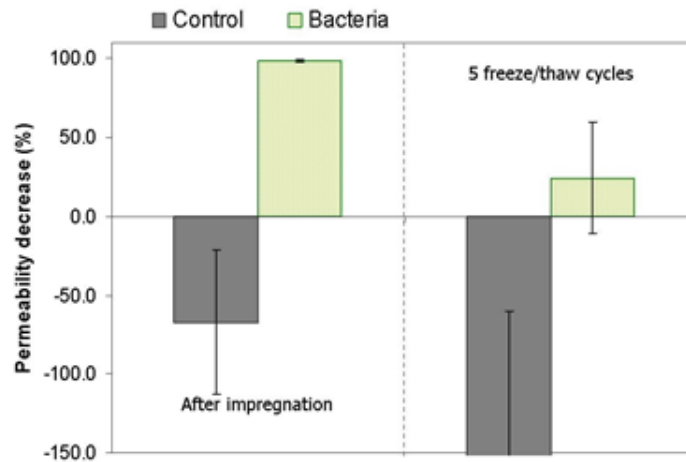


Figure 2. Water permeability of cracked control- and bacteria-based mortar specimens treated with liquid-based bacterial repair system before (left part of image) and after subjection to five freeze/thaw cycles (right part of image). Decrease of permeability was in both cases significantly higher in bacteria-based repair system treated specimens [6]

The developed cement-based repair mortar also featured, in addition to limestone-producing bacteria, PVA (polyvinyl alcohol) fibers. Latter fibers help to decrease shrinkage and improve better bonding between the freshly applied repair mortar and the underlying aged concrete. Micro cracks which might still occur during setting of the repair mortar are subsequently self-healed due to filling with limestone due to metabolic conversion of calcium lactate by bacteria which are both also included in the mortar (Figure 3).



Figure 3. Self-healing mortar applied in practice: a) Surface preparations, b) Application, c) Visible limestone formation (white lines) on the surface of the set repair mortar [7]

Conclusion of this study was that incorporation in of bacteria, which precipitate limestone under alkaline conditions, in the two novel developed repair products can significantly enhance functional properties such as water tightness and frost resistance in aged concrete constructions.

2.3. Bacteria-based ground stabilization to mitigate liquefaction and piping of granular sediments

Liquefaction, a process in which loose sands suddenly turn liquid, can result in dramatic erosion rates and thus loss of fertile agricultural land. A similar soil eroding process termed ‘piping’ is caused by rapidly flowing groundwater that can result in collapse of constructions such as dikes and dams. In this research project a solution to this problem is sought in soil bacteria which can stabilize and consolidate sand through metabolic production of calcium carbonate based binders and that way avoid ground liquefaction and piping phenomena. This proposed bio-based technology represents an alternative to traditional cement-based grouting techniques and is therefore expected to be more sustainable with respect to CO₂ footprint. In a series of initial studies van Paassen and colleagues [8, 9] established soil stabilization successfully by applying microbial-induced carbonate precipitation via enzymatic hydrolysis of urea (Figure 4).

However, after further analysis of this technology, the research team concluded that this urea-based process was not only costly but also much less environmental friendly than expected due to the massive production of ammonium requiring costly and energy intensive post treatment cleaning [9]. In the presently running research project the research team investigates alternative microbial-induced carbonate precipitation pathways which are superior to the urea pathway with respect to costs and sustainability performance. Using nitrate and organic compound rich industrial wastewater as nutrients the researchers established precipitation of calcium carbonate based minerals by endogenous microbial communities via the denitrification pathway [10]. In this research project it was concluded that this novel strategy is not only economically competitive to traditional cement-based grouting but also significantly more sustainable with respect to CO₂ footprint and environmental nitrogen loading.



Figure 4. Pilot scale (100m³) bio-grouting experiment by van Paassen and colleagues.
Image courtesy of Leon van Paassen, Delft University of Technology

2.4. Engineering of bacterial biofilms on buildings and infrastructure as a basis for natural protection

Bacteria are sometimes blamed for attacking building materials such as for example in the case of microbial induced corrosion of steel. However, bacteria could possibly also play a protective role, just depending on the type of metabolism, resulting in possible formation of protective compounds. Such a potentially positive role is investigated in this research project in which the aim is to find microbes or specific microbial communities who's concerted

metabolic activity result in protection of particularly steel constructions. In a series of studies performed on different field sites in the Netherlands it was found that specific mineral deposits are formed on the surface of steel sheet pilings (see Figure 5) present for up to 67 years in soil [11].

Analysis of the microbial communities associated with these mineral deposits revealed the presence of bacteria mainly related to methanogenic (methane forming) species of bacteria. Although methanogenic species in both fresh- and marine water environments and particularly sulfate-reducing bacteria in the marine environment are known to degrade steel by inducing corrosion, it was found in the present studies that particularly methanogenic bacteria subsequently protect steel due to formation of a dense layer of calcium- and iron carbonate based mineral deposits what prevents further corrosion. Ongoing research aims to further clarify this microbially induced protective mechanism, in order to enable active measures to stimulate these protective biofilms in situ, e.g. by providing specific nutrients or substrates to favor growth of protective microorganisms at the cost of material degrading ones.



Figure 5. Crusts of mineral deposits formed by microbial communities on the surface of sheet pilings. Image courtesy of Michael Asanajef, Delft University of Technology

2.5. Lift up Lowlands: upgrading of natural materials (bio-remediation of sludge) for sustainable lift up of low lying polder areas

Delta areas worldwide and particularly polders (reclaimed land areas) are often situated below the surface level of surrounding waters. Also land areas suffering from soil subsidence have to cope with regular flooding if water runoff cannot be adequately managed. Aim of this research project is to supplement (lift up) these low lying areas using dredged sediments from elsewhere. In The Netherlands rivers and some coastal regions are continuously dredged to enable commercial shipping activities. However, these dredging activities result in excess dredging sludge amounting to 100.000.000 m³ often of poor quality due to presence of organic contaminants. Strategy of the current research project is to create a win-win situation by applying sludge remediation, a process in which through microbial activity contaminated material is cleaned, making it suitable and valuable as building material to uplift low lying areas.

2.6. Towards the development of carbon dioxide neutral renewable cement

Portland based concrete is generally blamed for not being sustainable due to the high amount of CO₂ emitted to the atmosphere during the production process of cement. According to some studies between 5 and 10% of the total anthropogenic CO₂ is due to the production of Portland cement [12]. In order to substantially decrease the CO₂ footprint of cement a novel type of biomass-based binder is under development in this project. Certain types of biomass derived ashes such as rice husk ash and sugar cane bagasse are known to feature pozzolanic properties and are therefore suitable to replace at least a part of Portland cement in concrete mix designs. The main aim of this research project is to develop a functional hydraulic biomass-ash based binder that can fully replace Portland cement

in concrete product applications. Such as bio-based binder would be almost fully CO₂ neutral as the CO₂ produced during biomass combustion can be taken up again in the process of photosynthesis during biomass growth replacing the biomass that was combusted. In order to produce Portland cement-like minerals such as alite, belite, calcium aluminate, and calcium aluminoferrite, the input biomass must at least feature precursor elements required for the formation of these minerals. Second to the element/mineral composition of the input biomass, also the combustion process (temperature regime and process time) likely affects the type and hydraulic functionality of the minerals formed.

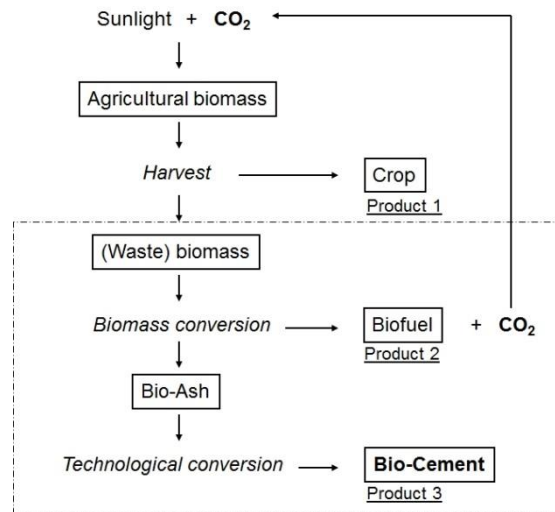


Figure 6. Scheme of biomass-based BioCement production. Its production is considered sustainable when, in contrast to production of Portland cement, CO₂ production and fixation are balanced. In this research project focus will be on processes depicted in the boxed part, thus starting with (residual) biomass from the agro-industrial sector.

Moreover, the main idea of this project is not to specifically grow crops to produce bio-based cement, but rather to use agricultural biomass-waste or by-products as an input source for biomass combustion. In this way two or three different products can be obtained from the same crop (Figure 6).

In a series of experiments it was shown that with proper pretreatment of ashes and a specific firing regime (ramp rate of 25°C/minute and an ultimate temperature for 4h at 1240°C) belite minerals could be formed [13, 14]. Conclusion of these studies is that production of a virtually CO₂ neutral hydraulic binder for concrete applications is possible providing that quality (mineral element composition) and combustion regimes of biomass input raw material is suitable.

3. Conclusions

Traditional geo- and civil engineering techniques are typically characterized not only by a high CO₂ footprint but also by massive use of finite resources while at the same time producing harmful emissions to humans and environment. In contrast, the bio-based processes and materials applied in the six research projects within the STW Perspective program ‘Bio-based geo- and civil engineering for a sustainable society’ demonstrate that a bio-based approach can provide in many cases an economically viable and environmentally more sustainable alternative to established traditional geo- and civil engineering techniques.

Acknowledgements

The six research projects discussed in this work with respective project numbers 11345, 11342, 11337, 11333, 11344 and 11338 have been financially supported by the Dutch Technology Foundation STW under the Perspective Program scheme.

References

- [1] H.M. Jonkers, V.A.C. Wiktor, M.G. Sierra-Beltran, R.M. Mors, E. Tziviloglou & D. Palin (2015) Limestone-producing bacteria make concrete self healing. Self healing materials - pioneering research in the Netherlands, S. van der Zwaag, E. Brinkman (eds.) IOS Press, © 2015. The authors and IOS Press. p 137-148
- [2] S. van der Zwaag (ed.) (2007) Self healing materials - An alternative approach to 20 centuries of materials science. Springer, The Netherlands
- [3] STW Perspective Program (2009) Bio-Based Geo & Civil Engineering for a Sustainable Society (BioGeoCivil). <http://www.stw.nl/nl/programmas/biogeocivil-bio-based-geo-civil-engineering-sustainable-society>
- [4] Sailer MF, van Nieuwenhuijzen EJ, Knol W. (2010). Forming of a functional biofilm on wood surfaces. Ecological Engineering 36: 163-167
- [5] Filippovych K, H Huinink, L van der Ven and OCG Adan (2015) Self healing biofilms for wood protection. Self healing materials - pioneering research in the Netherlands, S. van der Zwaag, E. Brinkman (eds.) IOS Press, © 2015. The authors and IOS Press. p 181185
- [6] Wiktor V, Jonkers HM (2014) Protection of aged concrete structures: application of bio-based impregnation system. AMS '14 Proceedings of the Int. Conference on Ageing of Materials & Structures Delft 26 – 28 May 2014, The Netherlands, pp. 295-301
- [7] Sierra-Beltran MG, Jonkers HM (2015) Crack self-healing technology based on bacteria. Accepted for publication 1st International Workshop on Self-Healing & Intelligent Materials 2015 (SHIM 2015), The Korean Association of Crystal Growth, 5-6 March 2015
- [8] Whiffin VS, van Paassen LA, and Harkes MP (2007), “Microbial carbonate precipitation as a soil improvement technique” Geomicrobiology Journal, 24(5), 417-423.
- [9] Van Paassen LA, Ghose R, van der Linden TJM, van der Star WRL, and van Loosdrecht MCM (2010a), “Quantifying biomediated ground improvement by ureolysis: Large-scale biogROUT experiment”, Journal of Geotechnical and Geoenvironmental Engineering, Vol. 136, 1721-1728.
- [10] Van Paassen LA, Daza CM, Staal M, Sorokin DY, van der Zon W, and van Loosdrecht MCM (2010b), “Potential soil reinforcement by biological denitrification”, Ecol Eng, 36, 168-175.
- [11] Kip, N., S. Janssen, M de Hollander, M. Afanasyev and H. van Veen (2016) Microbial induced corrosion inhibition: Methanogens predominate in mineral deposition layers on metal sheet piling. Nederlands Aardwetenschappelijk Congres, 7-8 April 2016, Veldhoven, The Netherlands
- [12] Worrell, E., Price, L., Martin, N., Hendriks, C., and Ozawa Meida, L. (2001) Carbondioxide emissions from the global cement industry. Annual Review of Energy and the Environment 26: 303-329
- [13] N.N. Carr and H.M. Jonkers (2014) Towards the development of CO₂-neutral cement (BioCement). Proceedings of the 34th Cement and Concrete Science Conference, 14-17 September 2014, University of Sheffield, pp. 173-177. Eitors S.A. Bernal and J.L. Provis. Published by The University of Sheffield.
- [14] Lorenzo Tosti, André Van Zomeren, Jan R. Pels, Natalie Carr, Rob N.J. Comans (2015) Development of new cement formulations containing paper sludge fly ash as secondary cementitious material. Proceedings of the 9th International Conference on the Environmental and Technical Implications of Construction with Alternative Materials - Resource Efficiency in Construction. Santander, SPAIN, 10–12 June 2015.



Sustainable Civil Engineering Structures and Construction Materials, SCESCM 2016

Full height rectangular opening castellated steel beam partially encased in reinforced mortar

Iman Satyarno^{a,*}, Djoko Sulisty^a, Dina Heldita^a, A. Talodaci Corte Real De Oliveira^a

^a*Department of Civil and Environmental Engineering Universitas Gadjah Mada, Indonesia*

Abstract

This paper discusses analysis and test results of full height rectangular opening castellated steel beams without encasing and with partially encasing using reinforced mortar. Each contains two types of beam span namely short span beams to study the shear failure mechanism and long span beams to study the flexural failure mechanism. Test results show that the beams without encasing have lower load capacity than the original section due to Vierendeel truss mechanism. On the other hand the application of partially reinforced mortar encasing in the long span beam can avoid the Vierendeel truss mechanism and increases the yield moment capacity around 3.5 times of original steel section yield moment. However the short span one failed in brittle shear mechanism due to diagonal crushing in the mortar and then followed by Vierendeel truss mechanism so that the flexural strength could not be achieved. Shear strength of the full height rectangular opening castellated steel beam partially encased in reinforced mortar is larger than the calculated conventional reinforced concrete shear capacity but is less than the steel web shear capacity. It is recommended that the shear strength is calculated using diagonal strut mechanism of the mortar to give more appropriate shear strength prediction. © 2017 The Authors. Published by Elsevier Ltd.

Peer-review under responsibility of the organizing committee of SCESCM 2016.

Keywords: beam, castellated, encased, flexural, shear, Vierendeel mechanism

1. Introduction

The most common pattern or shape of the hole in the web of castellated steel beams that has been known quite sometimes ago is hexagonal [1]. The main objectives of making castellated steel beam are to increase the steel section

* Corresponding author. Tel.: +62-818262438; fax: +62-274545675.

E-mail address: iman@tsipil.ugm.ac.id, imansatyarno@ugm.ac.id, iman_arno@eudoramail.com

flexural stiffness and strength without increasing the steel self weight [2]. These advantages can save some cost especially in mass production of long span beams [3]. If shear stress becomes dominant in the castellated beam, it is required to give stiffeners around the holes to increase the shear capacity [4]. Stress analysis of castellated steel beam can be calculated based on Vierendeel truss theory [1,2].

Steel encased in reinforced concrete method is used to avoid the steel from buckling that can be used for beams [5,6], columns [7,8], both columns and beams [9, 10, 11], or coupling beams [12,13]. There are two types of encased method namely fully encased and partially encased. In the fully encased method the whole steel section is covered by the reinforced concrete so that the top and the bottom flanges are not in the outermost position. In this case maximum strain developed in the steel is less than the one in the concrete. On the contrary, in partially encased method only the web is covered by the reinforced concrete, therefore maximum strain will develop in steel flanges that makes the application of the steel section can be more optimum.

This research was carried out to further optimize the application of steel in the partially encased method, that is by using new rectangular hole pattern castellated steel beam to be encased in reinforced mortar. The new hole pattern is designed to make full height rectangular opening castellated steel beam, see Figure 1.

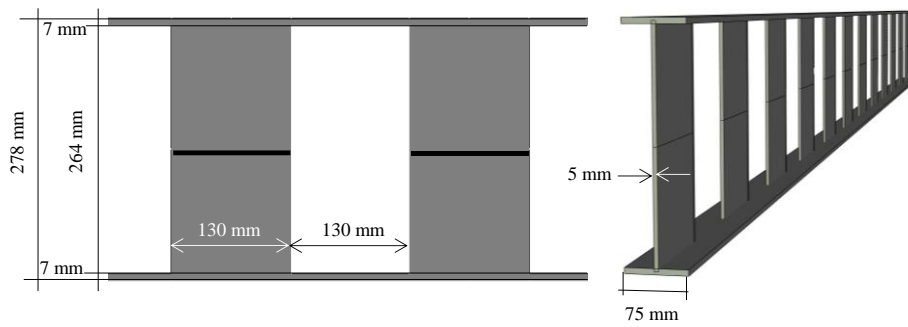


Figure 1. Full height rectangular opening castellated steel beams

2. Research Method

Two groups of specimens were made and analysed in this research. The first group was the full height rectangular opening castellated steel beams without encasing shown in Figure 1 that contains two beam specimens namely short span beam to study shear strength and long span beam to study flexural strength, see Figure 2. Two point loadings method was used in the tested beams which were supported using hinge at one end and roll at the other end. The full height rectangular opening castellated steel beam was made from IWF 150x75x5x7 section that had original section height $h = 150$ mm, width of flange $b_f = 75$ mm, flange thickness $t_f = 7$ mm, web thickness $t_w = 5$ mm, and the yield strength $f_{ysec} = 278$ MPa. Using this data it can be found that the original steel section has yield moment of 24 kNm. In the full height rectangular opening castellated steel beams the vertical and the horizontal cutting pattern made the width of hole in the web to be $B = 130$ mm, the height of hole $d = 264$ mm, and the height of castellated beam $h = 278$ mm or almost as twice as its original height of 150 mm as has been shown in Figure 1.

The second group of specimens was the same full height rectangular opening castellated steel beams mentioned above but were then partially encased in reinforced mortar as shown in Figure 3. Encasing process was carried out by firstly adding transversal and longitudinal reinforcements in the full height rectangular opening castellated steel beams. Two D16 reinforcing bars having yield strength $f_{yD} = 412$ MPa were used for the top and the bottom longitudinal reinforcement, while P8 reinforcing bar having yield strength $f_{yP} = 408$ MPa was used for the transversal reinforcement. It is noted that equal longitudinal reinforcement at the top and at the bottom flanges was used to maintain the steel ductile behaviour. Transversal reinforcement in the short span beam contains two steel hoops while the long span beam contains only one steel hoop. This transversal reinforcement was put at each edge of the web holes. Once the steel reinforcement has been added, the both sides of the web were then poured with flow mortar. The mix design of flow mortar for encasing material had the composition of water = 313 kg/m³, cement = 781 kg/m³, sand = 1172 kg/m³, and super plasticizer = 5.45 l/m³, that made the compressive strength of this flow mortar $f'_m = 53$ MPa.

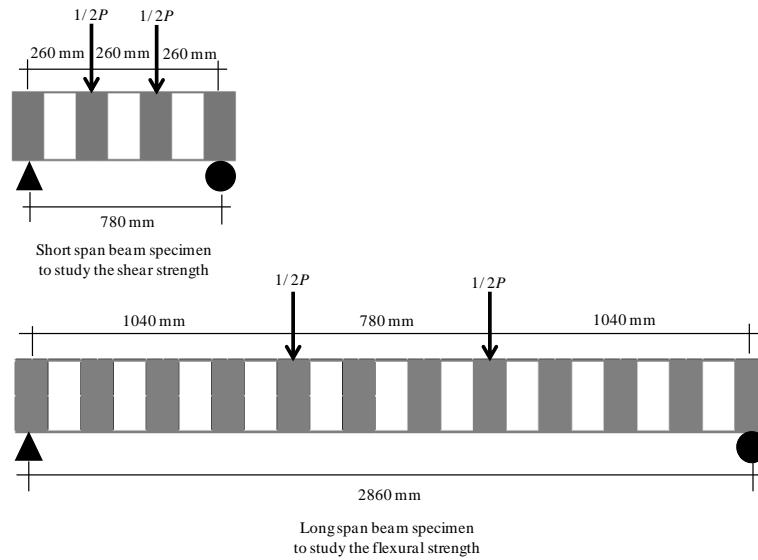


Figure 2. Short span and long span specimens of full height rectangular opening castellated steel beams

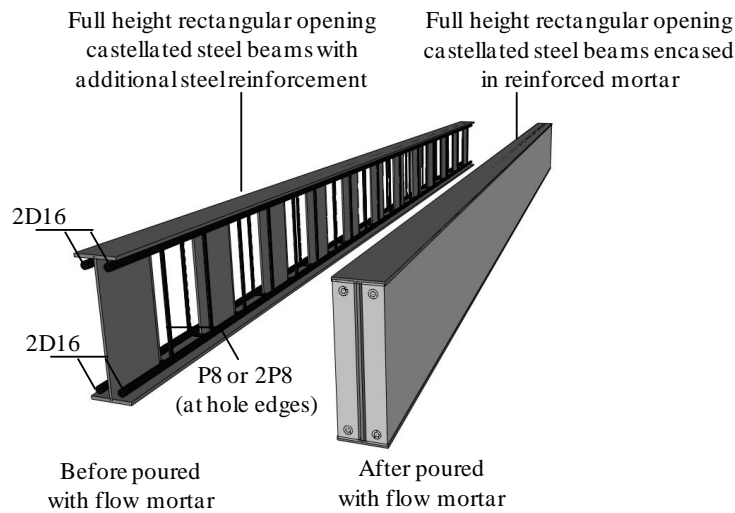


Figure 3. Full height rectangular opening castellated steel beam partially encased in reinforced mortar

2.1. Load capacity analysis of full height rectangular opening castellated steel beam

Load capacity analysis of full height rectangular opening castellated steel beam is carried out based on Vierendeel truss mechanism for common hexagonal opening [1]. However, simpler analysis is taken as the top and the bottom flanges are now having no web at all. Therefore under the Vierendeel truss mechanism the plastic hinges at flange ends will determine the yield shear strength of the beam V_y as

$$V_y = \frac{b_f t_f^2 f_{ysec}}{B} \quad (1)$$

where from the data mentioned above and Figure 1, Equation 1 will give $V_y = 7.9$ kN. It is noted that in Vierendeel truss mechanism, the load capacity of the beam only depends on the value of V_y and is not influenced by the beam span. This makes the short span beam and the long span beam will theoretically have the same load capacity. From Figures 2 it can be found that the full height rectangular opening castellated steel beam will have yield load capacity $P_y = 2V_y = 15.8$ kN.

2.2. Flexural strength analysis of full height rectangular opening castellated steel beam partially encased in reinforced mortar

The main function of reinforced mortar encasing in the full height rectangular opening castellated steel beam is to avoid Vierendeel truss mechanism so that the section flexural strength can be achieved. As the steel section and the longitudinal reinforcement are symmetrical, the section flexural strength analysis can be simplified by assuming that the flexural strength is provided by the summation of each material flexural strength, see Figure 4. Flexural strength provided by the mortar, M_m is

$$M_m = S_m f_m = \frac{1}{6} (b_f - t_w) (h - 2t_f)^2 f_m \quad (2)$$

where S_m = elastic section modulus of mortar, f_m = stress developed in the outer most position of mortar. Flexural strength provided by the longitudinal reinforcement, M_{sD} is

$$M_{sD} = 2F_{sD} y_1 = 2A_{sD} f_{sD} (0.5h - t_f - P_8 - 0.5D_{16}) \quad (3)$$

where A_{sD} = area of longitudinal reinforcement, f_{sD} = stress developed in longitudinal reinforcement, P_8 = diameter of transversal reinforcement, D_{16} = diameter of longitudinal reinforcement. Flexural strength provided by the flanges, M_{sf} is

$$M_{sf} = 2F_{sf} y_2 = 2A_{sf} f_{sf} (0.5h - 0.5t_f) \quad (4)$$

where A_{sf} = area of flange, f_{sf} = stress developed in flange. In yield condition it is assumed that maximum stress developed in mortar f_m is its tensile strength that can be taken as $0.1f'_m$ while $f_{sD} = f_{yD}$ and $f_{sf} = f_{ysec}$. Therefore the yield moment can be calculated as

$$M_y = M_{my} + M_{sDy} + M_{sfy} \quad (5)$$

where

$$M_{my} = \frac{1}{6} (b_f - t_w) (h - 2t_f)^2 0.1f'_m \quad (6)$$

$$M_{sDy} = 2A_{sD} f_{yD} (0.5h - t_f - P_8 - 0.5D_{16}) \quad (7)$$

$$M_{sfy} = 2A_{sf} f_{ysec} (0.5h - 0.5t_f) \quad (8)$$

Using the data mentioned before, the yield moment of full height rectangular opening castellated steel beam partially encased in reinforced mortar can be found to be 83 kNm or 3.5 times the yield moment of original steel section which is 24 kNm. This 83 kNm yield moment correlates to the yield load of 159 kN for the long span beam and 636 kN for the short span beam.

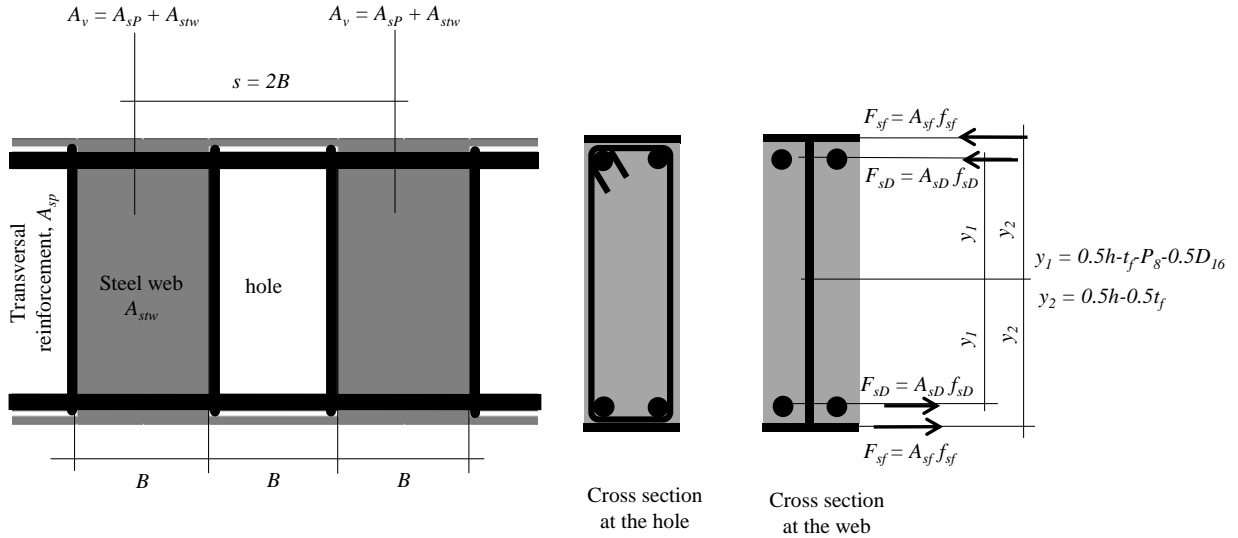


Figure 4. Steel reinforcement details for calculating flexural and shear strength of full height rectangular opening castellated steel beam partially encased in reinforced mortar

2.3. Shear strength analysis of full height rectangular opening castellated steel beam partially encased in reinforced mortar

The shear strength of castellated steel beam partially encased in reinforced mortar can be calculated by using two methods. In the first method the shear strength is calculated using the common reinforced concrete beams [14] where the shear strength is provided by the mortar V_m and by the transversal reinforcement V_s . As shown in Figure 4, transversal reinforcement A_v consists of steel hoop A_{sp} and steel web A_{stw} where the spacing is $s = 2B$. Therefore according to [14], the shear strength will be

$$V = V_m + V_s = 0.17\sqrt{f'_m}bd + \frac{(A_{sp}f_{yP} + A_{stw}f_{ysec})d}{2B} \quad (9)$$

where, b = width of the mortar section which is taken as b_f , d = depth of the mortar section which is taken as $h - 2t_f$, f'_m = mortar compressive strength, f_{yP} = yield strength of transversal reinforcement, f_{ysec} = yield strength of steel web, B = width of the web hole. However according to [14] the value of V_s shall be limited to

$$V_s \leq 0.66\sqrt{f'_m}bd \quad (10)$$

Using Equations 9 it can be calculated that $V_m = 25$ kN, $V_s = 539$ kN for the long span beam, $V_s = 706$ kN for the short span beam, and the maximum V_s from Equation 10 is 95 kN. It can be seen that the value of V_s from Equation 10 is much smaller than the calculated V_s from Equation 9. If the limitation of V_s from Equation 10 is applied, the shear strength of the specimen according to [14] will be only 120 kN and this correlates to the maximum load capacity $P = 240$ kN.

The second method to calculate the shear strength is by using diagonal strut mechanism of the mortar as shown in Figure 5. In this mechanism the shear strength V is controlled by the axial load capacity of the diagonal strut of the mortar that depends on the size of B , d , h_s , and the mortar compressive strength f'_m as shown in Equation 11.

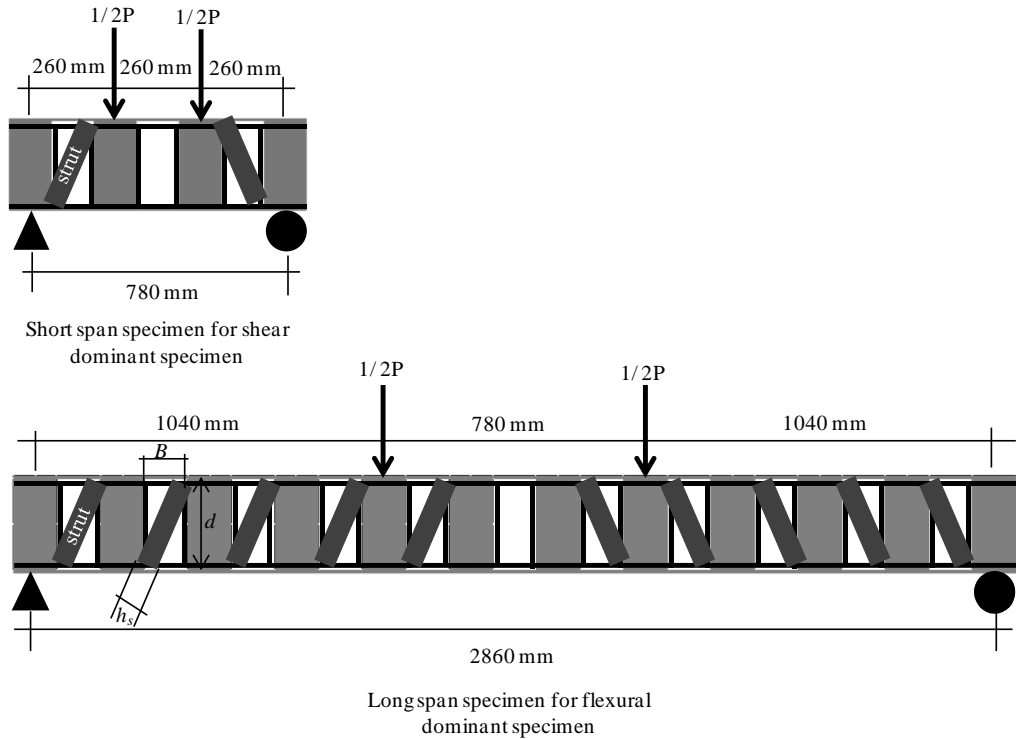


Figure 5. Diagonal strut mechanism of the mortar in full height rectangular opening castellated steel beam encased in reinforced mortar

$$V = bh_s f'_m \frac{d}{\sqrt{B^2 + d^2}} \quad (11)$$

Using the data mentioned above and Equation 11, the shear strength can be calculated using various values of h_s as shown in Table 1. It is noted that the shear capacity of the steel web itself is $ht_w f_{ytw} = 386$ kN that correlates to $P = 772$ kN.

Table 1. Value of V for variou h_s and the correlated value of P

h_s	V (kN)	P (kN)
40	143	286
60	214	428
80	286	571
100	357	714

3. Test Results and Discussions

This section discusses the comparison of the analyses explained above and the laboratory test results of short span beams [15] and the long ones [16].

3.1. Load capacity of full height rectangular opening castellated steel beam

As discussed above, the Vierendeel truss mechanism will make the load capacity of the full height rectangular opening castellated steel beam does not depend on the beam span. Figure 6 shows the load-displacement relation under Vierendeel truss mechanism of the long span beam and the short one from the test results and the calculated yield load capacity P_y . It can be seen that the yield load capacity of the both beams from the test results are quite similar. Meanwhile the calculated yield load capacity P_y can give adequate prediction of the tested beams yield load capacity. However, the short span beam looks stiffer than the long beam as the short span beam has less cumulative displacement due to Vierendeel truss mechanism than the long span beam. Both beams also do not show elasto-plastic behaviour, the higher stiffness in the post elastic condition can be caused by the effect of tension stiffening due to large displacement effect especially in the short span beam.

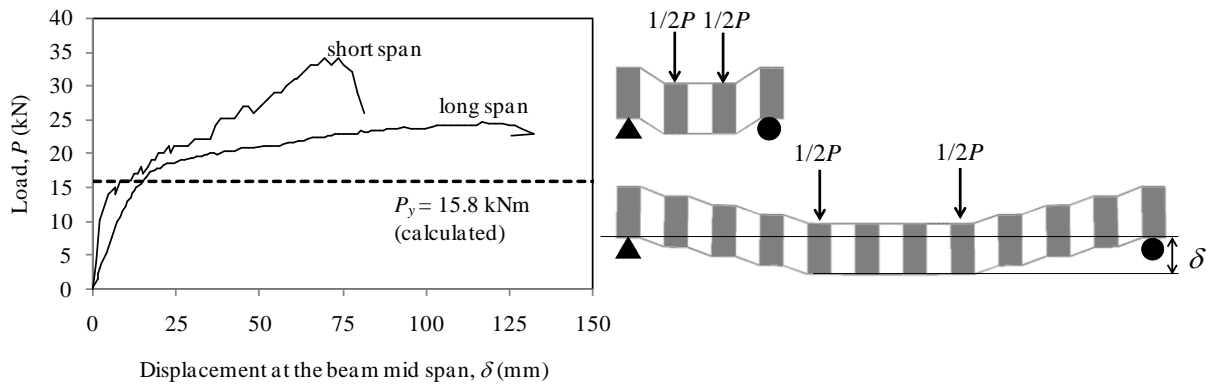


Figure 6. Load-displacement relation of full height rectangular opening castellated steel beam under Vierendeel truss mechanism

3.2. Flexural strength of full height rectangular opening castellated steel beam partially encased in reinforced mortar

Figure 7 shows moment-displacement relationship of the short span beam and the long span beam. Theoretically flexural yield capacity shall be the same between the short span beam and the long one, that is $M_y = 83$ kNm. However it can be seen from the figure that the short span beam does not reach its yield moment capacity due to shear failure occurred prior to the yield moment could be reached, therefore the short beam failed in a brittle manner. On the other hand the long span beam could reach its yield moment so that the beam failed in ductile manner. In Figure 7 it can also be noted that the application of Equations 5 to 8 can predict quite well the yield moment of full height rectangular opening castellated steel beam partially encased in reinforced mortar that failed in flexure.

3.3. Shear strength of full height rectangular opening castellated steel beam partially encased in reinforced mortar

As mentioned before the tested short span beam failed in shear after diagonal crushing in the strut mechanism of mortar around the web hole and then was followed by Vierendeel truss mechanism, see Figure 8. Figure 9 shows the comparison of short span beam load capacity of test result, calculated flexural load capacity, and several calculated shear load capacities, where the real shear load capacity of the short beam is 582 kN. This real shear load capacity is less than the load capacity provided by the flexural strength which is 636 kN or by the steel web which is 772 kN, but higher than the calculated shear load capacity based on [14] which is 240 kN. Adequate prediction of the shear strength can be achieved by the method of diagonal strut mechanism of the mortar with the value of $h_s = 80$ mm as shown in Table 1 which is 571 kN. However, further study is still required in order to calculate analytically the appropriate value of h_s for any given size of web opening.

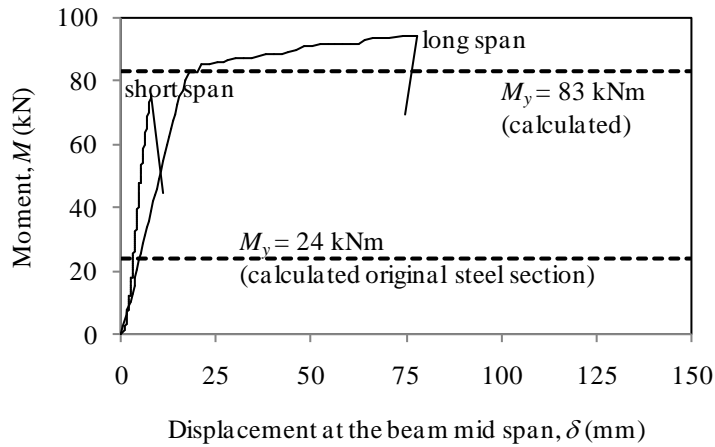


Figure 7. Moment-displacement relation of full height rectangular opening castellated steel beam partially encased in reinforced mortar

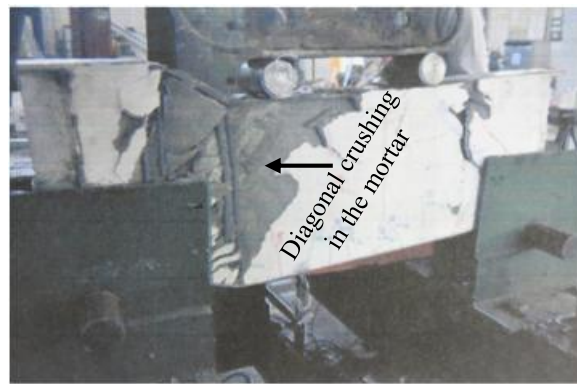


Figure 8. Brittle shear failure due to diagonal crushing of strut mechanism in the mortar of short span beam that causes Vierendeel truss mechanism [15]

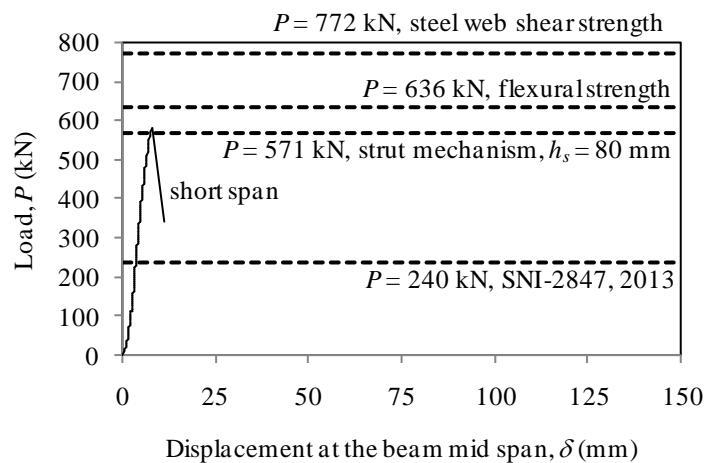


Figure 9. Shear load capacity of full height rectangular opening castellated steel beam partially encased in reinforced mortar of short beam

4. Conclusions

From the above discussions the following conclusions can be made.

- Full height rectangular opening pattern in the web of castellated steel beam can increase the height of steel section to be almost as twice as its original section height but the load capacity decreases due to Vierendeel truss mechanism.
- Reinforced mortar encasing method can prevent the full height rectangular opening castellated steel beam from Vierendeel truss mechanism so that the flexural yield strength can be achieved and is much higher than the original one. In this research the yield moment capacity of full height rectangular opening castellated steel beam partially encased in reinforced mortar is 83 kNm or increase 3.5 times from its original section yield moment which is only 24 kNm.
- Diagonal strut mechanism of the mortar at the web holes can be used to calculate the shear strength of full height rectangular opening castellated steel beam partially encased in reinforced mortar but further study is still required to analytically determine the appropriate size of h_s .

References

- [1] Boyer, J. P., 1964, Castellated Beams—New Developments, AISC National Engineering Conference, Omaha, Nebr., May 1964.
- [2] Das, P.K., and Srimani, S.L., 1984, Handbook for the Design of Castellated Beam, Central Mechanical Engineering Research Institute, Durgapur, Mohan Pramlari for Oxford & IBH Publishing Co.
- [3] Estrada, H., Jimenez, J. J. , and Aguiñiga, F., 2006, Cost Analysis in the Design of Open-Web Castellated Beams, Building Integration Solutions, ASCE.
- [4] Anupriya, B. and Jagadeesan, K., 2014, Shear Strength of Castellated Beam with and without Stiffeners Using FEA (ANSYS 14), International Journal of Engineering and Technology (IJET), Vol 6 No 4 Aug-Sep 2014.
- [5] Weng, C.C., Yen, S.I., and Jiang, M.H., 2002, Experimental Study on Shear Splitting Failure of Full-Scale Composite Concrete Encased Steel Beams, Journal of Structural Engineering, 2002.128:1186-1194.
- [6] Ali, A.A., Sadik, S., N., and Abdul-Sahib, W.S., 2012, Strength and Ductility of Concrete Encased Composite Beams, Engineering & Technology Journal, Vol.30 , No.15 , 2012.
- [7] Nagashima, T and Takiguci, K, 1996, Seismic Strength of Small Size Steel Encased Reinforced Concrete Columns with High Strength Materials, Paper No. 593, Eleventh World Conference on Earthquake Engineering.
- [8] Weng, C.C. and Yen, S.I., 2002, Comparisons of Concrete-encased Composite Column Strength Provisions of ACI Code and AISC Specification, Engineering Structures 24 (2002) 59–72.
- [9] Chen, C.C, Li, J.M., and Weng, C.C., 2005, Experimental Behaviour and Strength of Concrete-encased Composite Beam–columns with T-shaped Steel Section Under Cyclic Loading, Journal of Constructional Steel Research 61 (2005) 863–881.
- [10] Chen, C., C., and Lin, K.T., 2009, Behavior and Strength of Steel Reinforced Concrete Beam–column Joints with Two-side Force Inputs, Journal of Constructional Steel Research 65 (2009) 641–649.
- [11] Chen, C.C., Suswanto, B., Yu-Jen Lin, Y., J, 2009, Behavior and Strength of Steel Reinforced Concrete Beam-column Joints with Single-side Force Inputs, Journal of Constructional Steel Research 65 (2009) 1569-1581.
- [12] Gong, B. and Shahrooz, B.M., 2001, Steel-concrete Composite Coupling Beams — Behavior and Design, Engineering Structures 23 (2001) 1480–1490.
- [13] Motter, C.J., Wallace, J.W., Klemencic, R., Hooper, J.D., and Fields, D.C., 2012, Large-Scale Testing and Analysis of Concrete Encased Steel Coupling Beams under High Ductility Demands, 15th World Conference of Earthquake Engineering, Lisboa.
- [14] SNI-2847, 20013, Requirements of Structural Concrete for Buildings, BSN (Badan Standarisasi Nasional), Indonesia
- [15] Helda, D., 2012, Shear Behaviour of Rectangular Hole Pattern Castellated Beam with Reinforcement and Mortar Composite, Master Thesis, Post Graduate Program, Department of Civil and Environmental Engineering, Universitas Gadjah Mada, Indonesia
- [16] Oliveira, A., T., C., R., D, 2012, Flexural Behaviour of Rectangular Hole Pattern Castellated Beam with Reinforcement and Mortar Composite, Master Thesis, Post Graduate Program, Department of Civil and Environmental Engineering, Universitas Gadjah Mada, Indonesia



Sustainable Civil Engineering Structures and Construction Materials, SCESCM 2016

Supply chain management strategy for recycled materials to support sustainable construction

Mochamad Agung Wibowo^{a,*}, Elizar^a, Moh Nur Sholeh^a, Hadjar Seti Adji^b

^a*Diponegoro University, Jl. Prof Soedharto, SH, Semarang, 50275, Indonesia*

^b*PT Perusahaan Perumahan Persero (Tbk), Jakarta*

Abstract

Sustainable construction as a construction method is a beginning to gain traction among Indonesian contractors, but with the dearth of research, knowledge, socialization and strategic support in this field, there are many obstacles towards *en masse* adoption in Indonesia: to be applied “effectively” and to become part of a “strategic method”. The concept of Sustainable Construction primarily emphasizes the wise use of resources (primarily natural resources), thereby systematically guaranteeing the fulfillment of future needs. However, the use of recycled materials is still hampered by the difficulty of field implementation; this is attested by the low scores attained in green building certification. This study will analyze the strategies needed to support sustainable construction in relation to supply chain management for materials, which have not been implemented well in Indonesia, whereas it has the highest impact in contributing to the effectiveness of sustainable construction. The aim of study is to analyze supply chain performance in materials of construction projects. The measurement used is the Supply Chain Operations Reference (SCOR) model with perfect order fulfillment and overall value at risk as a Key Performance Indicator (KPI). The result of the study is the percentage of material that could be used by the management of supply chain. Once the KPI is more fulfilled by perfect order fulfillment, the use of material is more complete to support sustainable construction.

© 2017 The Authors. Published by Elsevier Ltd.

Peer-review under responsibility of the organizing committee of SCESCM 2016.

Keywords: supply chain management, recycled materials, SCOR and sustainable construction

* Corresponding author. Tel.+: +62-24-7460053 fax: +62-24-7460055

E-mail address: agung_wibowo8314423@yahoo.co.uk

1. Introduction

In order to accelerate the economic growth in various regions, the Government of Indonesia encourage the development of infrastructure with the target of investment is 2.000 trillion rupiah in 2025. Planning of infrastructure development includes the technical and management matters such as cost, quality, time, safety and environment. Along with the development of infrastructure, supply chain has become one of the topic for research in construction management subject [1].

Any construction project always needs resource projects as a component input in the construction process. One of them is material. Material is one of the project resources that were quite dominant in determining the quality of the construction [2]. The construction industry has a great impact on the environment in the form of natural resources that are used as well as the solid waste that is generated, and they could harm the surrounding environment. The previous research states that the sheer number of solid waste generated by the construction is 20-30% of construction projects in Brazil, and 1-10% in Netherlands [3]. To anticipate the issues related to environmental impacts, it is necessary to use waste management as part of the construction project management [4]. Therefore, in this study will analyze the construction supply chain management which is to reduce waste by using Key Performance Indicator (KPI) of Supply Chain Operations Reference (SCOR) and see the cause.

2. Literature Study

2.1. Sustainable Construction

Sustainable construction is a process whereby, over time, sustainability is achieved. The concept of sustainability must be applied into construction industry to influence the manner in which a project shall be conducted to strike a balance between conserving the environment and maintaining prosperity in development [5]. Environmentally sustainable building construction has experienced significant growth during the past decade [6]. Furthermore, some local governments are adopting green building providing permitting and financial incentives or standards and regulations for sustainable development. In another study, sustainable construction faces economic challenges at different areas [7]. The first is macroeconomic area that the goals of sustainable construction are being implemented in individual countries in which the share of construction output is decreasing. The second is mesoeconomic area that the construction sector depends on the implementation of the goals of sustainable development across the national economy as a whole.

2.2. Supply Chain Management

Supply chain management is the integration of key business processes from end user through original suppliers that provides products, services, and information that add value for customers and other stakeholders [8]. Supply chain management is ultimately about influencing behavior in particular ways and particular directions [9]. There are four specific roles in construction, see Fig. 1.

2.3. Supply Chain Operations Reference (SCOR)

Supply Chain Operations Reference (SCOR) model provides a unique framework that connects performance metrics, best practices, processes, and people into a unified structure [11]. The frameworks will supports communication between supply chain partners and enhances the effectiveness of supply chain management, related supply chain improvement activities, and technology. SCOR is a consensus model. SCOR is developed and continues to evolve with the direct input of industry leaders who manage global supply chains and use it daily to analyze and improve the performance of their groups. It features an intentionally broad scope and definitions that can be adapted to the specific supply chain requirements of any application or industry. There are 11 Key Performance Indicators (KPI) in SCOR. These KPI are perfect order fulfillment, order fulfillment cycle time, upside supply chain flexibility, upside supply chain adaptability, downside supply chain adaptability, overall value at risk, supply chain management cost, cost of goods sold, cash to cash cycle time, return on supply chain fixed assets, and return on working capital.

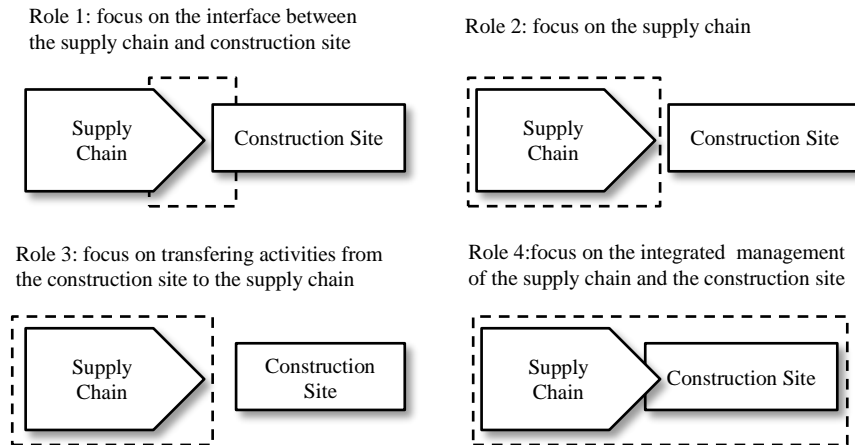


Fig. 1. The four specific roles in construction [10]

2.4. Waste in Construction

Waste in construction is defined as the difference between the value of those materials delivered and accepted on site and those used properly as specified and accurately measured in the work, after the deducting cost saving of substituted materials and those transferred elsewhere [12]. As the information flows and matures through this process, the tasks performed add value to the information, transform it from its initial state of raw data to the completed ready to build data. However, there are not everything that begins from raw data results useful information and the team recognize this through the application of the seven manufacturing waste categories to information, list in Table 1.

Table 1. Seven Waste Categories [13]

No	Waste	Description
1	Overproduction	Too much detail, unnecessary information, redundant development, over-dissemination, pushing rather than pulling data
2	Transportation	Information incompatibility, communication failure, multiple sources, security issues
3	Waiting	Information created too early or unavailable, late delivery, suspect quality
4	Processing	Unnecessary serial effort, too many iterations, unnecessary data conversions, excessive verification, unclear criteria
5	Inventory	Too much information, poor configuration management, complicated retrieval
6	Unnecessary Movement	Required manual intervention, lack of direct access, information pushed to wrong sources, reformatting
7	Defective Product	Lacking quality, conversion errors, and incomplete, ambiguous, or inaccurate Information, lacking required tests/verification

3. Research Method

Various research have conducted, either of research in supply chain management strategy. In Indonesia, is still needs conducted research for supply chain management for materials. The aim of study is to analyze supply chain performance in materials of construction projects. The measurement used is the Supply Chain Operations Reference (SCOR) model with perfect order fulfillment (POF) and overall value at risk (VaR) as a Key Performance Indicator (KPI). The result of the study is the percentage of material that could be used by the management of supply chain. Once the KPI is more fulfilled by perfect order fulfillment, the use of material is more complete to support sustainable construction. Furthermore, causes of waste material is obtained through interviews with the team using the instrument supplier questionnaire. Flow chart of research method is shown in Figure 2.

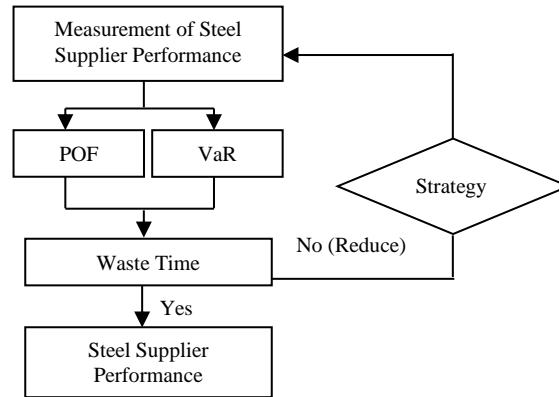


Fig 2. Flow Chart of Research Method

Perfect order fulfillment and overall value at risk was chosen from several KPI of SCOR because it is based on literature review and validation to the project very closely related to sustainable construction. In KPI of perfect order fulfillment, more complete delivery of materials to the project is better. While on the KPI of overall value at risk, the risk that occurred during the procurement of materials is better. 2 KPI’s which will help to measure in view of waste in construction projects relating to steel suppliers.

4. Result and Discussion

Measurements were made with a view reference to the scale of the existing performance compared with the results of calculations on each indicator and then determined a scale of performance per indicator. The scale of each performance then totaled and averaged so it could be seen how was the overall value of the supply chain in this steel material. Steel supplier performance measurement was shown in the Table 2.

Table 2. Value of KPI

No	KPI	Operational Definition	Application in Construction	Scale	Value	Category	Result of Analysis
1	Perfect order fulfillment	The percentage of orders delivered in full, delivery performance to customer commit date, documentation accuracy, and perfect condition.	The percentage of steel material order that fulfillment in order, documentation accuracy, and perfect condition.	5	> 90%	Excellent	90%
				4	81% - 90%	Good	
				3	71% - 80%	Average	
				2	61 % - 70%	Poor	
				1	≤60%	Execrable	
2	Overall value at risk	The value of the risk borne by the company as a whole	The value of the supplier risk when there are order or it send steel materials.	5	> 90%	Excellent	80%
				4	81% - 90%	Good	
				3	71% - 80%	Average	
				2	61 % - 70%	Poor	
				1	≤60%	Execrable	

Based on the table above there was a scale, value, and category of KPI assessment. A scaling of the concept Linkert scaled with a range of values of 1 to 5. Determination the value based on the study of various references in the literature determine the highest and smallest value. While the determination of the category followed the existing scale with the category of excellent, good, average, poor, and execrable.

Delivery of materials from suppliers to the project had always pursued in good condition and complete. But in fact there might be constraints in the delivery. Product defect occurred, damaged on delivery, the calculation of the amount of material that was incomplete sometimes became a limiting factor. The value of perfect order fulfillment was 90%. Reinforcing steel company basically had been already anticipating the risks that would occur in the supply chain

activity. However, as the company was still modest scale distributors, identification of risks did not so maximum. The value of overall value at risk was 80%.

It means, there is 10% waste for perfect order fulfillment and 20% for overall value at risk. Base of interview by supplier and analyze, cause factor of waste was shown in Table 3.

Table 3. Cause factor of waste

Cause factor of waste	Perfect order fulfillment	Overall value at risk
Poor weather conditions	√	√
Ordering of material is not within specifications	√	√
Damaged material		√
Slow information flow between parties	√	√

The causes factor of waste of perfect order fulfillment were poor weather conditions, ordering of material was not within specifications, and slow information flow between parties. Poor weather conditions such as rain, floods, and hurricanes could hinder the delivery of materials. Ordering of material was not within specifications resulting material could not be used and had to be returned. Slow information flow between parties led to the delay orderings and shipping materials. While the causes of overall value at risk were poor weather conditions, ordering of material was not within specifications, damaged material, and slow information flow between parties.

4. Conclusion

Based on the result and discussion, it can be concluded that the supply chain management strategy for material of steel is measuring performance which is a critical part of the supplier relationship management process because management needs to assess the success of the firm's relationships. The other processing teams communicate to the supplier related to performance to the accounting teams who tie these metrics back to the profit of both the firm and the supplier, and report the results both internally and to the supplier. The objective of supply chain management is to create the most valuable result for the entire supply chain network, including the end-customer. Successful supply chain management involves the coordination of activities within the firm and between members of the supply chain. Supply chain management strategies can support investment in sustainable construction.

The performance indicators in measuring the performance of the supply chain based on the SCOR model are composed of perfect order fulfillment and overall value at risk. The results of measurements on steel suppliers show that the value of perfect order fulfillment is 90 % while the overall value at risk by 80 %. It shows that there are about 10 % of waste when measuring perfect order fulfillment and 20 % waste when measuring the overall value at risk. Waste is caused by poor weather conditions, Material order that is out of specifications, and slow information that flows between parties to perfect order fulfillment. While waste of overall value at risk is caused by poor weather conditions, Material order that is out of specifications, damaged material, and slow information that flows between parties.

For further research might be added regarding the performance indicators measured. It also increase the number of respondents, so adding material analysis in supply chain management may reduce the construction waste.

References

- [1] M. A. Wibowo and M. N. Sholeh, "The analysis of supply chain performance measurement at construction project," *Proceeding The 5th International Conference of Euro Asia Civil Engineering Forum (EACEF-5)*, p. 25 – 31, 2015.
- [2] W. I. Ervianto, *Save the Earth Through the Green Construction*, Yogyakarta: Andi Offset, 2012.
- [3] L. Ekanayake and G. Ofori, "Building Waste Assessment Score: Design-Based Tool," *Journal Building and Environment*, 2001.
- [4] Q. Zhu and J. Sarkis, "Relationships between operational practices and performance among early adopters of green supply chain management practices in Chinese manufacturing enterprises," *Journal of Operations Management*, p. 265–289, 2004.
- [5] N. Z. Abidin, "Sustainable Construction in Malaysia – Developers' Awareness," *Proceeding of World Academy of Science, Engineering and Technology*, 2009.
- [6] L. B. Robichaud and V. S. Anantmula, "Greening Project Management Practices for Sustainable Construction," *Journal of Management*

in *Engineering*, p. 48–57, 2011.

- [7] R. Bon and K. Hutchinson, "Sustainable construction: some economic challenges," *Building Research & Information*, p. 310–314, 2000.
- [8] D. M. Lambert and M. C. Cooper, "Issues in Supply Chain Management," *Industrial Marketing Management*, pp. 65-83, 2000.
- [9] J. Storey, C. Emberson, J. Godsell and A. Harrison, "Supply chain management: theory, practice and future challenges," *International Journal of Operations & Production Management*, vol. 26, pp. 754-774, 2006.
- [10] R. Vrijhoef and L. Koskela, "The four roles of supply chain management in construction," *European Journal of Purchasing & Supply Management* 6, pp. 169-178, 2000.
- [11] S. C. Council, Supply Chain Operations Reference (SCOR®) model, USA: Cypress,, 2010.
- [12] S. Nagapan, I. A. Rahman, A. Asmi, A. H. Memon and R. M. Zin, " Identifying Causes of Construction Waste-Case of Central Region of Peninsula Malaysia," *Journal of Integrated Engineering*, pp. 22-28, 2012.
- [13] H. L. McManus and R. L. Miilard, "Value Stream Analysis and Mapping For Product Development," in *Proceedings of the International Council of the Aeronautical Sciences*, 2002.



Sustainable Civil Engineering Structures and Construction Materials, SCESCM 2016

Experimental evaluation of masonry infill walls of RC frame buildings subjected to cyclic loads

Mochamad Teguh^{a,*}

^aIslamic University of Indonesia, Kaliurang Street KM 14.5, Yogyakarta, 55584, Indonesia

Abstract

Masonry infill walls of reinforced concrete frame structures are commonly used for non-engineered and engineered buildings. For this establishment, exterior walls and interior partitions are made of masonry for producing a cost-effective solution for building purposes. Although walls are usually considered as a non-structural element of reinforced concrete frame structures, the masonry infill walls contribute significantly to the seismic building performance. The interaction effect between bounding frame and infill wall is a complicated issue in the experimental test. This paper presents experimental investigations of masonry infill walls of RC frame buildings under cyclic in-plane loads. Three typical reinforced concrete frames with and without infill masonry walls were experimentally conducted to seek their structural behavior in terms of stiffness, strength and ductility of the structures. In this research, tie-beam and tie-column (practical beam and column) components applied to non-engineered buildings were adopted to perform typical reinforced concrete frames. Their hysteretic behavior of RC frames as well as the effect of gaps between the frame and the infill on the structural behavior are briefly discussed.

© 2017 The Authors. Published by Elsevier Ltd.

Peer-review under responsibility of the organizing committee of SCESCM 2016.

Keywords: structural behavior; stiffness; strength and ductility; infill masonry wall; cyclic in-plane load; non-engineered building.

1. Introduction

Seismic response of building structures to strong earthquake frequently produces in excessive and uncontrollable lateral displacements as well as serious damages to structural and non-structural elements. Consequently, this may accumulate damage sustained under repeated load reversals affecting to the lateral stability of the building due to the load-displacement effect [1, 2]. Reinforced concrete structures, for instance, accumulate damage resulting from cyclic

* Corresponding author. Tel.: +62-274-898471; fax: +62-274-858330.

E-mail address: m.teguh@uii.ac.id

inelastic deformations in a way that is completely different from that for steel structures. Given this condition, drift control requirement in the design of multi-story building should be considered to limit overall drift index (R) or inter-story drift index (d) in order to meet the building codes like SNI 1726-2012 [3], where drift can be determined based on the magnitude of the lateral displacement at the top of the building relative to its base. Considering the concept of earthquake resistant design for the high-rise building structure, earthquake load dominated tends to occur rather than gravity load dominated [4].

In some seismic-prone countries, residential buildings are constructed using both reinforced concrete (RC) and unreinforced masonry walls. Despite of their popularity, there is a general lack of knowledge concerning the seismic behavior of such mixed systems and they are often designed using oversimplifying assumptions. Buildings with masonry infill walls in reinforced concrete (RC) frames are commonly used in all around the world [5]. Most of masonry infill walls are widely used as partition walls because of their lightweight nature, ease of construction, cost-performance efficiency, and architectural attractiveness. There has been at least two controversy assumptions in the design of masonry buildings, i.e., firstly infill walls are unaccounted for the design assuming they serve as additional elements that may increase the stiffness of the RC frame and provide better deformation control for the structure, secondly the presence of infill walls may endanger the seismic design philosophy for frame action due to the damage imposed on the boundary elements. Both arguments are probably true when the level of lateral deformation demands is taken into account in the design consideration. Utilizing infill walls in frame structures causes their strength, stiffness, and displacement ductility increased.

The seismic response of RC frames with masonry infill walls has become a major investigation topic. An experimental investigation of masonry infill walls of RC frame buildings under cyclic in-plane loads presented in this paper is undertaken to seek its structural behavior in terms of stiffness, strength and ductility of each structure. Based on the experimental tests, the structural performance of RC frames can be evaluated by comparing to each structural behavior. Most importantly, this research finding may help engineers in understanding the contribution of infill walls based on experimental data for more accurate seismic assessment of RC frames applied to non-engineered buildings. This research is motivated to develop structural design of appropriate masonry based construction method in urban areas especially in Indonesia.

1.1. Masonry Materials and Construction System

A variation of raw building materials with different compositions is widely used for the production of traditionally and industrially made masonry units. Mortar is usually composed of lime, cement, and sand in variety of proportions, and mixed with water. In fact, the mortar can be added with or without additives depending on its application. To reinforce the masonry wall, steel reinforcing bars of different shapes and quantities embedded and connected to RC columns in mortar are often used to increase their strength contribution. Every masonry wall has its own specific mechanical characteristics, they are generally expected to produce a homogeneous structural material in resisting to permanent and temporary actions. Not all materials, however, can be encountered together depending on which materials may be composed together in a structure. In practice, the masonry construction system consists of: (a) unreinforced (plain) masonry, consisting of mortar and masonry units; (b) confined masonry, utilizing masonry units, mortar, reinforcing steel and concrete, (c) reinforced masonry, composing masonry units, mortar, reinforcing steel, and concrete infill. In fact, the unreinforced masonry has mechanical properties such as strength and ductility inferior compared to confined masonry and reinforced masonry.

The masonry units either from brick or concrete block can be solid or hollow and made from fired clay, concrete, calcium silicate or natural stone. The most common masonry units used over the world are burned clay brick and concrete block. Mortar strength can be specified based on its variation comprising lime or a mixture of cement, lime, sand, and water. Different mortar variation produces masonry properties vary from one structure to others depending on the properties of the interaction between components, type of units, and mortar used. In this research, the masonry infill walls were made of clay brick and concrete block mounted with mortar using ratio of 1:4 cement-coarse sand, and mixed with water. In addition to the clay brick material, it is made of clayey earth, consisting of 30-40% clay and 60-70% earth, which is mixed with water. Straw is often added to the mix of clay and earth (7-10 kg per m³ of earth) in order to prevent cracking. In an attempt to improve the compressive strength of the units, cement or gypsum or fly

ash is occasionally substituted as stabilizer and/or filler [6]. The clay brick and concrete block are usually dried under the sun for a couple of days.

In this research, all materials encompassed concrete block, clay brick, mortar, concrete material (cement, coarse sand, and gravel), and reinforcing steel were used domestic products. This research investigates structural performance of walling systems considering their construction methods which are applicable to non-engineered houses. These masonry products are commonly produced either by hand- or machine-made (fabricated), and they may cause material qualities differently. Consequently, each masonry product produces random quality on its characteristic and precision. Hand-made concrete blocks and fabricated clay bricks were used to prepare specified specimens. For the best wall resistance, it should be selected fabricated concrete blocks or brick masonry for walling system [7]. Furthermore, each material used in this research was carefully observed as listed in Table 1.

1.2. Structural Behavior of Confined Masonry Wall

The masonry walls have a main economic interest and contribute significantly to the building performance. Even though infill walls do not respond to load-bearing function, however they give significant contribution to seismic behavior of buildings. Given this condition, adequate structural performance of the masonry walls is essential to avoid the occurrence of severe in-plane damage resulting very large economical losses, and the out-of-plane expulsion affecting to additional large risk of human life. Two different construction systems of masonry wall, i.e, confined masonry and RC frame infill wall masonry have been investigated by some previous researchers [4, 7-12]. In this research, a construction system of confined masonry was used in all specimens except for the bare frame. Masonry structural walls are generally restrained on four sides with RC tie-beams and tie-columns, which are intended to carry vertical and/or horizontal loads, and they are designed to perform as a moment resisting frame. Whilst, in the construction system of RC frame infill wall masonry is constructed in vice versa. Both construction systems produce different structural behavior in withstanding seismic actions. In this research, the experimental tests were conducted to evaluate the structural behavior of each specimen subjected to cyclic loads.

Based on the experimental investigations and lessons learned after earthquakes, the confined masonry produces in improving the connection between structural walls, the stability of slender structural walls, and the strength and ductility of masonry panels. In contrast, ignoring the effect of the infill panels on the structural behavior may underestimate the stresses that develop in some elements during seismic actions. Consequently, such an oversight could lead to premature failures and increases life safety risks. In addition, this system has reduced the risk disintegration of masonry panels damaged by the earthquake. In this case, vertical and horizontal confining elements should precisely meet at the corners and recesses of the building, and at all joints as well as wall intersections. In other words, the reinforcement detail should be well-designed considering the concept of earthquake resistant building [3].

2. Experimental Program

2.1. Material Properties

The foundation component was reinforced and confined with rebar diameter of 13 mm having a confinement pitch of 125 mm. The common dimension of tie-beams and tie-columns was 120x120 (mm) with a length of 3300 mm, height of 3350 mm, and the rest dimension is detailed in Fig. 1. The tie-beams and tie-columns were reinforced with four longitudinal bars of 10 mm diameter and confined with a bar of 8 mm diameter giving a confinement pitch of 150 mm.

In preparing for the best experimental tests, each specimen was restrained with a strong foundation component which was sufficiently bolted at the rigid floor in order to avoid tilting problems during the specimen tested. Given this reason, the foundation was reinforced with higher compressive strength of concrete and tensile strength of reinforcing steel than other components such as tie-beams and tie-columns. With regard to seek more contribution of the confined masonry wall, the compressive strength of concrete of the tie-beam was provided less strength compared to the tie-column. Table 1 briefly presents material properties used in this research.

It was observed that the masonry walls with and without plaster were also tested with their dimensions of 475x595x140 mm and 475x595x110 mm respectively. The compressive strength of both walls are 1.82 MPa and 2.56 MPa. These are comparable with the compressive strength of 2.18 MPa which is computed using an empirical formula. Depending on the compressive strength of masonry wall, the modulus of elasticity can be accounted for at 2215.61 MPa and 1783.06 MPa respectively. The average strength of mortar is 7.49 MPa with ratio of 1:4 cement-coarse sand, which is very good for constructing the masonry wall. All materials used in this research including their usage are briefly presented in Table 1 explaining their strength and modulus of elasticity.

Table 1. Observed material properties.

No.	Materials	Diameter (mm)	Average tensile strength (MPa)	Average compressive strength (MPa)	Modulus of elasticity (MPa)	Description
1.	Reinforcing steels	13.00	484.31		2.0×10^5	Foundation
		10.00	368.33		2.0×10^5	Tie-beam & tie-column
		8.00	338.50		2.0×10^5	Shear reinforcement
2.	Concrete			22.03	2.2×10^4	Foundation
				18.13	2.0×10^4	Tie-beam
				14.17	1.8×10^4	Tie-column
				6.44	2.2×10^3	With plaster
3.	Clay brick			6.44	2.2×10^3	With plaster
4.	Concrete block			2.62		Low strength material
5.	Mortar			7.49		Mixture ratio: 1:4 cement-course sand

Fig. 1 shows a typical in-plane instrumentation installed at each specimen. The instrumentation consists of strain gauge and Linear Variable Differential Transformer (LVDT). The strain gauge is a device used to measure strain on an object, whilst the LVDT is a well-established transducer design which has been used throughout many decades for the accurate measurement of displacement and within closed loops for the control of positioning. Table 2 describes the instrumentation used in this research. Different positioning of the instrumentation on the bare frame was made with less numbers of instrumentation installed. Meanwhile, the instrumentation on both confined concrete block and clay brick masonries were installed more devices.

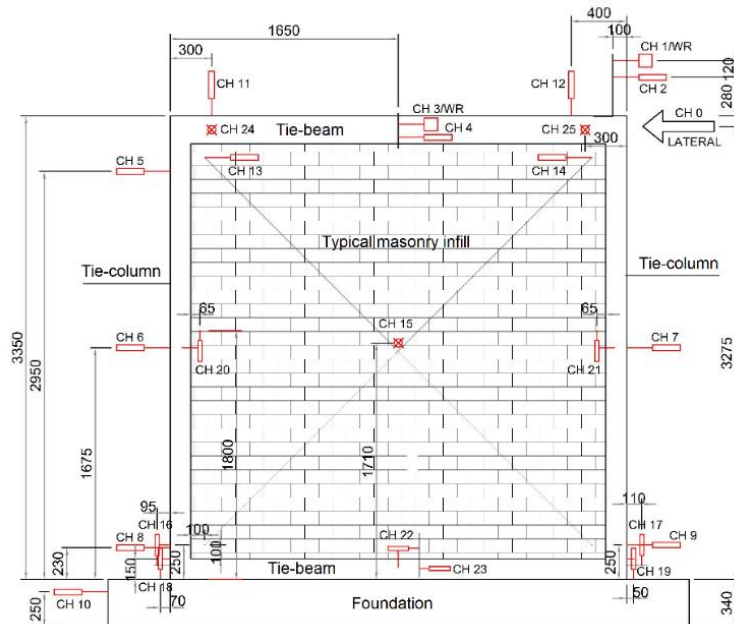


Fig. 1. Frame dimensions and typical in-plane instrumentation.

In general, the strain gauges and transducers were placed at specified objects to measure the strains and displacements at certain locations. The measured objects were positioned at the longitudinal reinforcement, confinement, concrete, anchorage, and other critical points. The most important effects of the interaction between the infill masonry and the frame were crack development either in the frame or in the wall, load-displacement response, and crack development creating the risk of brittle failure.

Table 2. Allocation of devices installed

No.	Type of specimen	Installed strain gauge (SG)	Installed LVDT (Transducer)	Description
1.	Bare frame	36	19	
2.	Confined concrete block	46	25	4 SG's installed in concrete at each b/c joint
3.	Confined brick	46	25	

2.2. Experimental Setup

The aim of the experimental campaign is to evaluate structural behavior of the practical RC frames used in non-engineered buildings, with and without infill masonry walls, constructed according to the traditional building process. Three specimens consisting of a bare frame, a confined concrete block masonry, and a confined brick masonry were investigated under in-plane cyclic loads until they reached a predetermined value (2% drift). Fig. 2 depicts experimental setups for two different types of specimen. The main component of the testing facilities as well as the hydraulic equipment and loading frame are shown in Fig. 2.

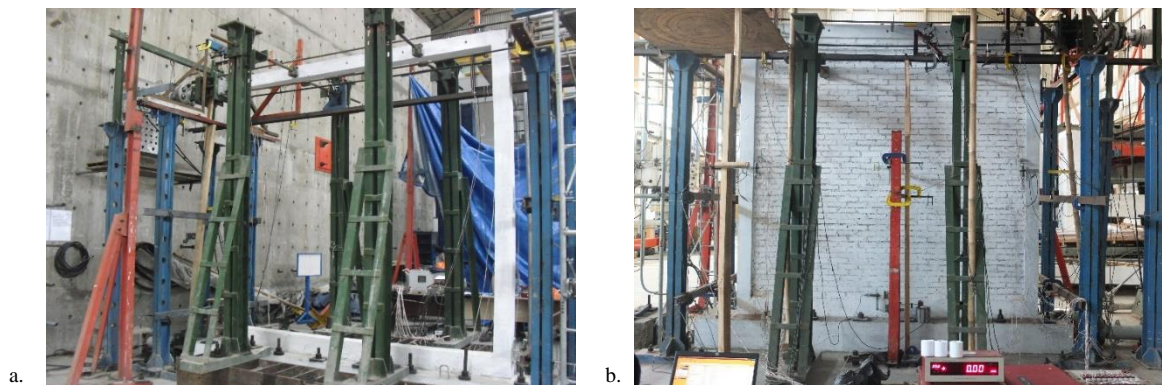


Fig. 2. Experimental setups: (a) bare frame; (b) typical confined masonry walls.

2.3. Test Procedure

All specimens having the same dimension and reinforcement were examined subjected to fully reversed quasi-static cyclic loads with normal rate of loading. The lateral loads were imposed utilizing displacement-controlled movements of the hydraulic jack following the specified displacement history. Testing was stopped when the maximum lateral load at specified cycle was reduced up to 80% of the ultimate load assuming that 20% loss in lateral load resisting capacity. At each load cycle, the crack propagation was recorded to plot the cracking patterns at failure for all specimens. Other data were precisely measured using the installed devices and stored in the data logger and PC unit for further data processing.

3. Results and Discussion

During strong ground motions subjected to earthquake, structures suffer several cycles of large reversals of lateral forces [13]. In the design of seismic philosophy, the members are usually allowed to be stressed beyond their working stress limit and at this condition the members experience cracking and yielding. The interaction between the infill walls and the RC frame members subjected to in-plane cyclic loads was examined experimentally in this study [14]. Three RC frame specimens, one of which was featured without infill walls while the other two with infill walls, were tested. The frame specimens were designed in such a way utilizing practical dimensions of RC column and beam members, so called tie-column and tie-beam members, in order to simulate the failure of the structural and non-structural components due to lateral cyclic loads. The frame specimens were quasi-statically pushed and pulled in horizontal direction at the top of center beam-column joint under displacement control to investigate the structural behavior of the RC frames, with a focus on the effects of infill walls. A special attention was emphasized on the physical quantities and phenomena of great interest in this study include the collapse resistance force and mechanism, strain variation and crack development in structural and non-structural components, and failure modes of the infill walls and the frames.

The masonry walls have been widely employed in existing RC building structures either as external infill or internal partitions. Although the masonry walls practically interact with the main structural members and, therefore, they affect the seismic response of RC frames, however the mechanical contribution of masonry infill walls are generally neglected in practice-oriented structural analyses. Simulating the actual dynamic behavior of these components and evaluating their effect on the global seismic response of RC structures have recently become a great attention by the scientific community [2, 5, 6, 8], nevertheless, the procedure has not been established so far for considering their contribution of masonry infills in practice-oriented seismic analyses of RC frames.

3.1. Hysteretic Behavior of Bare Frame

The mode of failure of the bare frame was generally combined flexural yielding at column bases and at beam-column joints, and bond deterioration of the beam reinforcement in the confined core of the joint region. Fig. 3 presents the load-displacement hysteretic behavior of the bare frame representing a full scale graph (Fig. 3a) and a zoomed hysteretic loop (Fig. 3b). Fig. 3 depicts the maximum displacement of 90.14 mm and the lateral load resisting capacity of 5.77 kN.

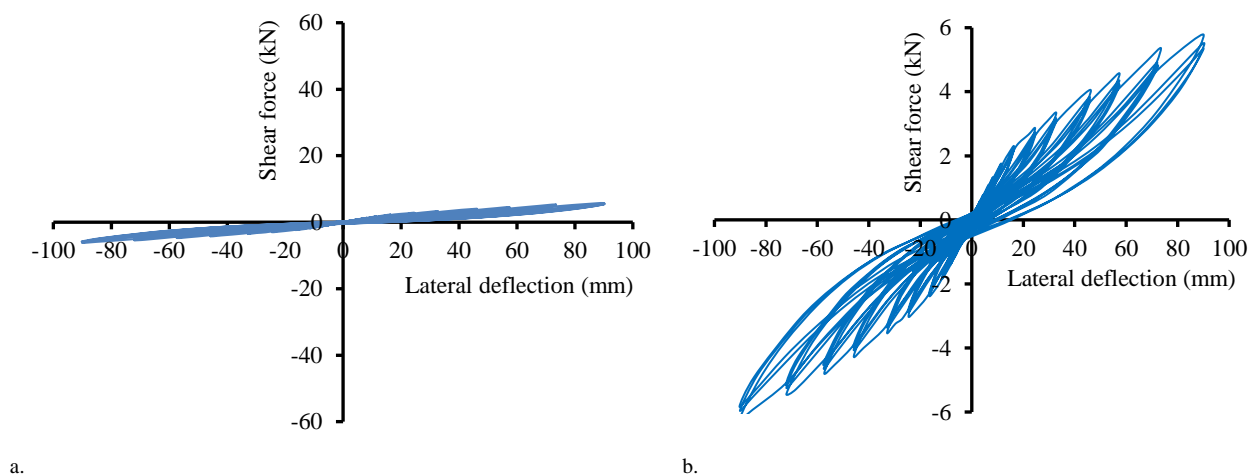


Fig. 3. Hysteretic loops of RC frame: (a) bare frame; (b) zoomed hysteretic loop

It should be noted that the tie-beams and tie-columns used to form a bare RC frame were small cross sections, i. e., 120x120 (mm) and the column height in total was 3350 mm. For this condition, the columns were vulnerable to buckle in-plane frame direction subjected to cyclic shear forces. Consequently, the bare frame was very weak to resist the

lateral loads and its strength was also very low due to the high slenderness ratio of their columns. In addition, the small column stiffness of RC bare frame (first specimen) contributed to significant lateral deflections following the shear load increased.

3.2. Hysteretic Behavior of Masonry Infilled Frame

Fig. 4 presents hysteretic behavior of both confined masonry walls showing that the concrete block masonry is more brittle compared to the brick masonry when they are subjected to cyclic in-plane loads. Based on the hysteretic loops for both specimens, it can be concluded that the confined brick masonry wall produces higher displacement ductility than the confined concrete block masonry wall. At the initial stages, both specimens demonstrate a little bit rigid and linearly elastic behavior resulting relatively high capacity from infill wall contribution, however their rapid strength and stiffness degradation are occurred when the infill walls start crushing. In other words, the very low compressive strength of concrete block significantly contributed to strength degradation of the second specimen. Given this condition, the second specimen produced different ultimate loads when quasi-statically pushed and pulled lateral loads were cyclically applied to it.

Most importantly, although the masonry walls were not plastered at both sides, the confined concrete block masonry wall (second specimen) and the confined brick masonry wall (third specimen) exhibited typical masonry infilled frame behaviors. The hysteretic behavior of masonry infilled frame, therefore, can be summarized based on a typical failure accompanied by excessive sway deformations.

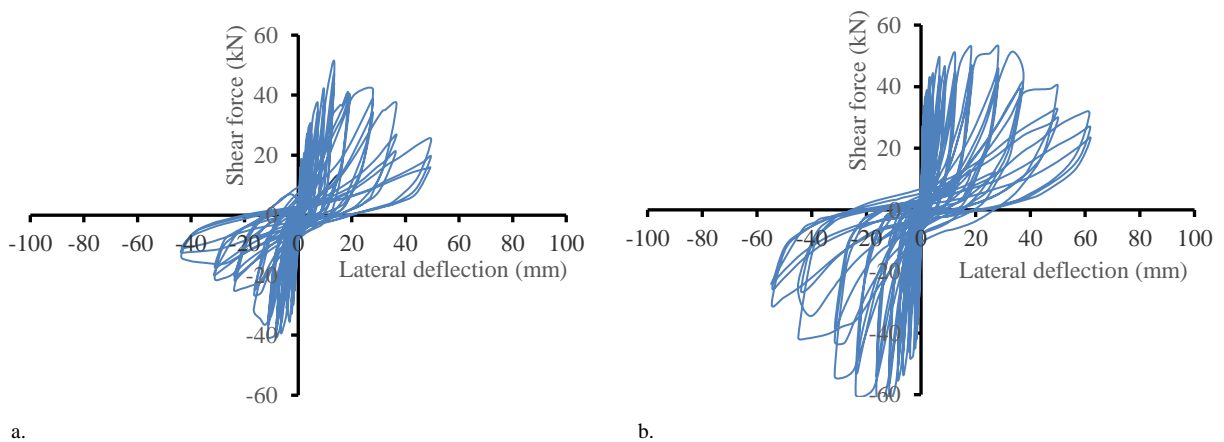


Fig. 4. Hysteretic loops: (a) confined concrete block masonry; (b) confined brick masonry

It was observed in the second specimen that the maximum displacement was 46.09 mm and the lateral load resisting capacity was 50.4 kN as shown in Fig. 4a. Whilst the third specimen slightly reached higher values of the maximum displacement and the lateral load resisting capacity compared to the second specimen. The maximum displacement and the lateral load as depicted in Fig. 4b were 61.99 mm and 52.8 kN, respectively.

3.3. Strength Contribution of Confined Masonry Wall

It has been discussed in earlier sections that infill walls are generally given for functional and architectural purposes and they are considered as non-structural elements. Given this reason, their strength and stiffness contributions are ignored in the design practice due to the difficulty involved in analysis and design as well the uncertainty of the non-integral action between infill wall and the frame. An infill wall, however, tends to interact with the RC frame when subjected to seismic forces when the structure performance is significantly increased in strength arising from the non-structural components accompanied with the increase in initial stiffness of the frame structure. This non-structural element also shows energy dissipation characteristics (Fig. 4) under earthquake loading as the frame components compress the infills at some locations producing strut action to the frame (Fig. 7 and Fig. 8).

Fig. 5 presents envelopes of hysteretic loops for all specimens showing that the shear forces resisting capacity for the infill walls on both second and third specimens are quite similar at the direction of pushed loads, but they are contrarily different their maximum shear loads at the direction of pulled loads. The strength for all specimens is not comparable since the bare frame is very weak in withstanding the shear force, whilst other two specimens of infill walls demonstrate significant contribution to their strength and ductility to prevent sudden damages on the walls.

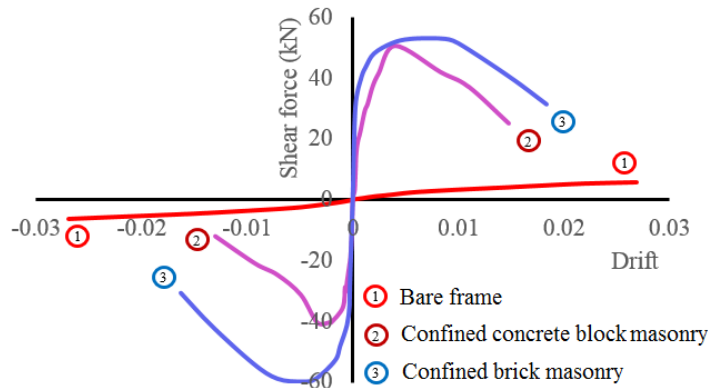


Fig. 5. Envelops of hysteretic loops for all frames

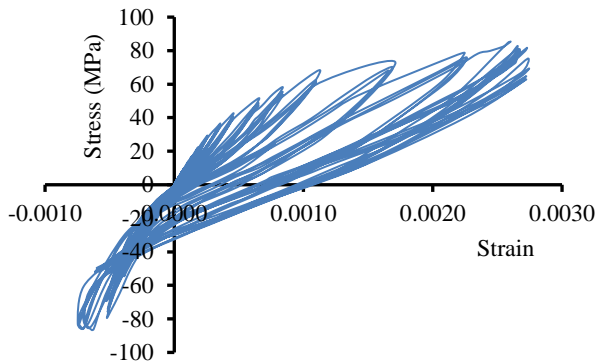
3.4. Typical Damage and Failure Mode

Referring to numbers of literatures, the infill walls contribute in stiffening of the RC frame and can increase the stiffness of the RC frame 4 to 20 times. Their in-plane action vary with the level of lateral loads applied to the frame. The infills and the frames are expected to have composite action at very low lateral loads, and thus the stiffness of the system is too large. When the lateral load increased, the infills start cracking at the frame-infill interface. Furthermore, the separation between frame and infill takes place at the locations where there is tension. At the locations where the infill gets compressed, there forms a diagonal strut action.

Fig. 6 to Fig. 8 show configurations of the all specimens and cracking patterns at failure. As discussed in earlier sections that the bare frame produces maximum lateral deflections up to 90.14 mm subjected to very low lateral load of 5.77 kN. Consequently, cracks propagated at both columns along their heights, at the top beam-column joint and the column base were totally collapse due to the maximum of concrete strain of 0.003 was reached and the strain of main reinforcement at the beam-column joint was over the yield strain of reinforcing steel of 0.0016 as shown in Fig. 6a. The strain values were measured using the strain gauge installed at specified locations (Fig. 6a). As marked a red circle at the top beam-column joint (Fig. 6b), the stress-strain relationship shows the flexural reinforcement has already yielded since the frame produces significant lateral deflection. Flexural crack patterns have dominated at both columns, and the total failures occur at the top and bottom beam-column joints.

Different typical damage conditions were occurred at both infill walls (Fig. 7 and Fig. 8) due to many factors involved in the infill walls. The yield strain of reinforcing steels at the column base is shown in Fig. 7a. Meanwhile, the failure modes of the second specimen have occurred in-plane and out-of-plane directions as a result of low compressive strength of concrete (Fig. 7b). In this specimen, the concrete block masonry wall and the left column base were totally collapse. The third specimen (Fig. 8) gave higher strength contribution and stiffer wall compared to the second specimen because of the compressive strength of clay brick was higher than concrete block. At both column bases were not seriously damage, but at the both top beam-column joints suffered serious damage. The yield strain of reinforcement (Fig. 8a) as well as the maximum concrete strain (Fig. 8b) were reached producing modes of failure on the brick wall. Fig. 8a shows how the stress and the strain of the main reinforcement at the joint were achieved over the yield stress and strain. The failure mechanism depends very much on the strengths of the frame and the infill wall. Failure mechanisms of masonry infilled frames with rigid connection are complicated due to the uncertainty of infill

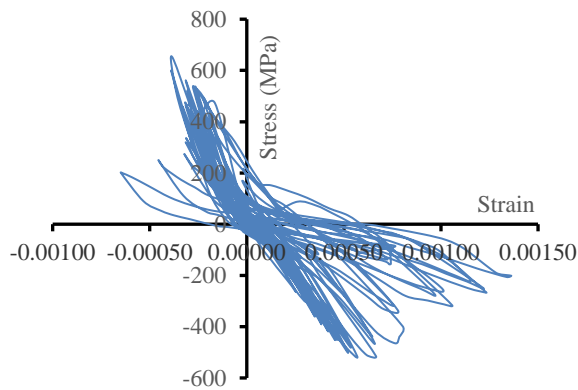
wall-frame interaction. The failure modes approximately include diagonal crack, horizontal slip, corner crushing and some combination of the above failure modes.



a.

b.

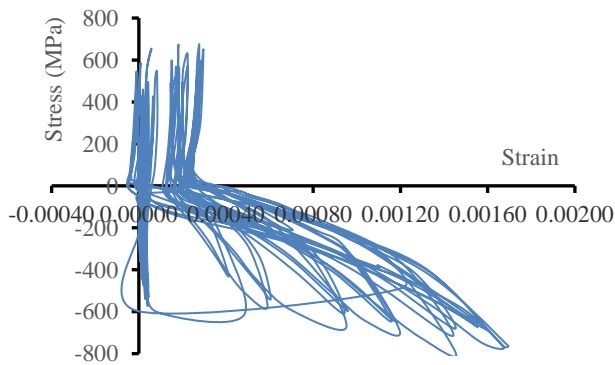
Fig. 6. Configuration of the first specimen and the cracking patterns at failure: (a) yielded flexural steel at top joint; (b) deformed shape



a.

b.

Fig. 7 Configuration of the second specimen and the cracking patterns at failure: (a) yielded flexural steel at bottom joint; (b) mode of failure



a.

b.

Fig. 8. Configuration of the third specimen and the cracking patterns at failure: (a) yielded flexural steel at top joint; (b) mode of failure

4. Conclusions

The infill walls provide significant contribution in the improvement of whole lateral stiffness of the structure. Strong infill walls have often prevented collapse of relatively flexible and weak RC frames. The structural behavior of RC frames with concrete block and brick masonry infills depend on the composite action of the frame and the infill. The structural response is quite complex as it involves an interaction of infill behavior, RC frames behavior, and length of contact between infill and frame.

The test results showed that the infill walls can provide alternative load paths for transferring the load originally only supported by the beams, and thus, improve the collapse resistance capacity of the RC frame. The infill walls, however, may reduce the ductility of the RC frame and may change the failure mode of the frame. The effect of infill walls in the RC frames can be summarized as follows: (a) enhance maximum resistance but reduce ductility of the frames; (b) change strains distributions in tie-beam and tie-column members; (c) change the cracks development and failure mode of the frames. It is concluded that the infill walls may affect (i.e., either improve or impair) the performance of RC frames against collapse in different aspects. The infill walls can have a beneficial effect on the structural response, provided that they are placed regularly throughout the structure, and that they do not cause shear failures of tie-columns.

Acknowledgements

This study is part of the 1305/K5/KM/2014 a multi-year research project (2014-2016). The author would like to acknowledge the Directorate General of Higher Education, Ministry of Research, Technology and Higher Education, for the financial support of this research, and the Department of Civil Engineering, Faculty of Civil Engineering and Planning, Islamic University of Indonesia, for giving the utilization of experimental devices.

References

- [1] T. Turgay, M. C. Durmus, B. Binici, G. Ozcebe, Evaluation of the predictive models for stiffness, strength, and deformation capacity of RC frames with masonry infill walls, *J. Struct. Eng., ASCE*, Vol. 140, No. 10 (2014) 140-148.
- [2] E. Martinelli, C. Lima, G. D. Stefano, A simplified procedure for nonlinear static analysis of masonry infilled RC frames, *Eng. Struct.* 101 (2015) 591-608.
- [3] BSN, Procedure of earthquake resistance for a building structure and non-building (SNI 1726-2012), Jakarta: BSN Press, 2012.
- [4] M. Tomazevic, Series on innovation in structures and construction – vol. 1: earthquake-resistant design of masonry buildings, Fulstrand Offset Printing, Singapore, 2006.
- [5] A. Furtado, H. Rodrigues, A. Arede, H. Varum, Experimental evaluation of out-of-plane capacity of masonry infill walls, *Eng. Struct.* 111 (2016) 48-63.
- [6] F. Christy, D. Tensing, and M. Shanthi, “Experimental study on axial compressive strength and elastic modulus of the clay and fly ash brick masonry,” *Journal of Civil Engineering and Construction Technology*, vol. 4 (4) (2013) 134-141.
- [7] M. Teguh, Structural behaviour of precast reinforced concrete frames on a non-engineered building subjected to lateral loads, *International journal of engineering and technology innovation*, vol. 6 no. 2 (2016) 92-104.
- [8] H. Jiang, X. Liu, J. Mao, Full-scale experimental study on masonry infilled RC moment-resisting frames under cyclic loads, *Eng. Struct.* 91 (2015) 70-84.
- [9] J. S. Kuang, Y. P. Yuen, Effect of out-of-plane loading on in-plane behavior of unreinforced infilled RC frames, *Proc. Of the international conference on computing in civil and building engineering*, University of Nottingham, UK (2010) 1-2.
- [10] D. J. Kakaletsis, C. G. Karayannis, Influence of masonry strength and openings on infilled R/C frames under cyclic loading, *J. Earthquake Eng.* 12 (2) (2008) 197–221.
- [11] H. Kato, T. Goto, and H. Mizuno, Cyclic loading tests of confined masonry wall elements for structural design development of apartment houses in the Third World, *Earthquake engineering, tenth world conference*, Balkema, Rotterdam (1992) 3539-3544.
- [12] P. G. Arteris, Lateral stiffness of brick masonry infilled plane frames, *Journal of structural engineering*, August (2003) 1071-1079.
- [13] C. Umarani, S. B. Gnanappa, Structural behavior of reinforced concrete frames with confined infill under cyclic loading, *International journal of earth sciences and engineering*, vol. 03, No. 06 (2010) 904-911.
- [14] M. Teguh and L. Makrup, Model design of an earthquake resistant precast non-engineered house and development of retrofitting method on post-earthquake damage, *Research Report No. 1305/K5/KM/2014*, Directorate General of Higher Education, Ministry of Education and Culture of Indonesia, UII Press, Sept. (2014) 85 p.



Sustainable Civil Engineering Structures and Construction Materials, SCESCM 2016

Nanostructured oxide thin films for sustainable development

Paolo Mele^{a,*}, Shiv J. Singh^a, Shrikant Saini^b, Alok K. Jha^c, Malik I. Adam^d

^aResearch Center for Environmentally Friendly Materials Engineering, Muroran Institute of Technology, Hokkaido, 050-8585, Japan

^bDepartment of Materials Science and Engineering, University of Utah, 84112 Salt Lake City, Utah, USA

^cDepartment of Materials Science and Engineering, Kyushu Institute of Technology, Kitakyushu 804-8550, Japan

^dDepartment of Mechanical Engineering, University Tenaga Nasional, UNITEN, 43000 Kajang, Selangor, Malaysia

Abstract

In the effort to emancipate mankind from fossil fuels dependence and minimize the CO₂ emissions, efficient transport and conversion of energy is required. Advanced materials such as superconductors and thermoelectrics are expected to play an important role in sustainable science and development. We propose an overview of our recent progress on nanostructured thin films of superconducting and thermoelectric oxides. Superconducting properties of YBa₂Cu₃O_x and thermoelectric properties of Al-doped ZnO are described in relation to preparation techniques, experimental conditions, substrates used, structure and morphology. We especially discuss a nanoengineering approach for the enhancement of energy transport and energy conversion efficiency of oxide thin films compared to their corresponding counterpart of bulk materials.

© 2017 The Authors. Published by Elsevier Ltd.

Peer-review under responsibility of the organizing committee of SCESCM 2016.

Keywords: superconductors; thermoelectrics; thin films; oxides; pulsed laser deposition; artificial pinning centers; nanodefects; phonon scattering

1. Introduction

These days, mankind has been starting to face many difficult issues: energy problems, environmental problems, water shortage problems and so on. It is a common feeling that new advanced materials will play an important role in the current challenge to develop alternative and sustainable energy technologies to reduce considerably our dependence on nuclear and fossil fuels and eliminate greenhouse gas emissions [1, 2].

* Corresponding author. Tel.: +81-143-46-5646; fax: +81-143-46-5644.

E-mail address: : pmele@mmm.muroran-it.ac.jp

In particular, superconducting [3] and thermoelectric [4] materials seem fit to solve the energy puzzle since they can provide efficient energy transport and conversion, respectively.

Superconductors can transport electrical current without dissipation if cooled down at the appropriate temperature. Superconducting bulks and single crystals are quite important for the study of the basic physical properties, however for practical applications, such as direct current transport or winding of magnets, development of superconducting wires and tapes is strongly required. In order to be disclosed to the practical applications (lossless current transportation, winding of magnets and so on), superconducting materials should possess not only T_c , but also J_c (critical current density) and pinning force ($F_p = J_c \times B$, where B is the external magnetic field) as large as possible to cover a wide range of intended applications. Introduction of nanosized artificial pinning centres (APCs) was widely used to strongly enhance J_c and F_p of high temperature superconductors (HTSC) like $YBa_2Cu_3O_x$ (YBCO, $T_c = 92$ K) in magnetic field [6, 7]. Main advantage of HTSC towards conventional superconductors like NbTi or Nb_3Sn is the possibility to use nitrogen (boiling point: 77K) instead of helium (boiling point: 4.2K) as coolant. Impressively, in the past ten years or so, the nano-engineering approach to control microstructure, distribution, concentration and dimensionality of APCs has been demonstrated to be a powerful tool to produce YBCO thin films with excellent performances. Comprehensive review on the state of the art characteristics of YBCO wires and tapes can be found in [8].

Thermoelectrics can convert heat into electrical energy without moving parts. Efficient, small and light-weight thermoelectric modules are instrumental for recycling waste heat in a wide range of temperatures: gases from industrial plants, car engines, and even domestic stoves. In order to improve the efficiency of the thermoelectric conversion, the adimensional figure of merit $ZT = \sigma S^2 T / \kappa$ (where σ = electric conductivity, S = Seebeck coefficient; T = temperature and κ = thermal conductivity) must be increased. To date, the best performance is given by alloys like Bi_2Te_3 or Sb_2Te_3 , whose key feature is the presence of natural nanosized defects which act as efficient phonon scatterers for the depression of κ and the consequent increase of ZT [9]. On the other hand, oxides have been recognized as promising candidates for practical utilization as thermoelectric materials since they are more stable than metallic materials in oxidizing environments over wide temperature range [10]. Indeed, oxides possess important characteristics, such as their benign nature, abundant supply, and cost effectiveness. More recently, researchers start to focus of thermoelectric oxide thin films which are easier to be functionalized at the nanoscale with respect to the bulk oxides. Overview on the recent status of research on thermoelectrics oxide thin films can be found here [11].

This contribution will briefly highlight our recent progresses on high quality nanostructured films of superconducting and thermoelectric oxides with strongly enhanced properties for sustainable energy applications

2. Experimental procedure

A Lambda Physik KrF excimer laser ($\lambda = 248$ nm) was used for fabrication of $YBa_2Cu_3O_7$ (YBCO) superconducting thin films doped with $BaSnO_3$ (BSO), Y_2O_3 and $BSO+Y_2O_3$ on $SrTiO_3$ (STO) substrates. The Pulsed Laser Deposition (PLD) conditions were: energy density $E = 5$ J/cm², deposition temperature (T) = 800 °C, oxygen partial pressure (pO_2) = 200 mTorr, repetition rate (f) = 10 Hz, substrate to target distance (d) = 60 mm. For the deposition of pure YBCO thin film, a pristine YBCO target was ablated for 6000 laser pulses while for YBCO films added with nanodefects, YBCO+BSO mixed targets (YBCO added with x wt% of the BSO phase, being x 2, 4, 6 and 8%) and YBCO+ Y_2O_3 surface-modified targets (in this case a slice of Y_2O_3 , which percentage of total target area is denoted as $A\%$, is stuck on the surface of the target for periodical ablation and $A\%$ was varied as 2.5, 5.44, and 9.22%) were used. YBCO+BSO+ Y_2O_3 films were prepared in multilayer fashion, alternating YBCO+BSO and YBCO+ Y_2O_3 layers by periodic switching of the two targets.

Superconducting transition temperature (T_c), J_c/B characteristics ($T=77$ K, $B//c$, $B=0\sim 9$ T) and $J_c/B/\theta$ angular dependences ($T=77$ K, $B=1$ T, being θ the angle between B and c axis of the film) were measured by physical properties measurement system (PPMS, Quantum Design, USA). The thermoelectric 2% Al-doped ZnO (AZO) thin films were grown on STO, Al_2O_3 and fused silica substrates by the PLD technique using a Nd:YAG laser ($\lambda = 266$ nm). The PLD conditions were: $E = 4.2$ J/cm², $T = 300\text{--}600$ °C, $pO_2 = 200$ mTorr, $f = 10$ Hz, $d = 35$ mm. 2 % Al was found as the best doping in bulk. The electrical conductivity versus temperature (σ - T) characteristic was measured by a conventional four-probe technique from 300 to 600 K with a homemade apparatus. The Seebeck coefficient was

measured by a commercially available system (MMR Technologies, USA) The crystallinity and the orientations of both superconducting and thermoelectric thin films (θ - 2θ scans, rocking curves, Φ scans) as well as c axis lengths were determined by XRD (Bruker D8 Discovery). Cross-sections of all films were analysed by transmission electron microscopy (TEM, JEOL).

3. Results and discussion

3.1. Superconducting thin films

Nanoengineering approach with the incorporation of nanosized artificial pinning centres has been considered to improve the pinning performance of YBCO thin films.

At first, we tried adding BSO to YBCO films grown on STO substrates by PLD [12]. By ablation of mixed BSO-YBCO targets with increasing BSO content (2~8 wt%), we obtained high quality YBCO thin films incorporating BSO in form of nanorods, which are classified as one-dimensional APCs (1D-APCs). YBCO films added with 4 wt% BSO have huge $F_p^{\text{MAX}} = 28.3 \text{ GN/m}^3$ (77K, 3T, B//c). However, J_c is intrinsically anisotropic with the direction of applied magnetic field (with a maximum for B//c axis) and this is a critical issue for practical applications, since the value of J_c is desired to be constant in all directions of applied magnetic field.

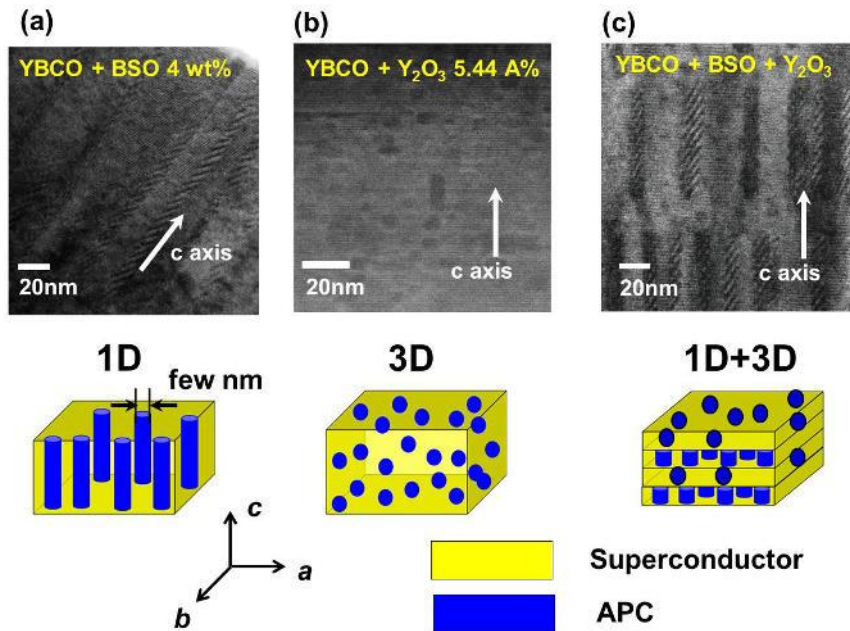


Fig. 1. Typical TEM-cross-sectional images (first row) and schematic representations (second row) of YBCO films added with artificial pinning centers (APCs) of various dimensionality: (a) 1D-APCs: YBCO with 4wt% c -axis aligned BSO nanorods; (b) 3D-APCs: YBCO with randomly dispersed 5.44 A% Y_2O_3 nanoparticles; (c) 1D+3D APCs: YBCO multilayer added with alternating 1D-APCs (BSO nanorods) and 3D-APCs (Y_2O_3 nanoparticles)

To solve this issue, we tried the incorporation of Y_2O_3 nanoparticles (three-dimensional APCs, 3D-APCs) inside the YBCO film. Areas of Y_2O_3 sectors on YBCO target were increased (2.51%, 5.44% and 9.22% of the YBCO pellet area). Randomly distributed Y_2O_3 particles, whose density was proportional to the area of sector, were incorporated in YBCO films. Consistent with the microstructure, J_c was isotropic. The 5.44 A% Y_2O_3 added sample presented $F_p^{\text{MAX}} = 14.3 \text{ GN/m}^3$ (77K, 3T, B//c) which is significantly large, though inferior to the value reported in YBCO-BSO films with the same conditions. We further used the single vortex dynamics model to account

for vortex pinning in the samples. The 5.44A% Y_2O_3 -YBCO film result shows a good agreement with the model fit up to $B = 4$ T [13].

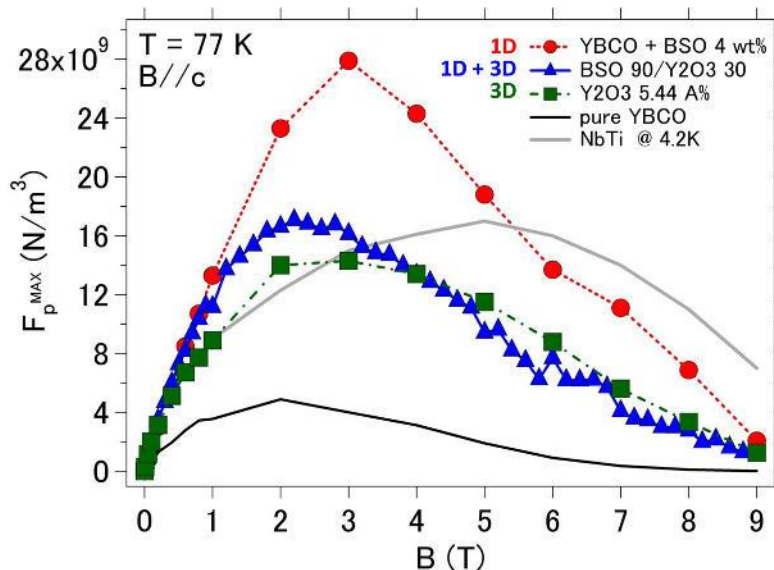


Fig. 2. Global pinning force ($F_p = J_c \times B$) at 77K (B/c) of YBCO films added with APCs of various dimensionalities: 1D-APCs (YBCO +4wt% BSO; 3D-APCs (YBCO+5.44 A%) Y_2O_3 nanoparticles; 1D+3D APCs (YBCO+BSO+ Y_2O_3). F_p of pure YBCO film is reported as reference; F_p of NbTi tape (at 4.2K) is plotted as a milestone.

Ultimate approach was combination of advantages of 1D- and 3D-APCs pinning, with coexistence of BSO nanorods and Y_2O_3 nanoparticles. Multilayered films, alternating YBCO+ Y_2O_3 and YBCO+BSO layers were prepared in PLD chamber by switching YBCO+ ~2A% Y_2O_3 and YBCO+ 4wt% BSO targets. Different combinations, varying the thickness of layers, were tried. Best result was obtained with the combination [(90 nm YBCO+BSO) / (30 nm YBCO+ Y_2O_3)] \times 3 presenting $F_p^{MAX} = 17.6$ GN/m³ (77K, 2.2T, B/c) [14].

3.2. Thermoelectric thin films

Several oxides are promising for thermoelectric applications [10] : the best performance for bulk oxide so far (has been reached by doped p -type $Ca_3Co_4O_9$ [15] and n -type ZnO [16]: $ZT \sim 0.45$ at 1000K in both cases.

In our research on thermoelectric oxide thin films we focused at first on ZnO, a semiconductor with wide direct band gap (3.3 eV), well known for its versatile applications (optics, solar cells, electrodes, gas sensors, biophysics, etc.). ZnO can also be regarded as low-cost, nontoxic, stable thermoelectric material for space applications, solar- thermal and electrical-energy production.

Epitaxial thin films of $Zn_{0.98}Al_{0.02}O$ (AZO) films were fabricated by PLD on several substrates: $SrTiO_3$ (STO), Al_2O_3 and fused silica. TEM images reported in Figure 3 demonstrate typical columnar growth of the films on STO and Al_2O_3 , while films grown on silica present thin natural buffer layers with randomly oriented grains. As summarized in Figure 4, at $T_{dep} = 400$ °C, films deposited on silica always shows higher values of ZT in comparison with films deposited on Al_2O_3 and STO: at $T = 600$ K, $(ZT)_{silica} = 0.045$, $(ZT)_{STO} = 0.03$ and $(ZT)_{Al_2O_3} = 0.04$. Furthermore, all the films have larger ZT in comparison with the correspondent bulk material: $(ZT)_{bulk} = 0.013$. Since the values of σ and S did not change dramatically on the different substrates, we attribute the enhancement of ZT values of the thin films to the fact that the values of κ of ZnO films at room-temperature are smaller than the value of corresponding bulk (25~35 W/m \times K [17, 18]. In numbers, $\kappa_{STO} = 6.5$ W/m \times K [11], $\kappa_{Al_2O_3} = 6.90$ W/m \times K [11] and $\kappa_{silica} = 4.89$ W/m \times K [19]. The depression of κ in thin films is due to several factors: enhanced phonon scattering by intrinsic defects of the films (point defects, dislocations, impurities, pores); phonon scattering at the grain

boundaries; phonon scattering at the interface between film and substrate.

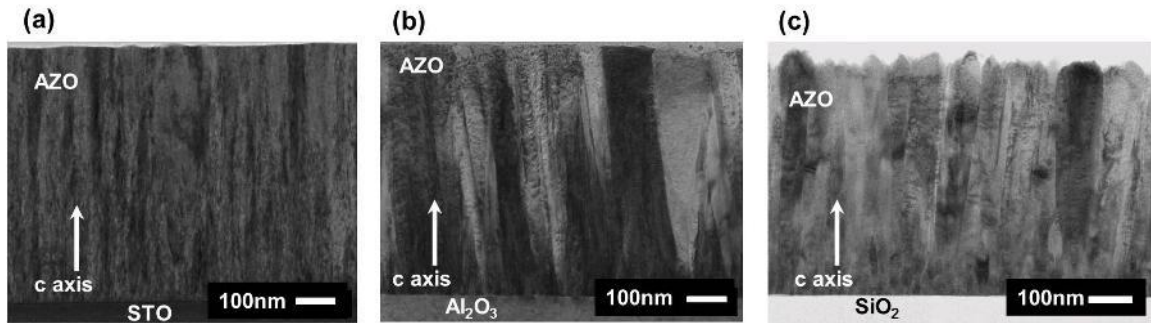


Fig. 3. Typical TEM-cross-sectional images of AZO thin film grown on several substrates at 400 °C: (a) STO; (b) Al₂O₃; (c) fused silica: natural buffer layer can be observed on the SiO₂ substrate..

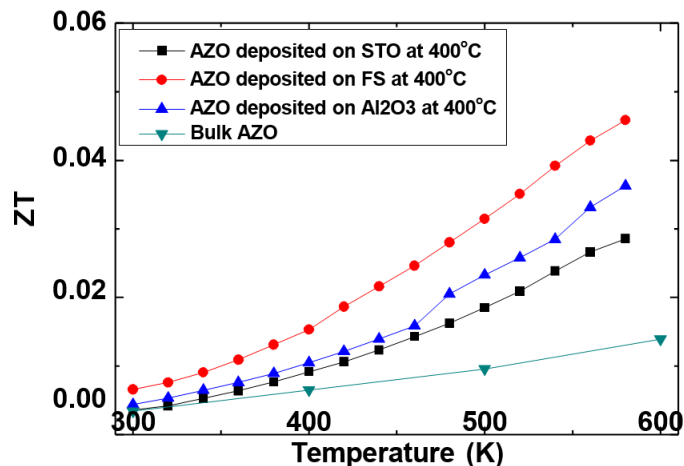


Fig. 4. Figure of merit ($ZT = \sigma S^2 \times T/\kappa$) of AZO films deposited on several substrates at 400 °C. Behavior of the corresponding bulk material is reported for comparison

4. Outlook and perspective

The results presented in this paper indicate that the nanoengineering approach by PLD method can produce a variety of complex nanocomposite oxide thin films with unique properties for sustainable applications. High-quality films of superconducting oxides (YBa₂Cu₃O_x: YBCO) and thermoelectric oxides (Al-doped ZnO: AZO) were prepared and characterized.

In the case of YBCO thin films, the nanoengineering approach is at very advanced level: satisfactory control of nanodefects size and distribution was achieved. The additions of several kinds of APCs are very effective in the enhancement of performances: large in-field pinning forces (F_p) at 77K and $B//c$ was obtained. Highlights are $F_{pMAX} = 28.3 \text{ GN/m}^3$ (3T) in YBCO added with 1D-APCs (4 wt% BSO nanorods); $F_{pMAX} = 14.3 \text{ GN/m}^3$ (3T) in YBCO added with 3D-APCs (5.44% Y₂O₃ nanoparticles); $F_{pMAX} = 17.6 \text{ GN/m}^3$ (2.2T) in YBCO 1D+3D-APCs multilayers, alternating BSO nanorods and Y₂O₃ nanoparticles. Despite such encouraging results, the performance of superconducting thin films still requires a breakthrough in order to realize full practical application. In particular, the irreversibility field (B_{irr}) needs to be improved. For example, a typical values of B_{irr} (77K) for our YBCO-BSO film is about 11T [12]. Recently, Xu et al reported $B_{irr} = 14.8\text{T}$ (77K) for MOCVD (Y,Gd)BCO doped with 15% vol Zr, although $F_{pMAX} = 14 \text{ GN/m}^3$ (at 6T) is about half the value obtained by us in the YBCO-BSO [20]. Therefore,

further exploration to expand the F_p and B_{irr} values if one had to have real applicable superconducting oxide thin films.

In the case of AZO thin films, promising values have been obtained, such as $\kappa = 4.89 \text{ W/m} \times \text{K}$ (300K) = ZT (600K) = 0.045 for AZO grown on silica. However, these values are still too low for the practical applications. First attempt preparing a tiny module based on 5 AZO and 5 $\text{Ca}_3\text{Co}_4\text{O}_9$ thin films legs was successful, though the output power was small: 29.9 μW with $\Delta T = 230 \text{ }^\circ\text{C}$ [21]. Further decrease of κ (to the range of 1-2 $\text{W/m} \times \text{K}$) and increase of ZT up to 2 at 1000K are the requirements for efficient recovery of waste heat [11] and improvement of module performance [21]. For these purposes, it is necessary to introduce and control additional artificial nanodefects to the films, following a similar path as for the superconducting oxide films

Acknowledgements

P.M. acknowledges partial financial support of JSPS KAKENHI, grant numbers 23226014 and 263901103. M.I.A. acknowledges partial financial support from MOHE, grant scheme number FRGS/2/2014/SG06/UNITEN/02/3.

We gratefully thank A. Ichinose, P. E. Hopkins, R. Guzman, L. Molina-Luna, H. Abe and H. Honda for the experimental support; K. Matsumoto, X. Obradors, J. Gazquez and T. Suzuki for insightful discussions.

References

- [1] V. Arunachalam and E. L. Fleischer (Eds.), *Harnessing Materials For Energy*, MRS Bulletin 33 (2008) 251-488
- [2] M. E. Green, L. Espinal, E. Traversa, E. J. Amis (Eds.), *Materials For Sustainable Development*, MRS Bulletin 37 (2012) 299-456
- [3] M. Tinkham, *Introduction To Superconductivity*, second ed., Dover, New York, 2004
- [4] D. M. Rowe (Ed.), *Thermoelectrics Handbook – Macro To Nano*, first ed., CRC Taylor & Francis, Boca Raton, New York, Upton, 2005
- [6] J. L. MacManus Driscoll, S. R. Foltyn, Q. X. Jia, H. Wang, A. Serquis, L. Civale, B. Maiorov, M. E. Hawley, M. Maley, D. E. Peterson, Strongly enhanced current densities in superconducting coated conductors of $\text{YBa}_2\text{Cu}_3\text{O}_{7-x} + \text{BaZrO}_3$, *Nature Mater.* 3 (2004) 439-443
- [7] T. Haugan, P. N. Barnes, R. Wheeler, F. Meisenkothen, M. Sumption, Addition of nanoparticle dispersions to enhance flux pinning of the $\text{YBa}_2\text{Cu}_3\text{O}_{7-x}$ superconductor, *Nature* 430 (2004) 867-870.
- [8] V. Selvamanickam, High Temperature Superconductor (HTS) Wires And Tapes, in: Z. Melhem (Ed.), *High Temperature Superconductors (HTS) for energy*, Woodhead Publ., Cambridge, 2012, pp. 34-62
- [9] R. Venkatasubramanian, E. Siivola, T. Colpitts, B. O'Quinn, Thin-film thermoelectric devices with high room-temperature figures of merit, *Nature*, 413(2001) 597-602
- [10] J. W. Fergus, Oxide materials for high temperature thermoelectric energy conversion, *J. Eur. Ceram. Soc.*, 32 (2012) 525-540
- [11] P. Mele, Nanostructured Thin Films of Thermoelectric Oxides, in: P. Mele, C. Li, S. Arisawa, T. Tsuchiya, T. Endo (Eds.), *Oxide Thin Films, Multilayers, and Nanocomposites*, first ed., Springer, Berlin, 2015, pp.109-155
- [12] P. Mele, K. Matsumoto, T. Horide, A. Ichinose, Y. Yoshida, M. Mukaida, S. Horii, R. Kita, Ultra-high flux pinning properties of BaMO_3 -doped $\text{YBa}_2\text{Cu}_3\text{O}_{7-x}$ thin films (M= Zr, Sn), *Supercond. Sci. Technol.* 21 (2008) 032002-032006
- [13] P. Mele, R. Guzman, J. Gazquez, T. Puig, X. Obradors, S. Saini, Y. Yoshida, M. Mukaida, A. Ichinose, K. Matsumoto, M. I. Adam, High pinning performance of $\text{YBa}_2\text{Cu}_3\text{O}_{7-x}$ films added with Y_2O_3 nanoparticulate defects, *Supercond. Sci. Technol.*, 28 (2015) 024002
- [14] P. Mele and M. I. Adam, Nanoengineered Pin-Spots Dimensionality for Vortex Power Harvesting on the Infield Performance of YBCO Thin Films, in: M. Miryala (Ed.), *Superconductivity: Applications Today and Tomorrow*, first ed., Nova Science Publishers, Inc (New York), 2016, pp. 169-213,
- [15] N. V. Nong, Chia.-Jyi Liu, M. Ohtaki, Improvement on the high temperature thermoelectric performance of Ga-doped misfit-layered $\text{Ca}_3\text{Co}_{4-x}\text{Ga}_x\text{O}_9+\delta$ ($x = 0, 0.05, 0.1, \text{ and } 0.2$), *J. Alloys and Comp.*, 491 (2010) 53-56
- [16] M. Ohtaki, K. Araki, K. Yamamoto, High Thermoelectric Performance of Dually Doped ZnO Ceramics, *J. Electr. Mater.*, 38 (2009) 1234-1238
- [17] P. Mele, H. Kamei, H. Yasumune, K. Matsumoto, K. Miyazaki, Development of Thermoelectric Module Based on Dense $\text{Ca}_3\text{Co}_4\text{O}_9$ and $\text{Zn}_{0.98}\text{Al}_{0.02}\text{O}$ Legs, *Met. Mater. Int.* 20 (2014) 389-397
- [18] P. Mele, S. Saini, H. Honda, K. Matsumoto, K. Miyazaki, H. Hagino, A. Ichinose, Effect of substrate on thermoelectric properties of Al-doped ZnO thin films, *Appl. Phys. Lett.* 102 (2013) 253903.
- [19] S. Saini, P. Mele, H. Honda, D. J. Henry, P. E. Hopkins, L. Molina-Luna, K. Matsumoto, K. Miyazaki, A. Ichinose, Enhanced thermoelectric performance of Al-doped ZnO thin films on amorphous substrate, *Japan. J. Appl. Phys.* 53 (2014) 060306.
- [20] A. Xu, L. Delgado, N. N. Khatri, Y. Liu, V. Selvamanickam, D. Abrahimov, J. Jarozynski, F. Kametani, D. C. Larbalestier, Strongly enhanced vortex pinning from 4 to 77 K in magnetic fields up to 31 T in 15 mol.% Zr-added (Gd, Y)-Ba-Cu-O superconducting tapes, *APL Materials* 2 (2014) 064111
- [21] S. Saini, P. Mele, K. Miyazaki, A. Tiwari, On-chip thermoelectric module comprised of oxide thin film legs, *Energy Conv. And Manag.* 114 (2016) 251-257.



Sustainable Civil Engineering Structures and Construction Materials, SCESCM 2016

Concrete structures for sustainability in a changing world

Petr Hajek^{a,*}

^a*Czech Technical University in Prague, Thakurova 7, Prague 6, 16629, Czech Republic*

Abstract

World is faced to increasing number of natural disasters and to increasing economical and social problems resulting in increasing migration of people, terrorism etc. The structures for sustainable future should be better prepared for the new conditions in a changing world. Concrete is due to its properties the most used man made material and gradually becomes a building material suitable for design of sustainable structures with high potential for needed environmental impact reduction. The use of advanced concrete technologies for new types of structures thus represents high potential for further development of built environment towards sustainability and resiliency.

© 2017 The Authors. Published by Elsevier Ltd.

Peer-review under responsibility of the organizing committee of SCESCM 2016.

Keywords: Type your keywords here, separated by semicolons ;

1. Introduction

Concrete is the most used construction material; even more concrete is the most used man-made material in the world. The production of concrete in the industrialized world annually amounts to 1.5-3 tone. Davidovits (1994) showed that chemical processes in production of 1 tonne of cement directly generate about 0.55 tonnes of CO₂ and the cement production technology requires the combustion of carbon-fuel up to 0.40 tonnes of CO₂. It means that during production of 1 tonne of cement approximately 1 tonne of CO₂ is generated and released to atmosphere, increasing total accumulation of atmospheric CO₂. As a consequence cement industry production was in the year 1987 responsible for about 5% of world CO₂ emissions. Considering continuing increase of cement production it is estimated that nowadays cement and concrete industry is responsible for about 7-8% of global CO₂ emissions.

* Corresponding author. Tel.: +420 739028773
E-mail address: : petr.hajek@fsv.cvut.cz

The world cement production has been 12 times increased in the second half of the last century [1]. The Figure 1 shows a development of cement production in different regions of the world presented by The European Cement Association – Cembureau [2]. From the graph on Figure 1a it is evident that the production of cement is significantly growing in developing countries in Asia, Africa and CIS (Commonwealth of Independent States – some former Soviet Republics) and slightly growing in America and Oceania. However, in Europe was the production in 2014 even lower in comparison to the year 2001. The dominant position keeps China with 56.5% of total world cement production in 2014 (see Figure 1b).

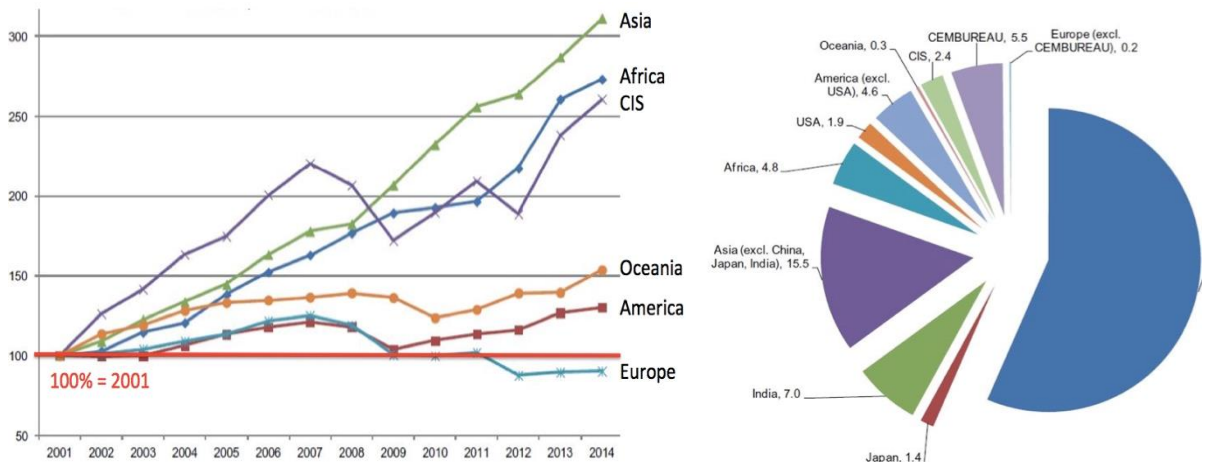


Fig. 1. (a) World cement production by region – evolution 2001-2014; (b) World cement production in 2014 by regions and countries in %; based on source Cembureau [2]

As a consequence of economy growth, especially in emerging countries, the demand for construction materials, including cement and concrete, is increasing. According to WWF report [3] the cement production in industrialized and developing countries in 2050 is estimated to be almost 5 times higher than in 1990, despite the need for reduction of total CO₂ emissions (!).

The current development of built environment leads to the need of replacement of some old existing buildings with new buildings. Consequently, the amount of demolished concrete structures is gradually increasing. This creates needs and potential for replacement of natural aggregate by recycled aggregate. The use of recycled concrete - as an aggregate for new concrete mixes, leads to saving of natural resources and helps to reduce the pressure on landfilling sites.

More over, high amount of production and use of concrete is associated with high transport needs and demands on production and demolition processes within the entire life cycle. This all has significant impact on the environment.

Current development of concrete, production technology and development of concrete constructions during last twenty years have led to improvement of technical parameters and in the same time reduction of environmental impacts. New types of concrete have due to mix optimization significantly better characteristics from the perspective of strength, mechanical resistance, durability and resistance to extreme loads. The use of new high performance concretes enables construction of more sustainable and resilient buildings or other types of structures.

Considering above specified global situation it is highly important to focus on an implementation of new technologies and construction techniques especially in emerging countries and regions with the highest cement production.

2. Sustainability and resiliency

2.1. Natural global changes and man-made disasters

World and its environment are steadily changing. This is a permanent process running from the birth of the Earth to present. However, nowadays we are faced to significantly increasing frequency of natural disasters and to increasing economical and social problems, incl. terrorism. Earthquakes, floods, storms, hurricanes, tornados, fires, tsunamis, volcanic events, heat and cold waves, extreme dry weather etc. are more and more frequent. According to a WMO (World Meteorological Organization) analysis [4] the years 2011-2015 have been the warmest five-year period on record, with many extreme weather events - especially heat waves - influenced by climate change. The probability of natural disaster is now nearly five times higher comparing to the 1970s, because of the increasing risks due to climate change – Figure 2a and 2b. In the same time we are faced to accelerating number of man-made disasters e.g. WTC New York terrorist attack September 11th, 2001 (Figure 2c), or current increasing number of terrorist attacks. As a consequence of natural and man-made disasters and socioeconomic situation in some regions and countries a human migration is increasing.



Fig. 2. (a) floods in the Czech Republic 2002; (b) earthquake Nepal 2015 (www.dylanxpowell.com); (c) terrorist attack WTC New York 2011 (www.youtube.com)

2.2. Sustainability and its evaluation

Sustainability is according to standard EN 15643-2 [5] “ability of a system to be maintained for the present and future generations”. With respect to the general definition of sustainability, the three essential pillars should be considered in the design, construction, use and other life-cycle phases of any construction, as follows:

- Environmental Performance,
- Social Performance,
- Economic Performance.

The built environment (buildings and civil engineering works) represents a key element in determining quality of life and contributes to cultural identity and heritage. The building and construction sector is a key sector in national economies; it has a significant interface with poverty reduction through the basic economic and social services provided in the built environment. Construction works absorb considerable resources and significantly contribute to the transformation of the whole environment. As a consequence construction works have considerable economic, environmental and social impacts. On the other hand they can to large extent influence level of resiliency of built environment in the changing natural and social conditions.

Sustainability assessment of structures is a combination of the assessments of environmental performance, social performance and economic performance taking into account the technical requirements and functional requirements of a structure (building, bridge, road etc.) or an assembled system (part of works), expressed at the structure level [6]. Most of the current standards, methodologies and tools are focused on the assessment of building sustainability.

However, the need for the development of methodologies and tools for sustainability assessment of infrastructure like bridges, roads, dams, etc., is increasing.

2.3. Resilience

Resilience is in general the capacity to adapt the system to changing conditions and to maintain or regain functionality and vitality in the stage of stress or disturbance [7]. It is the capacity to recover after a disturbance or interruption. According to the Resilient Design Institute “resilient design is the intentional design of buildings, landscapes, communities, and regions in order to respond to natural and man-made disasters and disturbances—as well as long-term changes resulting from climate change—including sea level rise, increased frequency of heat waves, and regional drought”.

It is essential to modify principles of structural design and construction technology for development and maintenance of buildings and all built environment in order to be more resilient. Of course consequently the reduction of environmental impacts (especially global warming) is urgently needed to slow down the process of climate change. Only resilient and environmental friendly structures in the built environment can be sustainable in the changing environmental as well as social situation of the forthcoming era

3. Advantages of concrete structures from sustainability and resiliency viewpoints

Concrete is due to specific mechanical and chemical properties advantages material for design and construction of sustainable and resilient structures. Main advantages of concrete structures from the viewpoints of sustainability and resiliency are:

- High thermal mass of concrete - Due to the density, concrete elements can serve as thermal energy storage. They are able to absorb and release heat or cold. This can contribute to energy savings associated with cooling and heating.
- Acoustic properties (improving air-born sound insulation properties) of concrete plane elements - Concrete walls and floors provide the mass that is required for effective reduction of sound transmission, particularly low frequency sounds.
- High fire resistance of concrete structures – In comparison to the most steel or timber structures concrete structures provide significantly higher fire resistance.
- High resistance of concrete structures against climatic effects (in environmental exposition) – High mechanical resistance of concrete structures; high durability of concrete surface (advantage for bridges, roads and other civil structures); resistance against floods, winds, frost, sun radiation, abrasion, etc. Durability and water tightness of HPC and UHPC.
- High durability, low maintenance requirements - especially in inside building environment, where concrete is protected against direct climatic impacts.

Above-mentioned advantages could be significant in designing new constructions as well as in old structures reconstructed for the new use [8, 9]. With respect to specifics of concrete presented as a strong and durable material it is possible to design and construct on this material bases robust structures with high level of resiliency when faced to the exceptional natural or man-made disaster situations.

3.1. Advantages of concrete structures from environmental viewpoint

- Secondary materials utilization - Utilizing supplementary cementitious materials in a composition of concrete mixture (fly-ash, granulated blast furnace, microsilica) it is possible to reduce the amount of embodied energy and embodied CO₂ and SO_x emissions.
- Recycled concrete can be utilized as aggregate substitutes in earthwork construction and up to some extent as an aggregate substitute in a new concrete production.
- Precast concrete elements in “tailor-made” manner enable waste reduction in production and also on construction site.

3.2. Advantages of concrete structures from economy viewpoint

- Long-term durability - Concrete in comparison to other materials (timber, steel etc.) enables longer service life of buildings. Concrete structures are usually more resistant to atmospheric action, they have a good capability of withstanding wear, and they do not subject easily to degradation processes. This also results in lower operating, maintenance and demolition cost.
- Less damages caused during disasters (due to high strength and fire safety) – lower economical impacts, lower costs for repair and reconstruction.
- Lower material cost, lower manipulation and transportation cost. Subtle concrete structures utilizing lesser amount of higher quality concrete could be cheaper, even though the unit cost of this type of concrete is higher than the unit cost of standard concrete types.
- Dismountable structures: Precast concrete structures can be designed as dismountable enabling consequential utilization of structural elements.
- Smaller thickness of peripheral structures can have a positive effect on construction economic efficiency (especially in areas with regulated size of built-up area).

3.3. Advantages of concrete structures from social viewpoint

- High structural safety and reliability, higher fire resistance – This includes also high resistance to natural effects during exceptional cases of natural disasters (floods, storms, winds, hurricanes, tornados, fires, earthquakes, etc.) and terrorist attacks.
- Acoustic properties – Due to high specific weight of concrete there can be improved air-born sound insulation of structure (floors and/or walls separating different operational areas);
- Thermal mass – Concrete (material with high specific weight) can contribute to thermal stability of internal environment and consequently to energy savings.
- Maintainability - Concrete surface produced in high quality can be easily maintained, cleaned and it has long durability.
- Flexibility – Character of concrete technology enables significant design flexibility due to the possibility of forming almost any element shape limited only by structural reliability requirements.
- Healthiness - Concrete is not the source of toxic emissions or volatile organic compounds.

4. Advanced technological and structural principles for sustainable concrete building structures

4.1. Optimization of concrete mixture – new types of concretes

New composite silicates with significantly better physical characteristics create realistic assumptions of achieving substantial effect from the perspective of material and energy savings. Some cases show that high performance concrete can be used for optimized shapes of reinforced concrete elements, which can be very subtle due to their mechanical parameters. Nowadays, use of concretes with compressive strength around 100 MPa is not exceptional. Also UHPC (UHPC – Ultra High Performance Concrete) with compressive strength over 150 MPa is already used for some specific construction elements in building construction and in construction of bridges. These types of concretes enable design with reduced material consumption and consequently with lower environmental impacts and with higher reliability and durability. Due to higher durability UHPC could be used also for special elements for external skin of buildings (Figure 4a) or city furniture (Figure 3a).

4.2. Utilization of recycled concrete and other secondary materials

Some secondary materials (waste recycling products from other processes) can be used for cement and concrete production, for production of mould elements or other components. Fly ash, slag or microsilica are used to increase strength and workability. They decrease consumption of energy intensive Portland cement due to their cementitious

properties. Recycled concrete from demolition can be used as backfill replacing natural aggregate. Recycled aggregate can be used to some extent as substitute to natural aggregate in new concrete.

4.3. Shape optimization – light subtle elements

Reduction of amount of needed concrete by shape optimization is one of the basic and traditional approaches. This can result in subtle lightened cross-sections of the elements. Their lower weight imposes lower load on supporting structures. Application of high performance concrete enables additional savings due to higher reduction of cross section dimensions. Cross section shape can be created using moulds, various types of lightening elements or by application of light-weight concrete. Mentioned techniques can lead to material savings from 30 to 70%.

4.4. Timber-concrete composite structures

An effective combination of different materials and structural concepts could lead to more sustainable and resilient structures.

The timber structures could have insufficient stiffness. The lack of mass in timber structures causes troubles with acoustics. Inflammability of wood limits the use from the perspective of fire safety. Thus the combination of concrete and timber elements can lead to advantageous structural and environmental solutions. In Figure 3b there is presented composite structure composed from timber glue laminated beams and thin top deck from UHPC. The thickness of the concrete deck is 30 mm and it is glued to the timber beam by glue based on epoxy resin.



Fig 3 (a) prototype of solar bench CapaSitty made from UHPC at University Centre for Energy Efficient Buildings, CTU (photo T. Vlach), (b) hybrid timber-concrete floor structure - UHPC 30 mm thin slab is glued to glue laminated beams; testing at CTU Experimental Centre.

4.5. Textile reinforced concrete utilization

Traditional approach based on the use of steel reinforcement is not applicable for very small thickness due to needed concrete layer protecting steel against corrosion. Textile reinforcement represents alternative to traditional steel reinforcement due to the non-corrosive properties. The concept of using textile reinforced concrete (TRC) was introduced in order to reduce the thickness and thus weight of elements and associated environmental impacts. On the Figure 4a there is a façade in Malmo, Sweden made from panels from TRC (13 mm thick TRC plate is fixed to steel bearing frame).

4.6. Concept of subtle concrete frame for energy efficient buildings

Nowadays, there is an increasing tendency to build multistory wooden based buildings. Multistory wooden based buildings are built from CLT (cross laminated timber) panels or using timber frames. However, there are limitations

in a space rigidity of multistory timber structures, in acoustic performance of timber floor structures and in a fire safety. The combination of light concrete frame with concrete floor structure and wooden based other parts of structure (envelope, partitions, roof structure) could solve some of these problems. Significant advantages of subtle elements are material and energy savings during production, transport, manipulation and construction on building site. Accumulative properties of RC floor structures can significantly contribute to thermal stability improvement of buildings indoor environment. This will mainly help buildings that need cooling in summer. On the other hand concrete frame represent stronger load bearing structure especially in comparison to timber structures. In the same time such composite structures will be more resilient and better prepared for extreme situations in a changing environment.

Figure 4b presents prototype of concrete structural subtle frame for construction of houses in passive energy standard. The concept is based on combination of subtle load bearing concrete frame with building envelope and other parts like partitions, roof structure etc. mainly from wood or other biobased materials.

Concrete precast elements are made from high performance concrete C80/95. Precast RC columns have a C shape with the cross section 180 x 250 mm. Floor structure has a flat lower ceiling without visible beams. There are tested two types of floor structures – both lightened with fillers from light concrete. Larger section has 8 x 8 m spans; smaller 8 x 6 m. Floor structure in larger section is formed from main prestressed beams and prestressed floor panels; shorter RC panels. On the second level of 8 x 8 m floor structure will be tested also effect of additional transverse prestressing by posttensioning – two way prestressed precast floor slab (see in the Fig. 4b prestressing cables in the holes prepared for prestressing).



Fig 4 (a) external façade panels from textile reinforced UHPC, construction Skanska CZ, Malmö, Sweden (photo Skanska), (b) prototype of HPC subtle frame for residential buildings under construction in University Center for Energy Efficient Buildings

5. Conclusion

Due to specific properties, concrete could be recognized in the most applications as a disaster resilient material. This is essential especially in current changing world. Mechanical properties of new types of concrete (HPC, UHPC, TRC) such as high compressive strength, durability, water tightness etc. create conditions for designing subtle structures that leads to saving up to 70% of material in comparison with ordinary concrete, and consequently to reduction of embodied CO₂ emissions. In the same time such structures could be more resilient in the situation of changing natural as well as social conditions.

Presented cases show potential of the use of new types of concrete in advanced structures. These structures could be sustainable and resilient in the forthcoming era with changed environment. Some of principles were demonstrated on results of experimental research performed by author and his team at the Czech Technical University in Prague and are presented on Figures 3 and 4.

Acknowledgements

The presented work has been supported by Czech Grant Agency, research grant GACR P104 13-12676S Advanced research of UHPC matrix for ultra thin elements with non-conventional reinforcement, Technology Agency of the Czech Republic research grant No. TA03010501 Optimized Subtle Frame for Energy Efficient Buildings and TE02000077 Smart Regions – Buildings and Settlements Information Modeling, Technology and Infrastructure for Sustainable Development.

References

- [1] P. Hajek, C. Fiala, M. Novotna, Sustainable Concrete – on the way towards sustainable building. In proc. World SB14 Barcelona – Creating New Resources, 2014
- [2] Cembureau, Cement & Concrete – Key facts & figures. The European Cement Association – www.cembureau.be, 2015 [3] WWF International (World Wide Fund for Nature): A blueprint for a climate friendly cement industry, 2008
- [4] WMO - World Meteorological Organisation - www.wmo.int and www.theguardian.com, 2015
- [5] EN 15643-2 Sustainability of construction works, Assessment of buildings – Part 2: Framework for the assessment of environmental performance, CEN, 2011
- [6] Fib Bulletin 71, Integrated Life Cycle Assessment of Concrete Structures, State-of-the art report, ISBN 978-2-88394-111-3, fib, 2013
- [7] Resilient Design Institute – www.resilientdesign.org
- [8] Hájek P, Novotna M, Fiala C., 2013, Sustainable Concrete for Sustainable Buildings, In. proc. SB13 Munich
- [9] Hájek P, Fiala C, Kynčlová M: Life Cycle Assessment of Concrete Structures – Step towards Environmental Savings, Structural Concrete, fib, 2011, vol. 12, no. 1, p. 13-22. ISSN 1464-4177.



Sustainable Civil Engineering Structures and Construction Materials, SCESCM 2016

Role of visualization technologies in safety planning and management at construction jobsites

Salman Azhar^{a,*}

^a*McWhorter School of Building Science, Auburn University, Auburn, Alabama 36849, USA*

Abstract

Workplace safety is significant to the construction industry throughout the world. Despite rigorous efforts of safety professionals and strong governmental enforcement of safety laws and regulations, there has not been a significant decline in fatalities, injuries and illnesses in the construction industry. Extensive research on this topic has indicated that the dynamic nature of the construction industry is one of the main reasons. Each construction project is unique and identifying all possible hazards and safety risks is always challenging. In recent years there has been a significant increase in the use of visualization technologies in different phases of the construction project life cycle. Visualization technologies such as Building Information Modeling (BIM), 4D simulations, and 3D Immersive Virtual Reality Environments can result in improved occupational safety by allowing architects, engineers, and contractors to visually assess jobsite conditions and recognize possible hazards before the construction proceeds. This paper presents three case studies that investigated the effectiveness of above-mentioned visualization technologies in developing, communicating and implementing construction site safety plans. The case studies results indicated that 3D/4D dynamic tools are more effective in safety planning and management as compared to the 2D static drawings because they closely simulate the actual jobsite conditions. In addition, the visualization technologies are found to be very effective in construction safety education and training in both formal and informal settings.

© 2017 The Authors. Published by Elsevier Ltd.

Peer-review under responsibility of the organizing committee of SCESCM 2016.

Keywords: Construction safety; visualization technologies; Building Information Modeling; 4D simulations; Virtual reality head gears

1. Introduction and background

Safety performance is of vital importance throughout the construction industry [1]. The accident rate in construction is among the highest in comparison to other industries all over the world [2]. Although dramatic improvements have

* Corresponding author. Tel.: +1-334-844-5383; fax: +1-334-844-5386.

E-mail address: salman@auburn.edu

taken place in construction technologies and processes in recent decades, the safety record in the construction industry continues to be one of the poorest [3]. Inappropriate work planning and supervision; insufficient communication between workers and supervisors; and lack of safety training and practices are identified as key contributing factors behind most fatalities and injuries [4].

Safety planning is an essential part of the construction planning process but is typically carried out to a certain extent separately from other project planning and control tasks [5]. Traditional safety planning relies on manual observations, gut-feelings and experience of the safety planner. A typical safety plan depicts what safety measures are necessary, when, where, and why. The link between planning for safety and work task execution is often weak: for example, many contractors use two-dimensional drawings (2D) or field observations to identify hazards. Since their approach is manual and based on experience and gut-feelings, the observed results can be error-prone due to subjective judgments of the decision maker [5].

Recently, there has been considerable interest in improving worksite safety through safer design and work method statements using Building Information Modeling (BIM) [6, 7]. A building information model allows constructors to visually assess jobsite conditions and recognize hazards [8]. The utilization of BIM technologies can result in improved occupational safety by connecting the safety issues more closely to construction planning, providing more illustrative site layout and safety plans, providing methods for managing and visualizing up-to-date plans and site status information, as well as by supporting safety communication in various situations, such as informing site staff about making safety arrangements in response to a particular risk or warning about various risks [9]. The use of BIM also encourages other project partners to involve in both risk assessment and planning [5].

Rajendran and Clarke [10] outlined the following areas where Safety and Health (S&H) professionals can use BIM technologies: (1) Design for safety; (2) Safety planning (job hazard analysis and pre-task planning); (3) Worker safety training; (4) Accident investigation; and (5) Facility and maintenance phase safety. For these tasks, S&H professionals can use 3D renderings generated from the BIM models and walk-throughs animations. In addition, 4D phasing simulations focused on the safety procedures can be generated to show how temporary safety elements and areas of concerns transition throughout the duration of a project. A byproduct of integrating safety with BIM is safety related training videos for construction workers. Using a BIM model for safety training creates a visual tool that allows on-site labor to understand the actual project conditions. It can also help cross the common language barriers associated with foreign workers because training is done through visualization [9]. Franconeri and Simmons indicated that animated stimulus with moving and looming stimuli captures the human attention-span for a significantly longer amount of time when contrasted with static imagery [11].

Eastman et al. reported two examples of the use of BIM in safety planning and management [12]. In the first project, a theme park, the project team modeled envelopes for testing rides to ensure that no activities were taking place during the testing period within the test envelope. Using 4D simulations, they identified a conflict and resolved it ahead of time. On a second project, a steel frame building in Yas Island of Abu Dhabi, massing cylinders were used to model the spaces occupied by the activities of the welding crews. Clash detection between cylinders was then used to identify possible exposure of workers to dangers posed by other teams from time to time.

1.1. Building information modeling for construction safety: scope and applications

The existing research studies on the utilization of BIM technologies for safety planning and management can be divided into the following categories: (1) Design for safety; (2) Design inspection and monitoring; (3) Safety planning; (4) Safety training; and (5) Facility management and emergency responses [7]. A brief summary of some of the important studies is presented below.

Ku and Mills evaluated potential of BIM as a design-for-safety (DfS) tool [13]. They indicated that BIM can facilitate early collaboration between architects/engineers and constructors, via automated checklists of rule-based safety information such as codes and regulatory information. Via a theoretical framework, they evaluated usefulness of BIM as a DfS tool and provided research suggestions for designing future BIM tools for safety. Based on this concept, Qi et al. designed a prototype Construction Safety Checking system. This tool automatically checks for fall hazards in a BIM model and provides design alternatives to the users [14].

Kim and Ahn used BIM technologies for temporary facilities planning of a building project [15]. They mentioned that the temporary facilities planning process is tedious and requires a lot of attention due to the following reasons:

Firstly, temporary facilities are generally not clearly delineated on the building drawings; secondly, the installation and dismantling of these facilities is one of the high risk activities on the jobsites; and thirdly, the designers typically overlook safety considerations in temporary facilities design which results in many safety hazards. They developed a prototype system for designing and depicting installation and de-installation of scaffolding in high rise building projects. Hu et al. used sub-building information models for 4D structural safety analysis during construction [16]. A sub-BIM is a subset of main BIM model and focuses on a certain part/phase/trade of the project. This concept is useful for complex projects where it is difficult to use a single BIM model for various analyses. The proposed approach was tested on the construction of the National Stadium of the 2008 Olympics. The authors claimed that their suggested approach is feasible, and resulted in remarkably reduced workload for safety planners. Sattineni and Azhar [17] investigated the movement of workers wearing Radio Frequency Identification (RFID) Tags in a BIM model. They indicated that this method of monitoring can be used to improve the safety and productivity of construction workers on a construction jobsite. Moreover this technique can also be used to track equipment and construction materials on a job-site thereby allowing S&H professionals to identify any associated hazards.

Bansal integrated a BIM model with a Geographical Information System (GIS) for predicting places and activities which have potential for accidents [18]. The prototype system was tested on a real life project in India. He concluded that the integration of geospatial information in a BIM model facilitates safety planners in examining what and where safety measures are required. Kiviniemi et al. [19] used 4D BIM models for managing and communicating construction safety plans. They demonstrated use of BIM for the following safety related activities: (1) Site layout and anti-crane collapse plan; (2) Wall demolition visualization; (3) Safety railing modeling; (4) Formwork plan with integrated fall protection; and (5) Design for safety model checking. They found that BIM-based safety demonstrations are an effective tool for discussing and communicating safety related issues at the jobsite with the project team. Kim suggested that a Building Life Cycle Management mechanism should be applied for the health and safety issues [20]. He demonstrated this concept with the help of several case studies where BIM technologies were used to address safety issues in the design, construction and post-construction stages.

Zhou et al. investigated application of 4D visualization technologies for safety management in metro construction [21]. The results show that the 4D visualization technologies can be effectively used to detect safety risks before and during the construction process and then provide preventive measures. Thus, timely decisions can be made to avoid accidents. Sijie *et al.* applied automated safety rule checking to Building Information Models and found it very useful [22]. Enshassi et al., found that “hazard identification and minimization” and “safety training and education” are the most important safety-related applications provided by BIM tools to improve safety performance in construction. Lack of universal use of BIM in the construction sector and insufficient training availability are the highest ranked barriers to adopting BIM in construction to improve safety [23].

2. Research aim and significance

The existing research studies have demonstrated the effectiveness of visualization technologies for safety planning and management however they have following limitations: (1) The end product of many studies is either a conceptual framework or a limited-functionality prototype system for demonstrating the main concept; (2) Most prototype systems were tested on hypothetical simplified “square form” buildings which represent a low level of complexity; and (3) The prototype systems were tested using “laboratory” settings with either no or very limited involvement of S&H professionals, site superintendents, and craft workers. This paper, via three case studies, demonstrates how designers, engineers, and contractors can utilize onsite BIM and other advanced visualization technologies for safety planning and management in real life projects. The presented study is unique because of: (1) It tested the advanced visualization technologies’ applications for safety in real-life complex building projects; (2) It utilized only those tools that are commercially available and well recognized in the construction industry; and (3) It exhibits how designers,

engineers, and contractors can use these advanced technologies to formally and informally educate and train their workers which in turn would help them to maintain high safety standards in their projects.

3. Research design

Case study approach is used in this paper for data collection and analysis. Fellows and Liu [24] found Case study as an effective strategy to research an experimental theory or topic using set procedures, often comprising of several different combinations of data collection such as interviews and documentary evidence, where the emphasis is towards investigating a phenomenon within a context. Case study is an appropriate research technique for an industry, like construction, that is project driven as well as composed of different types of organizations and businesses. There are many advantages for using case study to conduct research. Case studies utilize quantitative and qualitative data, or what is referred to as mixed methods research. This information can be drawn from a number of different types of sources such as documents, archival records and interviews to name a few. Hence the results of the case study research are technically sound, reliable, and highly valuable to both researchers and practitioners [24]. Three case studies are presented in this paper to illustrate the various advanced visualization technologies and their applications in safety planning and management. The research methodology and results of each case study are reported separately in the following sections.

4. Methodology and main findings

4.1. Case study 1: Recreation and wellness center at Auburn University, Auburn, Alabama, USA

The first case study demonstrates the applications of Building Information Modeling (BIM) and 4D simulation technologies for safety planning and management at the Recreation and Wellness Center project at the campus of the Auburn University (AU). In this project, four-dimensional (4D) phasing simulations, 3D walk-throughs and 3D renderings were utilized for identifying hazards and communicating safety management plan to the workers. The key project details are as follows: (1) Cost: \$50 million; (2) Size: 240,000 ft²; (3) Delivery system: CM agency; (4) Start date: October 2011; and (5) Completion date: July 2013. The exterior and interior renderings of the project are shown in Figure 2.



Fig. 1: Project renderings (Courtesy of: Robins and Morton & 360 Architecture).

Based on discussions with the project team, it was decided to use BIM and 4D technologies to address the “fatal four” construction fatalities and injuries namely: (1) falls; (2) struck by objects; (3) caught in/Between; and (4) electrocutions. It was further decided to develop following five safety plans: (1) excavation risk management plan; (2) crane management plan; (3) fall protection plan for leading edges; (4) fall protection plan for roofers; and (5) an emergency response plan. The following end products were shortlisted to develop the above-mentioned safety plans: (1) 3D renderings; (2) 3D Walk-through and fly-through animations; (3) 4D phasing simulations; and (4) Narrated videos for workers based on animations and simulations. The following software were selected for this purpose: (1)

Autodesk Revit® for modeling; (2) Google Sketchup® for creating 3D equipment, characters and related families; (3) Synchro® for 4D phasing simulations; (4) MS Project® for scheduling; and (5) Camtasia® and MS Movie Maker® for producing videos. The base BIM models of the project were acquired from the project architect. These models were used for hazards identification and development of BIM-based safety plans. The flowchart shown in Figure 2 outlines the workflow.

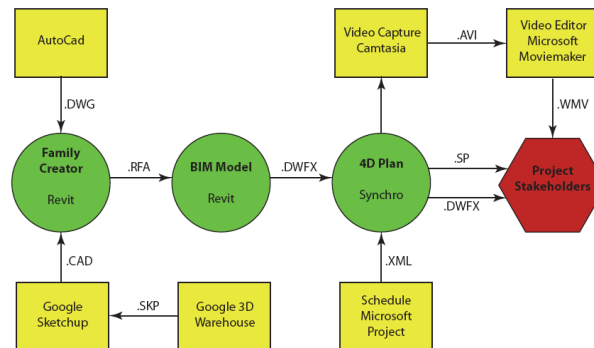


Fig. 2. The workflow for developing BIM-based safety plans, simulations and videos [6.9]

The purpose of the excavation risk management plan was to safely coordinate earthwork operations at the jobsite. The earthwork phase required excavation up to 8 ft deep and then installation of sheet piles to avoid cave-ins. In the BIM model, the researchers created sheet piling components consisting of a sheet pile section and a base re-shoring stand made of a steel beam and a solid steel tube. The sheet piles were arrayed around the indented ditch and the stands were then arrayed behind them. The site utility work included installation of reinforced concrete pipes for sewage. These activities were modeled using 4D simulations to coordinate excavation equipment operations at the jobsite. The crane management plan was prepared to: (1) identify swing radius of the crane to ensure its safe distance from the power lines and nearby temporary and permanent structures; and (2) identify what trade/crew would be utilizing crane at a particular day/ time. The fall protection plan for leading edges was prepared according to OSHA subpart M: Fall protection standards. Two types of fall protection railings were modeled: 2x4 wooden railings on the second level (concrete structure) that were bolted to the concrete slab and 3/8" steel aircraft cable railings on the third and higher levels of the project (steel structure).

After modeling the fall protection railing components, the railings were placed on the structural BIM model. While performing this process, the researchers were able to identify multiple fall hazards through the 3D view that were not easily identifiable in the 2D plan view such as not yet constructed stairwells and skylights. The modeled railings were then segregated by zones and levels, and the resulting railing sections were exported to Synchro® for developing 4D simulations. The 4D simulations provided complete details to the general and sub-contractors such as the location and date when the railings were to be installed or removed. Another fall protection plan was prepared for the roofing system. The entire roofing operation was simulated to identify any safety issues. These simulations were used to brief roof workers about work conditions and hazards on a constantly changing roof structure.

The BIM-based emergency response plan consisted of 5 sub-plans namely *Construction crew entrance/exit; construction equipment and deliveries route, temporary facilities and job trailer locations, emergency vehicle(s) route, and severe weather shelters* to orient workers with the construction site. Three dimensional (3D) walk-through animations and renderings were generated from the BIM models to communicate emergency response plan to the workers. Figure 3 illustrates screenshots of the Building Information Models and 4D simulations. More details about this case study can be found in [6] and [9].

The 3D walk-throughs and renderings, 4D simulations, and animation videos were used by the general contractor to communicate the site safety plan to the sub-contractors and workers. Both internal and external validations were performed to verify the research results and usefulness of this study.

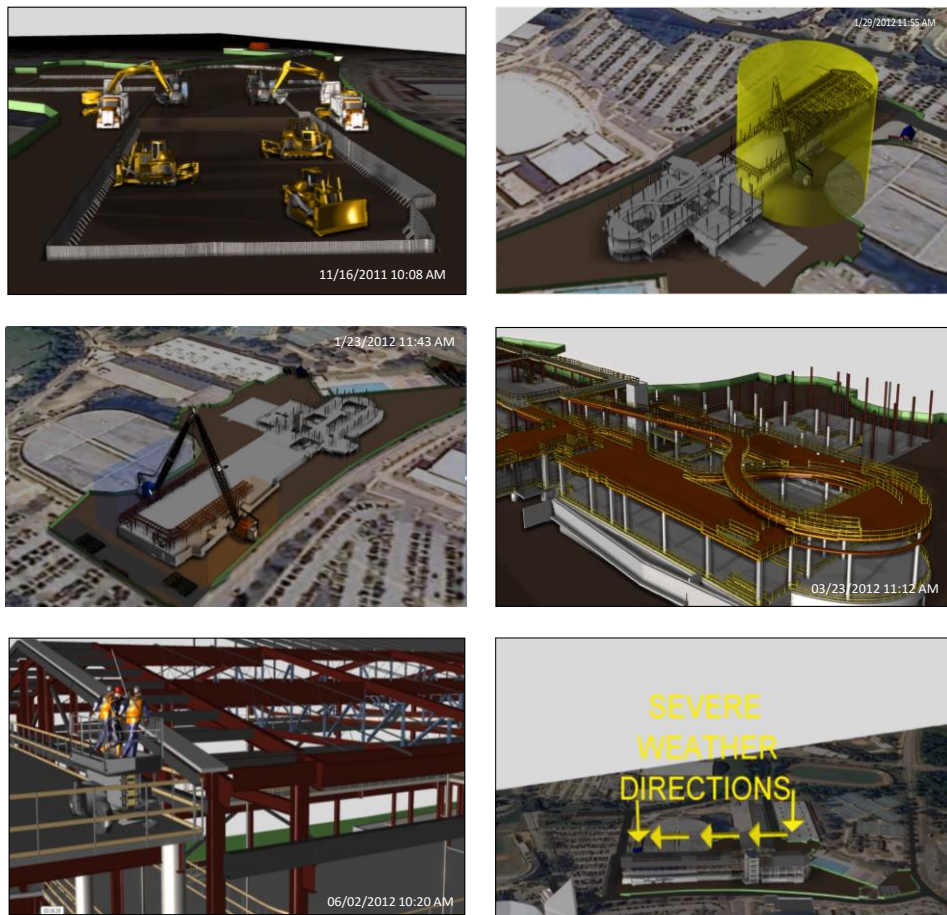


Fig. 3. Screenshots of BIM-based safety plans for AU Health & Wellness Center project [6, 9]

The site superintendent, site managers, and site safety staff were interviewed to identify the benefits and any pitfalls of BIM-based safety plans. The interviewees described three main perceived benefits: (1) improved communication of the safety plan to the construction personnel; (2) improved communication of the project's safety plan to the OSHA and the owner; and (3) logistical details of construction safety tasks being fully addressed in the preconstruction phase. Following are two excerpts from the interviews: (1) “.....BIM technology could have a very significant and positive impact on the safety planning and management...the 4D animations proved to be very helpful in the safety planning meetings and daily safety talks.....”; (2) “.....4D simulations are very helpful to fully involve owners in the safety process that may not be as fluent at visualizing safety practices from 2D drawings or written safety plans....”.

The group expressed some concerns on the extra cost that may be involved in developing the BIM-based safety plans. They also suggested a close collaboration between the BIM modeler(s) and site S&H staff to ensure 100% accuracy of the resulting models and simulations. The same group was also asked to complete a short questionnaire in an effort to compare the effectiveness of BIM-based safety planning to the traditional safety planning. These results indicate that the BIM-based safety planning is *moderately-to-highly* effective and accurate in identifying hazards and communicating safety plan to the workers. The survey group indicated BIM-based approach moderately better in incidents and accidents control at the site as compared to the traditional safety planning.

4.2. Case study 2: US Army Hospital, Fort Benning, Georgia

The second case study is a \$380 Million, 745,000 SF US Army hospital located in Fort Benning, Georgia on a 157 acre site. The primary facilities included both outpatient and inpatient medical facilities with ancillary services. The General Contractor (GC) was Turner Construction Company. Safety planning was not in the original scope for BIM services. The safety professional and the site superintendent made the decision to try and utilize BIM in their safety program for the following applications: *Identifying hazards and visualizing task with direct safety concerns; Illustrating clearances; Crane safety, location of fire extinguishers, and several other hazardous areas.* The data for this case study was collected via observations and personal interviews with the site safety staff. The following paragraphs depict our main findings. More details about this case study can be found in [25].

Before construction had begun, the safety professional and project engineers were able to use the BIM model to identify certain safety hazards that would arise on the site. These included overhead obstructions, falling object, personnel protection, entrance locations, underground obstructions, and fall Protection. In addition, through BIM they were able to visualize certain tasks and decrease the amount of safety unknowns such as: determined equipment access, reach, and landing area locations as shown in Figure 4; determined forklift manoeuvring routes; guard rail positions and where removable sections would be located; determined overhead personnel protection methods; and identified fall arrest and restraint anchor points.

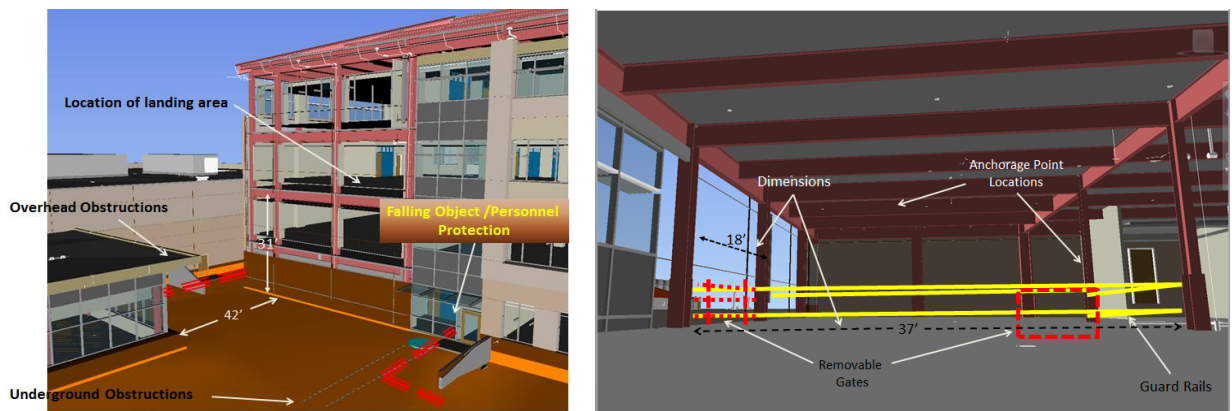


Fig. 4. Screenshots of BIM models used in morning safety meetings [25]

On this project, the GC used BIM to increase crane safety in multiple ways. First, they found the exact crane expected to be onsite and add it to the model (see Figure 5). Then an analysis was done on the swing radius, height, clearances, and placement of the crane to see what risk and hazards could arise while the crane is in use. This came in many of the confined spaces that a crane was needed. Also in one instance it was realized that the crane would not be big enough for that particular task by modeling the same crane that was being brought onsite. The safety professionals with GC also came up with using BIM to determine the locations and number of fire extinguishers that would be needed throughout the project (see Figure 5). The safety professional also had a meeting with the BIM team and figured out how to utilize the BIM model for their fall protection plan. They determined all the safety rails they would need, where they would be needed, and added them to the model. Also they determined anchor points that would be needed and added them to the model.

The GC also used BIM to visualize and model certain tasks in order to determine logistics and safety for complex issues. One great example was an excavation they modeled in BIM for gas tanks. They used BIM to model the slopes and found that it was not possible to keep the required slope on the excavation in the current place. It was decided to move the tanks eliminating hundreds of hours of work, rework, and possible unsafe conditions. The GC also used the BIM model for their subcontractors orientation. When a new subcontractor comes on site the GC safety professional sits down with their safety guy, foreman, or whoever will be in charge of safety and walks them through the BIM model at the current stage of the project. At this time he goes over any safety concerns, safety exits, or anything else that could be safety related to bring the contractor up to speed before their people ever walk on the site.

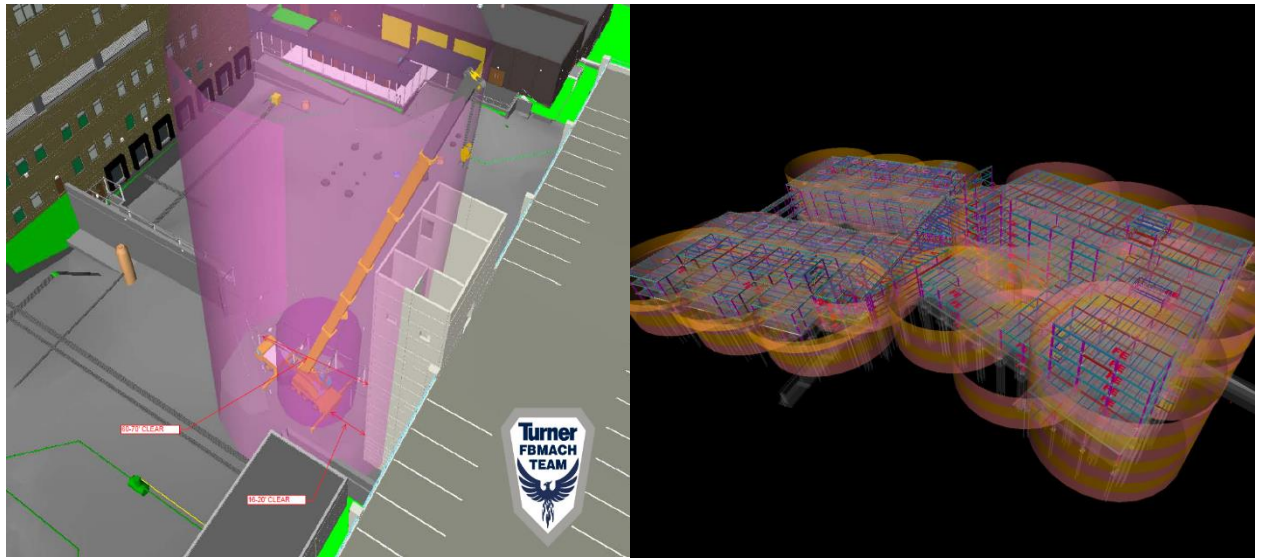


Fig. 5. Screenshots of BIM models depicting crane safety and fire extinguishers' placement plan [25]

Findings of this case study suggested the BIM models could be used to help with safety training, site layout, hazard identification, communication, collaboration, fall prevention, crane safety and accident investigation. There are numerous ways BIM can be utilized to increase the efficiency of safety programs with very little added effort and money.

4.3. Case study 3: Dudley Hall renovations, Auburn University, Auburn, Alabama, USA

The third case study is a renovation project (hereinafter called Dudley Hall renovation) on the campus of Auburn University. The project scope consisted of: Major exterior renovations; removal of existing brick; installation of rigid insulation and waterproofing to the CMU block backup wall; reinstallation of the previously removed brick. Also several walls were replaced by floor to ceiling storefront glazing. The building had to remain open and functional for students and faculty during the renovation process with limited street access. Photos taken during renovation are shown in Figure 6. More details about this case study can be found in [26].

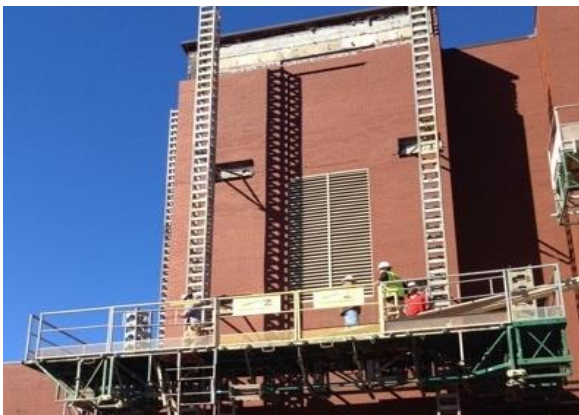


Fig. 6: Dudley Hall during renovation [26]

In this project, the research team moved one step ahead and tested the virtual reality headsets in conjunction with BIM technology. The rationale behind this decision was that Virtual Reality (VR) or immersive environment can

provide enriching experiences to users by simulating real world environments that is not possible through traditional methods. Virtual reality can recreate sensory experiences, which include virtual taste, sight, smell, sound, and touch (Luo, 2015). People gain 70 percent of information by vision, resulting in systems like HMDs that provide the visual component of immersion have been widely used to develop virtual environments. VR provides one of the best tools for accident reconstruction, training and hazard identification by immersing the trainee in an environment that is as real as possible. The use of high quality three-dimensional graphics, sound and dynamic simulation combine to form a uniquely engaging experience (Kizil and Joy, 2001). This research seeked answers to the following key questions: (1) Are VR headsets feasible for construction safety planning and training; (2) Does the VR headsets provides the same experience as the real-life construction environment; and (3) What are the limitations of VR headsets specifically in construction practice?

The VR headset used in this study is the Oculus Rift®. It is a light weight headset that allows a user to step into the VR environment and being able to “walk through” and “look” in any direction as shown in Figure 7.



Fig. 7: Components of Oculus Rift DK2. (Source: <https://www.oculus.com>)

For this case study, a BIM model of the Dudley hall was developed in Autodesk Revit®. The model depicted construction and renovation of the building at different phases. Construction equipment - a crane, scaffolding, tools, vehicles, debris removal, jobsite trailer, and construction fencing – were added in the model to simulate the active jobsite environment. This modeled environment served the basis for investigation of construction safety planning. The workflow of converting a BIM model into VR environment is shown in Figure 8. Unity 3D® software was used for creating VR environment and eventually viewing it via Oculus Rift®.



Fig. 8: Modeling workflow for developing a VR environment for safety training (Froehlich and Azhar, 2016)

It is important to note that the software capable of producing VR experiences are geared toward game development. The structure and file types differ than those traditionally used in the AEC industry. The following software were selected for this case study: (a) Autodesk Revit® for creating a BIM model; (b) SketchUp® for editing and exporting all the equipment, characters and related families needed onsite; (c) Autodesk 3Ds Max® for cleaning up the model; (d) Unity 3D® for rendering the model; and (e) Camtasia Recorder® and iMovie® for producing the videos. Oculus Rift headset is used to view the model in VR environment.

As shown in Figure 9, the BIM model of Dudley Hall was developed in Autodesk Revit®. Construction equipment, cranes, tools, vehicles and characters were imported from SketchUp®’s 3D Warehouse into Revit®. Use of these

publically accessible models enhanced the environment, as well as added efficiency to the process. The parametric nature of Revit required the developed model to be scrubbed of unnecessary information thus reducing the complexity and overall file size. The faces were combined by material type into layers, (this proved to be a key step for success once imported into Unity3D®). The file was then exported as an .FBX file type. Next the .FBX file was imported into Unity3D® where textures, materials, lighting, and trees were added. The following end products were produced in this phase: (a) 2D site plan captured from Unity3D®; (b) 3D site plan; (c) 3D site plan with immersive environment for Oculus Rift®; and a (d) video of the immersive environment.

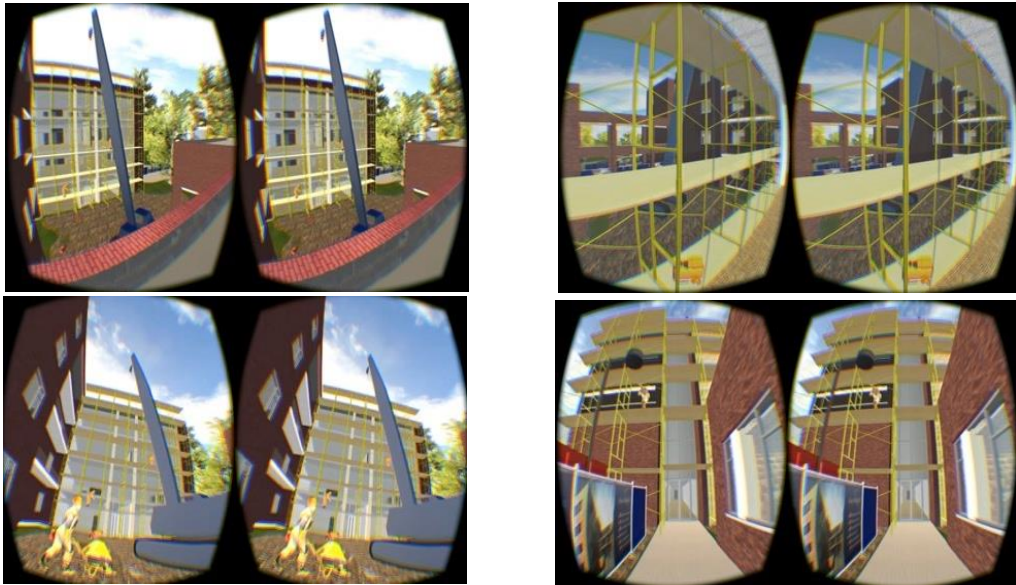


Fig. 9. Viewing VR environment through Oculus Rift – shows workers movement and site access (Froehlich and Azhar, 2016)

In addition to existing hazards’ identification, several scenarios were created for workers’ safety training such as: (1) Unsafe use of forklifts, (2) Inadequate fall protection, (3) Electrical hazards; (4) Falling objects; and (5) Tripping hazards. Figure 10 illustrates the electrical fire hazard scenario. More information about these safety training scenarios can be found in Congwen (2015).



Fig. 10. Electrical fire hazard Congwen (2015)

The project team members used Oculus Rift headset to view the created scenarios and provided their feedback. They considered ‘Safety Training’ as the best candidate for VR applications. Some specific comments were as follow: (1) “Very promising way to assess potential danger without being put in the actual situation.” (2) “It reminds me of a

game. It's very interactive and effective. I think it's an interactive idea for safety training and the immersive environment is definitely useful." Some users complained about the motion sickness which affected participants for various lengths of time. The motion sickness could be directly related to the amount of time spent in the VR environment. Participants stated that "using the Xbox game controller instead of the built-in head tracking eased the blurring associated with the movement". Collective feedback from participants indicated there is a strong interest in learning more about VR headsets in the construction industry. The participants interacting with the built scenarios and being able to identify key aspects as well as conflicts confirms VR as a viable option for construction safety management.

5. Conclusions and the Path Forward

These case studies demonstrated that BIM and VR technologies can be used as a new collaborative safety planning, management, and training tool. Through BIM models, 4D simulations and VR environment, designers, engineers, and constructors can take effective protective measures in the project planning phase to eliminate (or minimize) the construction site hazards. For example, contractors can use these technologies to identify hazards and communicate mitigation plans to the workers. Through 4D simulations and/or VR immersive environment, the site staff can visually identify the sequence of activities, and materials and equipment requirements before commencing work. They can discuss possible hazards and develop their specific safety plans. These visualization technologies can also be used during an accident investigation to recreate event sequence and the incident scene. In the absence of an existing 3D model, laser scanning technology can be used to capture point cloud for developing a 3D model. In fact, the Building Information Modeling (BIM) along with the 3D High Definition (HD) laser scanning has recently emerged as a powerful new platform for facilitating both engineering and administrative safety planning and management at the maintenance/retrofitting stages of a facility.

The utilization of BIM and VR technologies for safety management poses several challenges such as additional cost involved for developing/enhancing BIM models and/or VR environment; lack of knowledge of S&H personnel in using these tools; and technical issues such as non-availability of safety elements and equipment in BIM/VR software library. Last but not least challenge is human behavior which cannot be changed quickly. In that respect, the visualization technologies should not be considered as a panacea for solving all health and safety issues at the construction sites. These technologies will help to improve the safety situation but the overall improvement might be visible in several decades. We strongly believe that dynamic 3D/4D tools are always more helpful in hazards identification than 2D static drawings because they closely simulate the actual jobsite conditions. In this paper, we demonstrated the useful of BIM and VR technologies for identifying and communicating site hazards to the project team. The BIM/VR-based safety planning is particularly very useful for academic buildings projects that are typically constructed on an active college campus environment. The BIM and VR models and simulations can help university administrators to ensure safety of their students and staff and plan campus activities accordingly. It is hoped that these visualization technologies will become more wide spread in the coming months and years to help keep workers and projects safe which is the overall goal.

Acknowledgements

The author would like to acknowledge the following undergraduate and graduate students of Auburn University for contributing in this paper: Mr. Alex Behringer, Mr. Dehyrl Middleton, Ms. Congwen Kan, and Mr. Mark Froehlich.

References

- [1] Choudhry, M. R., Fang, D. and Ahmed, S. M., Safety management in construction: best practices in Hong Kong. *J. Prof. Issues in Eng. Edu. and Prac.*, 134 (1), 2008, 20-32.
- [2] Wu, H., and Fang, D., Safety culture in construction projects, *Proceedings of the CIB W099 International Conference on Modelling and Building Health and Safety*, Singapore, 2012.
- [3] Huang, X., and Hinze, J., Owner's role in construction safety, *J. Const. Eng. and Manage.*, 132 (2). 2006, 164-173.
- [4] Lappalainen J., Mäkelä T., Piispanen P., Rantanen E., Sauni S. Characteristics of occupational accidents at shared workplaces. *NoFS 2007 - Nordic Research Conference on Safety*, Tampere, Finland, 2007.
- [5] Sulvankivi, K.; Teizer, J.; Kiviniemi, M.; Eastman, C.M.; Zhang, S.; and Kim, K. Framework for integrating safety into Building Information

- Modelling. Proceeding of the CIB W099 International Conference on “Modelling and Building Health and Safety”, Singapore, 2012, pp. 93-100.
- [6] Azhar, S., and Behringer, A., a BIM-based approach for communicating and implementing a construction site safety plan, Proceedings of the 49th ASC Annual Conference, San Luis Obispo, CA, 2013.
- [7] Chi, S.; Hampson, K; and Biggs, H. Using BIM for smarter and safer scaffolding and formwork construction: A preliminary methodology. Proceeding of the CIB W099 International Conference on “Modelling and Building Health and Safety”, September 10-11, 2012, Singapore, pp. 64-73.
- [8] Azhar, S., “Building Information Modeling (BIM): trends, benefits, risks and challenges for the AEC industry, J. Leadership and Management in Eng., 11(3), 2011, 241-252.
- [9] Azhar, S.; Behringer, A.; Sattineni, A.; and Mqsood, T. BIM for facilitating construction safety planning and management at jobsites. Proceeding of the CIB W099 International Conference on “Modelling and Building Health and Safety”, September 10-11, 2012, Singapore, pp. 82-92.
- [10] Rajendran, S. and Clarke, B. Building Information Modeling: safety benefits and opportunities. Professional Safety, October 2011, pp. 44-51.
- [11] Franconeri, S., and Simons, D. Moving and looming stimuli capture attention. The Attention, Perception, and Psychophysics J., 65 (7), 2003, 999-1010.
- [12] Eastman, C; Teicholz, P.; Sacks, R; and Liston, K. BIM Handbook: A guide to Building Information Modeling for owners, managers, designers, engineers and contractors, 2nd ed., NY: John Wiley and Sons, 2011.
- [13] Ku, K., and Mills, T., Research needs for Building Information Modeling for construction safety. Proceedings of the 44th ASC National Conference, April 2-5, 2008, Auburn, Alabama, USA.
- [14] Qi, J., Issa, R. R. A., Hinze, J., and Olbina, S., Integration of safety in design through the use of Building Information Modeling. Proceedings of the 2011 ASCE International Workshop on Computing in Civil Engineering, Miami, FL, 2011.
- [15] Kim, H., and Ahn, H., Temporary facility planning of a construction project using BIM (Building Information Modeling), Proceedings of the 2011 ASCE International Workshop on Computing in Civil Engineering, Miami, FL, 2011.
- [16] Hu, Z.; Zhang, J.; and Lu, X., Development of a sub building information model for 4D structural safety analysis during construction. Proceedings of the International Conference on Computing in Civil and Building Engineering (ICCCBE 2010), Nottingham, UK, 2010.
- [17] Sattineni, A., and Azhar, S. Techniques for tracking RFID tags in a BIM model. Proceedings of the 27th International Symposium on Automation and Robotics in Construction, Bratislava, Slovakia, 2010.
- [18] Bansal, V.K., Application of geographic information systems in construction safety planning. Intl J. of Project Management, 29, 2011, pp. 66-77.
- [19] Kiviniemi, M., Sulankivi, K., Kähkönen, K., Mäkelä, T., & Merivirta, M., BIM-based Safety Management and Communication for Building Construction. A report published by VTT Technical Research Centre of Finland, Tampere, Finland, 2011.
- [20] Kim, I. (2012). New way of improving safety by adopting BIM-based quality checking process in the AEC industry. Proceeding of the CIB W099 International Conference on “Modelling and Building Health and Safety”, Singapore, 2012, pp. 11-21.
- [21] Zhou, Y., Ding, L.Y., and Chen, L.J. Application of 4D visualization technology for safety management in metro construction, J. of Automation in Construction, 34, 2013, pp. 25-36.
- [22] Zhang, S., Teizer, J., Lee, J-K., Eastman, C.M., and Venugopal, V. Building Information Modeling (BIM) and safety: automatic safety checking of construction models and schedules, 29, 2013, pp. 183-195.
- [23] Enshassi, A., Ayyash, A., and Choudhry, R.M. (2016). BIM for construction safety improvement in Gaza strip: awareness, applications and barriers, Intl. J. of Const. Management, DOI: 10.1080/15623599.2016.1167367.
- [24] Fellows, R.F., and Liu, A.M.M. Research methods for construction, Wiley, 2003.
- [25] Middleton, D., and Azhar, S., Case studies on applications of BIM for safety planning and management, Proc. of the Intl. Conf. on Safety, Construction Eng. and Project Management: Issues, Challenges and Opportunities in Developing Countries”, Islamabad, Pakistan, August 19-21, 2013.
- [26] Froehlich, M.A., and Azhar, S., Investigating virtual reality headset applications in construction, Proceedings of the 52nd ASC International Conference, Provo, UT, 2016.
- [27] Luo, Z. (Ed.), Robotics, automation, and control in industrial and service settings. Engineering Science Reference, Hershey, PA, 2015.
- [28] Kizil, M.S., Joy, J., What can Virtual Reality do for Safety? Peachpit Press, Berkeley, CA, 2001.
- [29] Congwen, K. Applications of 3D virtual reality headsets for safety training and jobsite organization, Graduate capstone, McWhorter School of Building Science, Auburn University, Auburn, Alabama, USA, 2015.



Sustainable Civil Engineering Structures and Construction Materials, SCESCM 2016

EN 206 Conformity Testing for Concrete Strength in Compression

Tam C. T^{a,*}, Daneti S. Babu^b, Li W^a

^a*Department of Civil & Environmental Engineering, National University of Singapore, Singapore*

^b*Concrete Specialist, Alliance Concrete Singapore Pte Ltd, Singapore*

Abstract

Concrete strength in compression is the common characteristic used in the design of concrete structures. However, in general, there are two different types of concrete specimens specified for the determination of concrete strength in compression. They are the standard 150mm diameter by 300mm length cylinders and the standard 150mm cubes. In the case where the maximum size of coarse aggregate is less than 40mm (1½ in.), 100mm diameter by 200mm length cylinders and 100mm cubes may be adopted. Cylinder specimens with aspect ratio (length/diameter) of 2 are likely to be closer to the uniaxial compressive strength as end friction effects at the platens tend to induced a more complex state of stress compared to that of a cubical specimen with aspect ratio of unity. Hence, the two types of test specimens do not provide the same measured strength for the same concrete. For the purpose of conformity testing, the consistency of test results is of greater interest than the magnitude of the measured strength of the concrete specimens. This paper reviews the issues concerning the two types of specimens, (cylinder or cube) and the size of the specimen in relation to maximum size of coarse aggregate used. Some experimental data for compressive strength at 3 strength classes for which slightly over 100 batches produced over several consecutive calendar months were tested. Three types of specimens, 150mm diameter by 300mm cylinders, 150mm cubes and 100mm cubes were adopted for testing at the age of 28-days. Maximum size aggregate of 20mm and CEM I cement were used for strength classes of C32/40, C50/60 and C65/80 achieved with added silica fume. The findings of these test regimes are summarised with recommendations for conformity testing based on EN 206 and its complementary British Standard BS 8500.

© 2017 The Authors. Published by Elsevier Ltd.

Peer-review under responsibility of the organizing committee of SCESCM 2016.

Keywords: Concrete; strength; cube; cylinder; conformity; sustainability

* Corresponding author. Tel.: +65 65166204; fax: +65 67791635.

E-mail address: ceetamct@nus.edu.sg

1. Introduction

Concrete strength in compression is the common characteristic used in the design of concrete structures. However, in general, there are two different types of concrete specimens specified for the determination of concrete strength in compression. They are the standard 150 mm diameter by 300 mm length cylinders and the standard 150mm cubes. Traditionally, design codes for concrete structures in different countries may adopt either type of standard specimens. In recent years with the trend towards globalization of construction practice and the promotion of ISO standards to ease international trades, the current European approach in design codes for concrete structure has adopted cylinder compressive strength in the design formulae. However, the conformity assessment of compressive strength may adopt either type of specimens. The corresponding characteristic strength in strength class is stated in terms of both types of specimens, e.g. C40/50 with the first value in cylinder and the second value in cube compressive strength. This paper reports on an a study of three selected strength classes, C32/40, C50/60 and C65/80 with three types of specimens, 150 mm diameter by 300 mm cylinders, 150 mm cubes and 100 mm cubes tested at the age of 28-days. The issues concerning the two types of specimens, (cylinder or cube) and the size of the specimen in relation to maximum size of coarse aggregate used are discussed. The findings of these test regimes are summarized with the recommendation for conformity testing based of EN 206 and its complementary British Standard BS 8500. Structure

2. Background

The design of concrete structures in accordance with BS EN 1992-1-1: 2004[1] adopts the characteristic cylinder compressive strength in its equations. EN 206: 2013[2] provides for conformity testing for concrete strength in compression using 150mm diameter by 300 mm length cylinders or 150 mm cubes only. The complementary standard to EN 206 in UK, BS 8500-2: 2015[3] has added provisions (clause 12.2) for the use of 100 mm cubes for conformity testing. The conformity criteria for 100mm cube specimens are to be the same as those for 150 mm cubes. Both BS EN 1992-1-1: 2004[1] and BS EN 206: 2013[2] provide for equivalent cube compressive strength corresponding to cylinder compressive strength. In general, up to strength class of C55/67, the ratio of 150mm cube compressive strength/150mm cylinder compressive strength is nominally 1.25 (with rounding to nearest 1 MPa). Above strength class of C55/67 up to C100/115, a constant difference of 15 MPa higher for cube compressive strength above that of cylinder compressive strength has been adopted. These relationships are examined at three strength classes, i.e. C32/40, C50/60 and C65/80. In addition, the ratio of 100mm cube compressive strength /150 mm cube compressive strength and the ratio of 100mm cube compressive strength/150 mm cylinder strength at these strength classes are also determined for the same three strength classes. The test results based on three specimens of each shape and size at the age of 28 days after standard curing are analyzed to provide an assessment of their relationships.

2.1. Relationship between cylinder and cube specimens

A From the many studies on the relationship between the two types of specimens in determining the compressive strength of concrete, the general consensus accepts the ratio of 150mm cube compressive strength/150mm cylinder compressive strength is nominally 1.25 in normal range of strength classes. EN 206: 2013[2] puts the limit at C55/67, but for above this strength class and up to C100/115, a constant difference of 15 MPa higher for cube compressive strength above that of cylinder compressive strength has been adopted. This difference has not received as much study, although the trend for the ratio of cube/cylinder strength has been observed to be decreasing with increasing strength classes, e.g. ratio for C60/75 = 1.25 and ratio for C100/115 = 1.15. Neville[3] stated that “in reality, there is no simple relationship between the strengths of specimens of these two shapes”. The difference in the measured strength between the cylinder specimen and the cube specimen is attributed to the difference in aspect ratio in relation to the restraining effect by the steel platen of the testing machine on the “lateral expansion of the concrete in the parts of the specimen near its ends”, estimated to extend to approximately “ $\frac{1}{2}d\sqrt{3}$ (where d is the lateral dimension of the specimen)” away from the ends, Neville[3]. Thus, in the case of a cube specimen, there is an overlapping of the affected end zones, but for a cylinder specimen with length/diameter ratio of 2, there is a middle zone free of this influence. Hence the measured strength of a standard cylinder specimen is lower than that of a standard cube specimen of the same lateral dimension. The combined influence of modulus of elasticity and Poisson’s ratio of steel and concrete determined the

degree and extent of the end restraint effect whilst the specimen is under load. For these four parameters, only the modulus of elasticity of concrete increases with increasing strength classes. This leads to a reduction in end restraining effect and a lower ultimate strength in the case of the cube specimen. Neville[3] also stated that the ratio of the strengths is “nearly 1 at strengths of more than 100 MPa (or 14000 psi).

2.2. Effect of specimen size on measured strength

Various standards specify the minimum size of the test specimen in term of the maximum size aggregate in the concrete. British standards allow 100mm cubes and 100mm by 200mm cylinders for maximum size aggregates up to 20mm and 150mm cubes and 150mm by 300mm cylinders for maximum size aggregate up to 40mm. ASTM standard requires the diameter of test cylinder to be at least 3 times the nominal maximum size of aggregate. EN 206: 2013[2] specifies only 150mm cubes and 150 by 300mm cylinders for testing of compressive strength of concrete. However, for up to 20mm maximum aggregate size, Clause 12.2 of BS 8500-2: 2015[4] permits the use of 100mm cubes for conformity testing with conformity criteria for 100mm cube specimens to be the same as those for 150mm cubes in EN 206: 2013[2].

3. Experimental Program

In view of the issues discussed above, a planned program of study has been conducted to provide data for three selected compressive strength classes, C32/40, C50/60 and C65/80 for which slightly over 100 batches produced and tested over several consecutive calendar months. Three types of specimens, 150 mm diameter by 300 mm cylinders, 150 mm cubes and 100 mm cubes were adopted for testing at the age of 28-days. The constituent materials for casting of all the concrete specimens are those commonly used in current RMC production in Singapore. The three concretes were produced by the same plant using Portland cement to BS EN 197-1: 2011[5] CEM I – 42.5 R, 20 mm maximum size granite and natural sand together with a superplasticiser to produce a consistence class of S4 given in BS EN 206: 2013[2] for designed concretes, over a period of several consecutive months. Silica fume (SF) to BS EN 13263-1: 2009[6] had been added only to produce C65/80 concrete. Table 1 shows the composition of the three concretes. All the specimens were cast within the RMC plant and demolded after 24 hours, then cured at $27 \pm 5^\circ\text{C}$ as recommended for Singapore testing laboratories under Annex ZZA of SS 544-2: 2014[7] until age of 28 days when they were tested at the saturated condition. No unexpected performance of the constituent materials was noticed during the period of this test program which used the same constituent materials for normal production of concrete in the same plant. All the three types of specimens were cast from the same batch of concrete. End preparation for all cylinder specimens was by grinding.

Table 1. Composition of concretes.

Strength Class	kg/m ³				
	Cement (SF)	Water	Fine Aggregate	Coarse Aggregate	Admixture
C32/40	395 (0)	175	776	990	5.39
C50/60	530 (0)	175	660	990	7.23
C65/80	550 (40)	150	590	990	11.31

3.1. Test Results

The test data of the three populations of concretes are analysed in terms of the following:

- for each concrete, the mean and standard deviation of all the test results (average of 3 specimens)
- for each concrete, the ratio of 150 mm cube/150 mm cylinder specimens ($f_c, 150 \text{ cu}/f_c, 150 \text{ cyl}$) for each batch of concrete
- for each concrete, the ratio of 100 mm cube/150 mm cube specimens ($f_c, 100 \text{ cu}/f_c, 150 \text{ cu}$) for each batch of concrete

- for each concrete, the mean of the ratio calculated in (b) and (c) above
- for each concrete, the mean of the ratio of 150 mm cube/150 mm cylinder specimens based on their characteristic values (f_{ck}), mean (f_m) and from (a) above
- for each concrete, (strength class C32/40 and C50/60), distribution of the ratio of 150 mm cube/150 mm cylinders ($f_{c,150cu}/f_{c,150cyl}$)
- for each batch of concrete for each concrete, distribution of the difference between 150 mm cube and 150 mm cylinders ($f_{c,150cu} - f_{c,150cyl}$) for strength class C65/80
- for each concrete; distribution of the ratio of 100 mm cube/150 mm cube specimens ($f_{c,100cu}/f_{c,150cu}$) for each batch of concrete
- for each concrete, (strength class C32/40 and C50/60), distribution of the ratio of 100 mm cube/150 mm cylinders ($f_{c,100cu}/f_{c,150cyl}$)
- for each batch of concrete for each concrete, distribution of the difference between 100 mm cube and 150 mm cylinders ($f_{c,100cu} - f_{c,150cyl}$) for strength class C65/80

[Note: the results of item (h) indicate that the ratios for ($f_{c,100cu}/f_{c,150cu}$) does not deviate significantly from 1.0 and hence for the case of 100mm cubes, the finding for analysis stated in item (i) and in item (j) is similar to the case for 150mm cubes in item (g) and in item (h). These are not included in this paper].

Tam et al (2015) (8) provided a summary of the data for items (a) to (d) stated above as shown in Table 2 and with Figure 1 showing the overlapping of the distribution of compressive strength of both 100mm cubes and 150mm cubes for each of the 3 strength classes. The findings are summarized as follows:

- The ratio of 150 mm cylinders/150 mm cubes for C32/40 based on characteristic strengths, ($f_{ck,150cy}/f_{ck,150cu}$) = 0.79 and based on mean strengths, ($f_{cm,150cy}/f_{cm,150cu}$) = 0.80
- The ratio of 150 mm cylinders/150mm cubes for C50/60 based on characteristic strengths, ($f_{ck,150cy}/f_{ck,150cu}$) = 0.82 and based on mean strengths, ($f_{cm,150cy}/f_{cm,150cu}$) = 0.83
- The difference between 150 mm cubes and 150 mm cylinders specimens for C65/80 based on characteristic strengths, ($f_{ck,150cu} - f_{ck,150cyl}$) = 12.9 MPa and based on mean strengths, ($f_{cm,150cu} - f_{cm,150cyl}$) = 12.7 MPa
- The ratio of 100 mm cube/150 mm cube for C32/40 based on characteristic strengths, ($f_{ck,100cu}/f_{ck,150cu}$) = 1.01(2) and based on mean strengths, ($f_{cm,100cu}/f_{cm,150cu}$) = 1.01(2)
- The ratio of 100 mm cube/150 mm cube for C50/60 based on characteristic strengths, ($f_{ck,100cu}/f_{ck,150cu}$) = 1.01(3) and based on mean strengths ($f_{cm,100cu}/f_{cm,150cu}$) = 1.01(3)
- The ratio of 100 mm cube/150 mm cube for C65/80 based on characteristic strengths, ($f_{ck,100cu}/f_{ck,150cu}$) = 1.01(4) and based on mean strengths ($f_{cm,100cu}/f_{cm,150cu}$) = 1.01(3)

The test results in Table 1 also provide the following additional findings:

- Standard deviations based on 3 specimens for each batch show generally an increasing trend with increase in compressive strength. The mean and the range of standard deviations for all the 3 types of specimens (100mm cube, 150 mm cube and 150 mm diameter by 300 mm length cylinders) for the three strength classes are shown in Table 3 The ratio of 150 mm cylinders/150mm cubes for C50/60 based on characteristic strengths, ($f_{ck,150cy}/f_{ck,150cu}$) = 0.82 and based on mean strengths, ($f_{cm,150cy}/f_{cm,150cu}$) = 0.83
- Since the mean, maximum and minimum values of standard deviation for the three types of specimens do not differ much for each strength class but the mean cylinder strength is always lower than the cube strengths, the coefficient of variation is higher for the cylinder specimens.
- The range of standard deviations increases with strength level for all three types of specimens indicating a higher degree of variability of test results as also reflected in the range of actual strength values in Table 3.

- For all 3 strength classes the coefficient of variation (standard deviation/mean) is approximately 2%. This is in agreement with the observation in relation to Figure 14.4 of Neville[3] that “for a constant degree of control, laboratory test data, as well as some results of actual site tests, have been shown to support the suggestion of a constant coefficient of variation for well-compacted concrete of different mix proportions with strengths higher than about 10 MPa”. Although other data from construction sites, e.g. Figure 14.6 of Neville[3], show that “coefficient of variation is constant up to some limiting value of strength but, for higher strength, the standard deviation remains constant”. This is not the case with the test data of the study conducted. The standard deviations based on 3 specimens for each batch show generally an increasing trend with increase in compressive strength. Hence, the issue of constant standard deviation or constant coefficient of variation remains to be controversial.

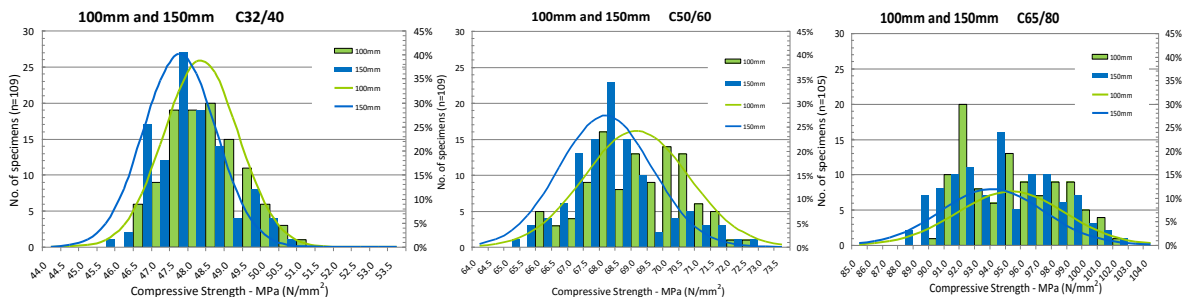


Fig. 1. Graphic distribution data of 100 mm cube and 150 mm cube compressive strength [8].

Table 3. Distribution of 100 mm cube and 150 mm cube compressive strength data [8].

	C32/40		C50/60		C65/80	
	100 mm	150 mm	100 mm	150 mm	100 mm	150 mm
Cube	100 mm	150 mm	100 mm	150 mm	100 mm	150 mm
Mean	48.1 MPa	47.5 MPa	68.9 MPa	68.0 MPa	94.2 MPa	93.0 MPa
Standard deviation	0.91 MPa	0.90 MPa	1.23 MPa	1.19 MPa	1.74 MPa	1.77 MPa
$f_{ck,cu}$	46.6 MPa	46.1 MPa	66.9 MPa	66.0 MPa	92.1 MPa	90.8 MPa
n	109	109	109	109	105	105

Table 4. Summary of standard deviations for compressive strength [8].

Specimen type for strength class	Standard deviation - MPa											
	Mean			Maximum			Minimum			Range		
	$f_{cu,100}$	$f_{cu,150}$	$f_{cyl,150}$	$f_{cu,100}$	$f_{cu,150}$	$f_{cyl,150}$	$f_{cu,100}$	$f_{cu,150}$	$f_{cyl,150}$	$f_{cu,100}$	$f_{cu,150}$	$f_{cyl,150}$
C32/40	0.91	0.90	0.94	1.98	1.82	2.99	0.17	0.16	0.21	1.81	1.66	2.78
C50/60	1.23	1.19	1.12	2.57	2.99	2.87	0.13	0.21	0.21	2.44	2.78	2.66
C65/80	1.74	1.77	1.86	4.45	5.20	3.84	0.29	0.29	0.54	4.16	4.91	3.30

4.1. Ratio of 100 mm cube/150 mm cube

It is generally expected that small size test samples tend to provide a higher measured compressive strength as reported by past researchers. However, the number of samples in these publications is limited. In this study, for each of the 3 strength levels, slightly over 100 batches were produced for which 3 specimens of 100 mm cube and 3 specimens of 150 mm cube were tested in each batch. The distribution of compressive strength at each strength level

is presented in Figure 2 where the overlapping of the distribution of the two sizes of cubes is clearly shown in all the 3 strength classes tested. In order to provide a better understanding of the test data, the distribution of the ratio ($f_{ci,100cu}/f_{ci,150cu}$) for each batch of the slightly over 100 batches in each strength class is presented in Figure 2(a) for C32/40, Figure 2(b) for C50/60 and Figure 2(c) for C65/80[8]. Figure 2 shows that although a wide range of the ratio is obtained for each strength class, from 0.95 to 1.07. Since around 100 batches (105 or 109) of each strength class were tested, the number of samples at a particular ratio represents approximately the percentage of test results that has been obtained.

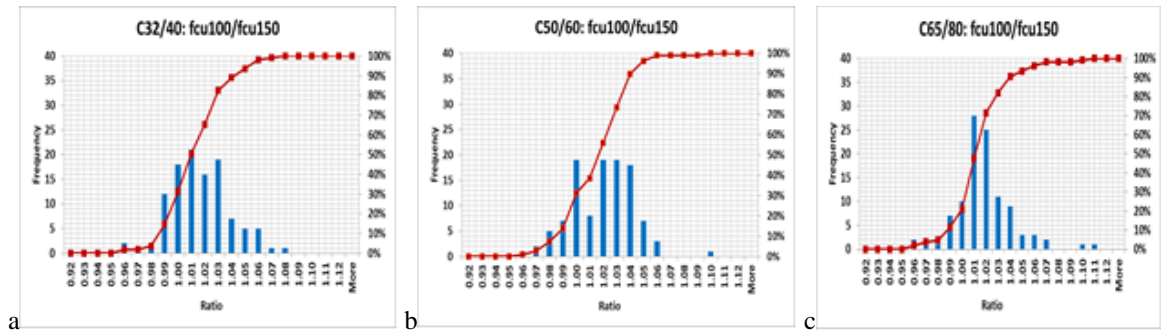


Fig. 2. Distribution of ration ($f_{ci,100cu}/f_{ci,150cu}$); (a) C32/40; (b) C50/60; (c) C65/80[9]

Firstly, the cumulative percentage of test results up to ratio of 1.0 in Figure 2(a) is 31%, for C32/40, in Figure 2(b) 31% for C50/60 and 21% in Figure 2(c) for C65/80. Hence, in 20% to 30% of cases of testing for cube compressive strength equal or higher strength for the 150mm cubes than corresponding 100mm cubes may occur. This implies that test results for 1 in 5 to 1 in 6 batches, the expectation that the small size cube specimens should show a higher strength may not happen. Cases of such contrary to generally expected test results have often been reported 100 mm cubes are used for plant production conformity testing and 150 mm cubes are taken on site as commonly specified. Particularly for small sample size adopted for assessment in site practice, the ratio can be either above or below unity as shown in the test data presented. The recommendation in clause 12.2 of BS 8500-2: [4] to consider the assessment of 100mm cubes with the same criteria for 150 mm cubes is supported by the large populations of over 100 batches of test data for each of the 3 strength classes.

4.2. Relationship between cylinder and cube compressive strength

The difference in measured compressive strength between 150mm diameter by 300mm length cylinder specimens and 150mm cubes is not due the difference in shape but the difference in aspect ratio (length/lateral dimension). From the experimental data, for C32/40, the mean ratio = 0.80 (51% of results), for C50/60, mean ratio = 0.83 (0.82 at 39%, 0.83 at 64%) and for C65/80, the mean ratio = 0.86 (50% at 0.85). There is a tendency for the ratio to increase with strength classes. In addition, both the minimum value and the maximum ratio also increased with strength class, 0.78 to 0.84 for C32/40, 0.79 to 0.87 for C50/60 and 0.81 to 0.95 for C65/80. For C65/80, the nominal difference of 15 MPa between 150mm cubes and 150mm diameter by 300mm length cylinders is indicated in Table 12 of EN 206: 2013[2]. The range of this difference obtained ranges from 5 MPa to 19 MPa, mean = 13 MPa (47%) and 64% of results up to 15 MPa. However, unlike experience with strength classes up to C55/67, there is much less published data on the relationship between cube compressive strength and cylinder compressive strength for C60/75 and above. Therefore, it is prudent to test of both types of specimens during the stage of initial tests in the development of high strength concrete to gain more data on this relationship, particularly with locally available materials for concrete production.

5. Sustainability in concrete strength assessment

Significant volume of concrete is used in the assessment of compressive strength of concrete for initial/trial mix testing, production conformity during production as well as samples taken on site at the time of delivery for conformity assessment in relation to the project specification. After testing the specimens have to be disposed as waste, at best sent to aggregate recycling plants. Hence, a reduction in the volume of concrete involved in such testing is a step forward towards a more sustainable concrete industry.

5.1. Specimen size

The adoption of the smaller size cube specimens has significant effect on the sustainable use of concrete, as the volume of each 150mm cube is more than sufficient to make 3 numbers of 100mm cubes. This smaller volume of concrete needed for routine testing in conformity assessment conserves materials resources for concrete and reduces the volume of waste for storage and later disposal after testing. In addition, curing capacity of existing facilities is able to cater for 3 times more test samples and time for testing and energy for loading are also reduced to achieve the same failure stress, besides easier handling of test specimens leading to better productivity and/or resource savings in the test laboratory. This green practice has been successfully implemented by Singapore HDB since 2007 and provides strong evidence for the local concrete industry to adopt this practice, a forward step towards a more sustainable concrete industry. It may be of interest to note that in the first edition of *Properties of Concrete*, Neville [10], on the section of “specimen size and aggregate size” the issue of recommended value for the ratio of the minimum dimension of the test specimen to the maximum aggregate size was stated as follows: “BS 1881: 1952 prescribes a test cube not smaller than 4 in. when $\frac{3}{4}$ in. aggregate is used, i.e. a ratio of 5-1/3, but 6 in. cubes may be used with $1\frac{1}{2}$ in. aggregate. A.S.T.M. Standard C192-57 limits the ratio of the diameter of the cylinder to the maximum aggregate size to 3, and the U.S. Bureau of Reclamation to 4. A value of between 3 and 4 is generally accepted as satisfactory”. Hence, it is convenient in practice for one size of cubes to cater for both 20mm and 40mm maximum aggregate size rather than due to technical requirement that 150mm cubes are commonly specified in evaluation of compressive strength.

5.2. Conformity testing

Conformity testing may be carried out using either cube or cylinder specimens. Specimen size of 100 mm cubes or 100 mm x 200 mm cylinders require less than 1/3 of the volume of concrete compared to 150 mm cubes or 150 mm x 300 mm cylinder. The saving in concrete volume needed plus the reduction in waste disposal of tested specimens is a significant green practice towards sustainability. The testing of cylinders requires end preparation by capping for normal strength levels and special non-bonded caps (up to 80 MPa – ASTM C1231-15[11] and grinding for higher strength classes. Besides the cost factor, time taken in end preparation is the other factor in routine production conformity testing. Cube specimens offer the more economic and time saving, even though cylinder strength is adopted in design equations. The confirmation of the suitability of the tabulated equivalency of cube to cylinder strength in EN 206: 2013[2] whenever a new designed concrete is developed during the initial testing stage is highly recommended, particularly for high strength concrete for which much less published data is available

5.3. Certification

In Singapore, all structural concrete must be supplied by RMC plants that have achieved certification by a Certification Body approved by the Singapore Accreditation Council since 2013. This is to replace the former practice of conducting 3 rounds of trial mixes for approval of a designed concrete for each project. In lieu of small population of data for each project, the total production statistics in each RMC plant for the same designed concrete are available for assessment by intending users. On site, only identity testing is carried out for specific volume of concrete or for specific type of structural element to assess if concrete supplied to site is verified to be in conformity with the in-plant production quality. Daneti et al[9] reported over the period of a year, when trial mixes were conducted for projects for the same concrete (C32/40) on dates for which the production data of the same time period show that the trial mix test

results were always higher than the mean strength of the production control data. Hence the production data is adequate for judging a certified designed concrete without the need for trial mixes.

6. Sustainability in concrete strength assessment

Only 3 strength classes up to C65/80 have been tested and until data from more concretes above C60/75 are available, the findings lead to the following observations:

- 100 mm cubes provide similar measured compressive strength as 150mm with only a very small difference which is of little practical significance in conformity assessment, particularly when small sample size of two or three specimens taken on site at delivery.
- Strength ratio in compression between 150 mm cubes and 150 mm diameter by 300 mm length cylinders tends to decrease with increasing compressive strength classes supporting the commonly accepted value of 1.25 up to C50/60 to 1.15 at C100/115 based on a constant difference of 15 MPa as provided in EN 206: 2013[2].
- Difference in compressive strength between 150mm cubes and 150 mm diameter by 300 mm length cylinders for C65/80 is about the same as the nominal value of 15 MPa in BS EN 206: 2013[2] for strength classes of C60/75 and above

Only 3 strength classes up to C65/80 have been tested and until data from more concretes above C60/75 are available, the findings lead to the following observations

References

- [1] J. Van der Geer, J.A.J. Hanraads, R.A. Lupton, The art of writing a scientific article, *J. Sci. Commun.* 163 (2000) 51–59.
- [2] W. Strunk Jr., E.B. White, *The Elements of Style*, third ed., Macmillan, New York, 1979.
- [3] G.R. Mettam, L.B. Adams, How to prepare an electronic version of your article, in: B.S. Jones, R.Z. Smith (Eds.), *Introduction to the Electronic Age*, E-Publishing Inc., New York, 1999, pp. 281–304.



Sustainable Civil Engineering Structures and Construction Materials, SCESCM 2016

Can self-healing mechanism helps concrete structures sustainable?

Senot Sangadji^{a,*}

^a*Civil Engineering Department, Faculty of Engineering, Universitas Sebelas Maret, Surakarta, Indonesia*

Abstract

Concrete is quasi-brittle material susceptible to cracking under tensile or shear stress. In case of continuous network of crack is formed, concrete structure becomes permeable and embedded rebar may be exposed to ambient air, hence escalating the risk of material degradation. On the other side, concrete infrastructures industry is facing pressing sustainability issues. Concrete production consumes high amount of energy and produces large amount of CO₂ emission. The scale of the problem is even greater in the event of many concrete structure premature failure which consumes more raw material for rebuilding. Designing new infrastructures for longer service life by improving concrete (materials and structure) durability is one solution to overcome the dilemma. One promising concept is by incorporating self-healing mechanism found in nature into cement-based materials / concrete structural element.

This paper presents inherent autogeneous healing which occur due to its heterogeneous nature of concrete. This contribution also demonstrates some laboratory proven bio-inspired techniques that makes concrete materials and/or structural element self-healing autonomously. It involved diverse methods across several categories. The methods designed have demonstrated to have a good prospect in making concrete structural element self-healing. Finally the paper concludes with the claim that If unavoidable cracks due to inherent brittleness in concrete could be self- sealed/healed/repared, concrete structure will certainly serve longer service life, making it more durable, therefore sustainable.

© 2017 The Authors. Published by Elsevier Ltd.

Peer-review under responsibility of the organizing committee of SCESCM 2016.

Keywords: Self-healing concrete, bacteria-based healing agent, Porous Network Concrete, Bio-inspired engineering.

* Corresponding author. Tel.: +62-82137659700

E-mail address: s.sangadji@ft.uns.ac.id

1. Introduction; What are the issues at stake[1]

Throughout history of human civilization, concrete has been gaining a remarkable success. Several layer of calcium carbonate had been utilized as mortar floor as old as nine millennia ago when archaeologist discovered it in Yiftah El in 1985. Concrete had been used as one of primary construction materials in the Roman era when they built Pantheon, unreinforced dome preserved under compression stress, which survives two thousand years up to now. A long history of cementitious material culminates in the modern concrete which demonstrate its noticeable performance in reinforced and prestressed concrete as well as development of ultra-high strength concrete.

Apart from its rich historical narratives, the success of concrete might also be justified by the claim that concrete is currently the most used man-made material. Data support the claim that the amount of concrete used for construction worldwide exceeds 12 billion tons annually, approximately 2 metric tons per person per year. Concrete - the second largest volume material utilized by human after water - is virtually irreplaceable for innumerable large infrastructure developments from the point of view of economy and ecology. It is hard to imagine the progress of modern civilization without concrete serving as major engineering material.

1.1. Pressing sustainability issue

Infrastructures is vital backbone for socio-economic activity and its development encourages productivity and growth. Many countries, primarily developing nations, invest in infrastructure not only to expand their capacity but to influence income distribution. On the other side, the construction, maintenance, refurbishment and demolition of these infrastructure requires huge amount of material cycle and intense energy demand leading into high ecological impact.

Concrete as major infrastructure material embodies energy and carbon emission approximately of about 0.95 MJ/kg and 0.35 kg C/kg, respectively. This value of energy input required from raw material extraction production process, and distribution to its place ready for use, is much lower than many other common construction materials. For instance steel embodied energy and CO₂ is 56.7 MJ/kg and 6.15 kg C/kg, while timber (exclude sequestration) has 8.5 MJ/kg and 0.46 kg C/kg, respectively. However, due to high rate of consumption abovementioned, cement and concrete still demonstrates total high energy demand and carbon emissions. These facts imply that efficient use of cement, concretes, and mortars will certainly save the total energy and reducing environmental impact in the life time of the infrastructure.

1.2. Inevitable cracks in concrete; challenge to durability, functionality, and cost of repair

Concrete encounters another challenge from that concrete is quasi-brittle material with properties weak in tension. This intrinsic brittleness is the reason steel reinforcement bar is installed in the tension cross section to carry tensile stress. Concrete cracks is important in this case since it trigger the activation of the steel bar. Within the prescribed crack limit, the crack opening as such may not fail the structure or hamper the overall safety, although it may expose the reinforcement bar to corrosive action from atmosphere.

Apart from macrocracks, microcracks are practically inevitable to the normal concrete. In the event when microcracks form continuous network, concrete will be permeable and the reinforcement bar may be open to ambient air. In this case continuous crack is used as easy mean for ingress of aggressive substances to enter and damage the concrete and corrode the rebar therefore concrete degrades and becomes more vulnerable.

Technically speaking, concrete can succeed a 50 years – or even longer – of life time even though it encounters several degradation processes, e.g. chemical ingress, freeze-thaw cycle, carbonation, etc. However, the presence of cracks triggers more serious problems and limits the concrete capacity to be durable

In many other cases cracks are not desirable. Cracks may threaten the tightness of the retaining structures, e.g. liquid containing structures tank wall, aqueducts, underground spaces, tunnels, etc., which undergo tensile forces. In these cases cracks may facilitate the flow of fluid – liquid or gas – into and out of the structures which considerably alters its serviceability, leads to unhealthy environments within a structure, and diminishes its functionality. In case of waste, highly toxic materials and radioactive disposal container, leakage through concrete is catastrophic and unacceptable.

The unexpected premature deterioration and fracture of concrete structures not only limit its service life, but also leads into another issue concerning huge inspection, maintenance and repair cost. Tougher issue emerges when the cracks are invisible and or inaccessible, such in the underground waste container structures which may impractical, if not impossible, to repair.

To get a deeper view of this economic pressure, consider few examples. The total amount of money for repairing and upgrading 10% of the US bridges which are considered functionally obsolete and structurally deficient is estimated at \$ 140 billion. In the UK, 45% of its construction and building industry activity is related to the repair and maintenance. In the Netherlands, one third of the yearly budget large civil engineering works must be spent on monitoring, maintenance, repair and upgrading. It is also estimated that the indirect cost and loss of productivity of traffic congestion caused by bridge (and tunnel) maintenance interruption is ten times higher than the direct maintenance cost, which may reach \$ 63 billion per annum in the US [2].

1.3. Tackling the challenge: durable concrete

From a materials perspective, Flatt et al [3], identify several solutions alternatives for tomorrow's concrete in overcoming the pressing problems of concrete sustainability:

1. Partial cement (clinker) replacement by supplementary cementitious materials
2. Development of alternative binders
3. Broader use of concrete mix designs that limit cement content
4. Recycling of demolished concrete in new concretes
5. Enhancement of durability (designing new infrastructures for longer service life)
6. Rehabilitation of existing infrastructures (extending the service life of existing infrastructures)

As durable concrete increase infrastructure sustainability and in turn will positively affect biosphere stability, this contribution focuses on emerging technology of making durable concrete. One promising concept is incorporating self-healing mechanism found in nature into cement-based materials.

This paper will survey several technology currently developed for the purpose of providing overview of mechanisms involved and category of mechanisms to help reader navigate in the vast panorama of cementitious based self-healing. This work also present some necessary condition for healing mechanism to happen, the potential and benefit of this technology. This work will be concluded by attempt to answer the question 'Can Self-Healing Mechanism Helps Concrete Structures Sustainable?', as well as providing outlook; a kind of probable scenario of self-healing cementitious materials.

2. Self-healing concrete; strategy, healing mechanisms and condition necessary

2.1. Self-healing materials; synthetic approach to healing in nature

Self-healing materials certainly take inspiration from nature. Healing in biological hard of soft tissue triggered by injury follows in general three overlapping steps in time; inflammatory response, cell proliferation, and tissue remodeling. Self-healing materials, mimicking its biological counterparts, are designed to possess the ability and perform self-repair and self-recovery of the materials pre-assigned properties and functionalities using built-in resources in the material. It follows deliberately accelerated artificial route in equally similar three steps after damage formed in material: actuation (triggering actions), transport of healing agents into fracture zone, and chemical repair. Damage in the material therefore is indeed necessary to trigger the healing process.

Similar approach is seen in the development of self-healing concrete. Concrete crack trigger the healing mechanism, either intrinsically or autonomously, then crack is healed at right on time quicker than its biological counterpart.

Explosion in number of literature of studies and development of self-healing concrete have been seen recently. Van Tittelboom [4] provides exhaustive literature review of concrete autogenic and autonomic healing of in her PhD thesis.

In its systematic in-depth analysis can be found on the different type of concrete healing mechanism, efficiency of various healing agents, suitable encapsulation techniques, triggering mechanism for autonomic action, and evaluation of recovered properties. State of the Art Report of RILEM TC-221 SHC entitled Self-Healing Phenomena in Cement-based Materials published in 2013 also provides extensive overview of the most recent progress [5].

In guiding advancement of this emerging field attempts to set-up general framework and definition were carried out by technical committee TC-075B from Japan Concrete Institute (JCI), RILEM committee TC-221 SHC, shown in figure 1.a. and Mihashi and Nishiwaki as can be seen in figure 1.b [6].

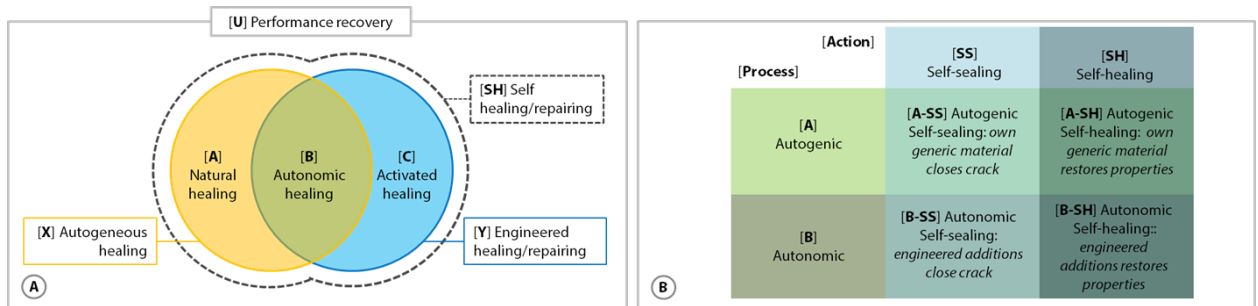


Fig. 1. [A] Self-healing classification proposed by TC-075B JCI depicted in Venn diagram. [B] Interpretation by Mihashi and Nishiwaki to the definition of self-healing materials proposed by RILEM TC-221 SHC.

Recently, H. Huang et al., [7] published a review of self-healing of cracks in cementitious materials. According to healing mechanisms implemented, Huang and co-worker suggest four categories, as follows: 1) autogenous self-healing, 2) self-healing based on mineral admixtures, 3) self-healing based on bacteria, and 4) self-healing based on adhesive agents.

2.2. Strategy 1: intrinsic autogeneous healing

It is well known that cement-based materials have inherent autogenic self-healing capacity [8]. According to Hearn, French Academy of Science had observed autogeneous healing of cracks in fractured culverts, pipes, and water retaining concrete structures in 1836, and Hyde had already studied the phenomenon at the end of the nineteenth century [9]. Van Breugel reports that Glanville in 1926 conducted research about these phenomena and at that time a distinction between self-sealing and self-healing was discussed which was then followed by Soroker et al in 1926 and research of cracks in bridges by Brandeis in 1937 [10].

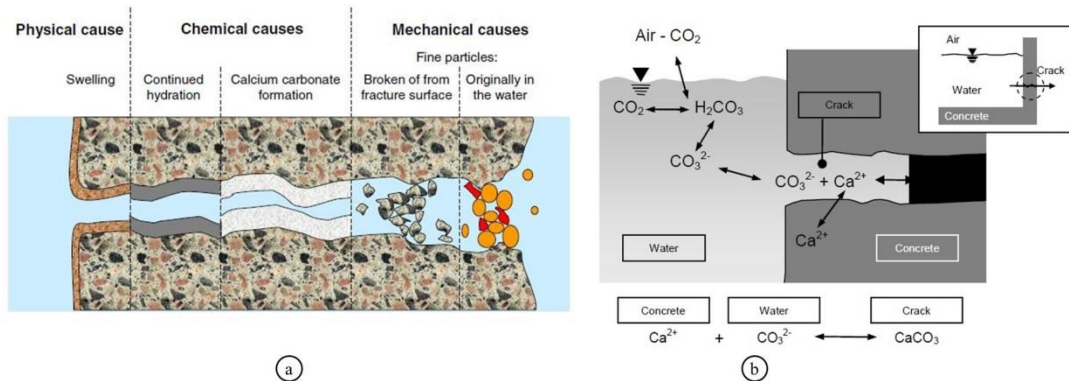


Fig. 2. (a). Classification of most possible causes of autogenic self-healing mechanism of concrete. The scheme appears in the thesis (pp. 4) of Nynke ter Heide [11]. The figure used in this work is reprinted from RILEM State-of-the-art Reports TC 221. (b) Autogenous self-healing involves intricate relation of media interfaces and ions in precipitating calcium carbonate from Mihashi and Nishiwaki [6].

A systematic study of concrete autogenic self-healing was carried out by Hearn [9]. It turns out that crack opening in concrete diminishes in time by means of several processes with a great number of literature demonstrating the evidence [12]. Four mechanisms show important contribution by which according to RILEM TC-221 SHC this recovery processes are classified into three causes [5] as depicted in figure 2.b.

- (1) Swelling of the cement matrix in proximity of crack tip due to absorbed water into hydrated cement paste.
- (2) Continuing hydration of unreacted cement particles due to lack of water during hydration process which in turn occupy crack void. This is the second important contribution to healing mechanism which is more pronounce in young concrete.
- (3) Dissolution of calcium ions (Ca^{2+}) which reacts with carbonate ions (CO_3^{2-}) from ambient environments and forms calcium carbonate (CaCO_3) which then precipitates at the crack faces. The mechanism, studied in great details by Edvardsen [13], is believed to be the most important contribution to the autogeneous healing [14]. The complex interaction of concrete matrix, interface and dissolved ions is depicted in figure 2.b.
- (4) Physical clogging of small particles crumbled from crack surface or carried by ambient water.

The efficiency of concrete autogeneous self-healing capacity is influenced by environmental action (e.g. the presence of water), temperature [12], mix composition [4] and is deemed higher with higher cement content promoting continued hydration. The later may be thought as in contrast with the demand of low cement content concrete to satisfy sustainability criteria.

On the other hand, autogeneous self-healing might be the reason for decreasing chloride ingress through the concrete cover and preventing corrosion of rebar. Klaas van Breugel suggests this innate ‘immune system’ makes concrete a material with high resistance. This beneficial feature may in turn promote longer concrete service life, though concrete structure was not designed taking into account its inherent autogeneous healing capacity [10]. The reason is because the probability of occurrence of the process and necessary conditions are not fully understood therefore possess low reliability to be taken into account in the design explicitly. However a limited crack width is allowed in the design of watertight container with respect to pressure and crack stability. Van Breugel asserts, “This in fact demonstrates that the self-healing capacity of ordinary concretes is considered a by-product of the material rather than a feature that could be manipulated by a sophisticated design of the mixture” [10].

Studies show provisions to elevate the success rate of autogenous self-healing are crack width, water availability, and crack closure. Smaller cracks have a better chance to heal. The presence of ambient water helps un-hydrated cement particles to form hydration product and seal the cracks. Re-closing the crack opening promotes higher rate of healing mechanism afore-mentioned.

Autogeneous healing in concrete is restricted to small crack width (up to 200 μm), presence of water and crack closure by means of compression [4, 15, 16]. Many research and developments have been dedicated to improve concrete inherent healing capacity. Several strategies and its combinations involve:

- (1) restricting crack width by embedding fibres in the concrete which takes form as: fibre-reinforced concrete (FRC) or strain hardening cementitious composites (SHCC) [17-19]. One successful example of SHCC is ECC (Engineered Cementitious Composites) developed by Li et al. which shows high ductility while ensuring that crack widths remain typically around 50 μm ;
- (2) closing crack opening by incorporating shape memory alloys [20-22] or shrinkable polymer tendons [23, 24];
- (3) providing additional water by means of super absorbent polymers (SAP) [25, 26] or water capsules; and
- (4) adding agents e.g. sodium monofluorophosphate [27, 28], microbes [29-32], to promote crystallization, precipitation of calcium carbonate and/or hydration.

This autogeneous healing, therefore, remained unreliable. This may be attributed to the fact that concrete is highly variable with respect to the composition of its ingredients. Certain compositions may promote healing while the other mixtures proportion might raise questions upon its healing capacity. As the presence of water is the prerequisite for certain autogenous healing mechanism to happen, for instance continued hydration, its highly improbable the healing will occurs in the element with limited contact to the ambient moisture. It is also hard to determine and to quantify the

sort of healing mechanism taking place in the structure over a certain period. Moreover, although there is no agreement upon certain values, autogeneous healing might occur only to very limited crack width.

Additionally, in quasi-brittle concrete, cracks are hard to control. Cracks tend to continue to increase once the critical value/characteristic length/crack thickness is reached, even in the decrease of tensile stress. Even worse is when the tensile crack is actively opening up and propagating due to constant (local) tensile stress, autogenous healing might be inadequate.

2.3. Strategy 2: engineered / autonomous healing

Overcoming this dubious healing capacity and having better ‘control’ on self-healing mechanisms, researchers purposefully develop ‘engineered healing’. Several developed methods are based on embedded capsule or embedded vessel (tube) by which healing agent flows out upon shell breakage by the crack. Heat evolution devices might be applied to promote accelerated reaction kinetics of healing agents [33].

2.3.1. Healing by means of capsule and vascular techniques

Dispersing capsules containing healing agents was proposed by Dry [34, 35] in the early nineties of the 20th century and successfully implemented in self-healing polymers by White et al. [36]. When the crack hits the capsule, its shell ruptures and healing agent is released and hardened upon contact with atmosphere or with polymeric crosslinking catalyst.

For implementation in cement based materials several examples may be presented. Yang et al. [37] successfully developed microcapsules with oil core and silica gel shell. Inside the shell, Yang and co-workers used commercially available methyl methacrylate (MMA) monomer as the healing agent and tri-ethyl-borane as the catalyst. Upon releasing the agent, polymerization of methyl methacrylate initiated by the catalyst may be achieved at room temperature and seal micro cracks decreasing permeability by approximately 66%. Van Tittelboom used brittle borosilicate glass and ceramic cylindrical capsules with internal diameter about 1.71 to 3.00 mm containing polyurethane with accelerator, epoxy resins, poly-acrylates, polyurethane and MMA. In case of using two compound agent, the capsules were connected two by two and placed manually in the concrete specimens.

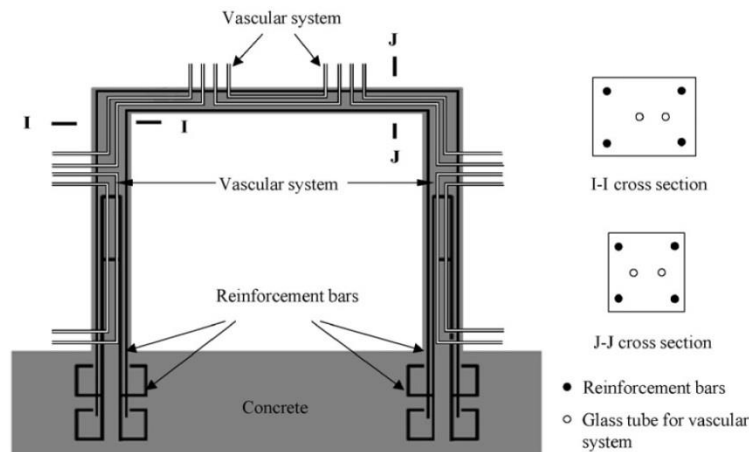


Fig. 3. Reinforced concrete frame with a vascular system for self-healing tested by Dry [34], reprinted from Huang et.al [7].

Joseph [38] used brittle borosilicate glass tubes containing cyanoacrylate (CA) cured in air in which one end of the tube is bent up and open to the air to supply the agent. This allowing continuous supply of the glue. As see in figure 3, Dry proposed a simple vascular system to supply healing agents to cracks zone by embedding some pipes in concrete and observed self-healing capacity rather high.

Nishiwaki et al. [33] developed a system where they embed organic film pipe containing healing agent and heating device made of ceramic fibre and conductive matrix. Upon crack formation the conductivity is reduced and the resistivity close to the crack increased therefore selectively induced heating and melt the thermoplastic film and released the healing agent.

Despite the promising results, some issues arise regarding the most efficient healing process and appropriate healing agent used in the concrete. The issues are:

- (1) Number and aspect ratio of capsules sufficient enough to ensure the random crack formation hit the capsules. In spherical capsules, there is tendency the crack surround the capsule instead of hit and break the capsule shell, by which scientists proposed elongated capsule or tube.
- (2) Vulnerability of the capsules during mixing. Brittle hollow capsule and tube can be damaged due to excess energy during mixing.
- (3) Placing and curing of concrete. Dispersing long brittle tube in the concrete is laborious.

To increase the survivability of the transport medium, the author designed Porous Network Concrete (PNC) [1, 39]. PNC is a hybrid system in which high permeability porous concrete is embedded in the interior or exterior of normal dense concrete. The porous network core constitutes alternate means for [1] channeling temporary or permanent materials to form a dense layer in the later stage and [2] distributing healing agent from the point of injection to cracks in the concrete main body, as depicted in figure 4. The autonomous healing mechanism in the PNC is designed by incorporating the feedback mechanism; once a certain crack width is sensed, an action to heal takes place. When a concrete structure receives loads and builds up internal stress, it deflects, cracks and deforms. Once the crack mouth opening reaches a certain prescribed value the healing agent is injected automatically. The proposed working principle is verified by mechanical and leakage (permeability, infiltration) testing.

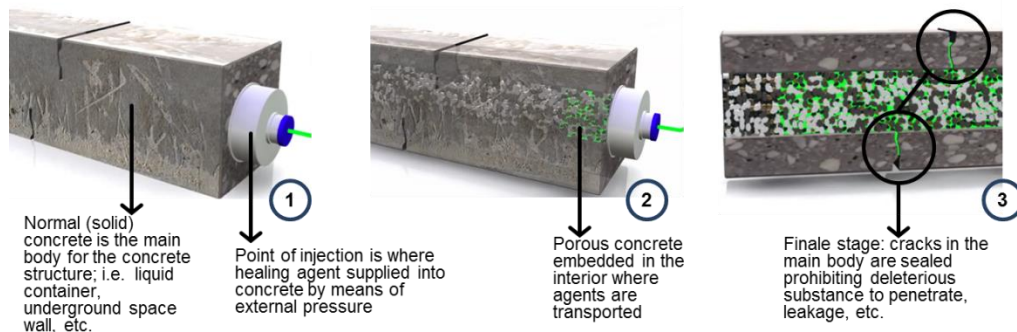


Fig. 4. The conceptual working principle of healing agent transport in the Porous Network Concrete.

2.3.2. Microbial mediated healing

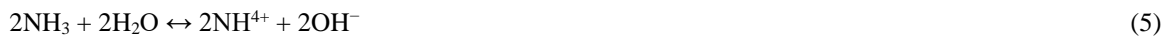
Several scientists have proposed and developed ideas around enhancing concrete durability by introducing bacteria to promote self-healing to seal crack. Microbiologically induced calcium carbonate precipitation, (MICP) form three different polymorphs: calcite, aragonite, and vaterite, via different pathways – e.g. urea hydrolysis, metabolic conversion of salt and carbon, denitrification.

2.3.3. Urea hydrolysis

In number of published studies, scientists investigated the potentials of bacteria to facilitate calcium carbonate precipitation by means of degrading urea to ammonia and carbon dioxide. Bang et al. [40] in 2000 published a study where *Bacillus pasteurii* immobilised in the Polyurethane was employed to precipitate calcite. Ramachandran et al.

[41] also used *B. pasteurii* and filled it in simulated cracks in mortar, meanwhile Bachmeier et al. [42] investigated *Escheria coli* and found the bacteria produced significant level of precipitation although less than *B. pasteurii*.

Researchers from Ghent University, Belgium, developed the system in which precipitation of calcite is based on major mechanism of enzymatic hydrolysis of urea. The bacteria used – *Bacillus sphaericus* – produce enzyme urease (urea amidohydrolase, E.C. 3.5.1.5) which catalyses the hydrolysis of urea into ammonium (NH_4^+) and carbonate ions CO_3^{2-} [31, 32, 43][115, 116, 231]. Van Tittelboom [4] elaborates the chemical reaction as follows; urea is internally hydrolysed by the bacteria producing carbamate acid and ammonia in equation 5.1. Carbamate is then hydrolysed into ammonia and carbonic acid at equation 5.2 which in turn develops new dissolved inorganic carbon balance (5.5) and increases pH of the concrete matrix.



These carbonate anions, $[\text{CO}_3^{2-}]$, in turn react with calcium cations, $[\text{Ca}^{2+}]$, present in the concrete matrix which are attracted into negatively charged bacteria cell wall in equation (7) and precipitate Ca-carbonates as expressed in equation (8) that fill the fissure in concrete structure [41].



Decreasing water permeability and crack sealing was observed in the specimen with *B. sphaericus* immobilized in silica gel or polyurethane by means of ultrasonic transmission measurement. Visual examination confirmed the sealing takes place in the crack surface [31, 32]. Despite the ease to control, the chemical reaction mechanism, however, may lead into problematic side effect for the environment due to two ammonium ions for each carbonate ion produced [4, 29]. Additionally, as Dhimi et al. [44] suggested, risks of concrete salt damage may arise from the production of ammonium molecules in hydrolysis of urea or where this ammonia is converted into nitric acid by nitrifying bacteria.

2.3.4. Metabolic conversion of nutrient

A different approach has been carried out by Jonkers and Schlangen [45], Jonkers et al. [29, 46, 47], and Wiktor and Jonkers [30] where they employed a different route to obtain bacteria mediated calcite precipitation. The bacteria metabolically convert nutrients-salt and change the micro chemical environment in their vicinity to be able to precipitate calcite. The requirements for the bacteria are that they should be alkaline resistant and oxygen tolerant. The reason is that they must survive in the highly alkaline concrete (fresh) matrix which is typically characterized by pH values between 11 and 13. They must also be viable for a prolonged period started from the mixing time. They should therefore also be able to form spores. The bacteria can be receptive to oxygen diffused in the concrete matrix. On the other hand the presence of oxygen is unnecessary if nitrate reduction is employed.

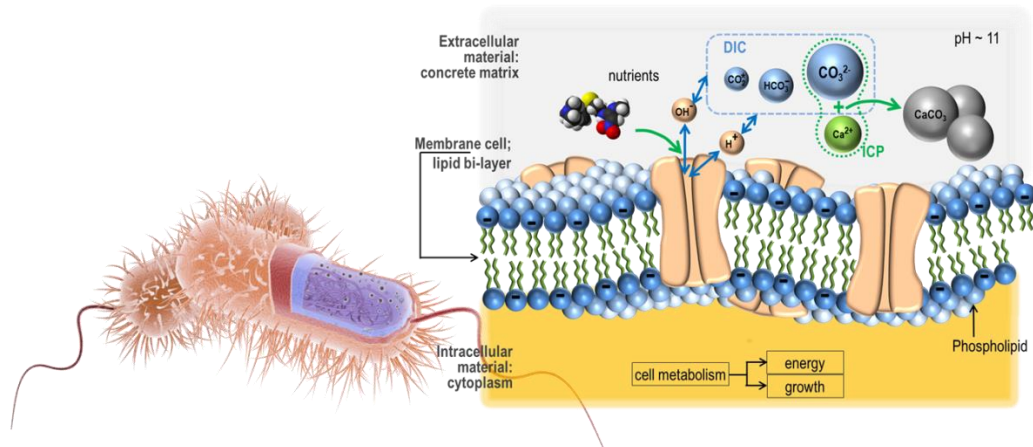


Fig. 5. Working mechanism of bio-based concrete healing developed at Microlab [1].

Figure 5 shows the working principle of bio-based concrete healing developed at Microlab, TU Delft. During the time bacteria is metabolizing nutrients and producing carbon dioxide, they change extracellular microenvironments leading to the bio-mineralization of Ca-Carbonate. The system working principles involves reaction of calcium cations, $[Ca^{2+}]$, present in the concrete which are then attracted into negatively charged bacteria cell wall and reacted with carbonate anions, $[CO_3^{2-}]$, in supersaturated state, as in eq. 7 and 8.

While the presence of bacteria may be thought as the nucleation point for bio-mineralization of calcium carbonates ($CaCO_3$), several factors influence the emergence of bacterially mediated $CaCO_3$ precipitation. These factors are:

- (1) the pH of the solution,
- (2) the presence of calcium ion $[Ca^{2+}]$, and
- (3) the carbonate equilibrium in the solution which is determined by concentration of dissolved inorganic carbon, (DIC) in the solution – which includes chemical species of carbon dioxide $[CO_2]$, carbonic acid $[H_2CO_3]$, bicarbonate anion $[HCO_3^-]$, and carbonate anion $[CO_3^{2-}]$, see DIC pool in the figure 3.

The reaction may be expressed as straightforward equilibrium suggested by Jonkers et al [47]. Bacteria metabolically convert 1 mole of calcium lactate, $Ca(C_3H_5O_3)_2$, into 1 mole of Ca-carbonate as in equation 9.



Jonkers et al. have developed and tested the concepts in which bacteria start to be activated in contact with ambient water present in cracked concrete, consume nutrients, and precipitate calcium carbonate which in turn fill the voids and seal the cracks. Wiktor and Jonkers encapsulated bacteria strain and nutrients into porous expanded clay to ensure viability and functionality of the bacteria after the concrete mixing.

3. Potentials and benefit of self-healing in concrete service life

Conceptually, the approach to make concrete structures – and structural (engineering) material in general – self-healing can be justified by studying both design strategy and philosophy. The prevailing concepts of making structures better is by making them stronger and stiffer. This can be achieved by making stronger and stiffer (structural/engineering) material or combination of materials. Within this philosophy, designers focus on preventing damage by increasing the strength of the material and therefore the load bearing capacity of the overall structures. This may adjourn the event when the first fracture develops. This philosophy is termed as Damage Prevention paradigm. Development of high and ultra-high strength material is the result of this productive and useful design philosophy.

As the damage formation is unavoidable during structures service life, damage monitoring is needed. Sooner or later any damage discovered requires repair and expenditure. Arguably, a certain level of damage will not create serious problem as long as it is neutralized by autonomous process of clearing of ‘healing’ the damage [48]. Even this certain limit of damage may be acceptable as a trigger for the inherent healing or repairing mechanism to start [49]. This pro-active Damage Management paradigm philosophy is the basis of emerging self-healing materials technology.

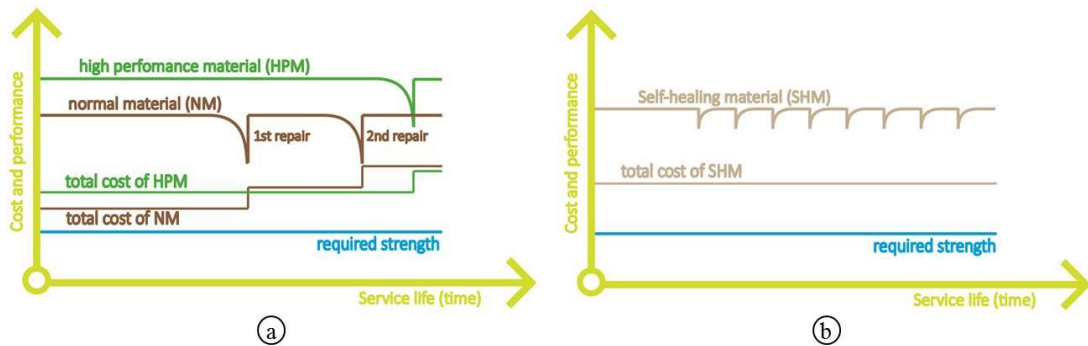


Fig. 6. a. Falling head permeability test, b. strain controlled three-point bending

Figure 6 shows conceptual diagram of performance of infrastructure and its cost over time. Once cracks formed, a degradation process starts until (expensive) repair raises the structure to its initial performance level. Applying damage prevention principle, longer service life of infrastructure can be achieved by using higher strength material, by which longer maintenance free period is achieved. As the initial investment is higher, however the total cost may be lower compare to ‘normal’ material which requires several repair actions for the same period of service. On the other side, by applying self-healing materials, damage is allowed and even triggers the autogeneous or autonomous self-healing mechanism. As there will be ‘no’ or very limited repair cost during service life the total cost may be competitive compared to normal and high strength material application.

4. Outlook; probable scenario of self-healing cementitious materials

Overview of the cementitious based self-healing has been presented in this paper involving autogenic and engineered mechanism. Autogeneous healing is inherent feature of the concrete which makes concrete show some kind of auto immunity from the aggressive environment. Because it is limited, this intrinsic mechanism required certain conditions to be effective. Some research tried to enhanced this innate character by means of controlling crack width, provide internal curing agent, and mineral admixture.

In order to control healing mechanism better engineered mechanisms have been devised. It involved several techniques for triggering, supplying healing agents, and crack sealing. The techniques utilized adhesive (polymeric) agents and microbes. The techniques developed have been proven effective to some certain extent under appropriate condition according to the literature.

Most of the self-healing techniques by now have been developed and studied in laboratory. Up to now there is no one-fit-for-all healing mechanisms. That is why, for practical applications self-healing techniques should be designed and implemented based on the concrete structures condition of service, taking into account necessary condition for the mechanisms to work. For instance water is necessary condition for autogeneous healing to work while on the contrary water might disrupt the mechanism based on polymerization of healing agents. The presence of carbonate and calcium ions is essential for bacteria induced calcite precipitation for crack sealing. These situation might even be more complicated with the requirement to have cost effective healing and continuous repeatable healing under complex load during concrete service life.

Can Self-Healing Mechanism Helps Concrete Structures Sustainable? It is well understood by many of the self-healing researcher that the healing mechanisms studied, designed and developed in their lab so far are adequate to some extent only and far from satisfactory. Even though how far healing mechanism takes place in the concrete

structures is still questionable, however, it can be contemplated if inevitable cracks due to inherent brittleness in concrete could be self-sealed/healed/repaired, concrete structure will certainly serve longer service life, making it more durable, therefore sustainable.

Acknowledgements

The author would like to thank the promotor, supervisor, mentors and many colleagues at Microlab, Section of Materials and Environment, TU Delft where the author studied self-healing materials and developed concrete healing mechanism. The author gratefully thank to the Government of the Republic of Indonesia for its financial support in the form of scholarship. The recent continuation of the study and investigation is funded by Universitas Sebelas Maret, Surakarta, Indonesia through Hibah Doktor Baru, 2016.

References

- [1] S. Sangadji, "Porous Network Concrete: a bio-inspired building component to make concrete structures self healing," Doctoral, Civil Engineering and Geosciences, Delft University of Technology, Delft, 2015.
- [2] M. Yunovich and N. G. Thompson. (2003, January 1, 2003) Corrosion of Highway Bridges: Economic Impact and Control Methodologies. *Concrete International*. Available: http://www.concreteinternational.com/pages/archives_abstracts_search_results.asp
- [3] R. J. Flatt, N. Roussel, and C. R. Cheeseman, "Concrete: An eco material that needs to be improved," *Journal of the European Ceramic Society*, vol. 32, pp. 2787-2798, 2012.
- [4] K. Van Tittelboom, "Self-Healing Concrete through Incorporation of Encapsulated Bacteria or Polymer-Based Healing Agents," Doctor, Faculty of Engineering and Architecture, University of Gent, Gent, Belgium, 2012.
- [5] K. V. T. Mario de Rooij, Nele De Belie, Erik Schlangen. (2013). *Self-Healing Phenomena in Cement-Based Materials*. 11. Available: <http://link.springer.com/book/10.1007/978-94-007-6624-2/page/1>
- [6] H. Mihashi and T. Nishiwaki, "Development of Engineered Self-Healing and Self-Repairing Concrete-State-of-the-Art Report " *Journal of Advanced Concrete Technology*, vol. 10, pp. pp.170-184, 2012.
- [7] H. Huang, G. Ye, C. Qian, and E. Schlangen, "Self-healing in cementitious materials: Materials, methods and service conditions," *Materials & Design*, vol. 92, pp. 499-511, 2/15/ 2016.
- [8] A. Neville, "Autogenous Healing—A Concrete Miracle?," *Concrete International*, vol. 24, pp. 76-82, November 1, 2002 2002.
- [9] N. Hearn, "Self-sealing, autogenous healing and continued hydration: What is the difference?," *Materials and Structures*, vol. 31, pp. 563-567, 1998/10/01 1998.
- [10] K. van Breugel, "Self-Healing Materials Concepts as Solution for Aging Infrastructure," in *37th Conference on Our World in Concrete and Structures*, Singapore, 2012.
- [11] N. ter Heide, "Crack healing in hydrating concrete," MSc, Faculty of Civil Engineering and Geosciences, Microlab, Delft University of Technology, Delft, 2005.
- [12] H.-W. Reinhardt and M. Jooss, "Permeability and self-healing of cracked concrete as a function of temperature and crack width," *Cement and Concrete Research*, vol. 33, pp. 981-985, 2003.
- [13] C. Edvardsen, "Water Permeability and Autogenous Healing of Cracks in Concrete," *ACI Materials Journal*, vol. 96, pp. 448-454, 7/1/1999 1999.
- [14] N. Hearn and C. T. Morley, "Self-sealing property of concrete—Experimental evidence," *Materials and Structures*, vol. 30, pp. 404-411, 1997/08/01 1997.
- [15] N. Ter Heide, E. Schlangen, and K. van Breugel, "Experimental study of crack healing of early age cracks," in *Knud Hojgaard conference on Advanced Cement-based Materials*, Lyngby, Denmark, 2005.
- [16] E. Schlangen, N. t. Heide, and K. v. Breugel, "Crack healing of early age cracks in concrete," in *Measuring, Monitoring and Modeling Concrete Properties*, M. Konsta-Gdoutos, Ed., ed: Springer Netherlands, 2006, pp. 273-284.
- [17] V. C. Li, Y. M. Lim, and Y.-W. Chan, "Feasibility study of a passive smart self-healing cementitious composite," *Composites Part B: Engineering*, vol. 29, pp. 819-827, 1998.
- [18] S. Qian, J. Zhou, M. R. de Rooij, E. Schlangen, G. Ye, and K. van Breugel, "Self-healing behavior of strain hardening cementitious composites incorporating local waste materials," *Cement and Concrete Composites*, vol. 31, pp. 613-621, 2009.
- [19] D. Homma, H. Mihashi, and T. Nishiwaki, "Self-Healing Capability of Fibre Reinforced Cementitious Composites," *Journal of Advanced Concrete Technology*, vol. 7, pp. 217-228, 2009.
- [20] Y. Sakai, Y. Kitagawa, T. Fukuta, and M. Iiba, "Experimental study on enhancement of self-restoration of concrete beams using SMA wire," 2003, pp. 178-186.
- [21] K. Yachuan and O. Jinping, "Self-repairing performance of concrete beams strengthened using superelastic SMA wires in combination with adhesives released from hollow fibers," *Smart Materials and Structures*, vol. 17, p. 025020, 2008.
- [22] Y.-c. Kuang and J.-p. Ou, "Passive smart self-repairing concrete beams by using shape memory alloy wires and fibers containing adhesives," *Journal of Central South University of Technology*, vol. 15, pp. 411-417, 2008/06/01 2008.

- [23] B. Isaacs, R. Lark, T. Jefferson, R. Davies, and S. Dunn, "Crack healing of cementitious materials using shrinkable polymer tendons," *Structural Concrete*, vol. 14, pp. 138-147, 2013.
- [24] A. Jefferson, C. Joseph, R. Lark, B. Isaacs, S. Dunn, and B. Weager, "A new system for crack closure of cementitious materials using shrinkable polymers," *Cement and Concrete Research*, vol. 40, pp. 795-801, 2010.
- [25] H. X. D. Lee, H. S. Wong, and N. R. Buenfeld, "Potential of superabsorbent polymer for self-sealing cracks in concrete," *Advances in Applied Ceramics*, vol. 109, pp. 296-302, 2010.
- [26] D. Snoeck, K. V. Tittelboom, S. Steuperaert, P. Dubruel, and N. D. Belie, "Self-healing cementitious materials by the combination of microfibrils and superabsorbent polymers," *Journal of Intelligent Material Systems and Structures*, March 15, 2012 2012.
- [27] K. Sisomphon, O. Çopuroğlu, and A. L. A. Fraaij, "Durability of blast-furnace slag mortars subjected to sodium monofluorophosphate application," *Construction and Building Materials*, vol. 25, pp. 823-828, 2011.
- [28] K. Sisomphon, O. Copuroglu, and E. A. B. Koenders, "Self-healing of surface cracks in mortars with expansive additive and crystalline additive," *Cement and Concrete Composites*, vol. 34, pp. 566-574, 2012.
- [29] H. M. Jonkers, "Self Healing Concrete: A Biological Approach," in *Self Healing Materials*. vol. 100, S. Zwaag, Ed., ed: Springer Netherlands, 2008, pp. 195-204.
- [30] V. Wiktor and H. M. Jonkers, "Quantification of crack-healing in novel bacteria-based self-healing concrete," *Cement and Concrete Composites*, vol. 33, pp. 763-770, 2011.
- [31] J. Wang, K. Van Tittelboom, N. De Belie, and W. Verstraete, "Use of silica gel or polyurethane immobilized bacteria for self-healing concrete," *Construction and Building Materials*, vol. 26, pp. 532-540, 2012.
- [32] K. Van Tittelboom, N. De Belie, W. De Muynck, and W. Verstraete, "Use of bacteria to repair cracks in concrete," *Cement and Concrete Research*, vol. 40, pp. 157-166, 2010.
- [33] T. Nishiwaki, H. Mihashi, B.-K. Jang, and K. Miura, "Development of Self-Healing System for Concrete with Selective Heating around Crack," *Journal of Advanced Concrete Technology*, vol. 4, pp. 267-275, April 26, 2006 2006.
- [34] C. M. Dry, "Three designs for the internal release of sealants, adhesives, and waterproofing chemicals into concrete to reduce permeability," *Cement and Concrete Research*, vol. 30, pp. 1969-1977, 2000.
- [35] C. Dry, "Procedures developed for self-repair of polymer matrix composite materials," *Composite Structures*, vol. 35, pp. 263-269, 1996.
- [36] S. R. White, N. R. Sottos, P. H. Geubelle, J. S. Moore, M. R. Kessler, S. R. Sriram, *et al.*, "Autonomic healing of polymer composites," *Nature*, vol. 409, pp. 794-797, 2001.
- [37] Z. Yang, J. Hollar, X. He, and X. Shi, "A self-healing cementitious composite using oil core/silica gel shell microcapsules," *Cement and Concrete Composites*, vol. 33, pp. 506-512, 2011.
- [38] C. Joseph, A. D. Jefferson, B. Isaacs, R. Lark, and D. Gardner, "Experimental investigation of adhesive-based self-healing of cementitious materials," *Magazine of Concrete Research*, vol. 62, p. 13, 2010.
- [39] S. Sangadji and E. Schlangen, "Self-Healing of Concrete Structures - Novel Approach Using Porous Network Concrete," *Journal of Advanced Concrete Technology*, vol. 10, pp. pp. 185-194, 2012.
- [40] S. S. Bang, J. K. Galinat, and V. Ramakrishnan, "Calcite precipitation induced by polyurethane-immobilized *Bacillus pasteurii*," *Enzyme and Microbial Technology*, vol. 28, pp. 404-409, 2001.
- [41] S. K. Ramachandran, V. Ramakrishnan, and S. S. Bang, "Remediation of concrete using micro-organisms," *ACI Materials Journal*, vol. 98, pp. 3-9, 2001.
- [42] K. L. Bachmeier, A. E. Williams, J. R. Warmington, and S. S. Bang, "Urease activity in microbiologically-induced calcite precipitation," *Journal of Biotechnology*, vol. 93, pp. 171-181, 2002.
- [43] W. De Muynck, D. Debrouwer, N. De Belie, and W. Verstraete, "Bacterial carbonate precipitation improves the durability of cementitious materials," *Cement and Concrete Research*, vol. 38, pp. 1005-1014, 2008.
- [44] N. K. Dhami, S. M. Reddy, and A. Mukherjee, "Biofilm and Microbial Applications in Biomineralized Concrete," in *Advanced Topics in Biomineralization*, D. J. Seto, Ed., ed: InTech, 2012.
- [45] H. M. Jonkers and E. Schlangen, "Crack Repair by Concrete-Immobilized Bacteria," presented at the the First International Conference on Self Healing Materials, Noordwijk aan Zee, The Netherlands, 2007.
- [46] H. M. Jonkers and E. Schlangen, "A two component bacteria-based self-healing concrete," 2009, pp. 119-120.
- [47] H. M. Jonkers, A. Thijssen, G. Muyzer, O. Copuroglu, and E. Schlangen, "Application of bacteria as self-healing agent for the development of sustainable concrete," *Ecological Engineering*, vol. 36, pp. 230-235, 2010.
- [48] S. van der Zwaag, "An Introduction to Material Design Principles: Damage Prevention versus Damage Management," in *Self Healing Materials: An Alternative Approach to 20 Centuries of Materials Science*. vol. 100, S. van der Zwaag, Ed., ed Dordrecht, The Netherlands: Springer, 2008, pp. 1-18.
- [49] K. van Breugel, "Is There A Market for Self-Healing Cement-Based Materials?," in *the First International Conference on Self Healing Materials*, Noordwijk aan Zee, The Netherlands, 2007.